

# Stellar populations in distant galaxies

**Gustavo Bruzual**

*Instituto de Radioastronomía y Astrofísica (IRyA)  
Universidad Nacional Autónoma de México, Campus Morelia  
Morelia, Michoacán, México*

IAU Symposium 395, Stellar populations in the Milky Way and beyond, Paraty, Brasil, November 2024

# IAU Regional Meetings

## 4th Latin-American Regional IAU Meeting (LARIM)

### Start date/time

November 18, 1984

### End date/time

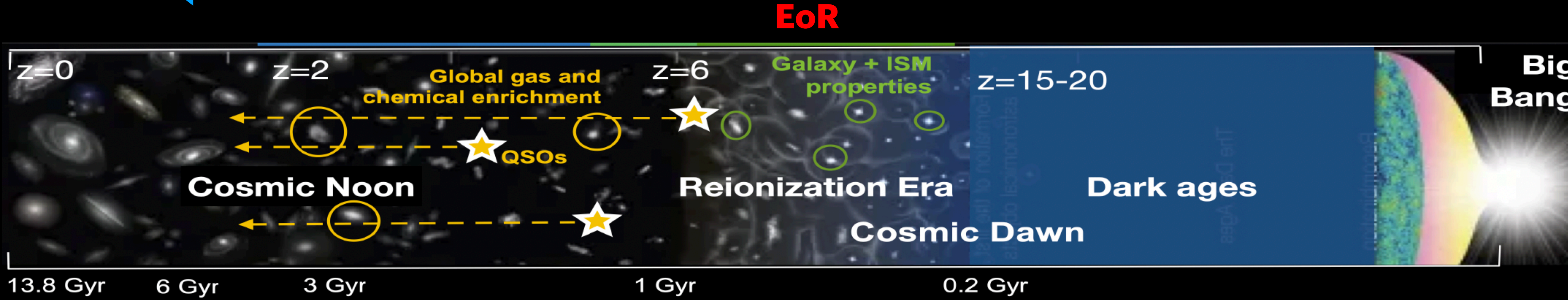
November 23, 1984

### Place

Rio de Janeiro,  
Brazil

**IV LARIM - Rio de Janeiro - November 18-23, 1984 (this week, 40 yrs ago)**

One of the objectives of JWST is to discover the first galaxies and the first stars in the EoR.



# Spectroscopic confirmation of two luminous galaxies at a redshift of 14

**Carniani et al. (2024):**

<https://doi.org/10.1038/s41586-024-07860-9>

Received: 11 May 2024

Accepted: 19 July 2024

Published online: 29 July 2024

Open access

 Check for updates

Stefano Carniani<sup>1✉</sup>, Kevin Hainline<sup>2</sup>, Francesco D'Eugenio<sup>3,4</sup>, Daniel J. Eisenstein<sup>5</sup>, Peter Jakobsen<sup>6,7</sup>, Joris Witstok<sup>3,4</sup>, Benjamin D. Johnson<sup>5</sup>, Jacopo Chevallard<sup>8</sup>, Roberto Maiolino<sup>3,4,9</sup>, Jakob M. Helton<sup>2</sup>, Chris Willott<sup>10</sup>, Brant Robertson<sup>11</sup>, Stacey Alberts<sup>2</sup>, Santiago Arribas<sup>12</sup>, William M. Baker<sup>3,4</sup>, Rachana Bhatawdekar<sup>13</sup>, Kristan Boyett<sup>14,15</sup>, Andrew J. Bunker<sup>8</sup>, Alex J. Cameron<sup>8</sup>, Phillip A. Cargile<sup>5</sup>, Stéphane Charlot<sup>16</sup>, Mirko Curti<sup>17</sup>, Emma Curtis-Lake<sup>18</sup>, Eiichi Egami<sup>2</sup>, Giovanna Giardino<sup>19</sup>, Kate Isaak<sup>20</sup>, Zhiyuan Ji<sup>2</sup>, Gareth C. Jones<sup>8</sup>, Nimisha Kumari<sup>21</sup>, Michael V. Maseda<sup>22</sup>, Eleonora Parlanti<sup>1</sup>, Pablo G. Pérez-González<sup>12</sup>, Tim Rawle<sup>13</sup>, George Rieke<sup>2</sup>, Marcia Rieke<sup>2</sup>, Bruno Rodríguez Del Pino<sup>12</sup>, Aayush Saxena<sup>8,9</sup>, Jan Scholtz<sup>3,4</sup>, Renske Smit<sup>23</sup>, Fengwu Sun<sup>2,5</sup>, Sandro Tacchella<sup>3,4</sup>, Hannah Übler<sup>3,4</sup>, Giacomo Venturi<sup>1</sup>, Christina C. Williams<sup>24</sup> & Christopher N. A. Willmer<sup>2</sup>

two luminous galaxies at  $z = 14.32^{+0.08}_{-0.20}$  and  $z = 13.90 \pm 0.17$ . The spectra reveal ultraviolet continua with prominent Lyman- $\alpha$  breaks but no detected emission lines. This discovery proves that luminous galaxies were already in place 300 million years after the Big Bang and are more common than what was expected before JWST. The most distant of the two galaxies is unexpectedly luminous and is spatially resolved with a radius of 260 parsecs. Considering also the very steep ultraviolet slope of the second galaxy, we conclude that both are dominated by stellar continuum emission, showing that the excess of luminous galaxies in the early Universe cannot be entirely explained by accretion onto black holes. Galaxy formation models will need to address the existence of such large and luminous galaxies so early in cosmic history.

**Z = 14**

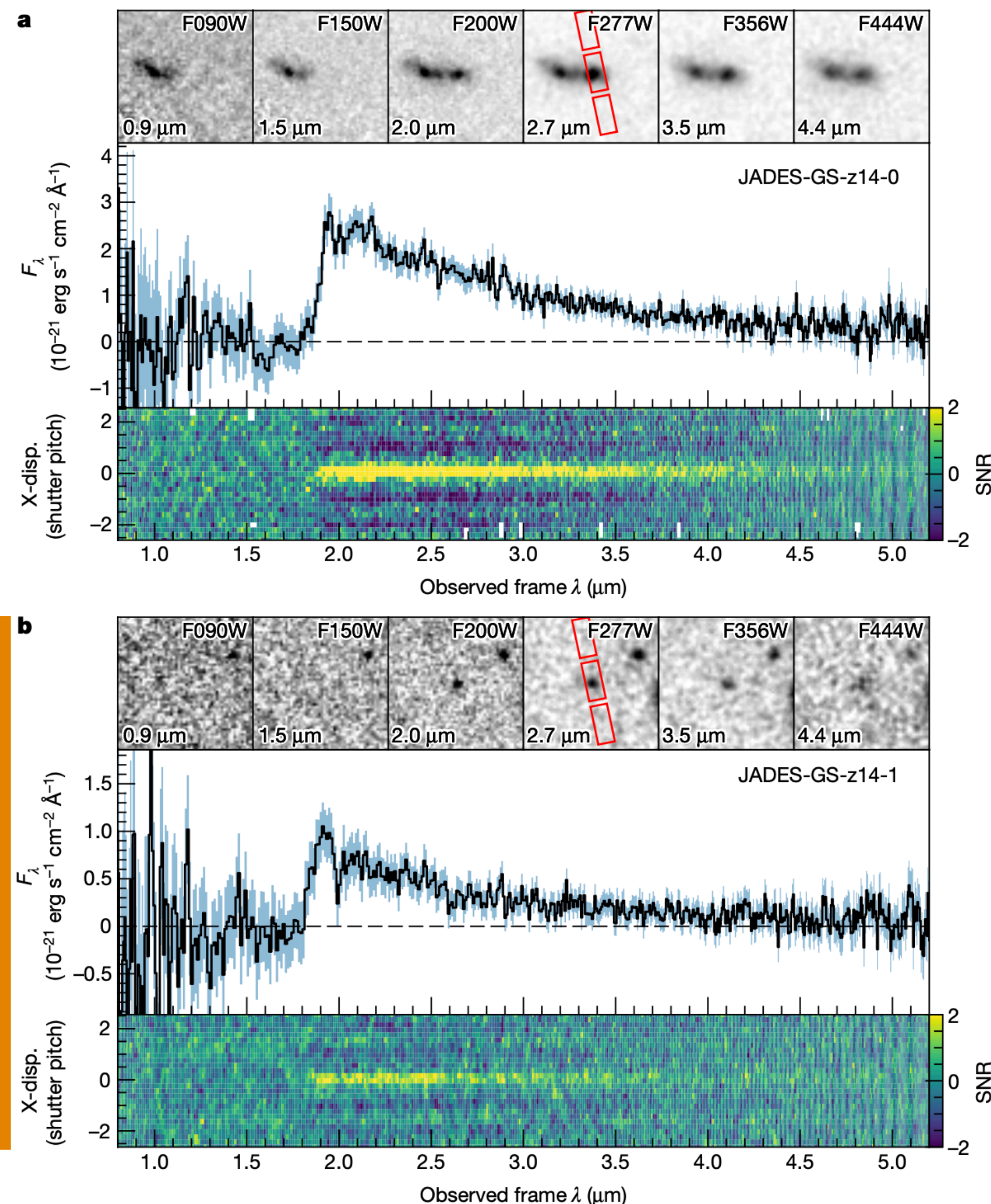


**Fig. 1 | Spectra of the two  $z \approx 14$  galaxies.** **a, b**, NIRSpect prism ( $R = 100$ ) spectra for JADES-GS-z14-0 (**a**) and JADES-GS-z14-1 (**b**). For each galaxy, the centre panel shows the 1D spectrum (black) and the associated  $1\sigma$  uncertainty (light blue). The bottom panels show the 2D spectrum of the signal-to-noise ratio (SNR) to better highlight the contrast across the break at roughly  $1.8 \mu\text{m}$ .

The 2D spectra illustrate the signal-to-noise ratio of the spectra as a function of wavelength and along cross-dispersion direction (X-disp.) Inset stamps in the top panels are cutouts of some of the NIRCам JADES images. The NIRSpect three-shutter slitlets are shown in red in each F277W image.

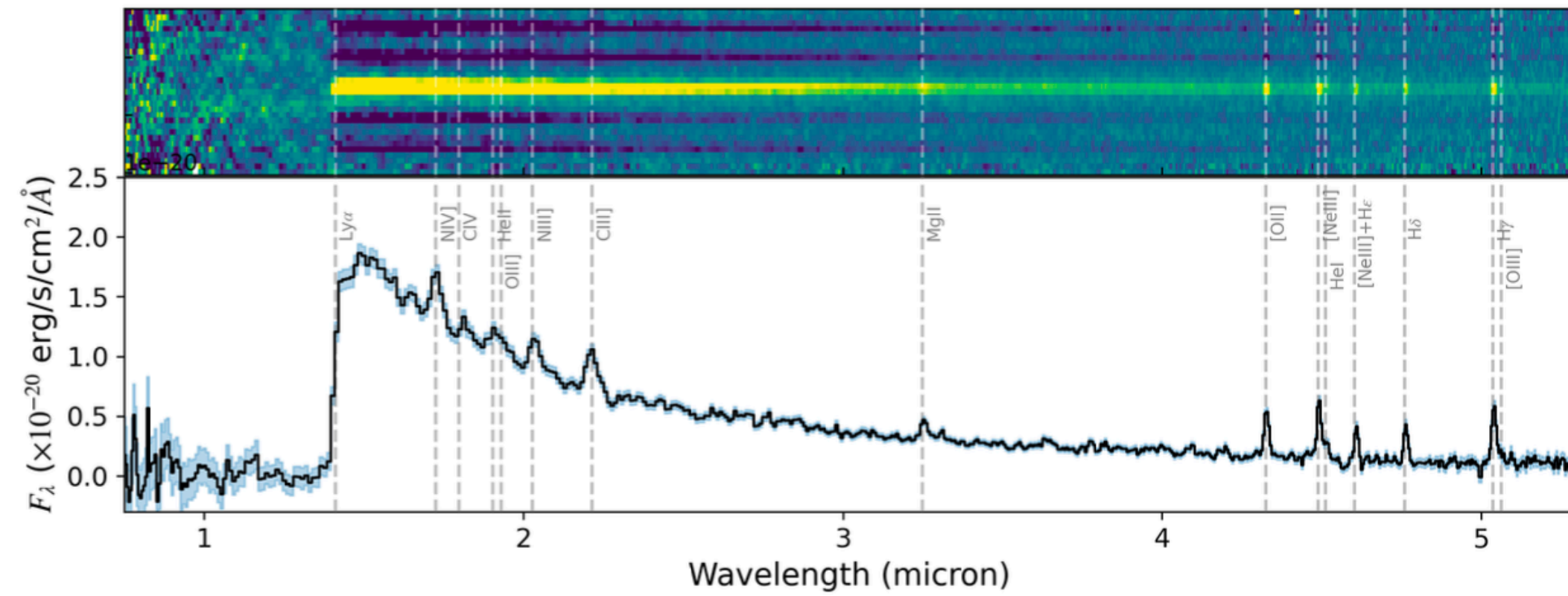


**Fig. 2.** 2D (top) and 1D (bottom) spectra of GN-z11 using the PRISM/CLEAR configuration of NIRSpec. The 1D spectrum has been extracted using a 3-pixel-wide aperture that leads to improved S/N in this highly compact object. Prominent emission lines present in the spectra are marked. The S/N of the continuum is high, and the emission lines are clearly seen in both the 1D and 2D spectra.

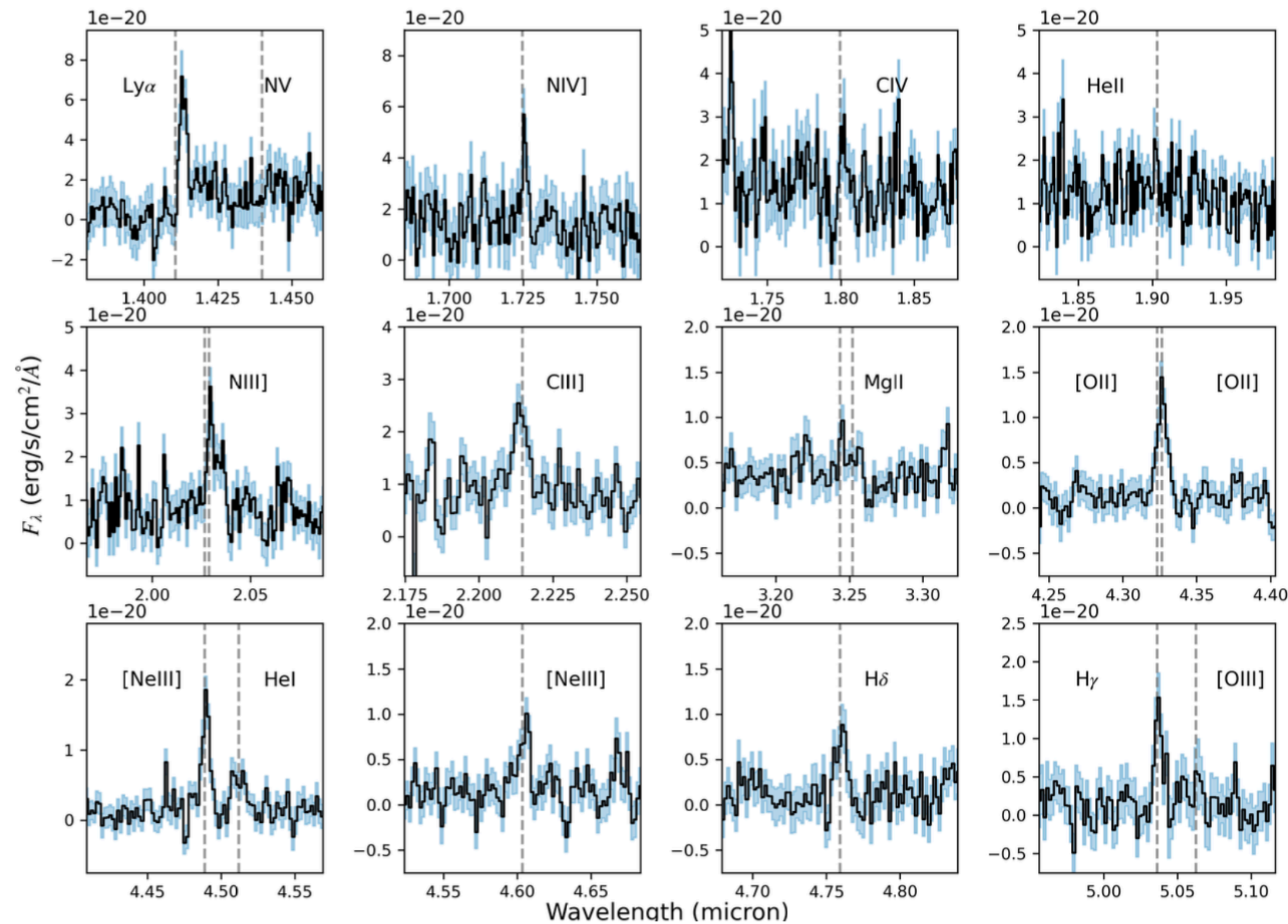


**Fig. 3.** Gallery of the most prominent emission lines seen in the GN-z11 spectrum from the medium resolution (R1000) gratings using a 3-pixel 1D spectral extraction.

**Bunker et al. (2023):**

**Lyman break galaxy at  $z = 10.6$**

(HI absorbs photons below 1215 Å)

**H, He, C, N, O, Ne, Mg emission lines visible**

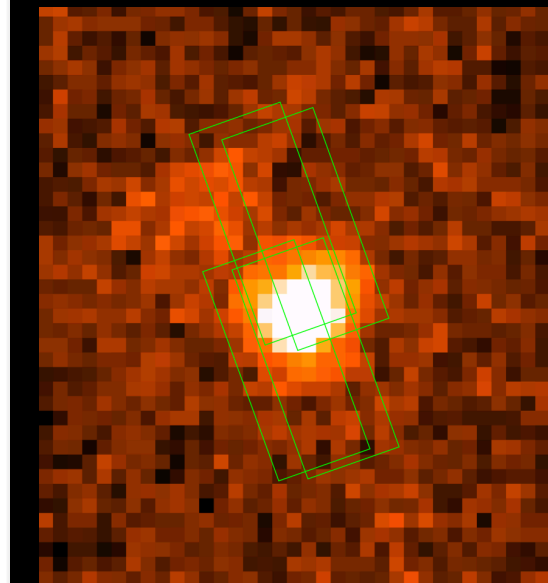


**Table 2.** GN-z11 physical parameters from BEAGLE SED fitting of the prism spectrum.

Parameter	GN-z11
$\log_{10}(M/M_{\odot})$	$8.73^{+0.06}_{-0.06}$
$\psi/M_{\odot} \text{ yr}^{-1}$	$18.78^{+0.81}_{-0.69}$
$\log_{10}(t/\text{yr})$	$7.27^{+0.19}_{-0.15}$
$\log_{10}(t_{\text{M}}/\text{yr})$	$7.01^{+0.1}_{-0.07}$
$\log_{10}(Z_{\text{neb}}/Z_{\odot})$	$-0.92^{+0.06}_{-0.05}$
$\log_{10} U_{\text{S}}$	$-2.25^{+0.97}_{-0.87}$
$A_{\text{V}}$	$0.17^{+0.03}_{-0.03}$
$\log_{10}(\xi_{\text{ion}}/\text{erg}^{-1}\text{Hz})$	$25.67^{+0.02}_{-0.02}$
$f_{\text{esc}}$	$0.03^{+0.05}_{-0.02}$

# Curtis-Lake et al. (2023):

## 4 Lyman break galaxies:

(HI absorbs photons below 1215 Å)

$z = 10.4, 11.6, 12.6, 13.2$

$Z = 0.01 - 0.04 Z_{\text{sun}}$

Mass = 10 - 100 Million  $M_{\text{sun}}$

Edad = 35 - 200 Myr

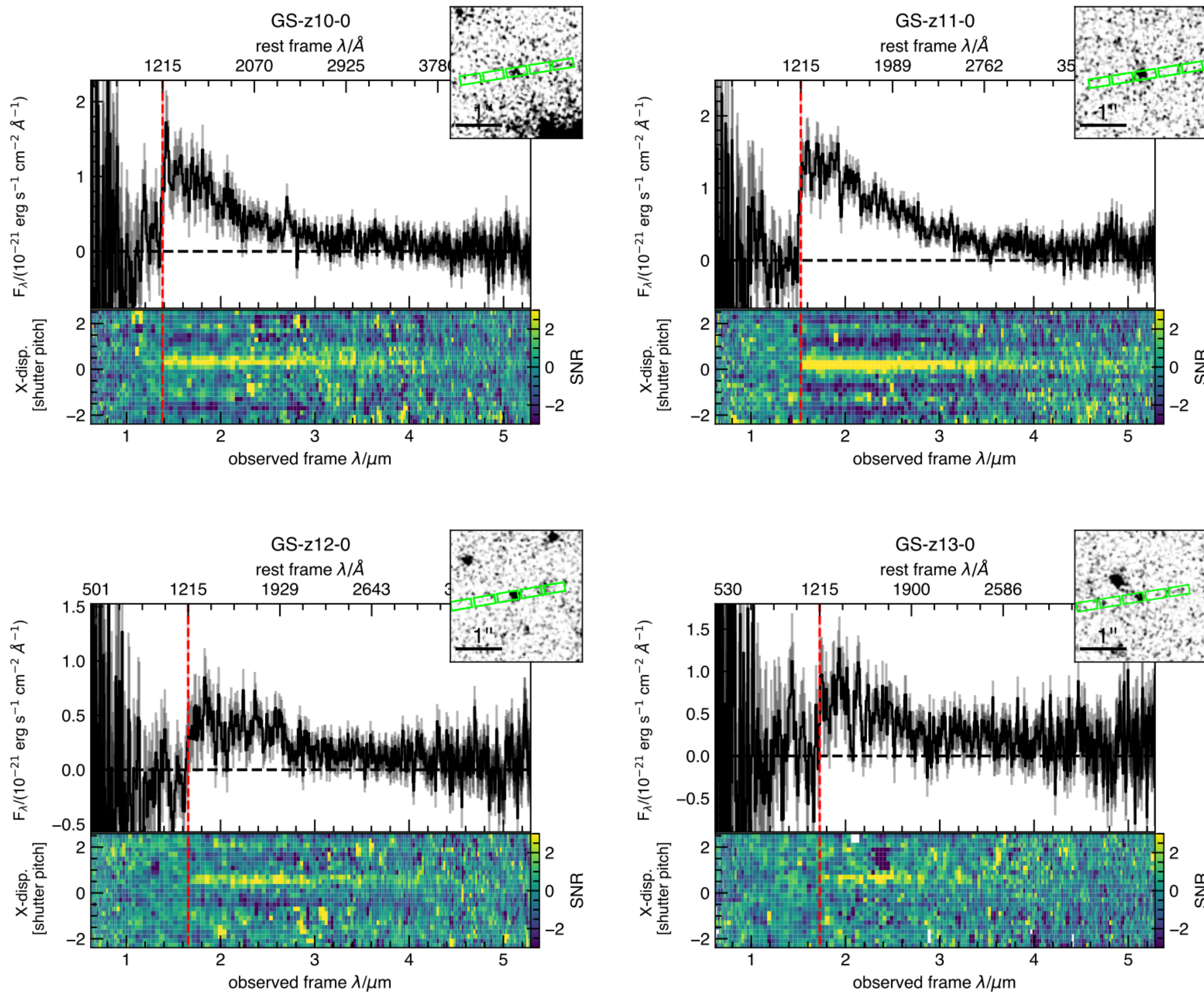


**Fig. 1** NIRSpect prism R  $\sim 100$  spectra for the four  $z > 10$  galaxies targeted for the first deep spectroscopic pointing of the JADES survey, JADES-GS-z10-0, JADES-GS-z11-0, JADES-GS-z12-0 and JADES-GS-z13-0. For each galaxy we display the 1D spectrum and associated  $1\sigma$  uncertainties (which are derived from standard error propagation through the reduction pipeline). In the bottom panel we show the 2D signal-to-noise ratio plot. The 2D plot is binned over four pixels in the wavelength direction to better show the contrast across the break. The inset panel in the top right-hand corner shows the NIRC4 F444W filter image with the three nodding positions of the NIRSpect micro-shutter 3-slitlet array aperture shown in green. The red dashed line shows  $1215.67\text{\AA}$  at the observed redshift  $z_{1216}$ .

**Table 1** Exposure times, redshifts (derived both from assuming the spectral break is at exactly  $1215.67\text{\AA}$  and accounting for the damping wing from a fully neutral IGM),  $2\sigma$  upper limits on emission-line equivalent widths (rest frame) for the C III]  $\lambda\lambda 1907, 1909$  He II  $\lambda 1640$  and [O II]  $\lambda\lambda 3726, 3729$  lines,  $2\sigma$  lower limits on the strength of the observed spectral breaks (measurements described in Methods 2), UV absolute magnitude,  $M_{\text{UV}}$ , and UV slope,  $\beta$  (measured directly from the spectra, see Methods 2.3) and BEAGLE-derived physical properties for the four objects. For the BEAGLE-derived properties we report posterior medians and limits in the  $1\sigma$  credible region.

JADES-ID	GS-z10-0	GS-z11-0	GS-z12-0	GS-z13-0
Full name	JADES-GS+53.15884-27.77349	JADES-GS+53.16476-27.77463	JADES-GS+53.16634-27.82156	JADES-GS+53.14988-27.77650
Exposure time (s)	67225.6	100838.0	67225.6	33612.8
$z_{1216}^*$	$10.38^{+0.07}_{-0.06}$	$11.58^{+0.05}_{-0.05}$	$12.63^{+0.24}_{-0.08}$	$13.20^{+0.04}_{-0.07}$
$z_{\text{HI}}^\dagger$	$10.37^{+0.03}_{-0.02}$	$11.48^{+0.03}_{-0.08}$	$12.6^{+0.04}_{-0.05}$	$13.17^{+0.16}_{-0.15}$
$EW(\text{C III]) \AA } 2\sigma$	$< 13.8$	$< 5.9$	$< 12.4$	$< 15.2$
$EW(\text{He II}) \AA } 2\sigma$	$< 14.8$	$< 6.0$	$< 13.5$	$< 15.4$
$EW(\text{O II}) \AA } 2\sigma$	$< 28.1$	$< 9.1$	$< 16.6$	$< 16.8$
$2\sigma$ break strength	$> 2.04$	$> 6.85$	$> 2.48$	$> 2.79$
$M_{\text{UV}}$	$-18.61 \pm 0.10$	$-19.34 \pm 0.05$	$-18.23 \pm 0.16$	$-18.73 \pm 0.06^\ddagger$
$\beta$	$-2.49 \pm 0.22$	$-2.18 \pm 0.09$	$-1.84 \pm 0.19$	$-2.37 \pm 0.12^\ddagger$
$\log(M/M_\odot)$	$7.58^{+0.19}_{-0.20}$	$8.67^{+0.08}_{-0.13}$	$7.64^{+0.66}_{-0.39}$	$7.95^{+0.19}_{-0.29}$
$\Psi/M \text{ yr}^{-1}$	$1.1^{+0.19}_{-0.16}$	$2.2^{+0.28}_{-0.22}$	$1.8^{+0.54}_{-0.43}$	$1.36^{+0.31}_{-0.23}$
$\log(t/\text{yr})^\parallel$	$7.54^{+0.25}_{-0.20}$	$8.35^{+0.08}_{-0.17}$	$7.36^{+0.75}_{-0.59}$	$7.84^{+0.23}_{-0.36}$
$\log(Z/Z_\odot)^\square$	$-1.91^{+0.25}_{-0.20}$	$-1.87^{+0.28}_{-0.18}$	$-1.44^{+0.23}_{-0.22}$	$-1.69^{+0.28}_{-0.31}$
$\tau_{\text{v}}^{\ddagger\ddagger}$	$0.05^{+0.03}_{-0.02}$	$0.18^{+0.06}_{-0.06}$	$0.17^{+0.20}_{-0.09}$	$0.10^{+0.08}_{-0.05}$
$\xi_{\text{ion}}^\S$	$25.46^{+0.07}_{-0.07}$	$25.43^{+0.06}_{-0.06}$	$25.72^{+0.16}_{-0.19}$	$25.47^{+0.10}_{-0.09}$

Oesch et al. (2023):

## Galaxy at $z=7.6$ with H and [OIII] emission lines at the EOR.

Oesch et al. 2023, MNRAS, 525, 2864

*The JWST FRESCO survey* 2867

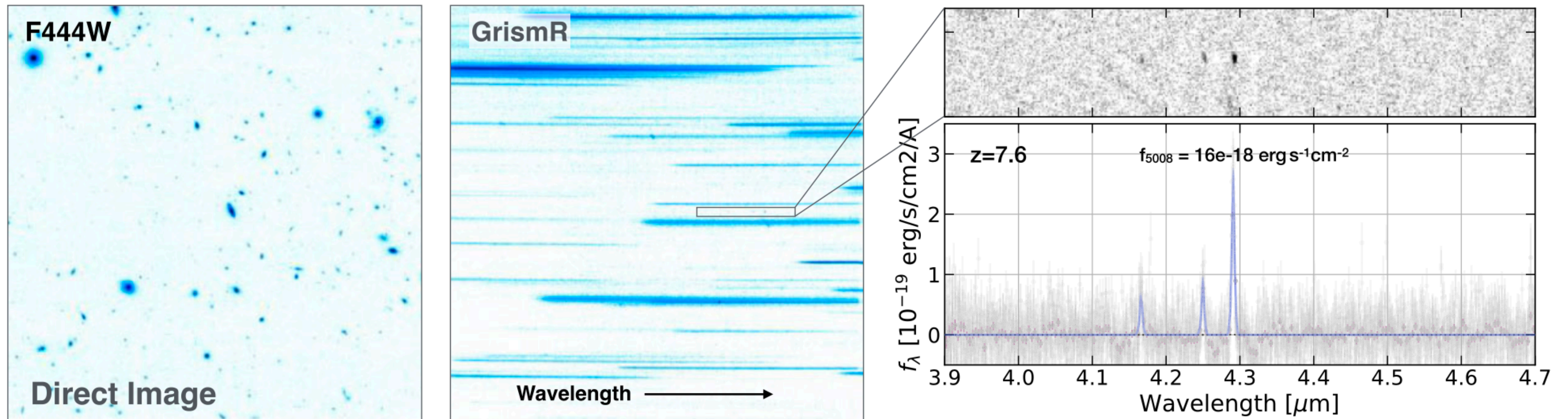


**Figure 2.** Example of FRESCO’s spectroscopic strategy. The left-hand panel shows a portion of the  $F444W$  direct image in the FRESCO-S field. The middle panel shows the associated GrismR data, from which FRESCO can identify EoR galaxies as emission line sources. Down to UV continuum magnitudes of 26.8,  $z = 6.7\text{--}9.0$  sources are expected to show three emission lines from the [O III] doublet as well as  $H\beta$ , resulting in unambiguous redshift identifications. For example, the right-hand panels show the 2D and the extracted 1D spectra of a source in the FRESCO-S field with an unambiguous grism redshift at  $z = 7.6$ .

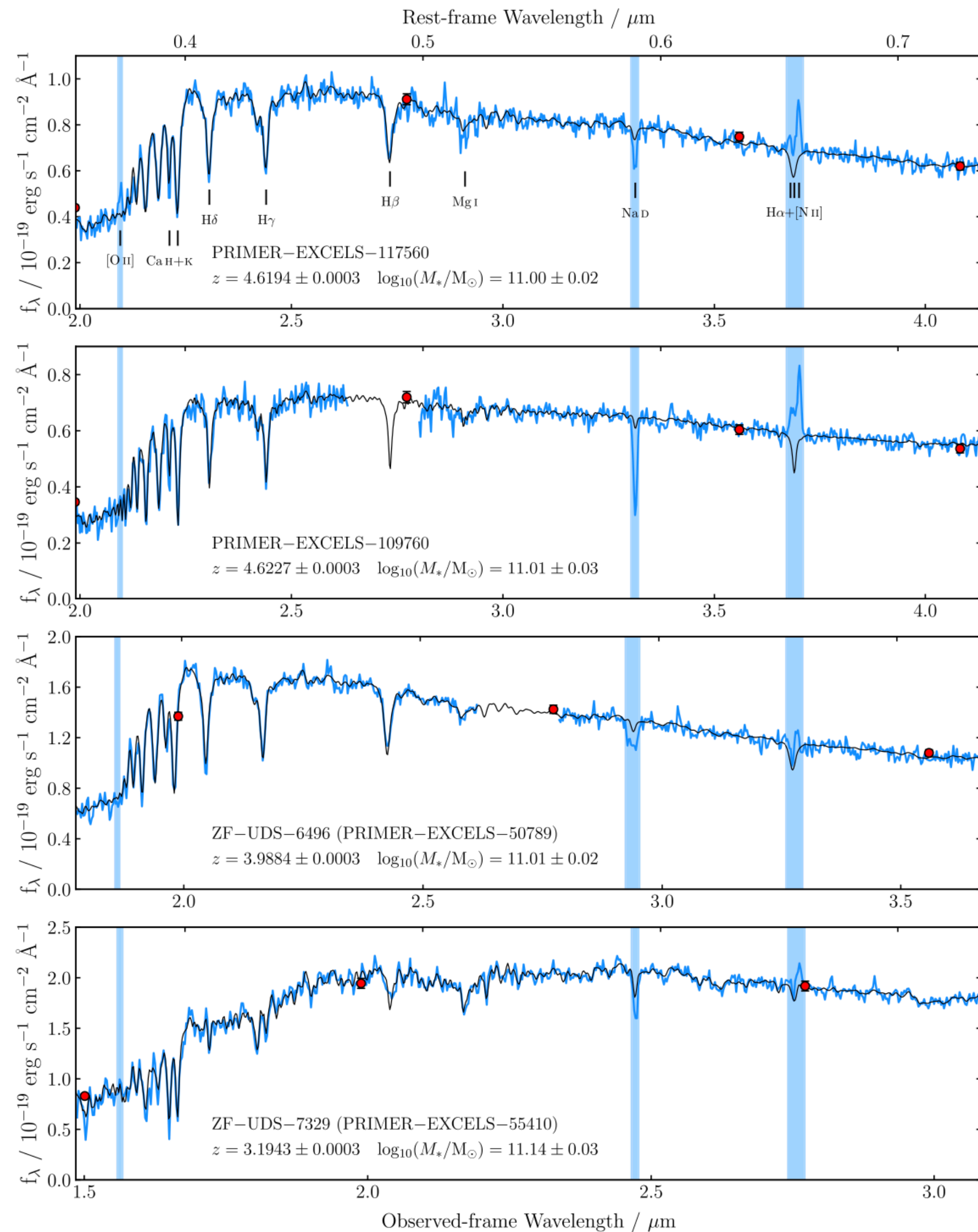


**Figure 3.** *JWST* EXCELS NIRSpec observations of our four ultra-massive quiescent galaxies at  $3 < z < 5$ ; zoom in on the rest-frame 3540–7350 Å region included in our BAGPIPES full-spectral-fitting analysis (see Section 4.3.1). The spectroscopic data are shown in blue, with PRIMER NIRCcam photometry shown as red points. The posterior-median fitted BAGPIPES models are shown with black lines. The vertical blue shaded regions were masked from the fits. The spectra and our full-spectral-fitting results are described in Section 5.

# Carnall et al. (2024):

Monthly Notices

of the

ROYAL ASTRONOMICAL SOCIETY

MNRAS **534**, 325–348 (2024)

Advance Access publication 2024 September 12

<https://doi.org/10.1093/mnras/stae2092>

## The *JWST* EXCELS survey: too much, too young, too fast? Ultra-massive quiescent galaxies at $3 < z < 5$

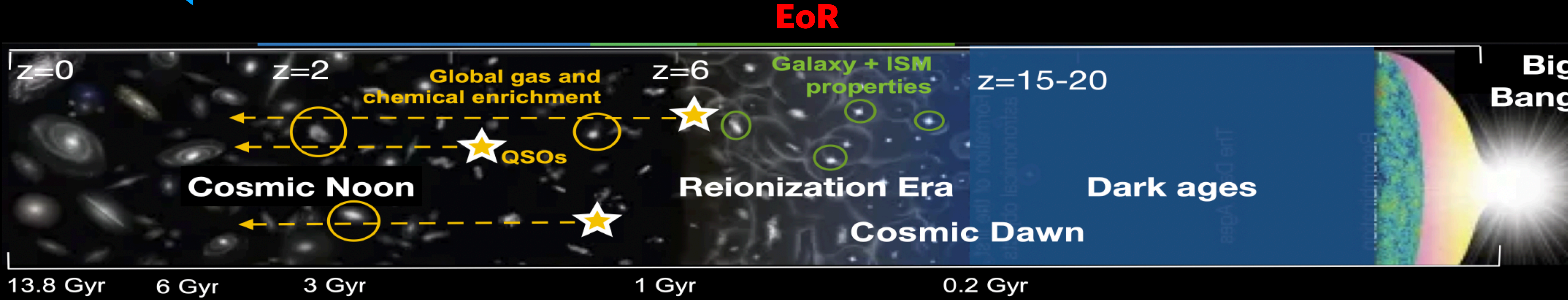
A. C. Carnall<sup>1</sup>,<sup>1\*</sup> F. Cullen<sup>1</sup>, R. J. McLure<sup>1</sup>, D. J. McLeod<sup>1</sup>, R. Begley<sup>1</sup>, C. T. Donnan<sup>1</sup>, J. S. Dunlop<sup>1</sup>, A. E. Shapley<sup>2</sup>, K. Rowlands<sup>3,4</sup>, O. Almaini<sup>5</sup>, K. Z. Arellano-Córdova<sup>1</sup>, L. Barrufet<sup>1</sup>, A. Cimatti<sup>6,7</sup>, R. S. Ellis<sup>8</sup>, N. A. Grogin<sup>9</sup>, M. L. Hamadouche<sup>1</sup>, G. D. Illingworth<sup>10</sup>, A. M. Koekemoer<sup>9</sup>, H.-H. Leung<sup>11</sup>, C. C. Lovell<sup>12</sup>, P. G. Pérez-González<sup>13</sup>, P. Santini<sup>14</sup>, T. M. Stanton<sup>1</sup> and V. Wild<sup>11</sup>

*Ultra-massive quiescent galaxies at  $3 < z < 5$*  335

**Table 3.** Derived parameters for our four EXCELS ultra-massive quiescent galaxies from the BAGPIPES full-spectral-fitting analysis described in Section 4.3.1, as well as the morphological analysis described in Section 4.4. The definitions of the parameters in our full-spectral-fitting analysis are given in Table 2. We also include the results we derived for GS-9209 in Carnall et al. (2023c). Parameters derived from our BAGPIPES full spectral fitting analysis are defined in Table 2. Morphological parameters were measured from F277W-band imaging.

Object ID	PRIMER-EXCELS-117560	PRIMER-EXCELS-109760	ZF-UDS-6496	ZF-UDS-7329	GS-9209
Redshift	$4.6194 \pm 0.0003$	$4.6227 \pm 0.0003$	$3.9884 \pm 0.0003$	$3.1943 \pm 0.0003$	$4.6582 \pm 0.0002$
$\log_{10}(M_*/M_\odot)$	$11.00 \pm 0.02$	$11.01 \pm 0.03$	$11.01 \pm 0.02$	$11.14 \pm 0.03$	$10.58 \pm 0.02$
$\text{SFR}/M_\odot \text{ yr}^{-1}$	$0^{+0.0001}_{-0}$	$0^{+0.004}_{-0}$	$0^{+0.000001}_{-0}$	$0.6 \pm 0.3$	$0^{+0.000003}_{-0}$
$\log_{10}(Z_*/Z_\odot)$	$0.35^{+0.08}_{-0.06}$	$-0.41^{+0.06}_{-0.06}$	$0.32^{+0.04}_{-0.05}$	$0.35^{+0.07}_{-0.08}$	$-0.96^{+0.04}_{-0.09}$
$t_{\text{form}}/\text{Gyr}$	$0.65 \pm 0.05$	$0.51 \pm 0.05$	$1.01 \pm 0.03$	$0.41 \pm 0.13$	$0.76 \pm 0.03$
$z_{\text{form}}$	$7.8 \pm 0.5$	$9.4 \pm 0.7$	$5.6 \pm 0.1$	$11.2^{+3.1}_{-2.1}$	$6.9 \pm 0.2$
$z_{\text{quench}}$	$7.1 \pm 0.8$	$6.7 \pm 0.9$	$5.4 \pm 0.2$	$6.3^{+1.2}_{-1.0}$	$6.5^{+0.2}_{-0.5}$
$A_V$	$0.38 \pm 0.06$	$0.84 \pm 0.09$	$0.49 \pm 0.05$	$0.23 \pm 0.07$	$0.02 \pm 0.02$
$a$	$1.61 \pm 0.03$	$1.57 \pm 0.04$	$1.57 \pm 0.04$	$1.55 \pm 0.04$	$1.71 \pm 0.03$
$\sigma_*/\text{km s}^{-1}$	$360 \pm 20$	$140 \pm 10$	$370 \pm 10$	$250 \pm 20$	$250 \pm 20$
$r_e/\text{pc}$	$610 \pm 10$	$310 \pm 10$	$730 \pm 10$	$910 \pm 10$	$220 \pm 20$
$n$	$4.7 \pm 0.1$	$5.1 \pm 0.2$	$3.7 \pm 0.2$	$2.5 \pm 0.1$	$2.3 \pm 0.3$
$e$	$0.63 \pm 0.01$	$0.32 \pm 0.01$	$0.50 \pm 0.01$	$0.77 \pm 0.01$	$0.58 \pm 0.01$
$\log_{10}(\Sigma_{\text{eff}}/M_\odot \text{ kpc}^{-2})$	$10.63 \pm 0.03$	$11.23 \pm 0.04$	$10.49 \pm 0.03$	$10.42 \pm 0.04$	$11.1 \pm 0.1$
$\log_{10}(M_{\text{dyn,eff}}/M_\odot)$	$10.86 \pm 0.05$	$9.71 \pm 0.07$	$10.71 \pm 0.02$	$10.94 \pm 0.07$	$10.3 \pm 0.1$

One of the objectives of JWST is to discover the first galaxies and the first stars in the EoR.



# First Stars (Pop III):

GALAXY GN - z11

## PRISTINE GAS CLUMP NEAR GN - z11

NIRCam Imaging



NIRSpec Microshutter Array Spectroscopy

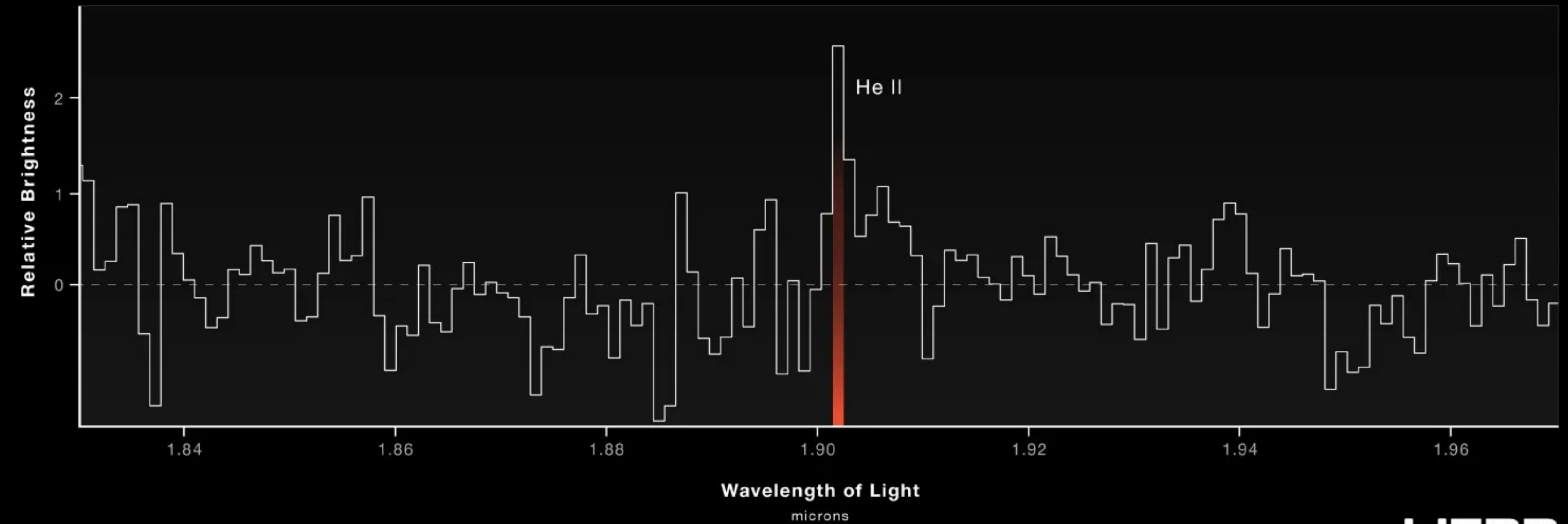


**Table 1.** Measured fluxes, EWs, and  $3\sigma$  limits in the apertures considered in this paper.

Emission line	Flux ( $10^{-19}$ erg s $^{-1}$ cm $^{-2}$ )	log(EW)[phot] ( $\text{\AA}$ )	log(EW)[spec] ( $\text{\AA}$ )
HeII clump small aperture			
HeII $\lambda$ 1640	$1.8 \pm 0.34$	$1.79^{+0.15}_{-0.25}$	$>1.18$
CIV1550	$<1.2$		
OIII]1665	$<1.0$		
CIII]1909	$<1.1$		
HeII large aperture			
HeII $\lambda$ 1640	$5.0 \pm 0.83$	$1.45^{+0.18}_{-0.32}$	$>1.08$
CIV1550	$<3.1$		
OIII]1665	$<2.5$		
CIII]1909	$<2.8$		
MSA offset aperture			
HeII $\lambda$ 1640	$3.4 \pm 0.9$	$1.99^{+0.18}_{-0.33}$	$2.16^{+0.13}_{-0.21}$
H $\gamma$	$<1.37$		

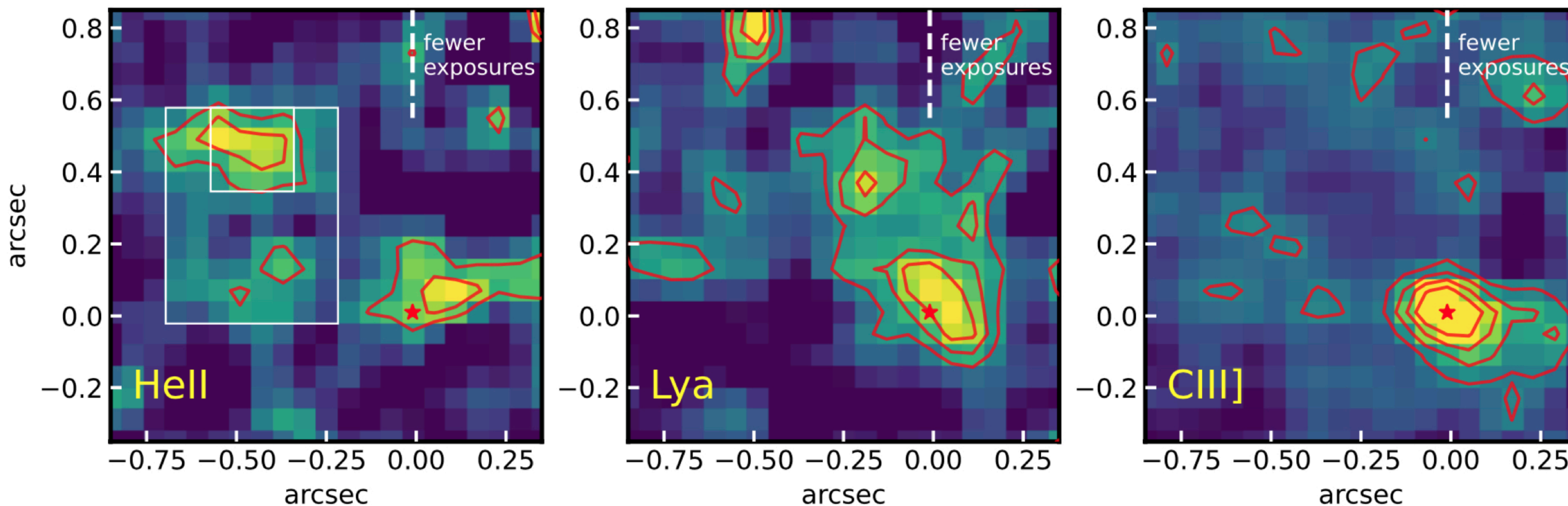
A&A, 687, A67 (2024)  
<https://doi.org/10.1051/0004-6361/202347087>  
 © The Authors 2024

## Maiolino et al. (2024)

## JADES

### Possible Population III signatures at $z = 10.6$ in the halo of GN-z11

Maiolino et al.: PopIII signatures at  $z=10.6$

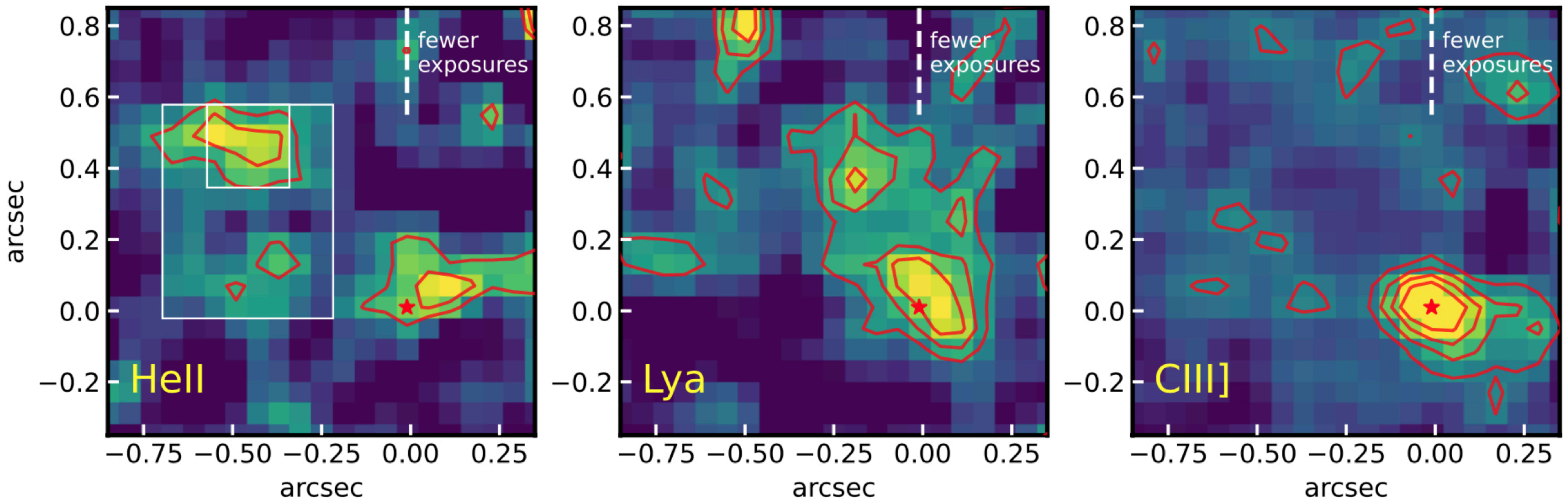


## Maiolino et al. (2024)

Galaxies detected so far in the EoR have the expected properties but contain heavy elements and hence are not formed by PopIII stars (H  $\gamma$  He).

Possibly PopIII stars can be detected via Integral Field Spectroscopy with JWST, which will allow to separate star forming regions of pristine composition from already polluted regions. With slit spectroscopy both populations are mixed and PopII stars dominate.

Maiolino et al.: PopIII signatures at  $z=10.6$



# Reionization

## Most of the photons that reionized the Universe came from dwarf galaxies

[Hakim Atek](#) , [Ivo Labbé](#), [Lukas J. Furtak](#), [Iryna Chemerynska](#), [Seiji Fujimoto](#), [David J. Setton](#), [Tim B. Miller](#), [Pascal Oesch](#), [Rachel Bezanson](#), [Sedona H. Price](#), [Pratika Dayal](#), [Adi Zitrin](#), [Vasily Kokorev](#), [John R. Weaver](#), [Gabriel Brammer](#), [Pieter van Dokkum](#), [Christina C. Williams](#), [Sam E. Cutler](#), [Robert Feldmann](#), [Yoshinobu Fudamoto](#), [Jenny E. Greene](#), [Joel Leja](#), [Michael V. Maseda](#), [Adam Muzzin](#), ... [Katherine E. Whitaker](#)  Show authors

[Nature](#) 626, 975–978 (2024) | [Cite this article](#)

**faintness.** Here we report an analysis of eight ultra-faint galaxies (in a very small field) during the epoch of reionization with absolute magnitudes between  $M_{UV} \sim -17$  to  $-15$  mag (down to  $0.005 L^{\star 10,11}$ ). We find that faint galaxies during the Universe's first billion years produce ionizing photons with  $\log(\xi_{ion}/\text{Hz erg}^{-1}) = 25.80 \pm 0.14$ , a factor of 4 higher than commonly assumed values.<sup>22</sup> If this field is representative of the large scale distribution of faint galaxies, the rate of ionizing photons exceeds that needed for reionization, even for escape fractions of order five per cent.

**8 ultra faint galaxies in a very small field**

**Rate of ionizing photons exceeds that needed for reionization even for escape fraction as low as 5%**

**Not QSO's, nor bright galaxies**

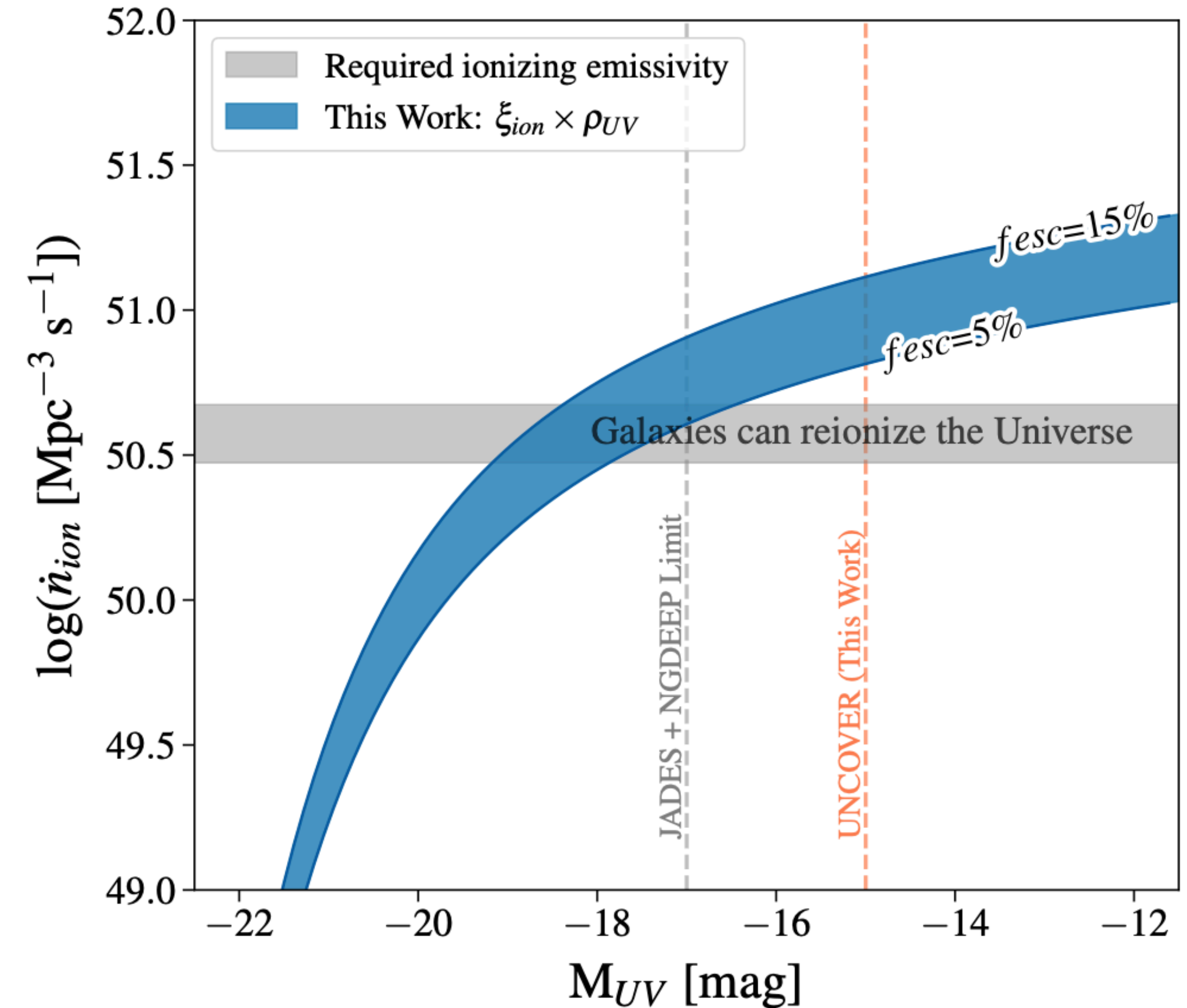


**Fig. 4:** The total ionizing emissivity of galaxies at  $z \sim 7$ . The total ionizing photon production rate density, derived from the prevalence and the ionizing efficiency of galaxies, as a function of the faint integration limit. The blue region delimits the two cases where  $f_{esc}=5\%$  and  $f_{esc}=15\%$ . The gray-shaded region is the threshold required to maintain the Universe ionized at  $z = 7$ . The gray vertical line marks the magnitude limit of the deepest *JWST* spectroscopic surveys to date. The orange vertical line shows the limit probed by this work. At this luminosity, galaxies produce enough radiation to reionize the Universe.

## Galaxy morphology from $z \sim 6$ through the lens of JWST<sup>★</sup>

M. Huertas-Company<sup>1,2,3,4,30</sup>, K. G. Iyer<sup>5,★★</sup>, E. Angeloudi<sup>1,4</sup>, M. B. Bagley<sup>7</sup> , S. L. Finkelstein<sup>7</sup>, J. Kartaltepe<sup>18</sup>, E. J. McGrath<sup>29</sup> , R. Sarmiento<sup>1,4</sup>, J. Vega-Ferrero<sup>1,4,9,10</sup>, P. Arrabal Haro<sup>6</sup>, P. Behroozi<sup>8,9</sup>, F. Buitrago<sup>10,11</sup> , Y. Cheng<sup>12</sup>, L. Costantin<sup>13</sup>, A. Dekel<sup>14,15</sup>, M. Dickinson<sup>6</sup>, D. Elbaz<sup>16</sup>, N. A. Grogin<sup>19</sup>, N. P. Hathi<sup>19</sup> , B. W. Holwerda<sup>17</sup>, A. M. Koekemoer<sup>19</sup>, R. A. Lucas<sup>19</sup>, C. Papovich<sup>20,21</sup>, P. G. Pérez-González<sup>13</sup>, N. Pirzkal<sup>22</sup>, L.-M. Seillé<sup>23</sup>, A. de la Vega<sup>24</sup>, S. Wuyts<sup>25</sup> , G. Yang<sup>26,27</sup>, and L. Y. A. Yung<sup>28</sup>

Huertas-Company et al. (2024)

## Complex morphological diversity already in place $\sim 1$ Gyr after the Big Bang

- The fraction of bulge-dominated galaxies increases at the high-mass end, even at  $z \sim 5$ , indicating that the processes of bulge formation in massive galaxies are already in place at these early cosmic epochs.
- The fraction of peculiar galaxies also increases with redshift, even in the NIR rest-frame, suggesting that the stellar mass distribution is more disturbed at high redshift, although the S/N may still affect this result.
- The high-mass end of the galaxy distribution ( $\log M_*/M_\odot > 10.5$ ) is dominated by undisturbed disk-like morphologies even at  $z \sim 5$ , indicating that disk formation may be in place at very early epochs.
- The fraction of early-type galaxies reaches  $\sim 70\%$  to  $\sim 90\%$  for massive ( $\log M_*/M_\odot > 10.5$ ) quenched galaxies, even at  $z \sim 5$ , suggesting that the connection between quenching and bulge growth is already established around  $\sim 1$  Gyr after the Big Bang.

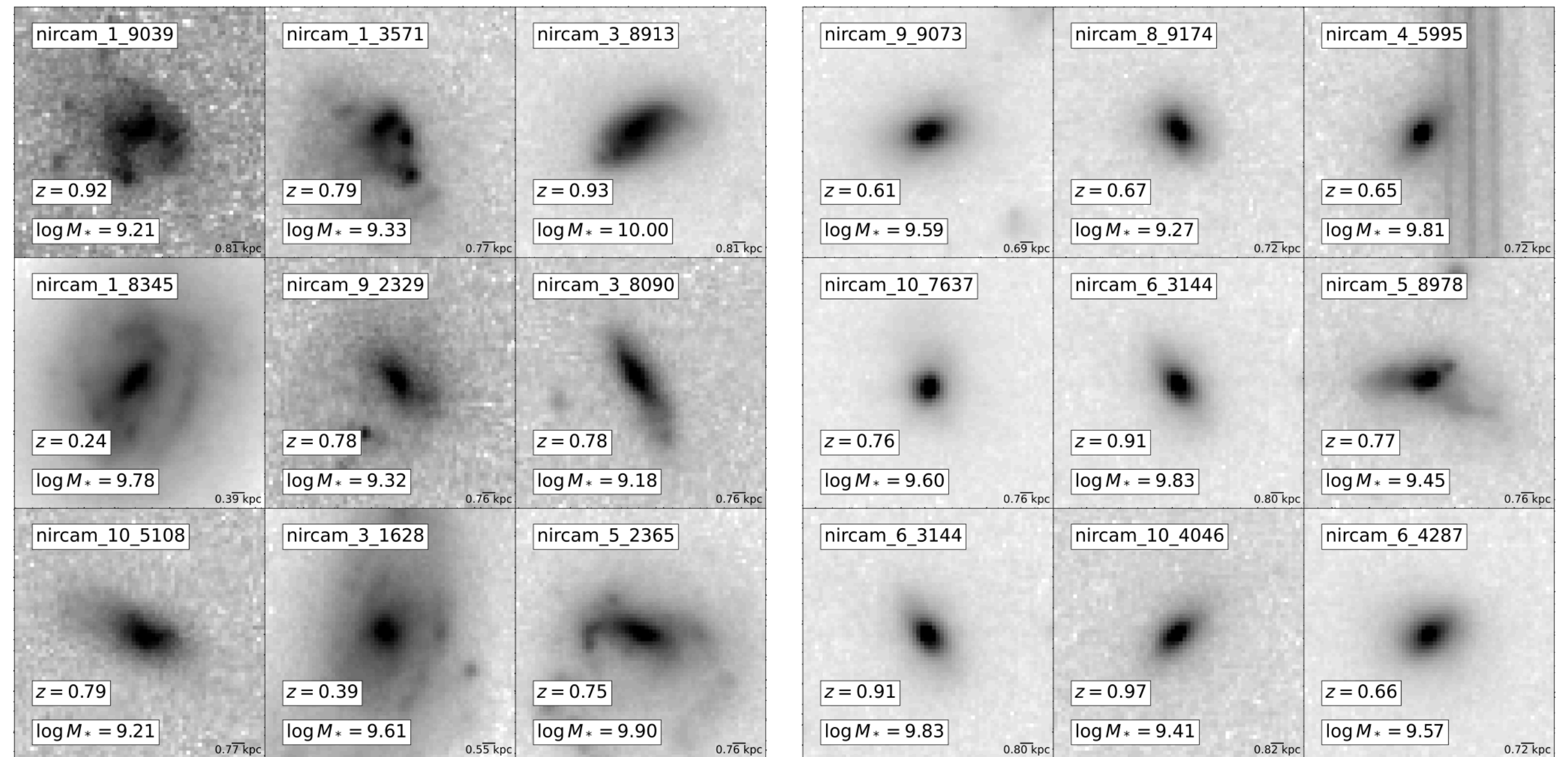
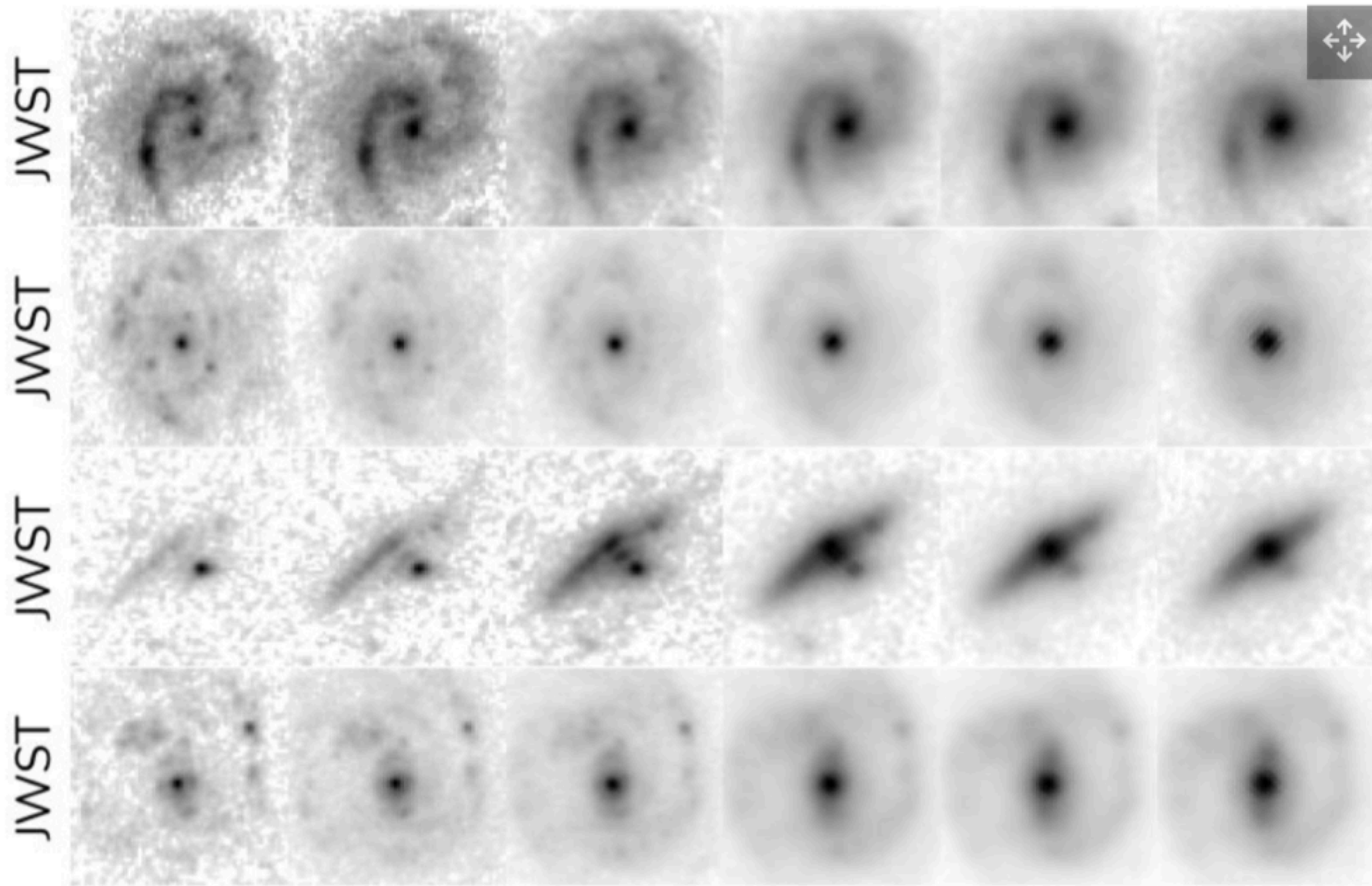


Fig. 18. Random example stamps of low mass ( $9 < \log M_*/M_\odot < 10$ ) star-forming galaxies with late-type (left panel) and early-type morphologies (right panel). Images are in the  $F200W$  filter.

# MW-like galaxies:



**Galaxies develop similar morphology to the MW already at 3.7 Gyr after the Big Bang (vs. ~ 6 Gyr predicted by theory).**

Images from JWST of the newly discovered Milky Way-like galaxies seen in the early universe. Each row shows a different galaxy as observed in the different infrared wavelengths where JWST takes imaging data.

(Image credit: L. Ferreira, C. Conselice)

# Little Red Dots (LRD's)

What is the nature of Little Red Dots and what is not, MIRI SMILES edition

PABLO G. PÉREZ-GONZÁLEZ <sup>1</sup>, GUILLERMO BARRO <sup>2</sup>, GEORGE H. RIEKE <sup>3</sup>, JIANWEI LYU <sup>3</sup>, MARCIA RIEKE <sup>3</sup>, STACEY ALBERTS <sup>3</sup>, CHRISTINA C. WILLIAMS <sup>4</sup>, KEVIN HAINLINE <sup>3</sup>, FENGWU SUN <sup>3</sup>, DÁVID PUSKÁS <sup>5,6</sup>, MARIANNA ANNUNZIATELLA <sup>1</sup>, WILLIAM M. BAKER <sup>5,6</sup>, ANDREW J. BUNKER <sup>7</sup>, EIICHI EGAMI <sup>3</sup>, ZHIYUAN JI <sup>3</sup>, BENJAMIN D. JOHNSON <sup>8</sup>, BRANT ROBERTSON <sup>9</sup>, BRUNO RODRÍGUEZ DEL PINO <sup>1</sup>, WIPHU RUJOPAKARN <sup>10,11</sup>, IRENE SHIVAEI <sup>1</sup>, SANDRO TACCHELLA <sup>5,6</sup>, CHRISTOPHER N. A. WILLMER <sup>3</sup>, AND CHRIS WILLOTT <sup>12</sup>

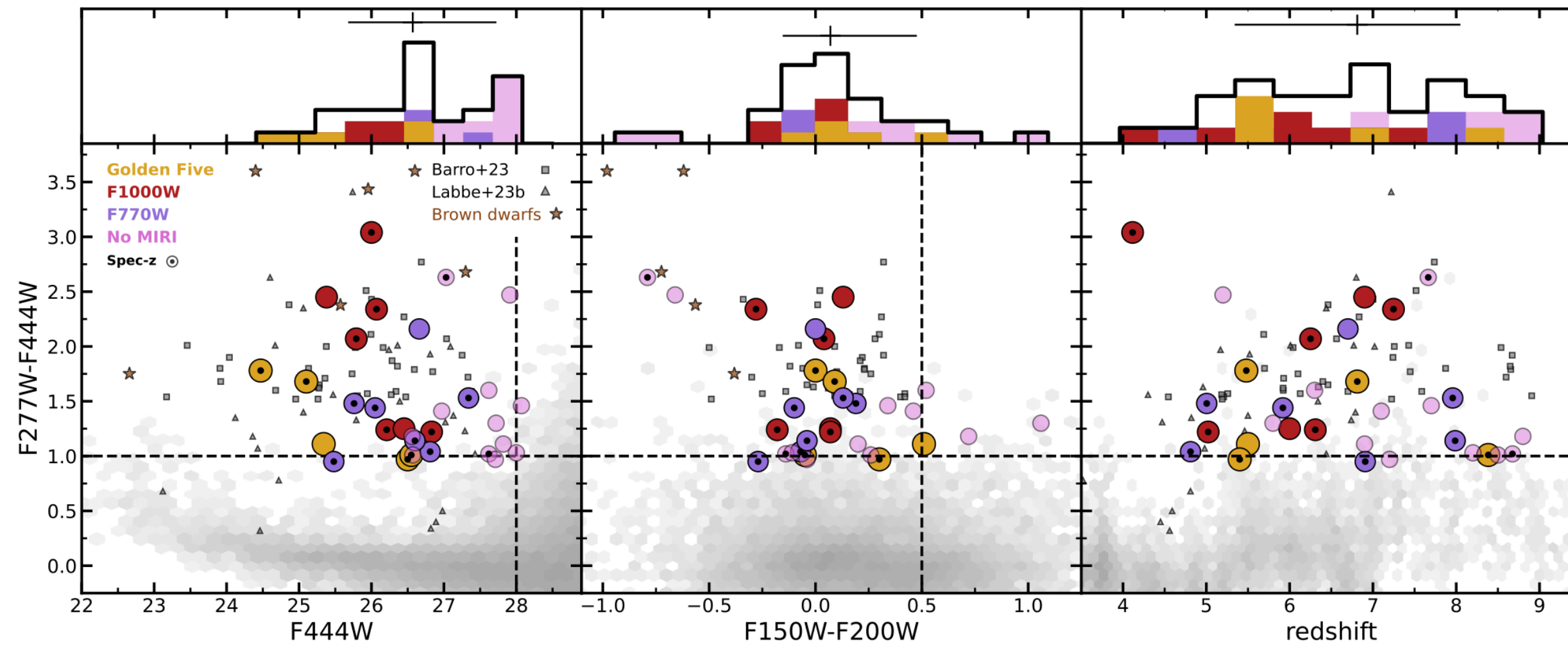
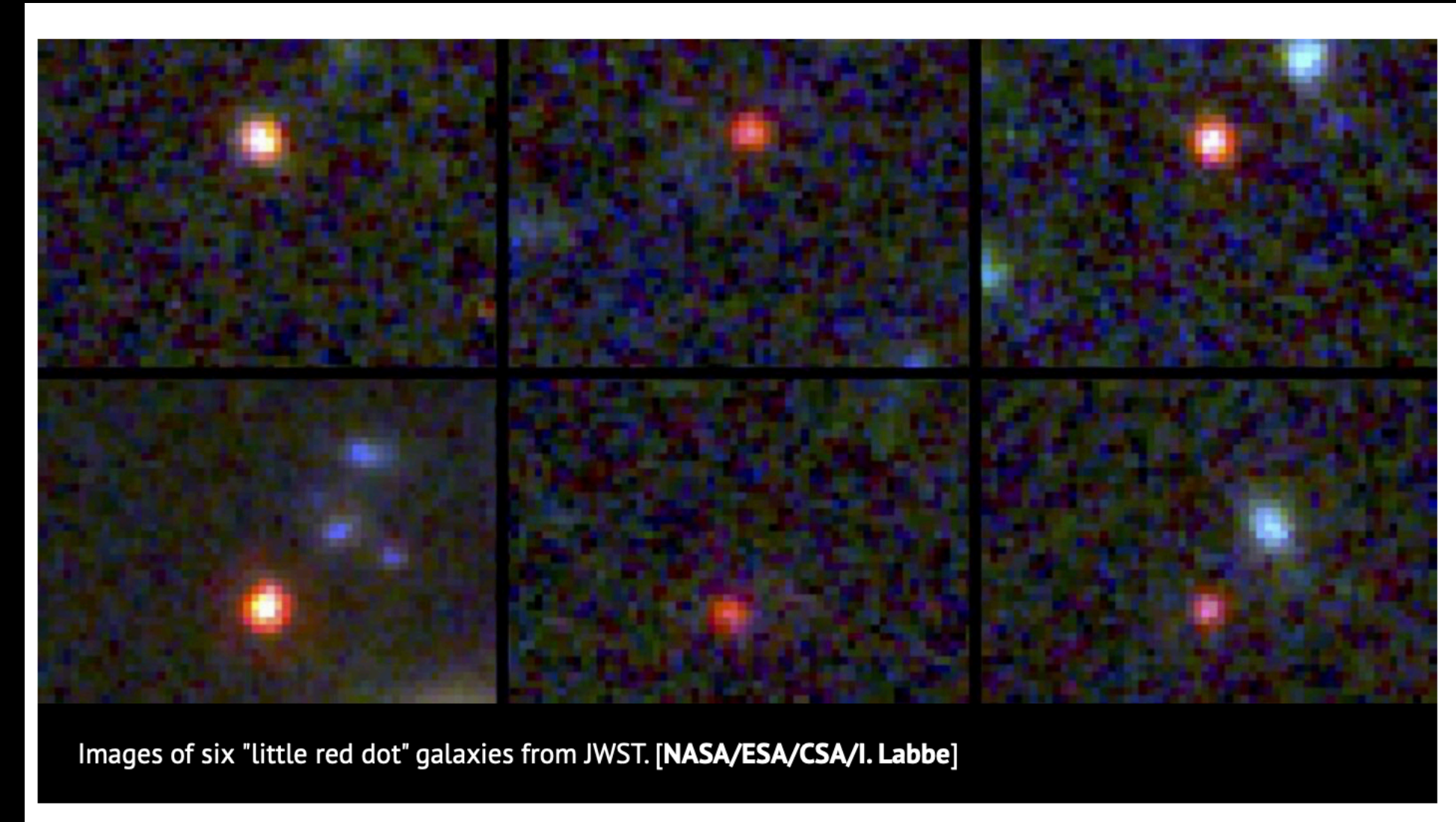


**Figure 1.** The left and central panels show the  $F_{277W} - F_{444W}$  vs.  $F_{444W}$  color-magnitude and  $F_{277W} - F_{444W}$  vs.  $F_{150W} - F_{200W}$  color-color diagrams, as well as histograms of NIRCcam colors, indicating the selection thresholds for LRDs ( $F_{277W} - F_{444W} > 1$  mag,  $F_{150W} - F_{200W} < 0.5$  mag and  $F_{444W} < 28$  mag; dashed lines) relative to the bulk of the JADES DR2 galaxy catalog. The different colors indicate the subsets of LRDs detected in different MIRI bands: up to F1280W and beyond (Golden Five galaxies), up to F1000W, up to F770W, or not detected in MIRI (at the SMILES depth). Comparison LRD samples from Barro et al. (2023) and Labbé et al. (2023b) in the CEERS and UNCOVER fields are shown with squares and triangles, respectively. The right panel shows the color vs. redshift diagram for the LRDs and JADES galaxies and the redshift distribution of LRDs (including median and quartiles). The 55% of the LRDs in our paper that have secure NIRSpect and NIRCcam-based spectroscopic redshifts are marked with a black dot.



## ABSTRACT

We study 31 little red dots (LRD) detected by JADES/NIRCcam and covered by the SMILES/MIRI survey, of which  $\sim 70\%$  are detected in the two bluest MIRI bands and 40% in redder MIRI filters. The median/quartiles redshifts are  $z = 6.9_{5.9}^{7.7}$  (55% spectroscopic). The spectral slopes flatten in the rest-frame near-infrared, consistent with a  $1.6 \mu\text{m}$  stellar bump but bluer than direct pure emission from active galactic nuclei (AGN) tori. The apparent dominance of stellar emission at these wavelengths for many LRDs expedites stellar mass estimation: the median/quartiles are  $\log M_{\star}/M_{\odot} = 9.4_{9.1}^{9.7}$ . The number density of LRDs is  $10^{-4.0 \pm 0.1} \text{ Mpc}^{-3}$ , accounting for  $14 \pm 3\%$  of the global population of galaxies with similar redshifts and masses. The rest-frame near/mid-infrared ( $2\text{--}4 \mu\text{m}$ ) spectral slope reveals significant amounts of warm dust (bolometric attenuation  $\sim 3\text{--}4$  mag). Our spectral energy distribution modeling implies the presence of  $< 0.4$  kpc diameter knots, heated by either dust-enshrouded OB stars or an AGN producing a similar radiation field, obscured by  $A(V) > 10$  mag. We find a wide variety in the nature of LRDs. However, the best-fitting models for many of them correspond to extremely intense and compact starburst galaxies with mass-weighted ages 5–10 Myr, very efficient in producing dust, with their global energy output dominated by the direct (in the flat rest-frame ultraviolet and optical spectral range) and dust-recycled emission from OB stars with some contribution from an obscured AGN (in the infrared).

# SFR density:

# Lilly - Madau Plot

Bouwens et al. (2023)

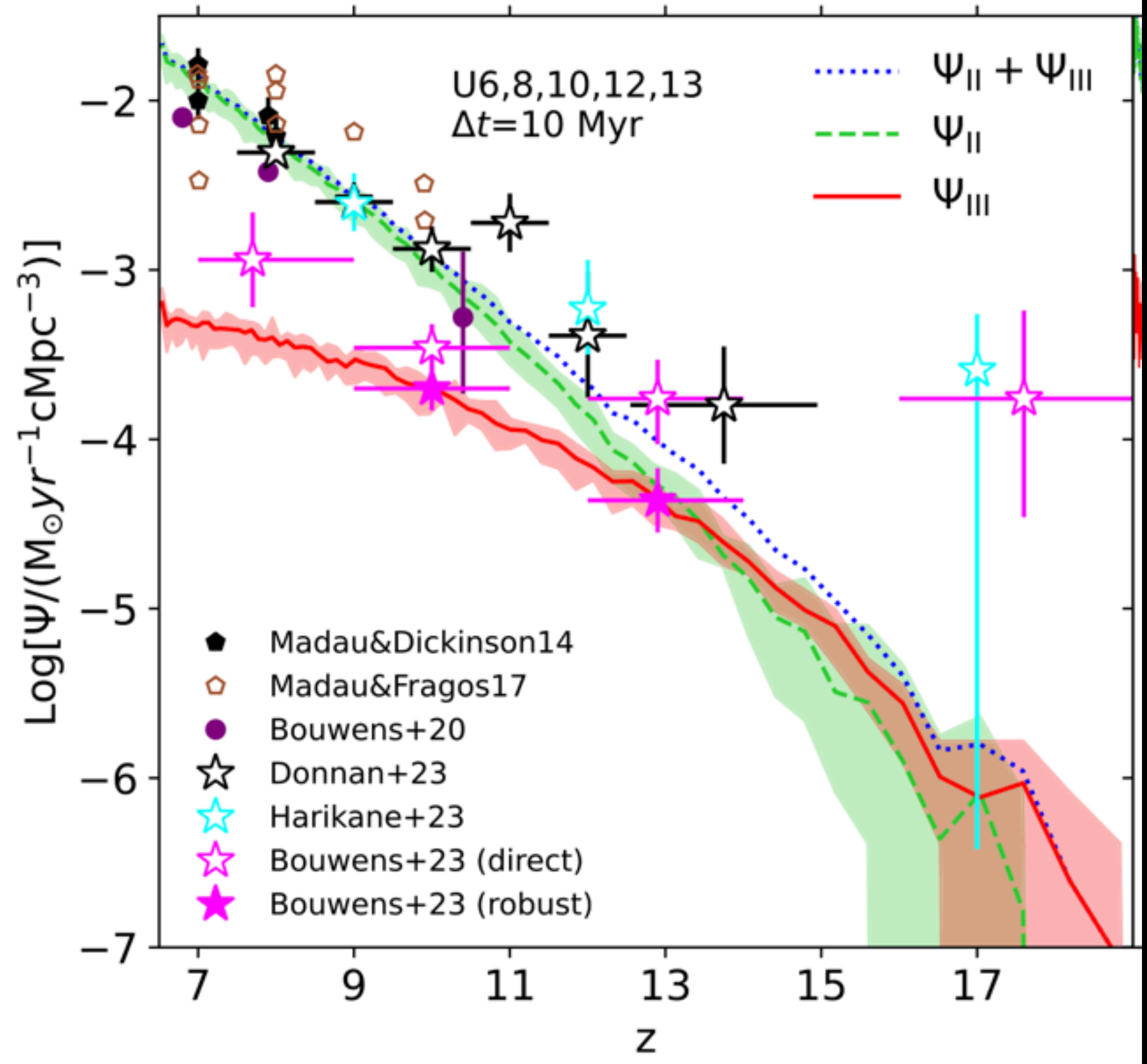
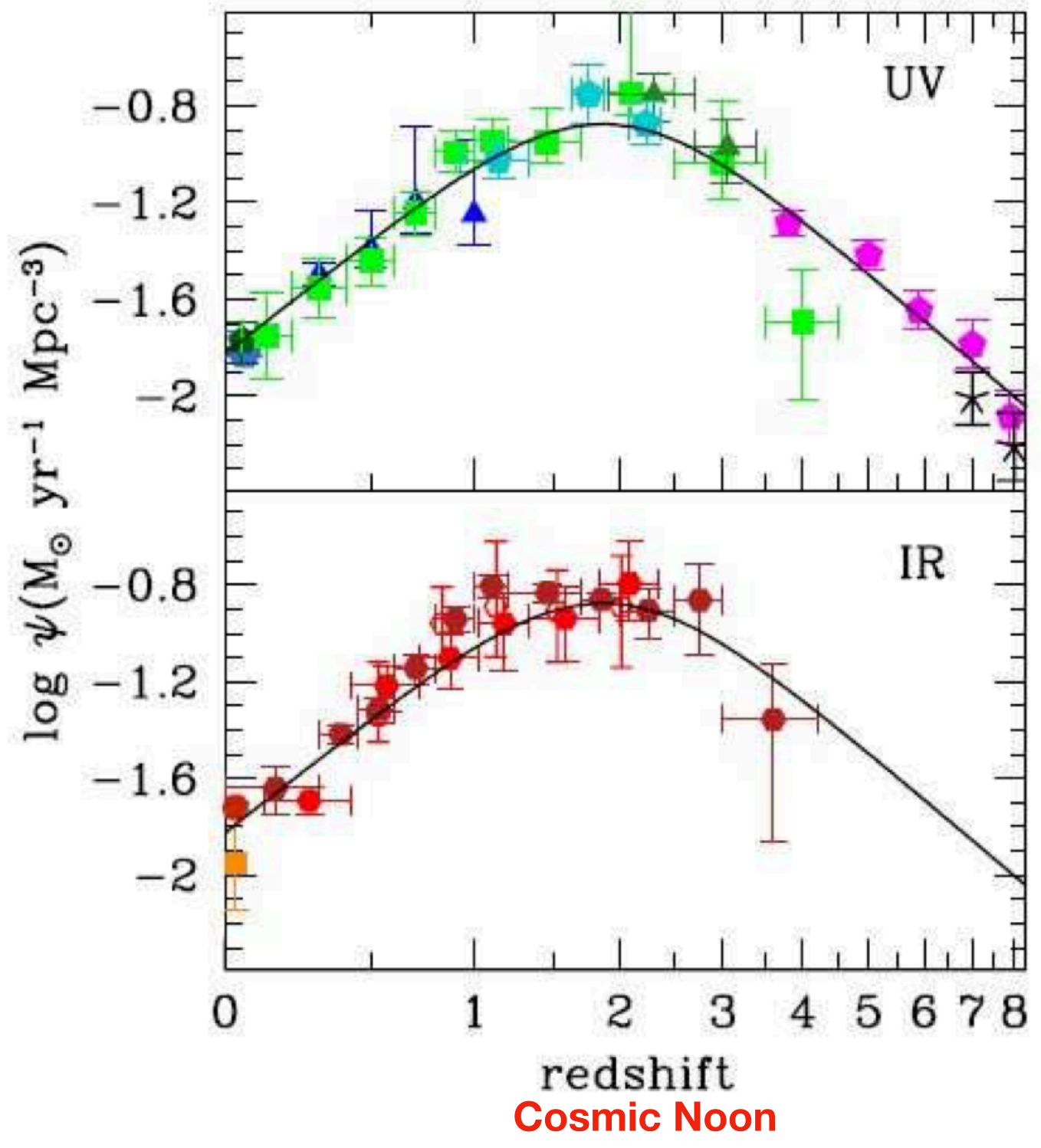
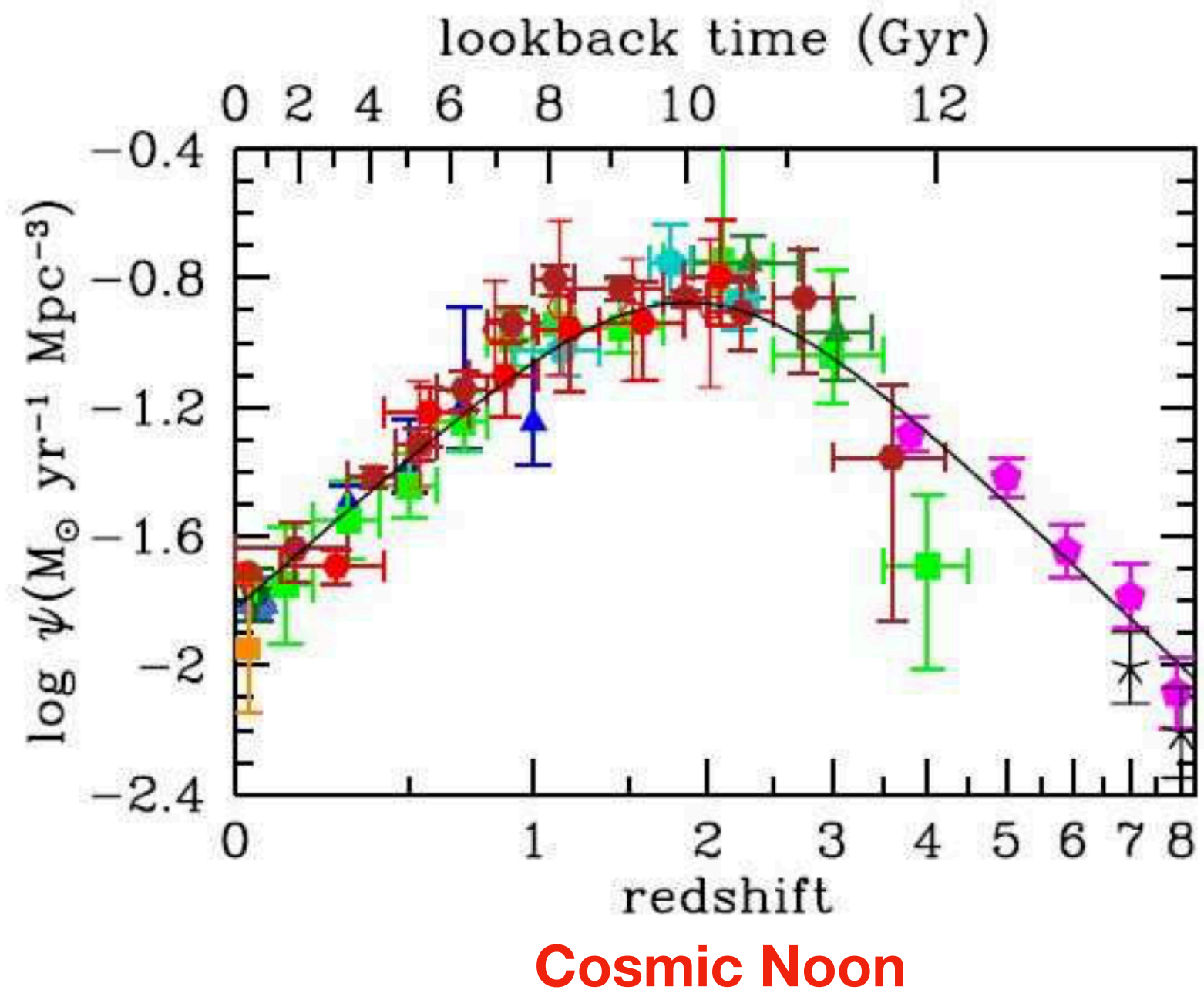


Figure 3.4 From Madau & Dickinson (2014): The history of cosmic star formation from (top right panel) FUV, (bottom right panel) IR, and (left panel) FUV+IR rest-frame measurements. The solid curve in the three panels plots the best-fit SFRD.

# Conclusions:

- JWST has detected large numbers of large and luminous galaxies made out of stars, present in the universe as early as 300 Myr after the Big Bang
- Hints on how to look for PopIII stars
- Reionization
- Morphology
- Little red dots

**Derived properties from spectral fits are model dependent (e.g., lacking binaries).**

## Nebular emission from young stellar populations including binary stars

Marie Lecroq <sup>1</sup>★ Stéphane Charlot <sup>1</sup>★ Alessandro Bressan,<sup>2,3</sup> Gustavo Bruzual,<sup>4</sup>  
Guglielmo Costa <sup>3,5,6,7</sup> Giuliano Iorio <sup>3,5,6</sup> Mario Spera <sup>2,8,9</sup> Michela Mapelli <sup>3,5,6,10</sup> Yang Chen,<sup>11,12</sup>  
Jacopo Chevallard <sup>13</sup> and Marco Dall’Amico<sup>5,6</sup>

**Include binary star evolution in our population synthesis models**

## Approach:

**Use the SEVN (Spectral EVolution for N-body) code to compute the distribution of binary stars in the HRD. SEVN works for binary stars with  $M_1, M_2 \geq 2 M_\odot$ . The binary stellar population is sampled stochastically assuming the Chabrier IMF for the primary stars. Binary parameters derived as in Sana et al. (2012). Use C&B stellar libraries to compute SED of binary population. We can then easily mix single and binary star models assuming a binary fraction.**

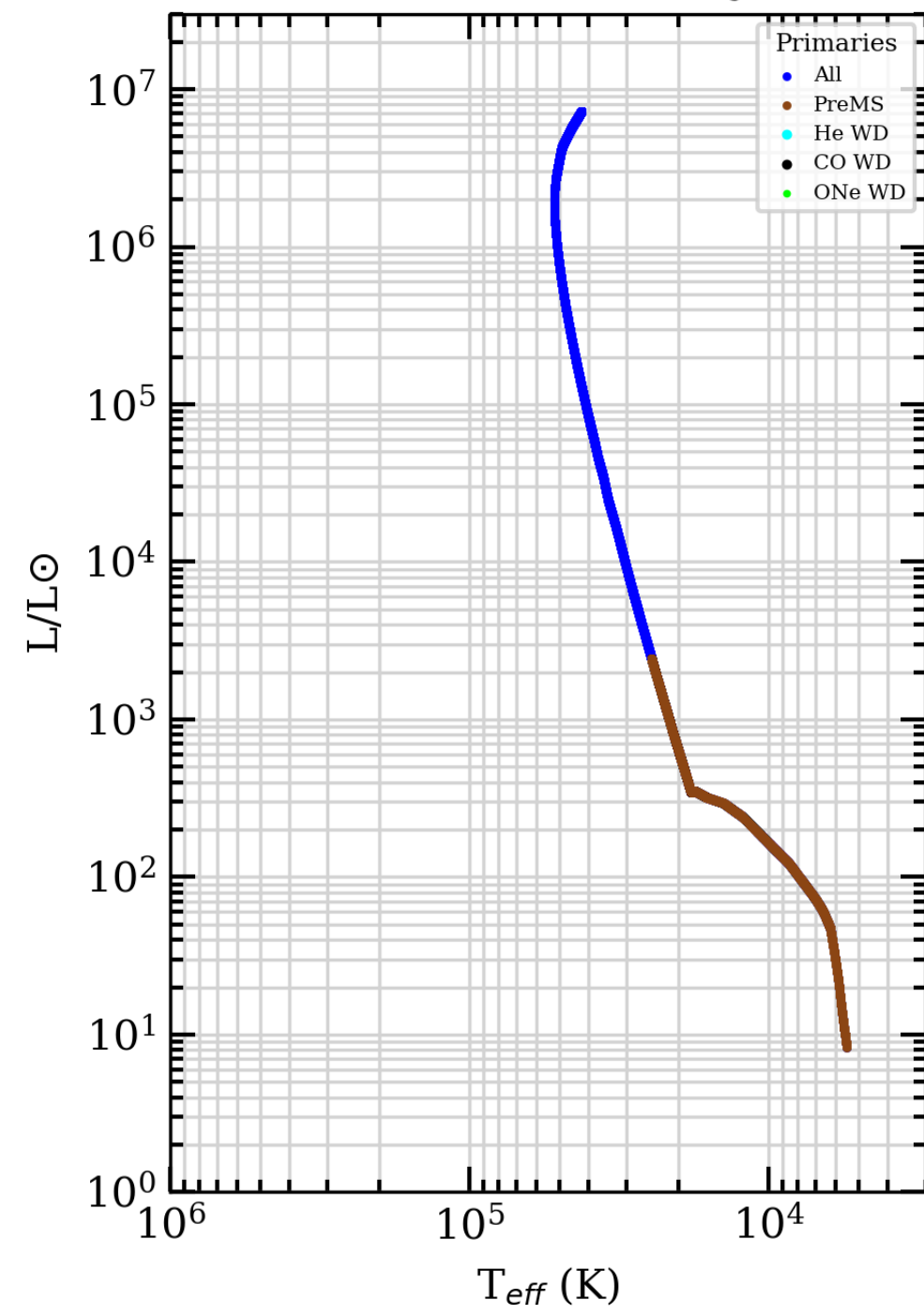
**SEVN:** Spera et al. (2015, 2019); Mapelli et al. (2017, 2020); Iorio et al. (2022)

## Note:

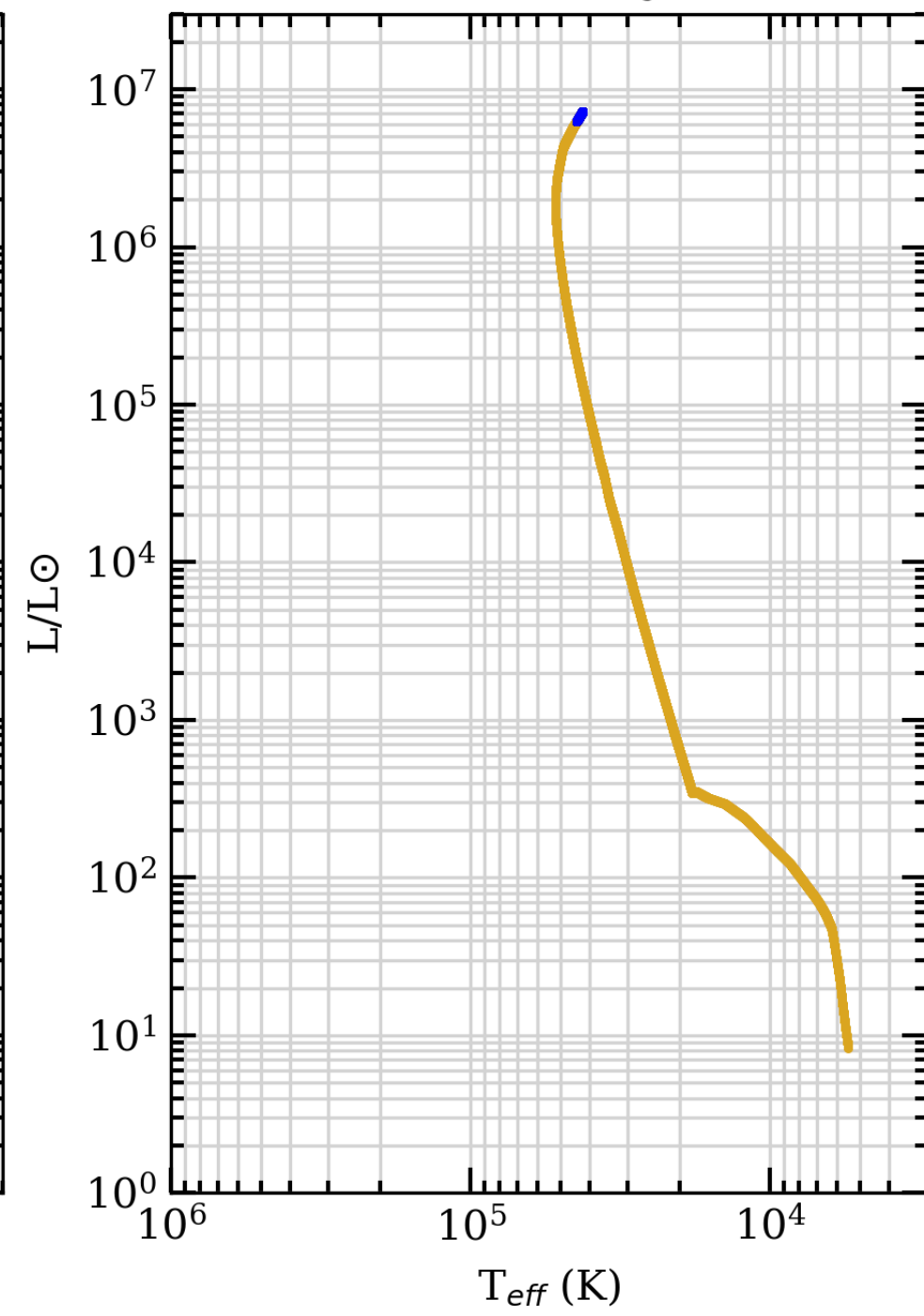
The SEVN code interpolates on the fly the stellar properties of each binary companion from existing isochrone tables for single stars, making it faster and more flexible than other binary stellar evolution codes like BPASS (Eldridge, Stanway +) and MESA (Mesa team) that follow the detailed evolution of each star in each pair.

- Single vs. binary star evolution in the HRD

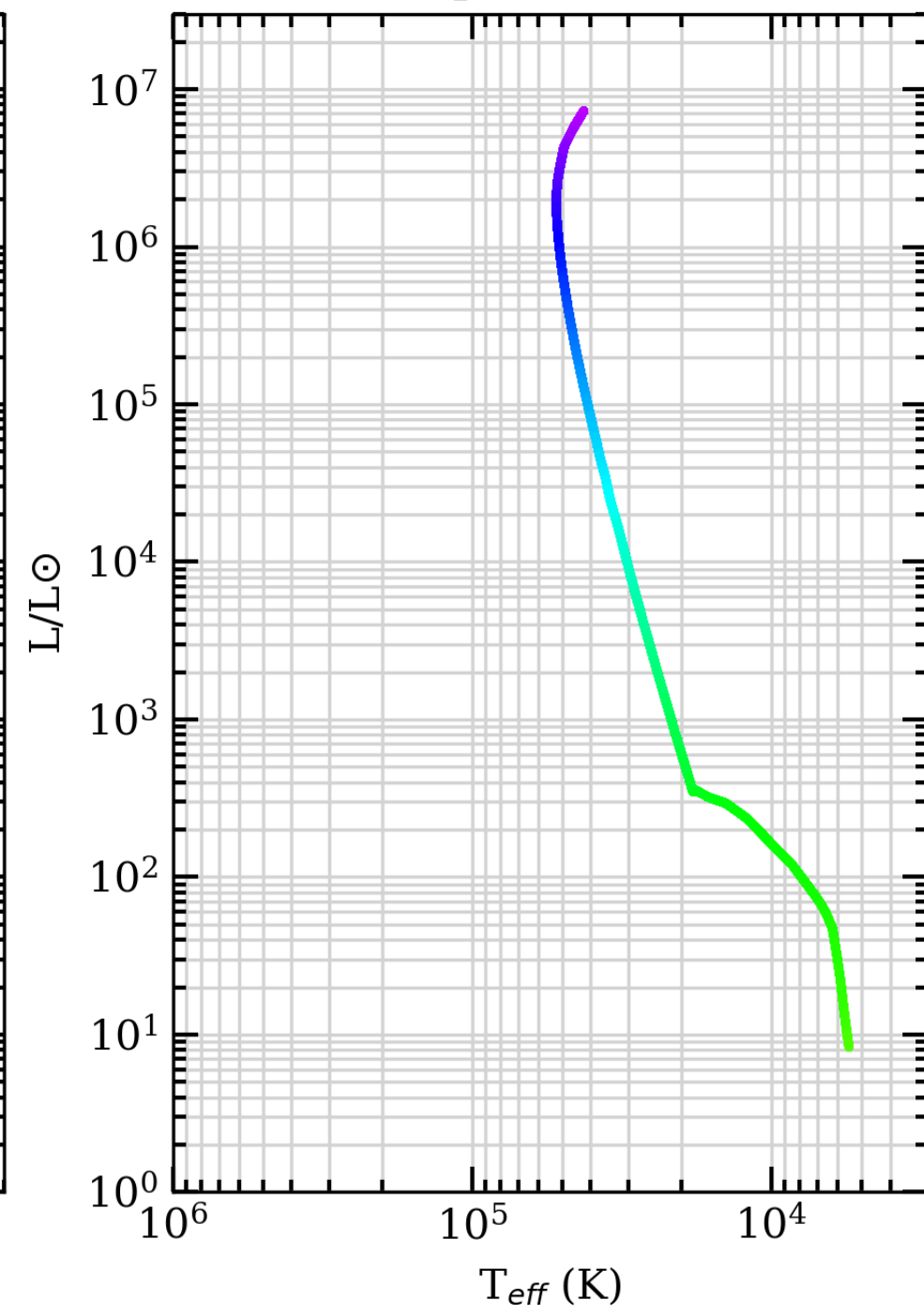
Z=0.004, t=1 Myr



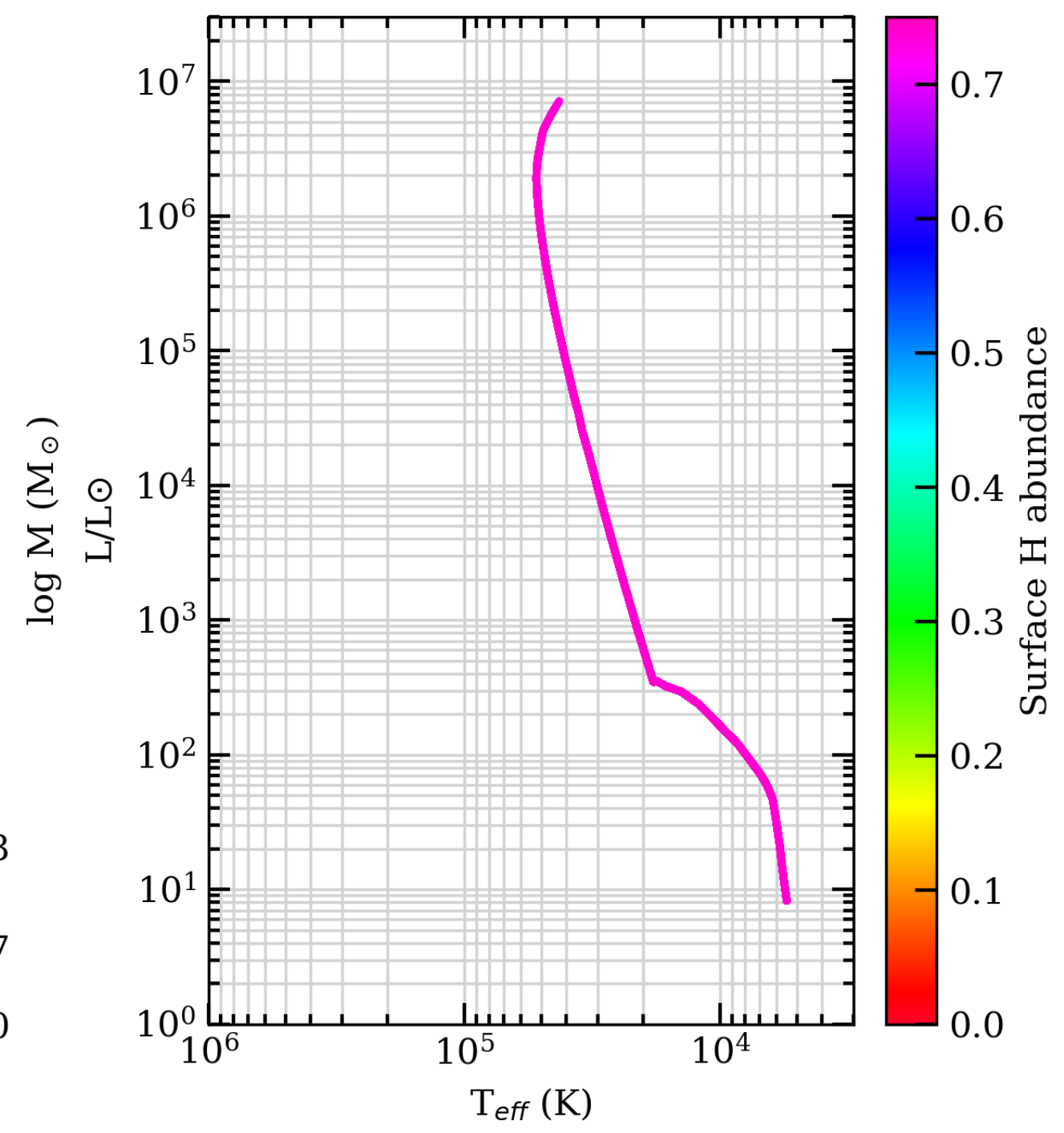
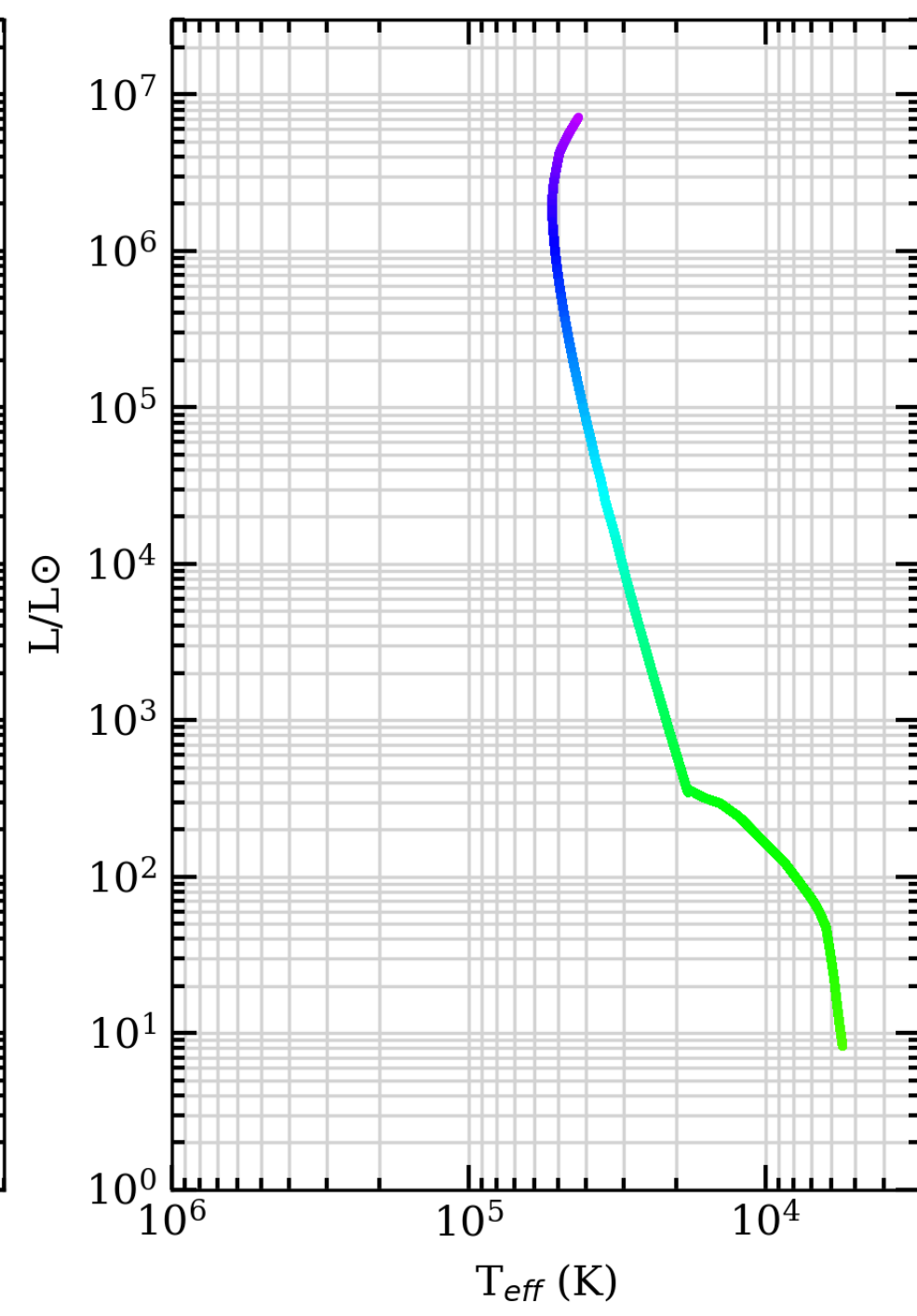
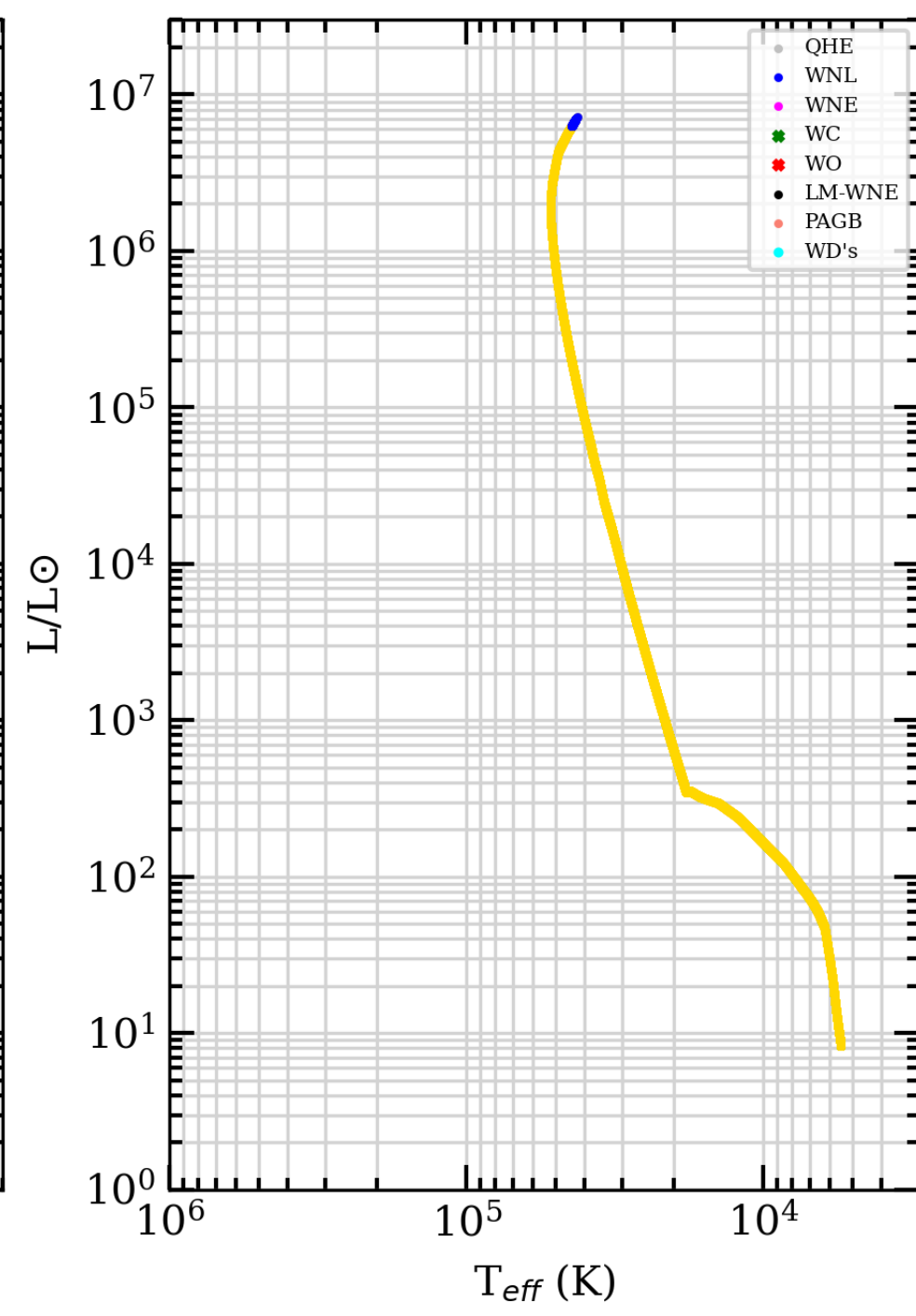
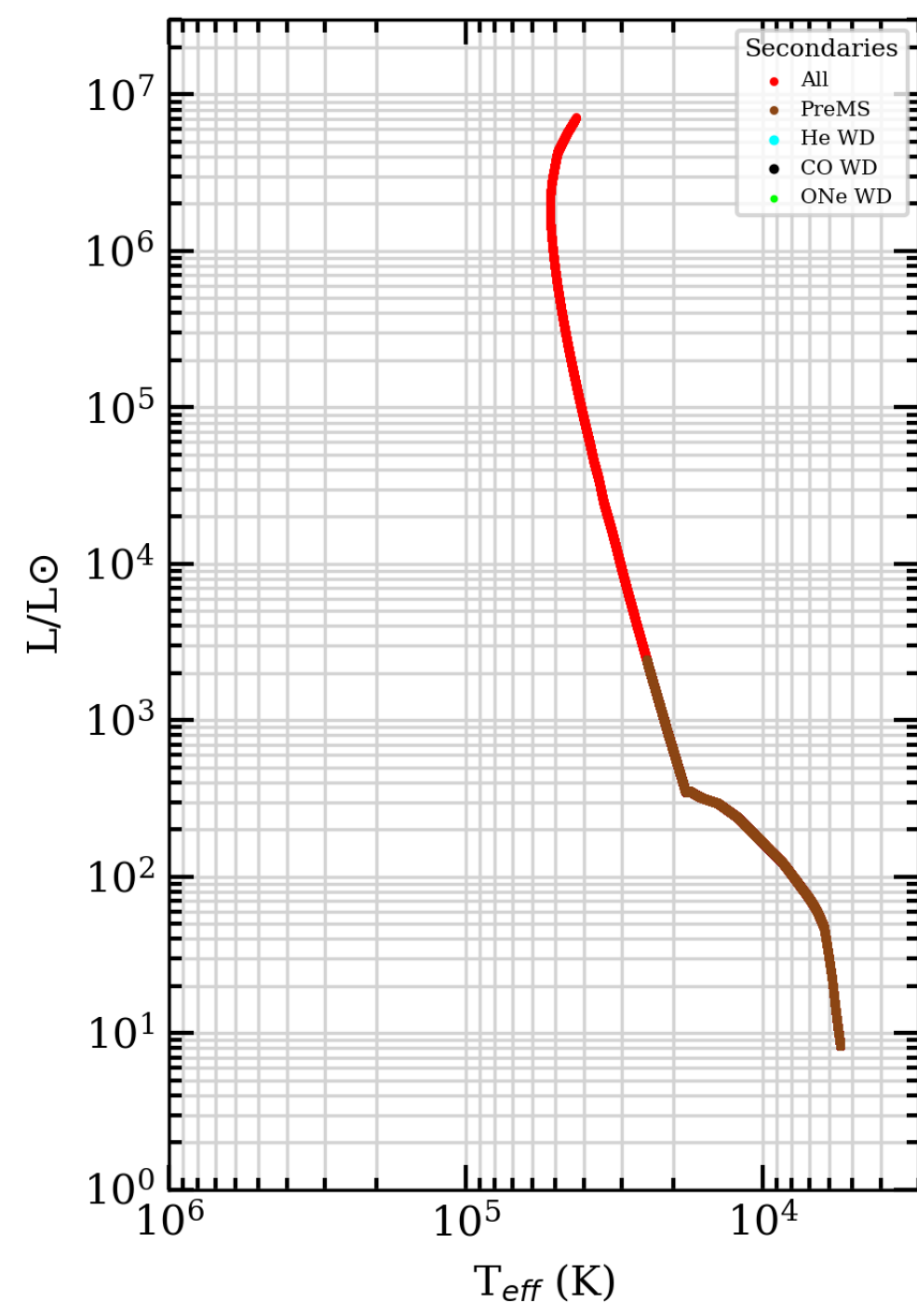
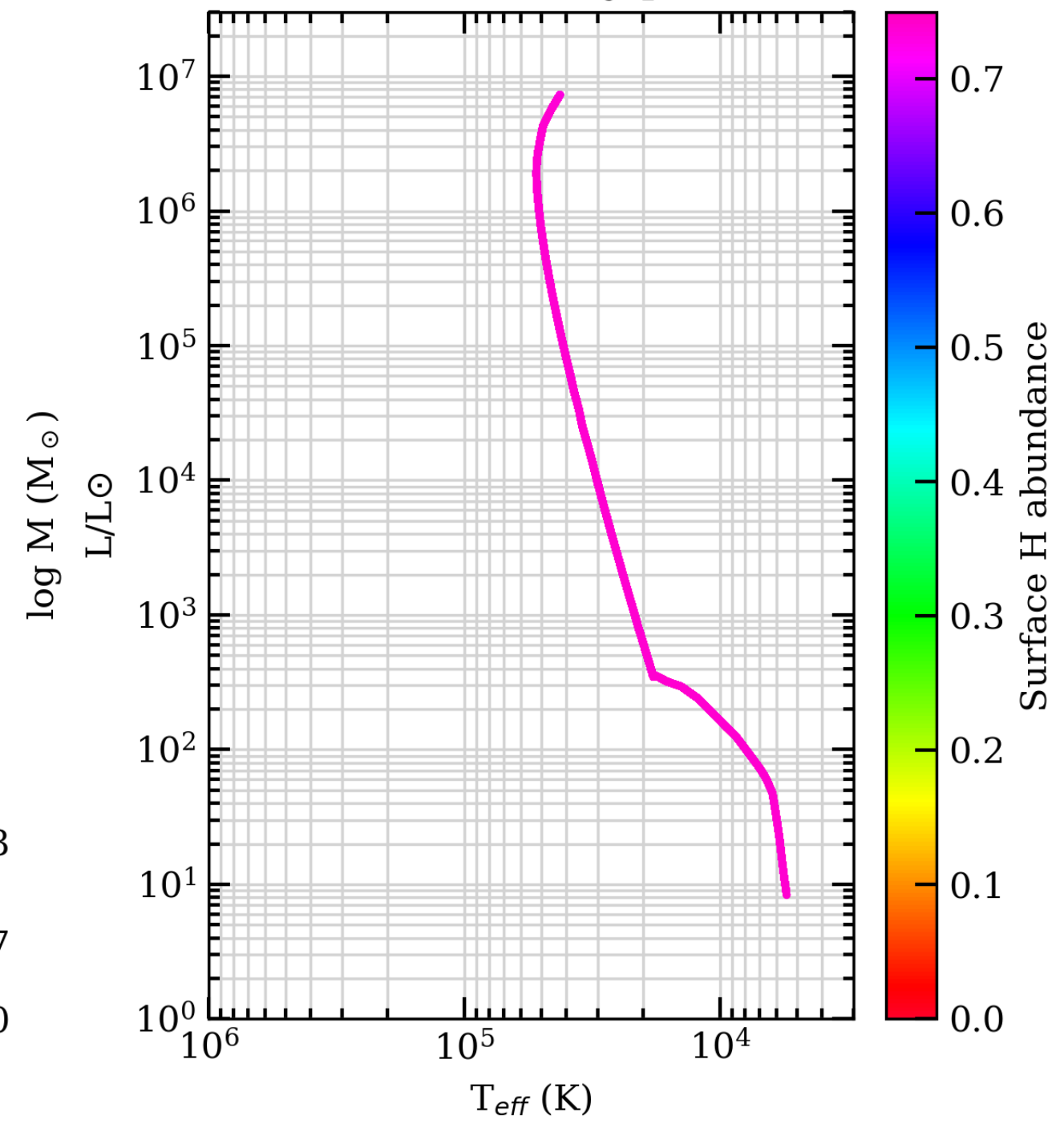
SEVN2.3 VLA binary star tracks



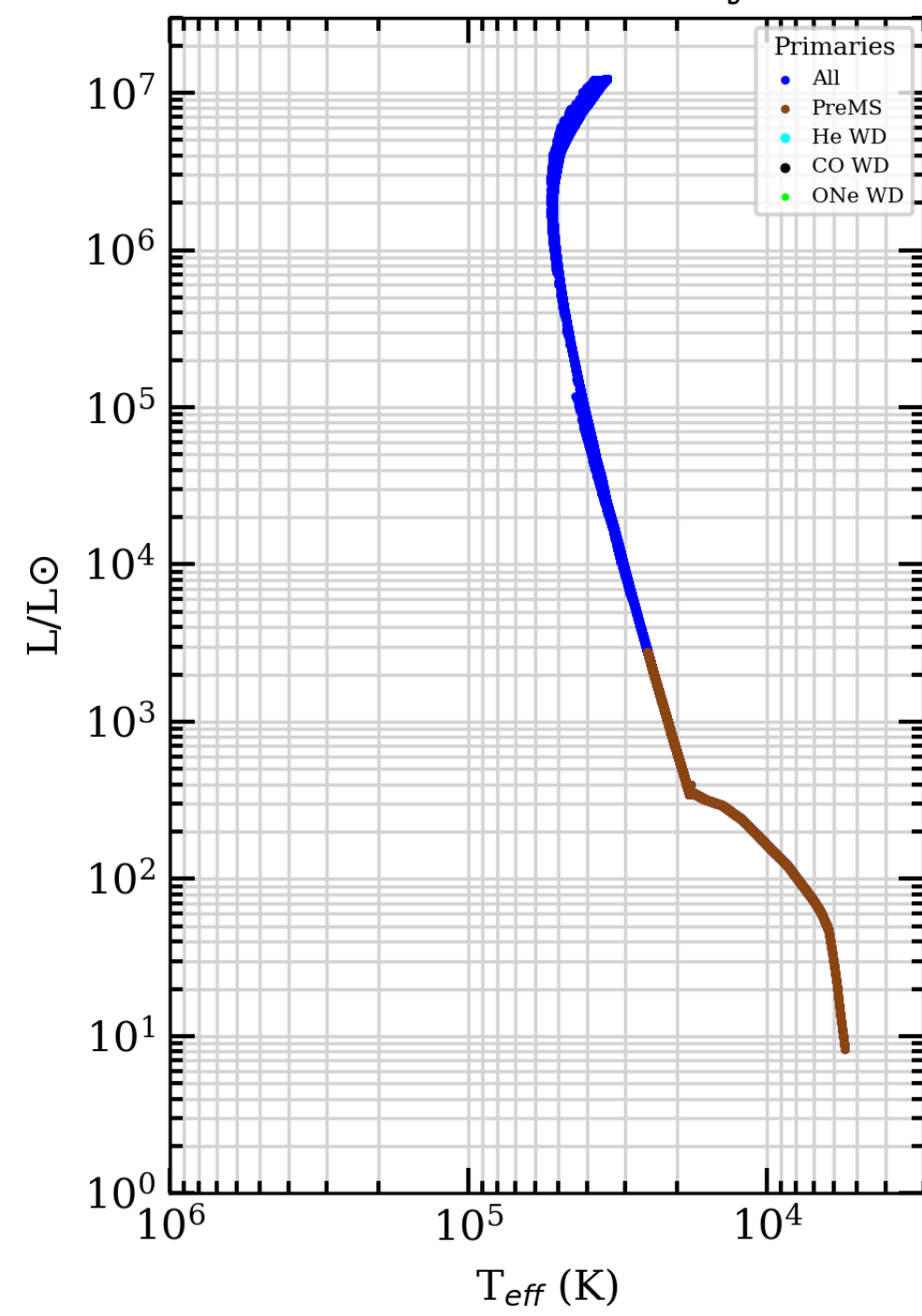
April 2023



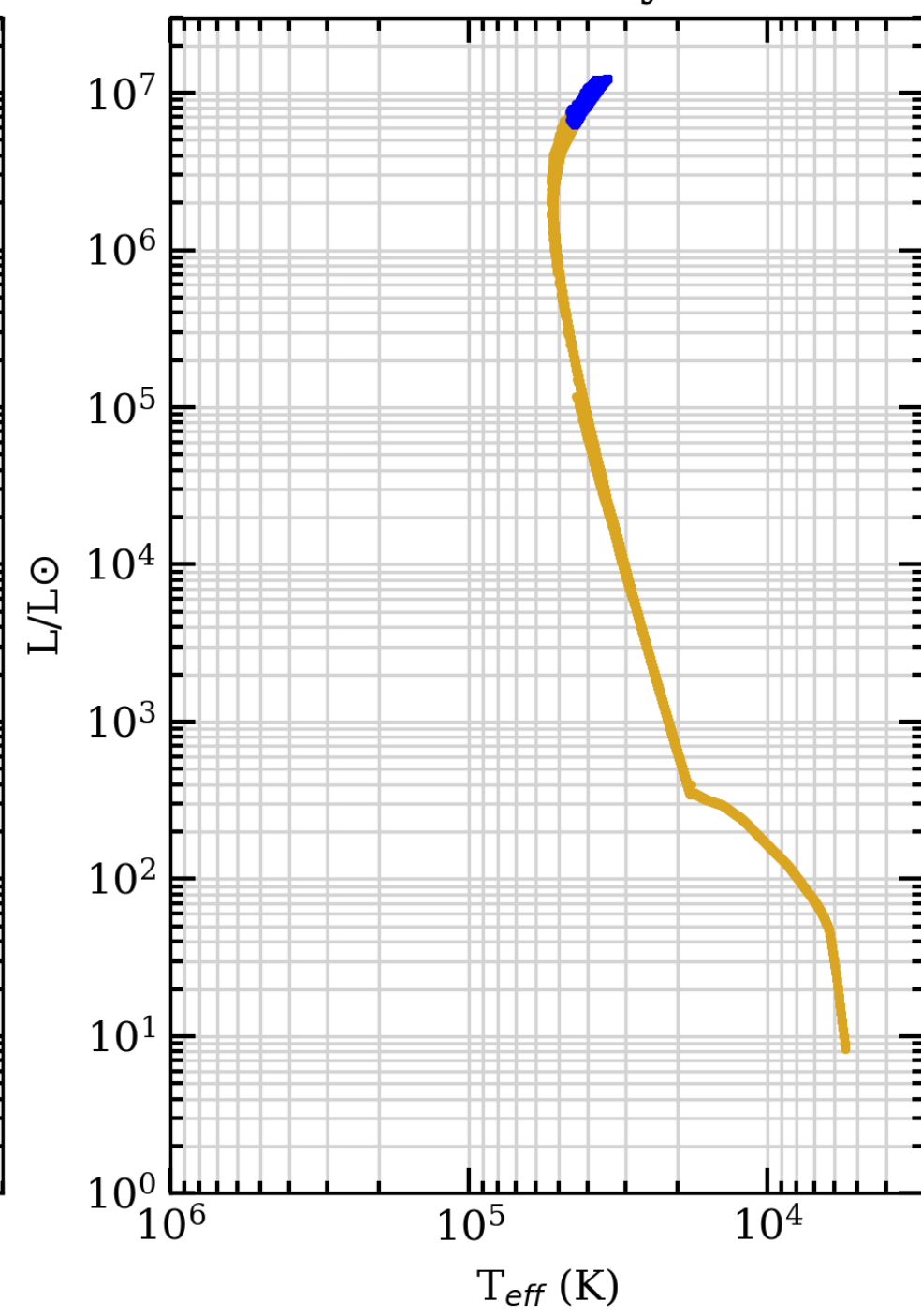
156250 binary pairs



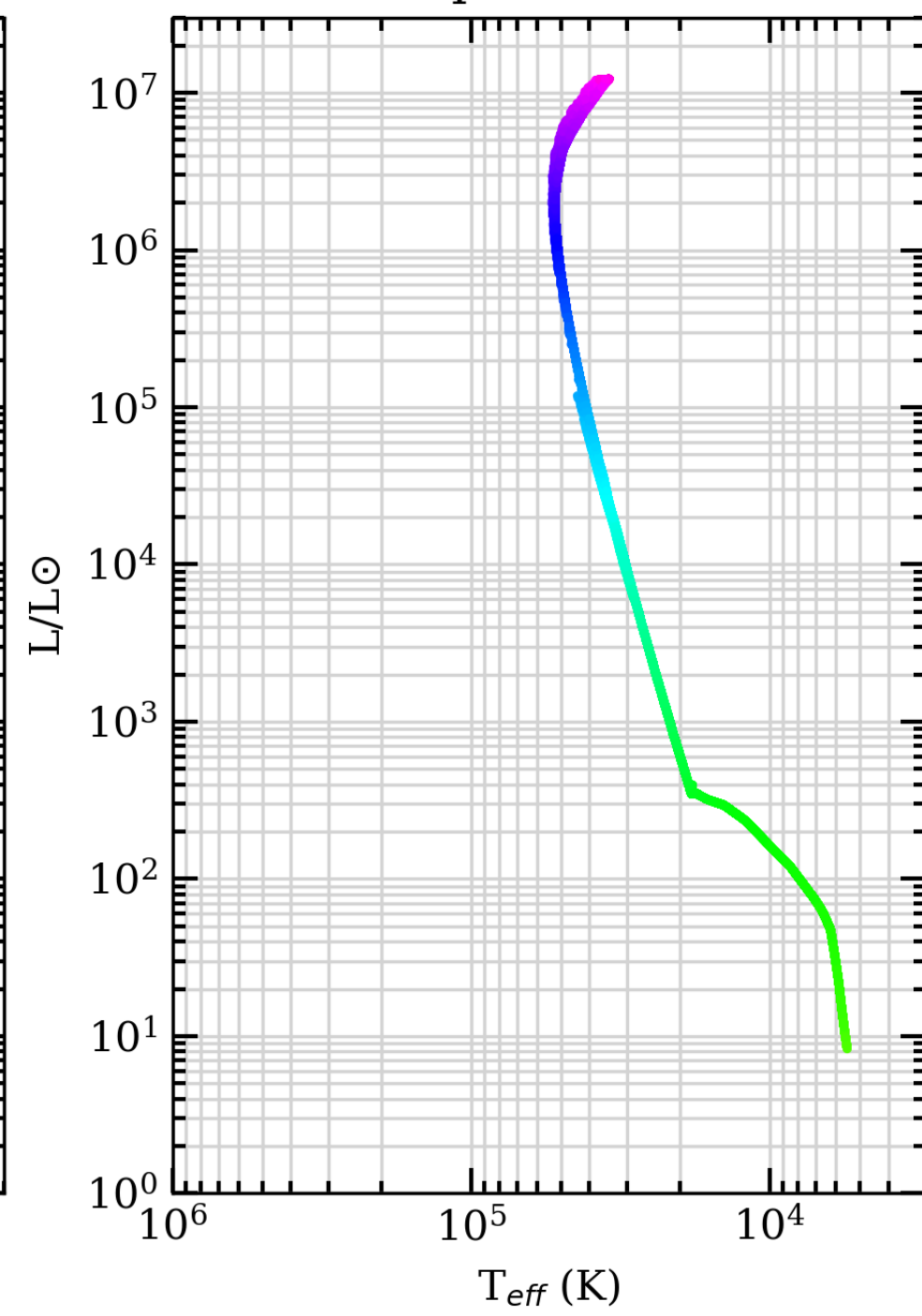
Z=0.004, t=1 Myr



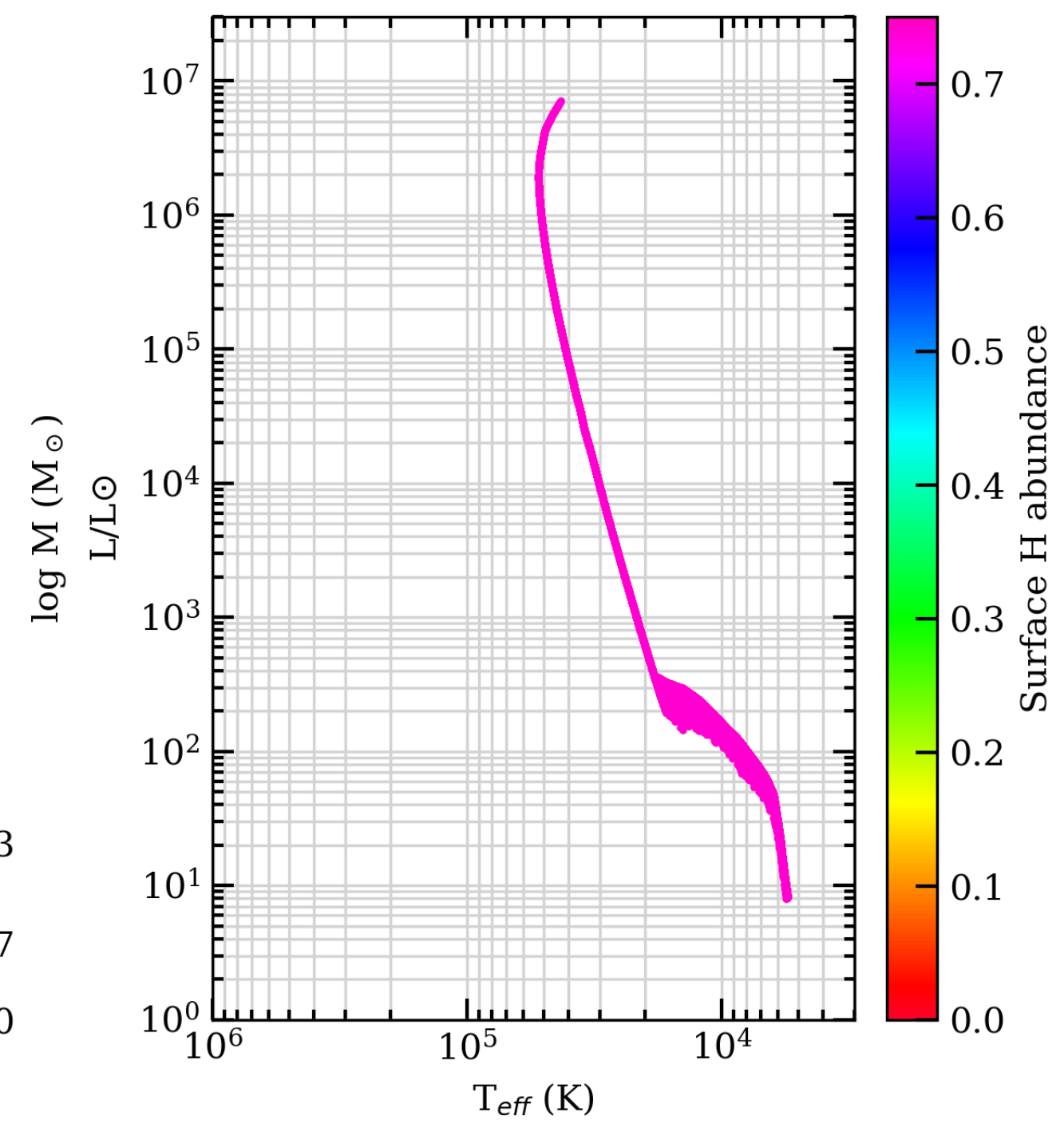
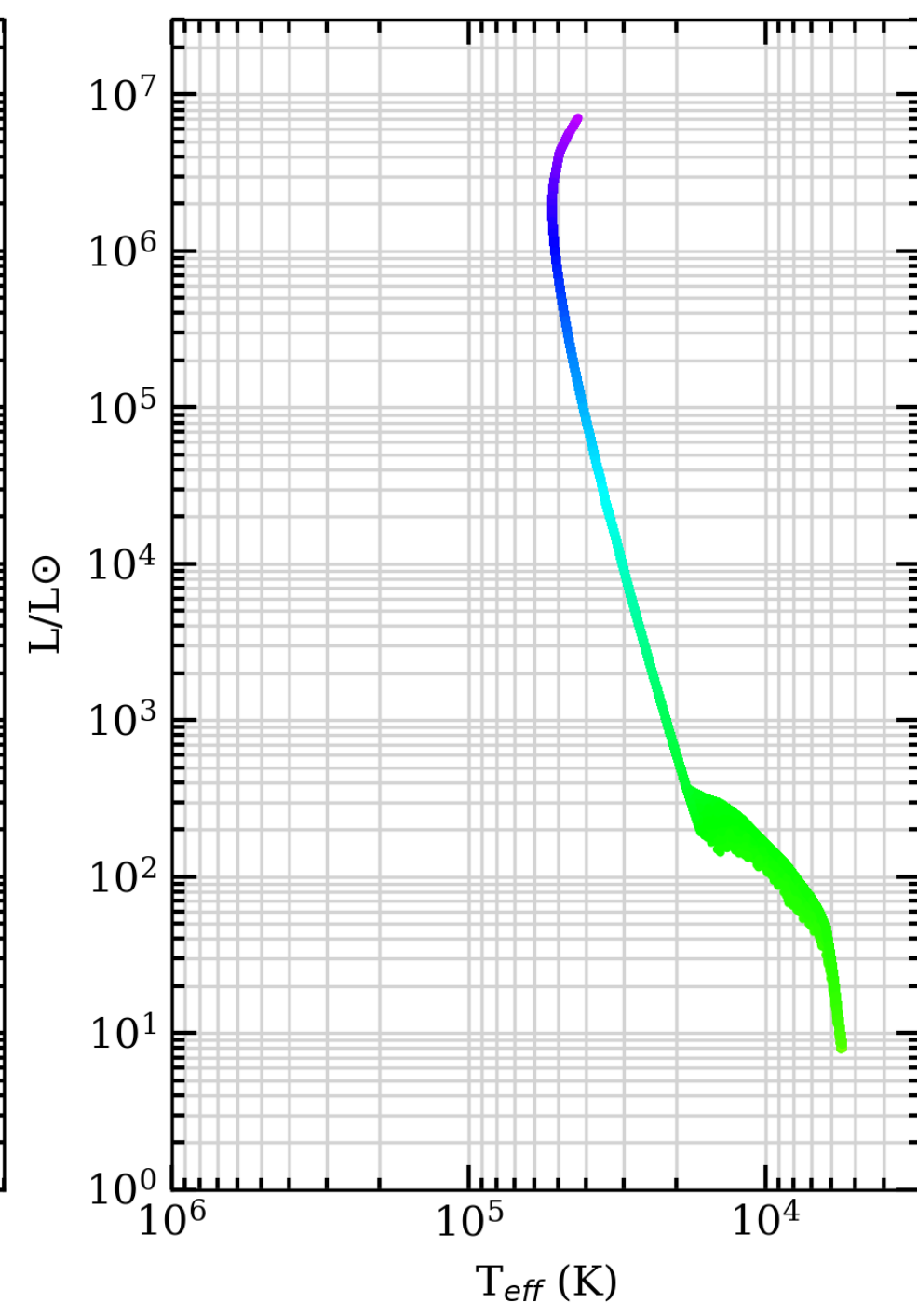
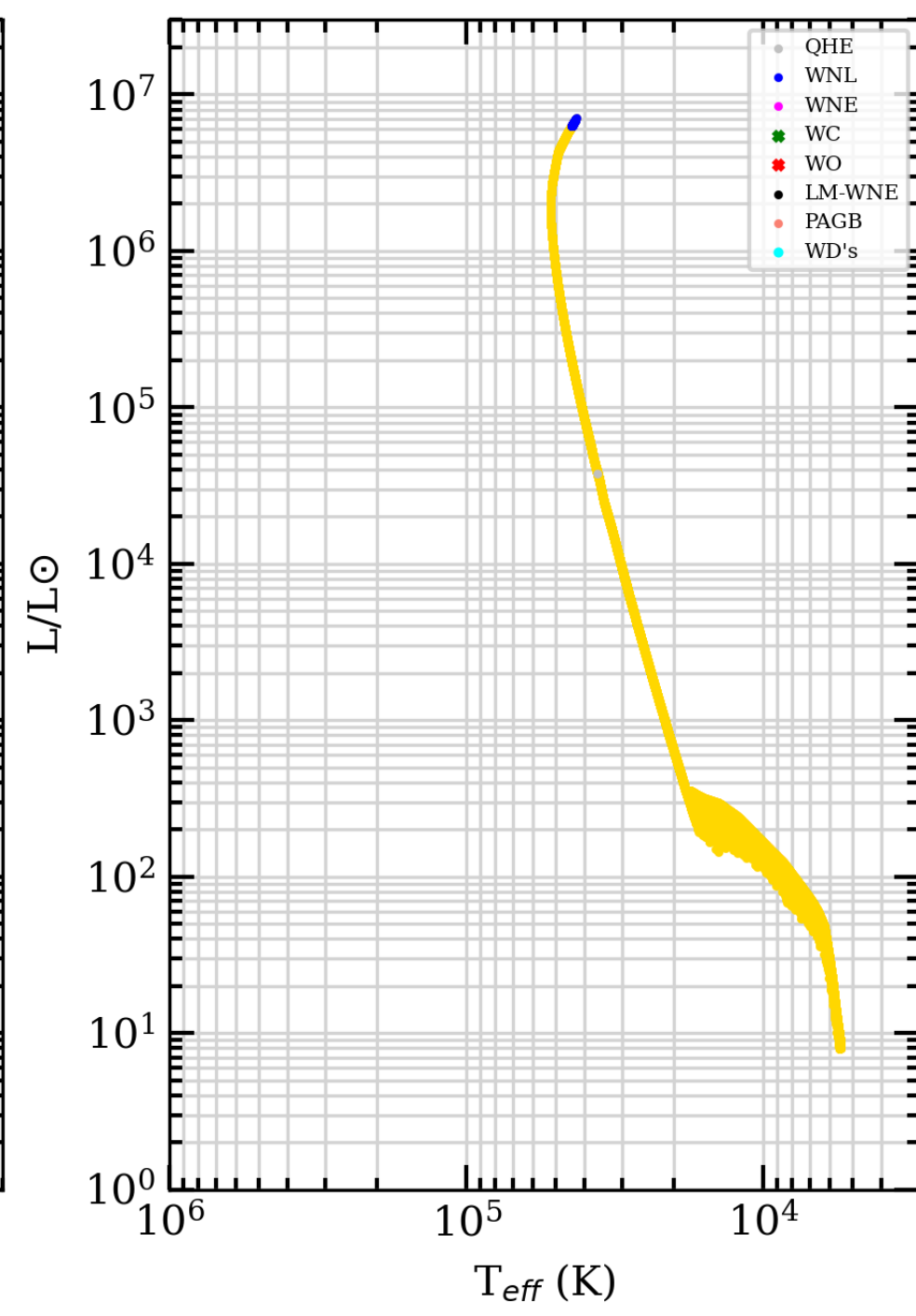
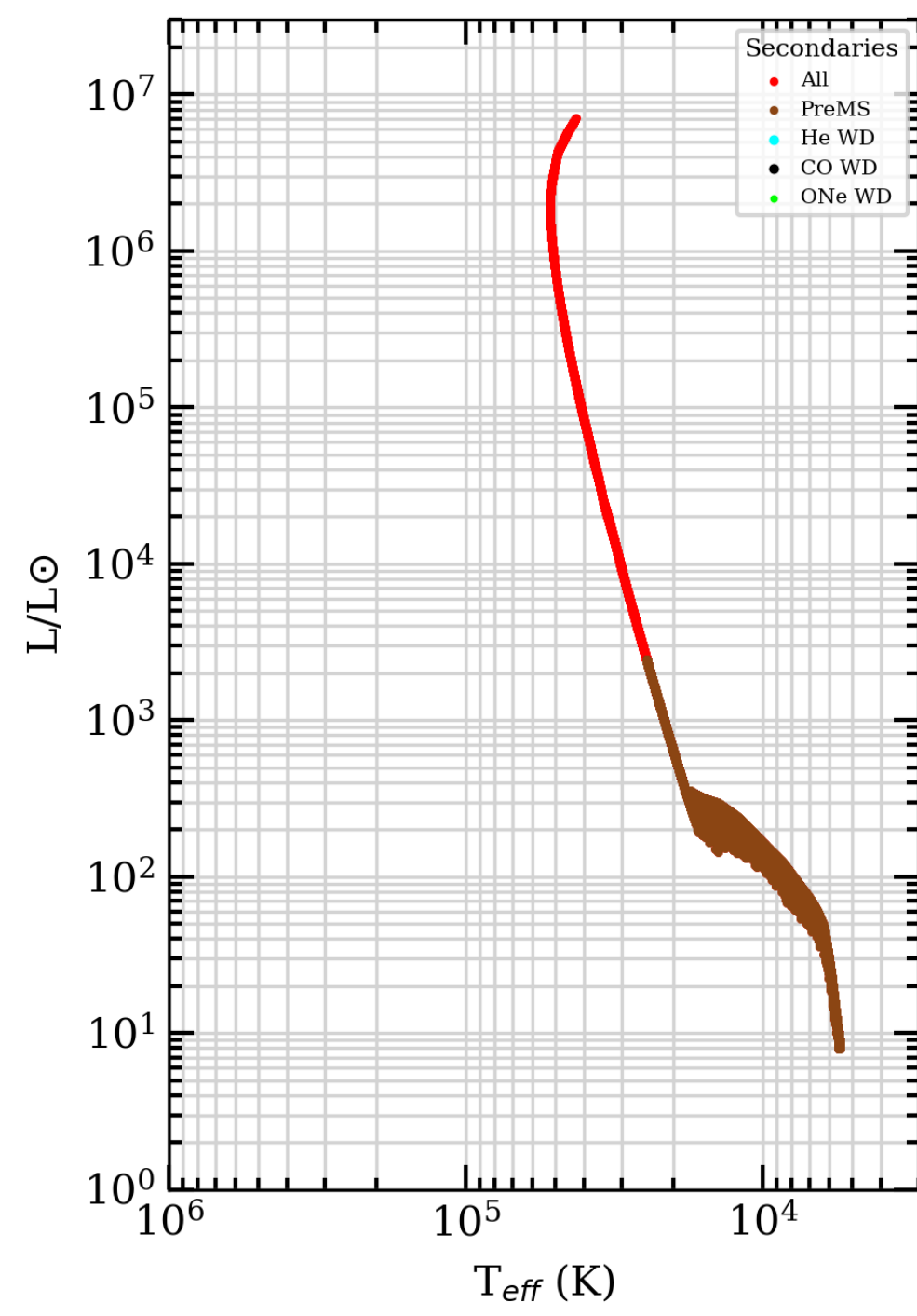
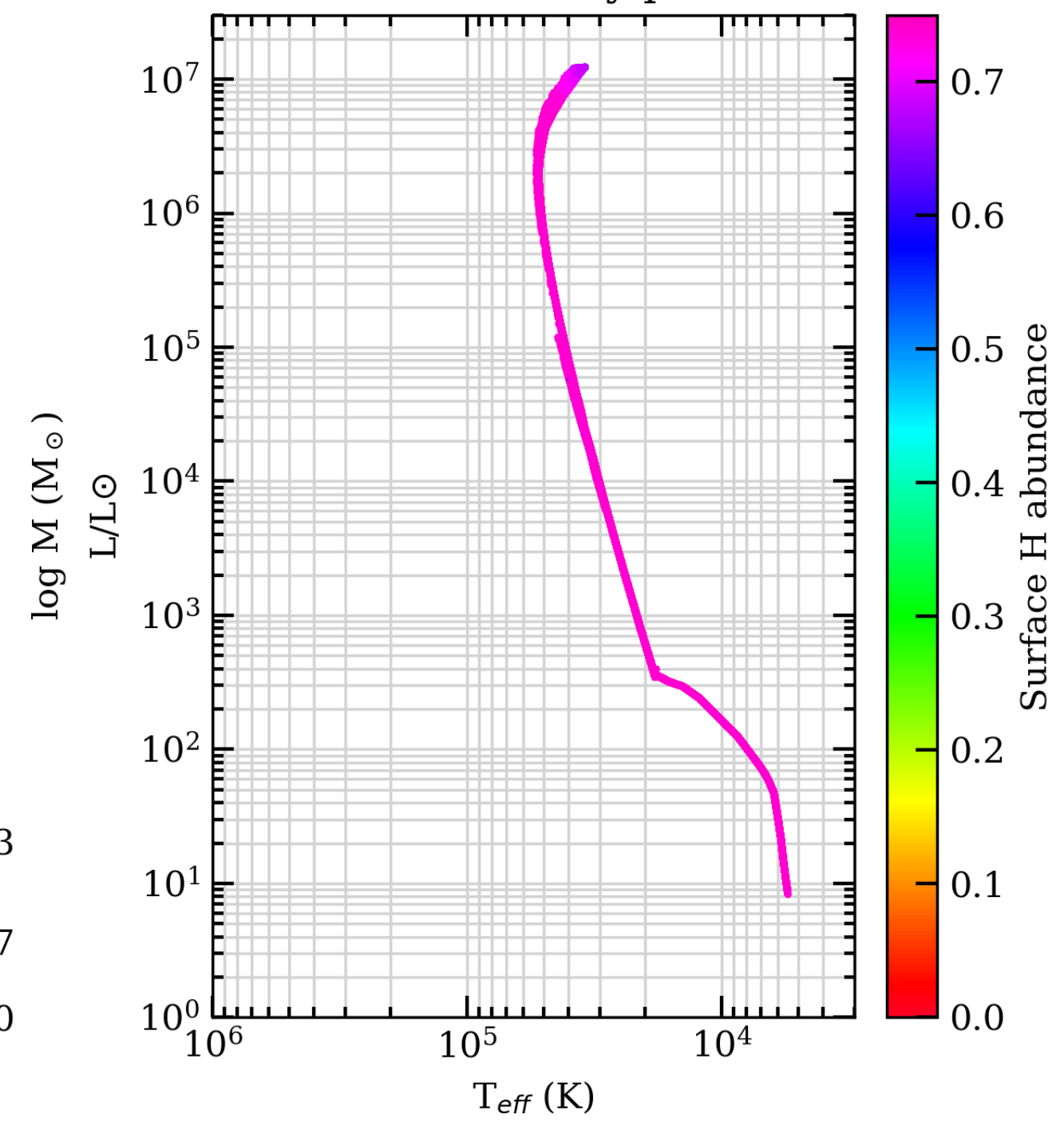
SEVN2.3 STD binary star tracks



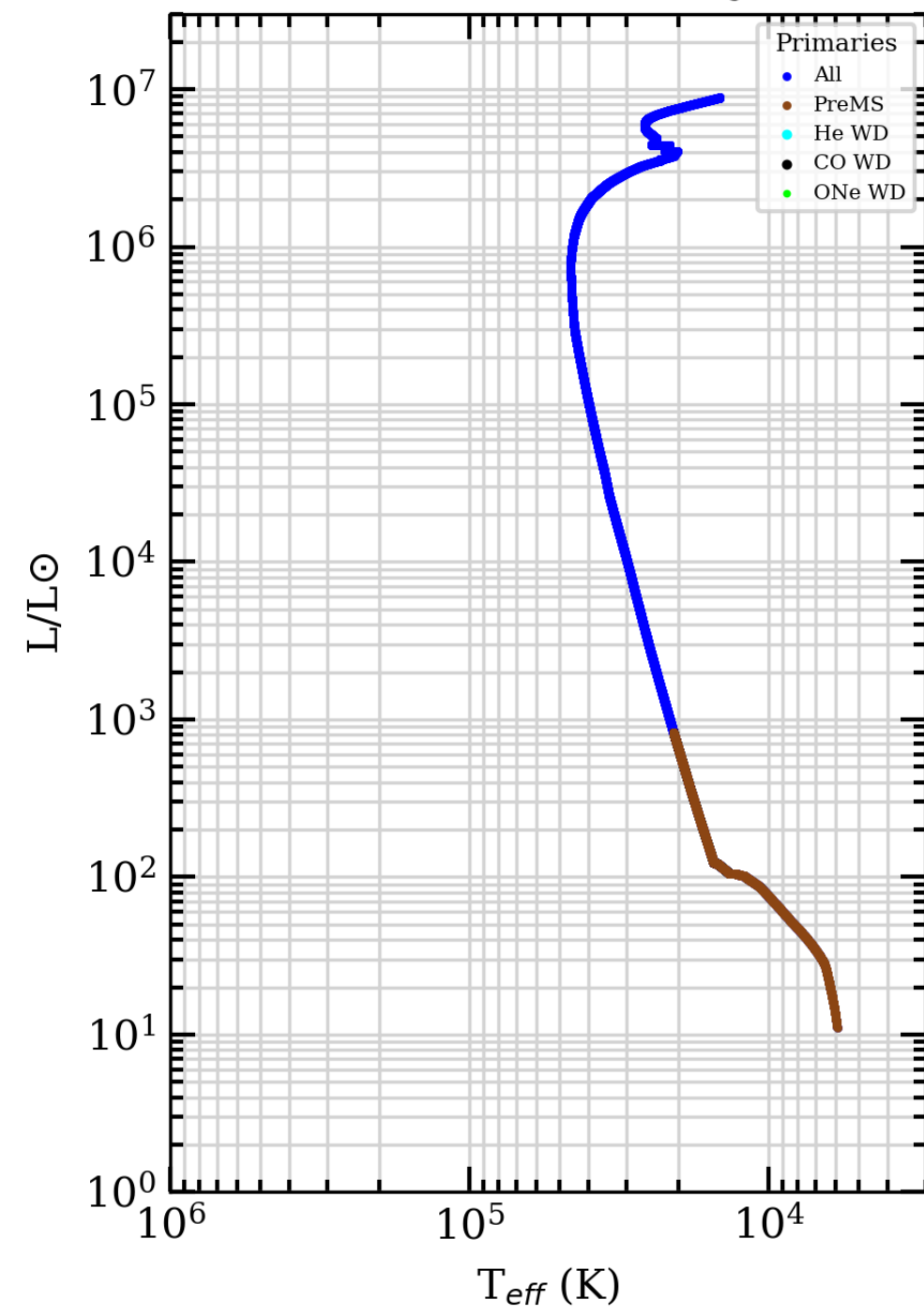
April 2023



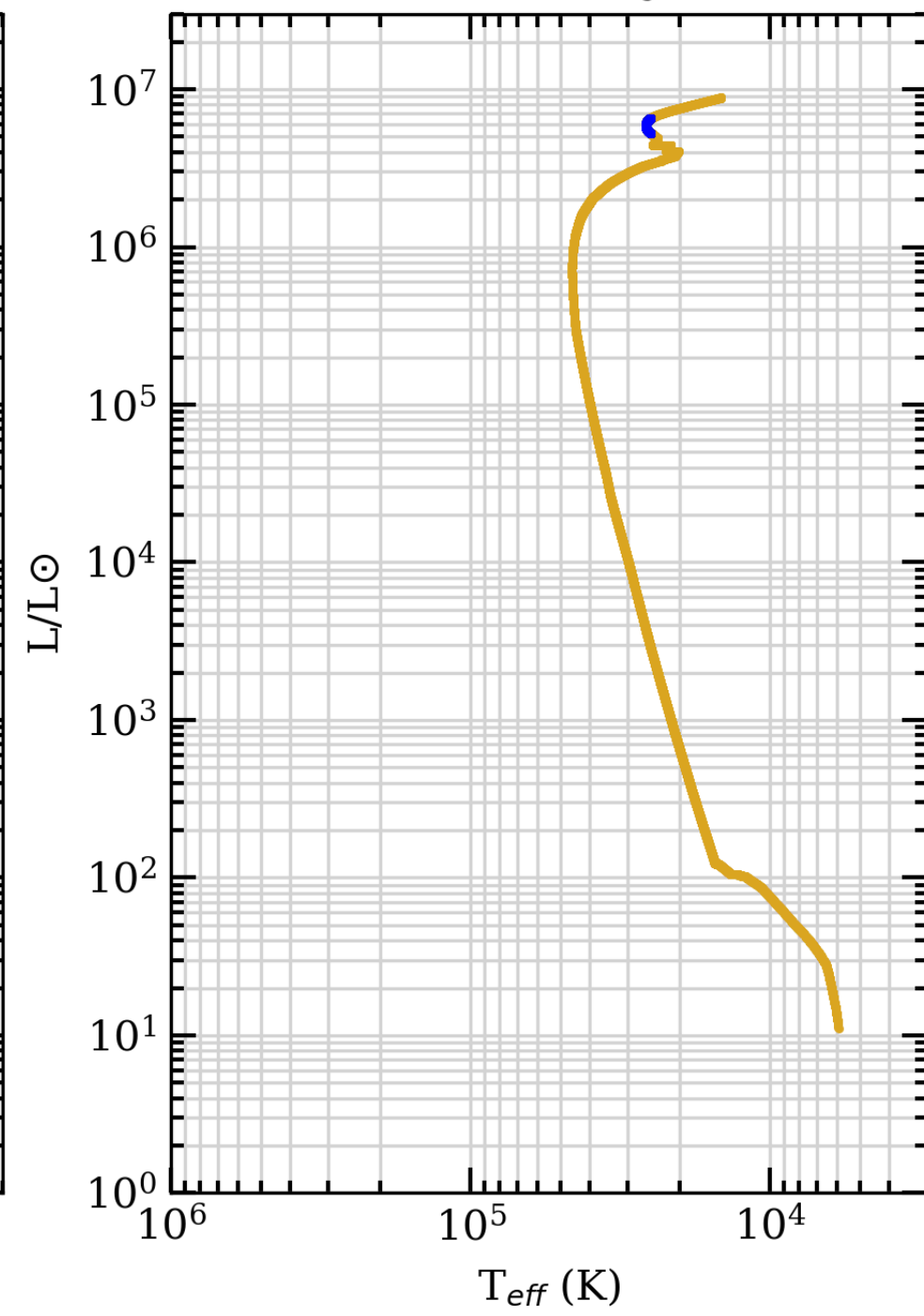
156250 binary pairs



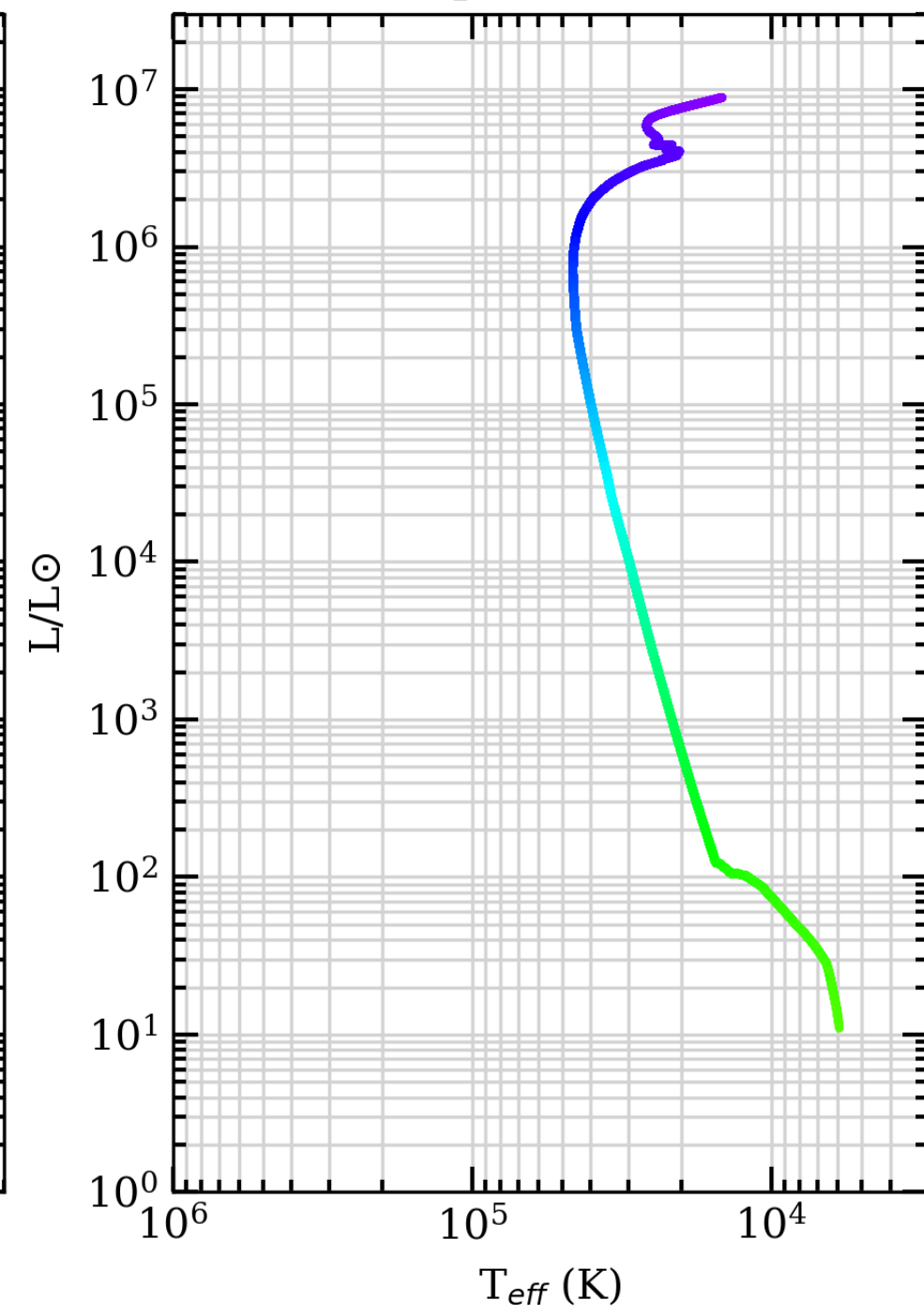
Z=0.004, t=2 Myr



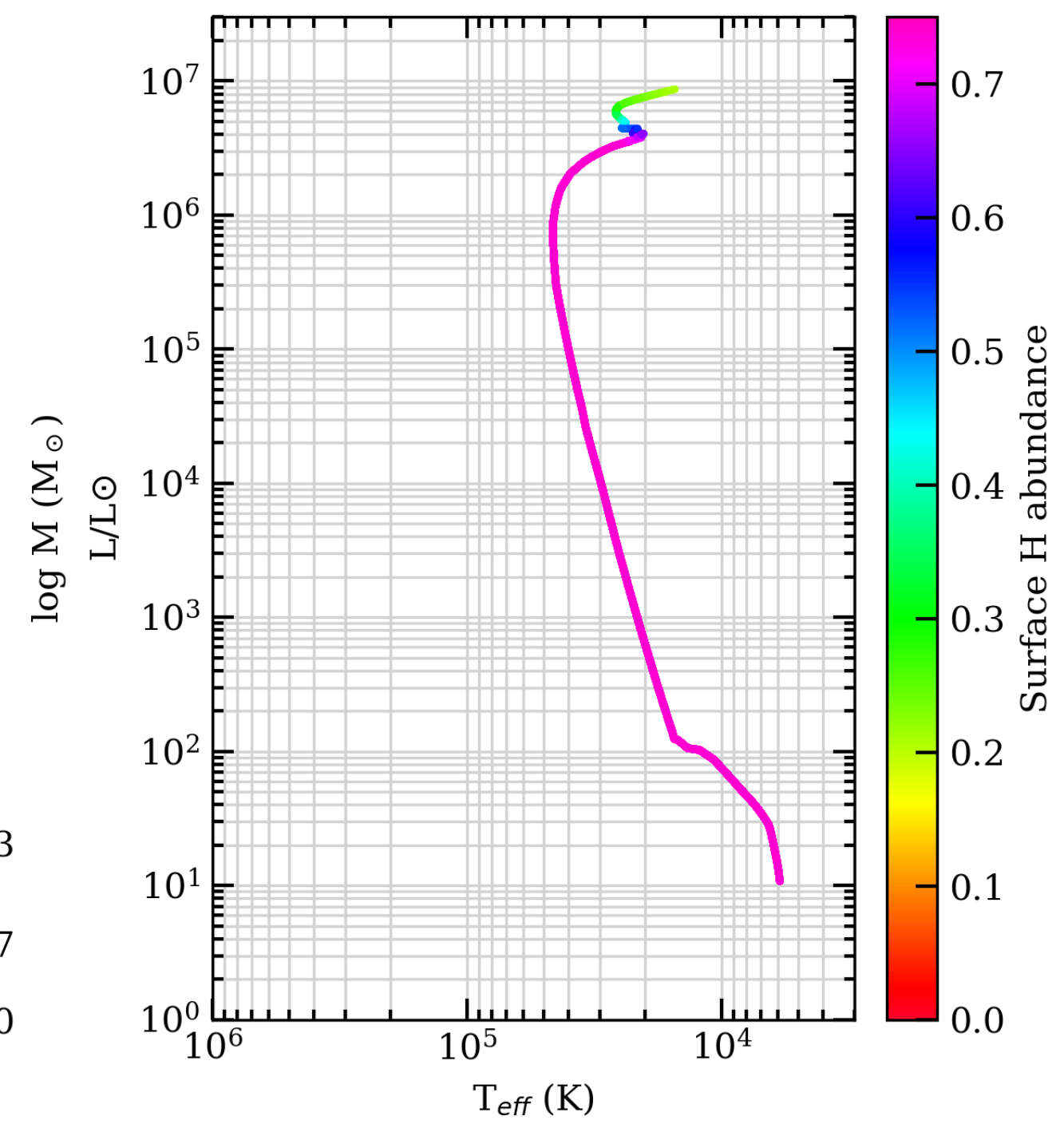
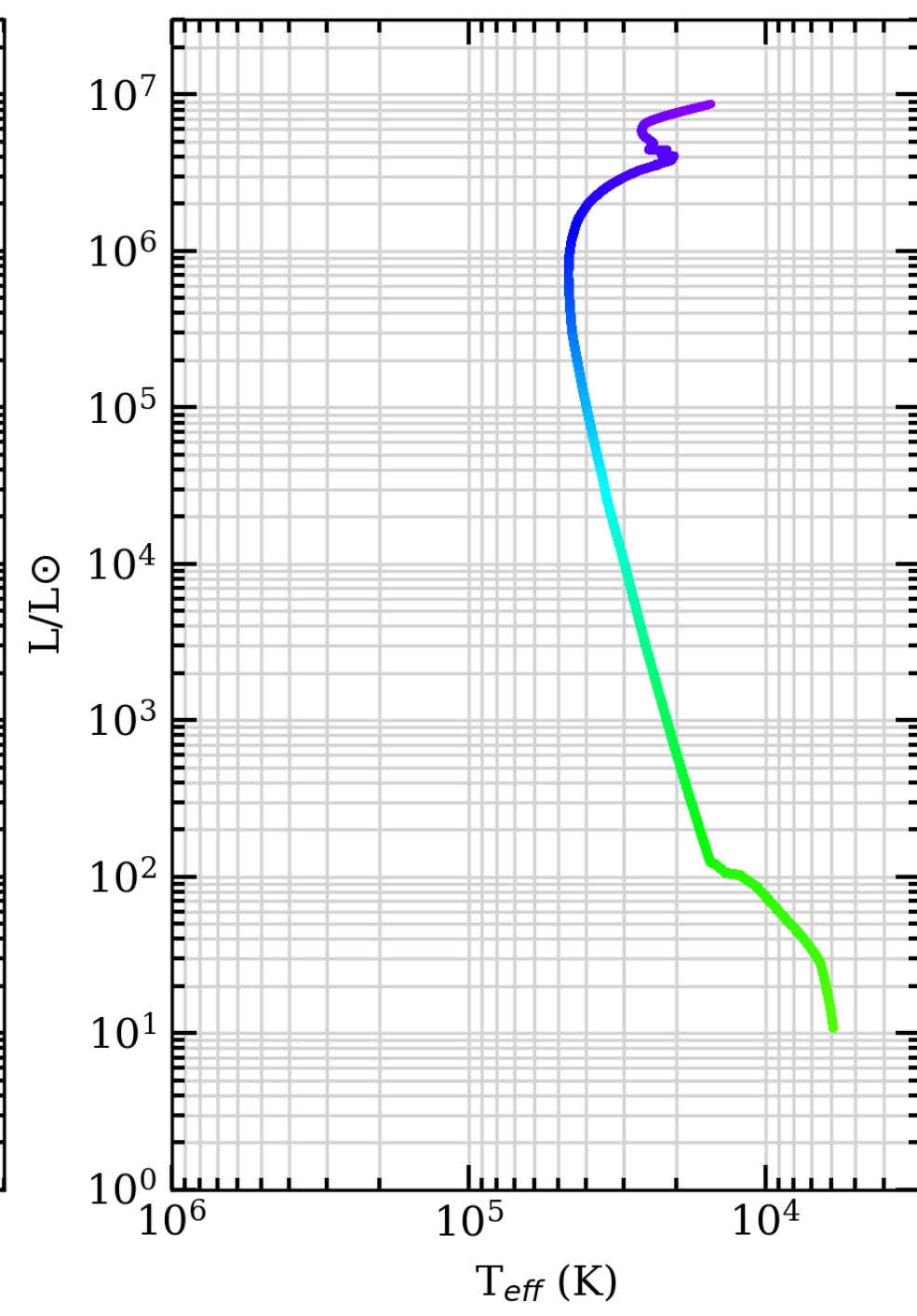
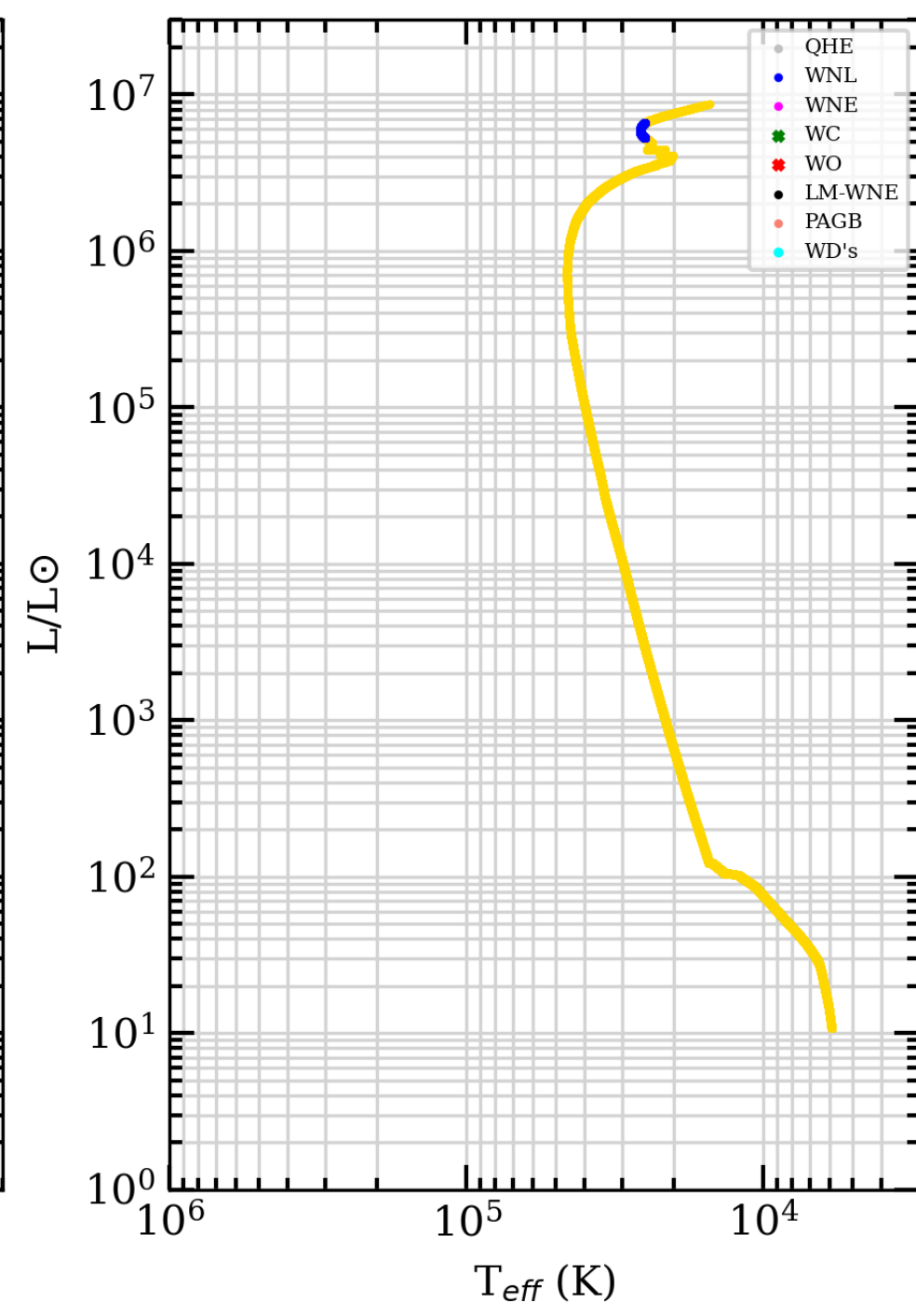
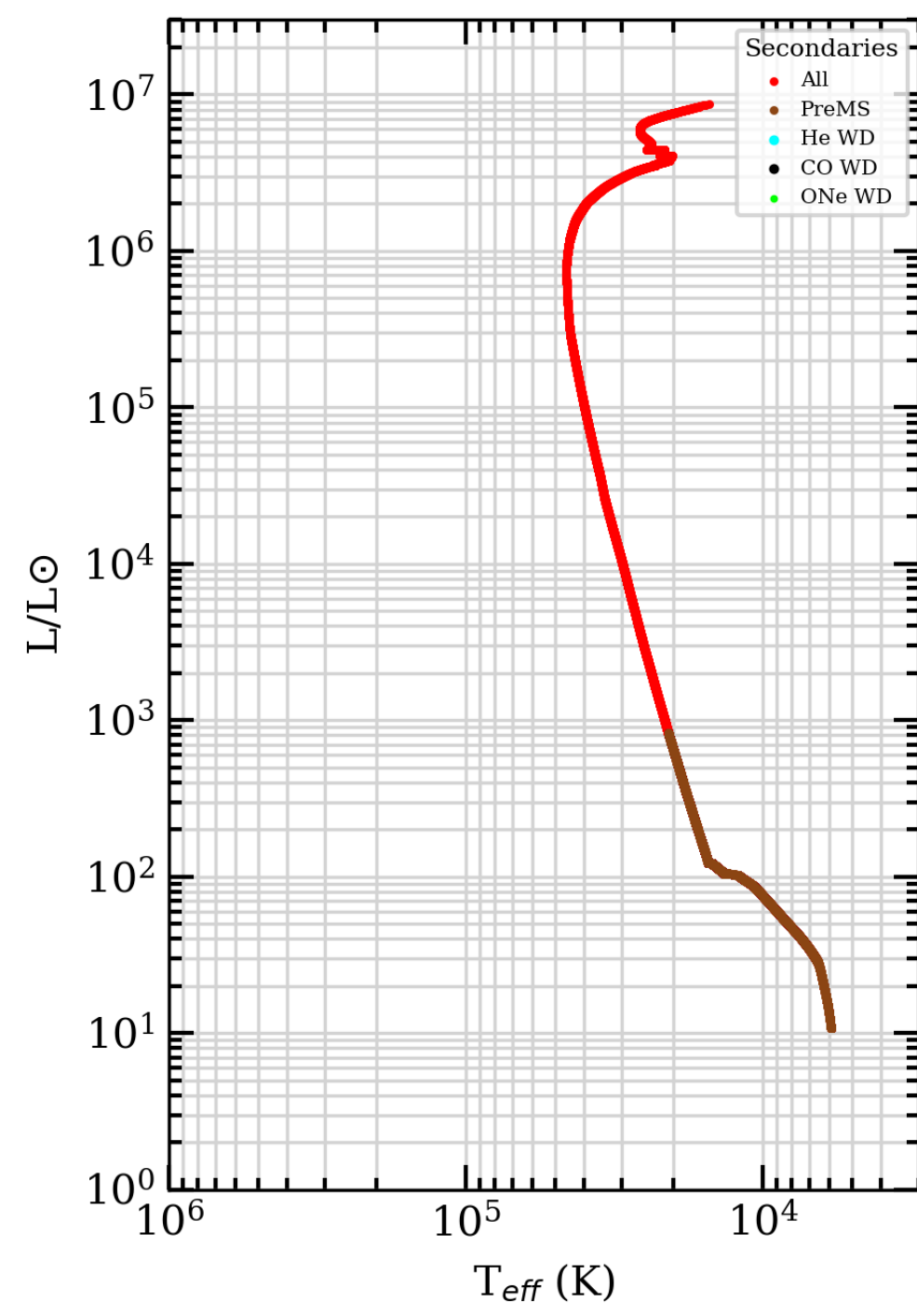
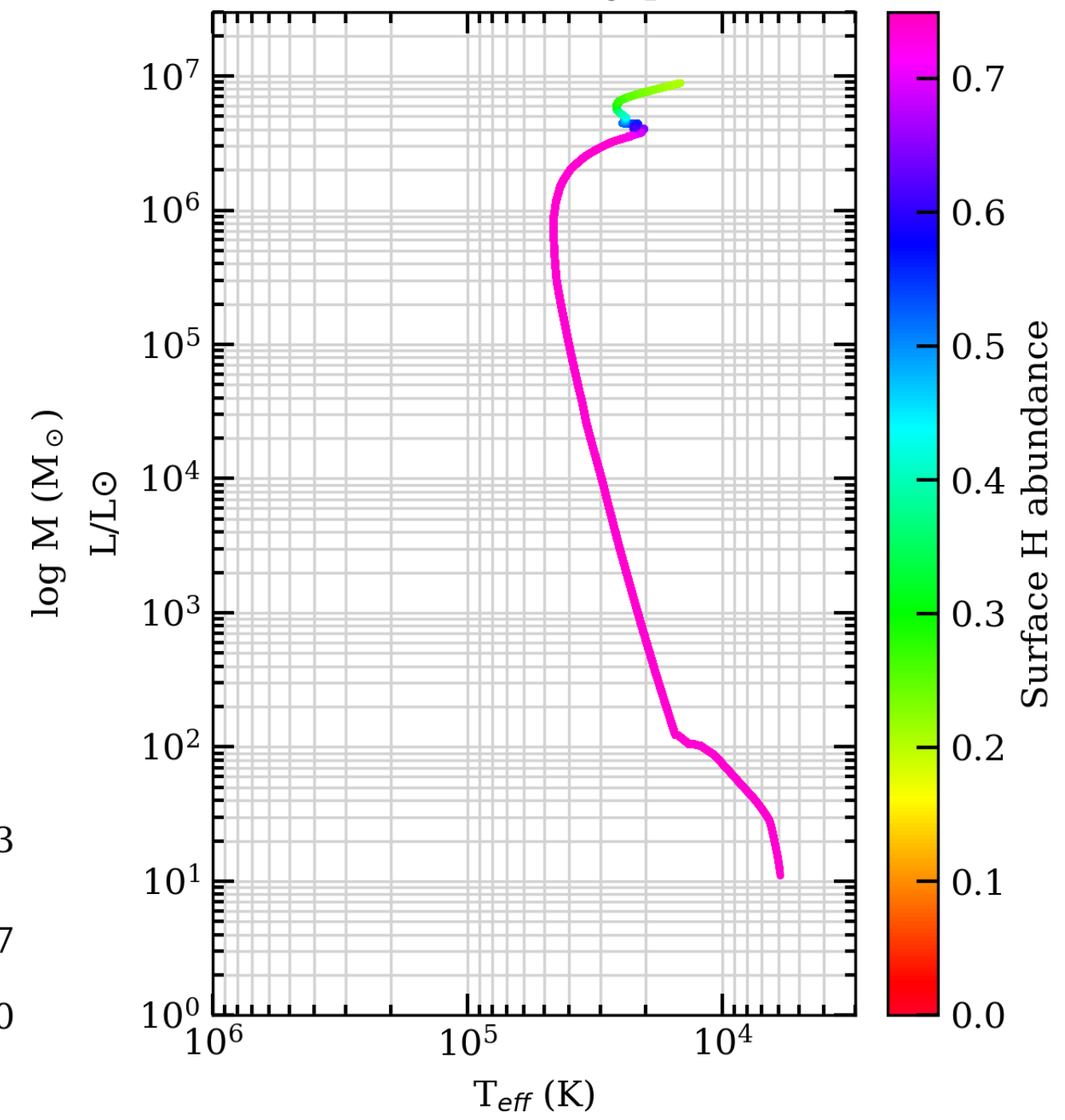
SEVN2.3 VLA binary star tracks



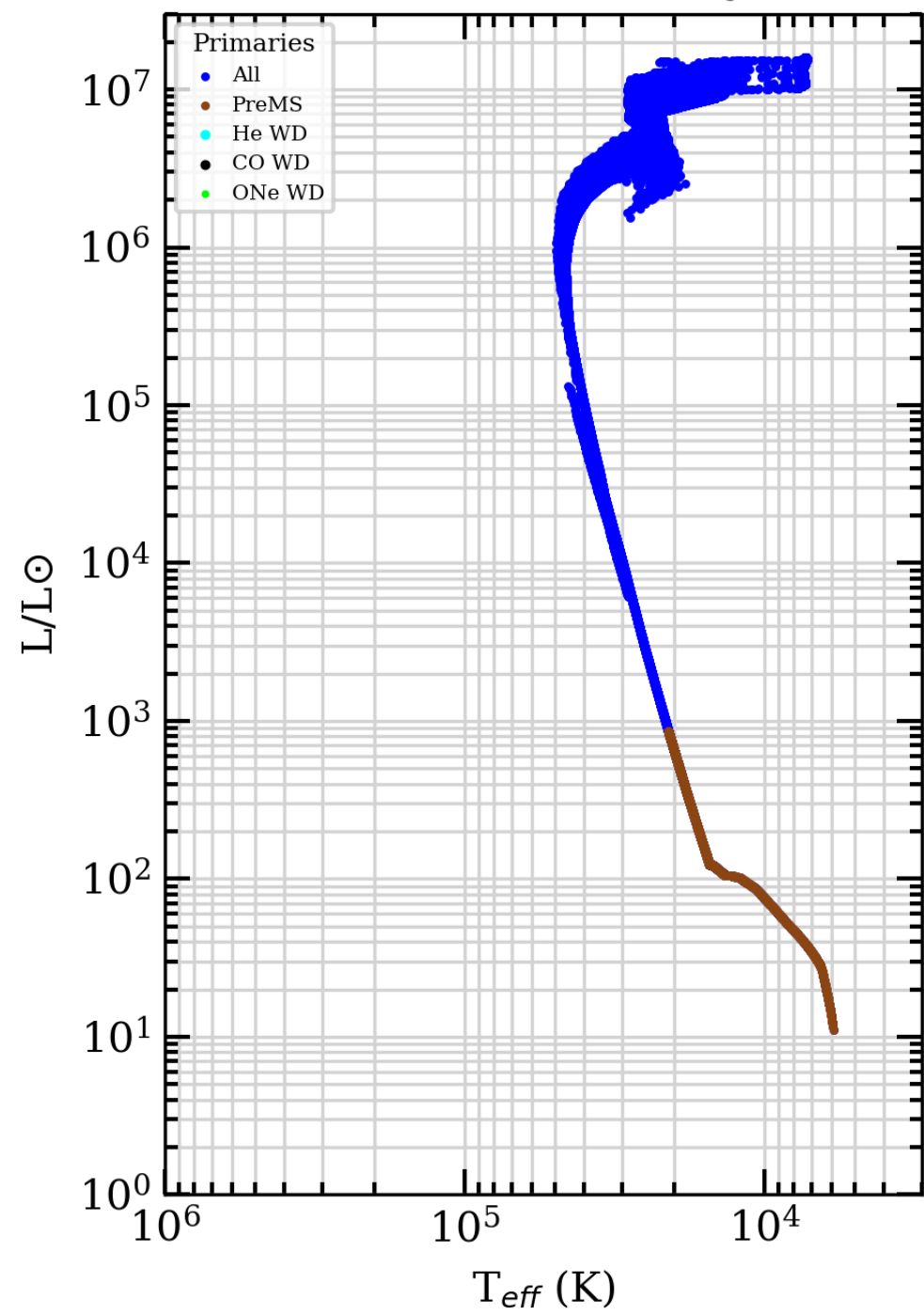
April 2023



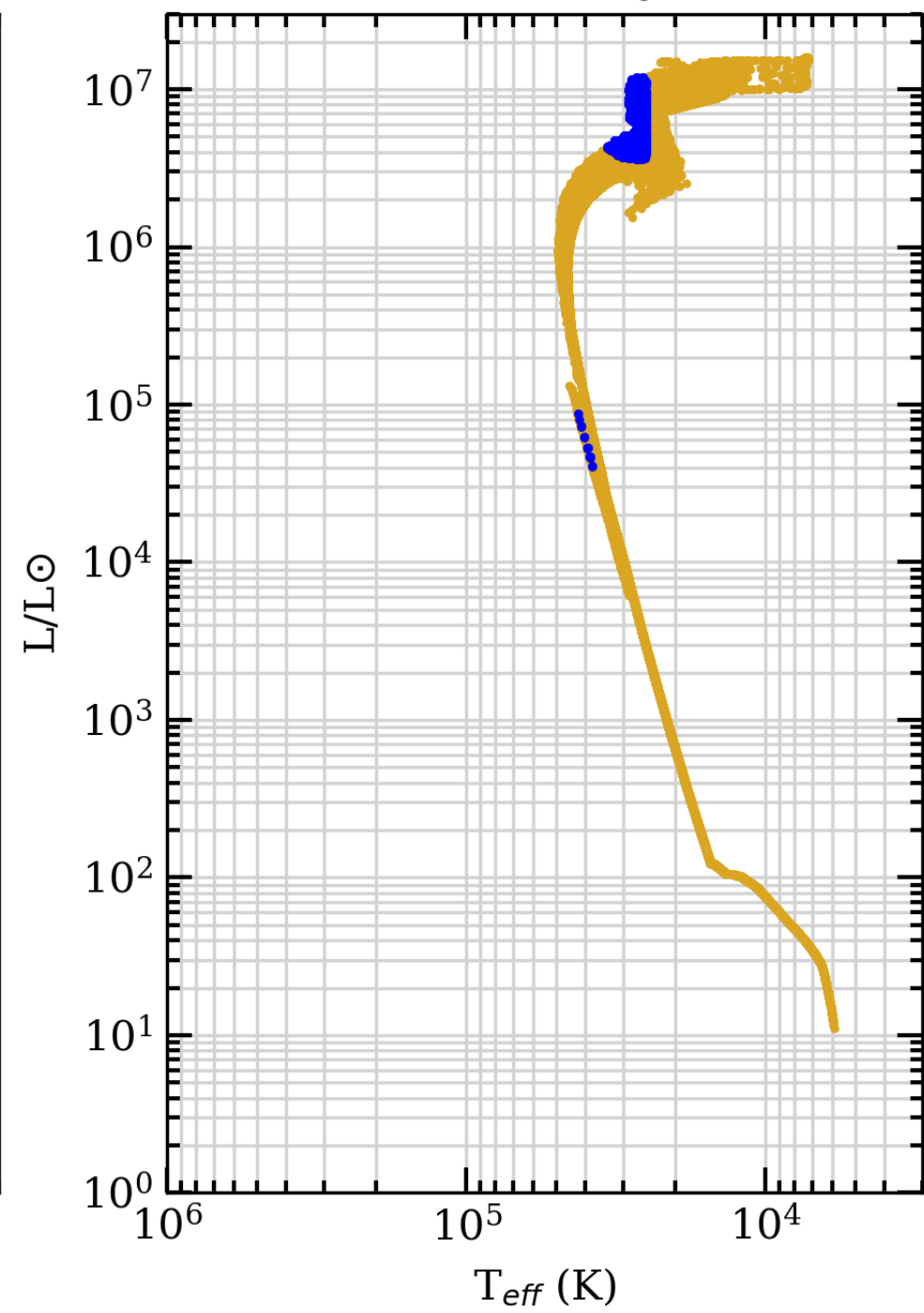
156250 binary pairs



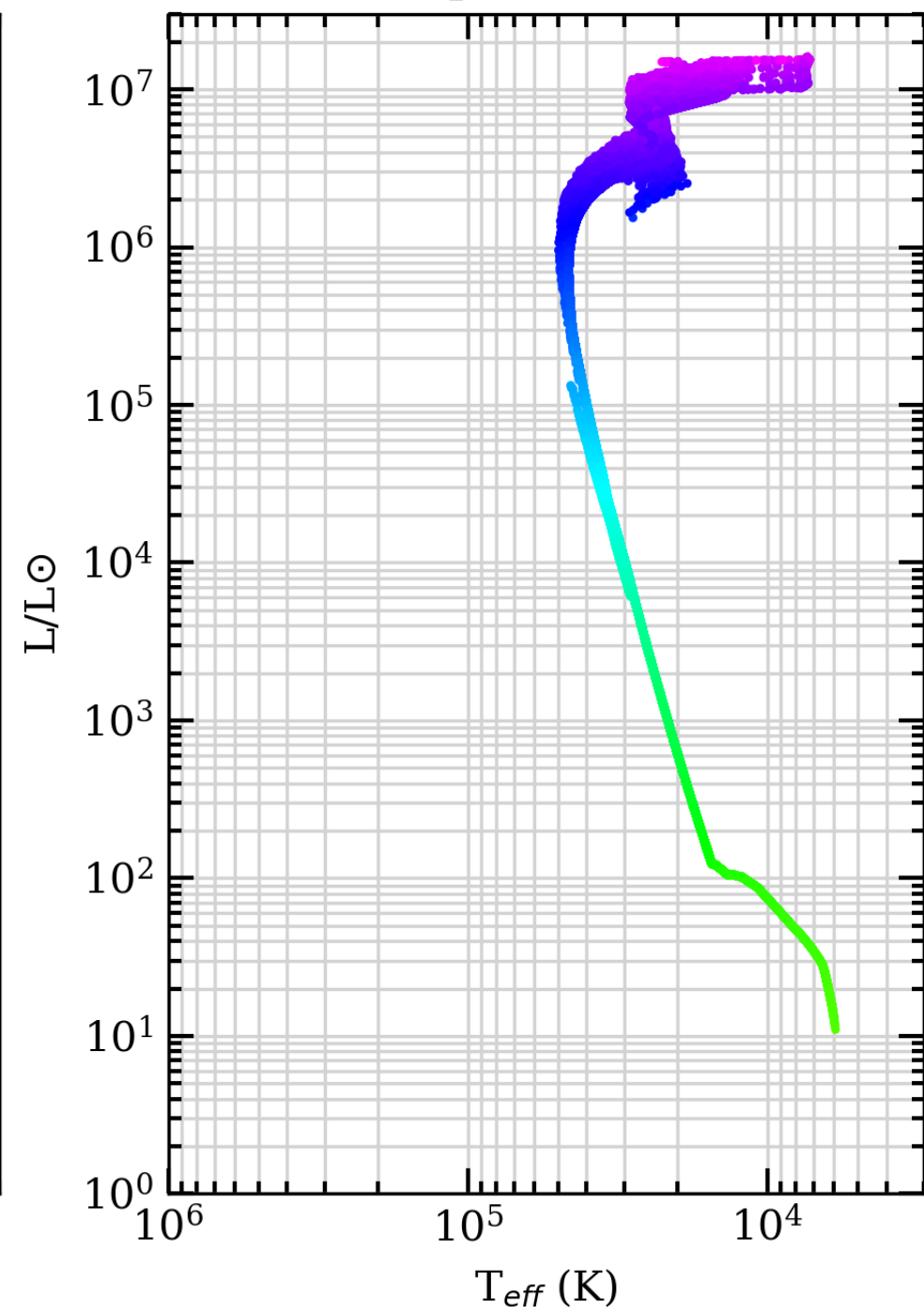
Z=0.004, t=2 Myr



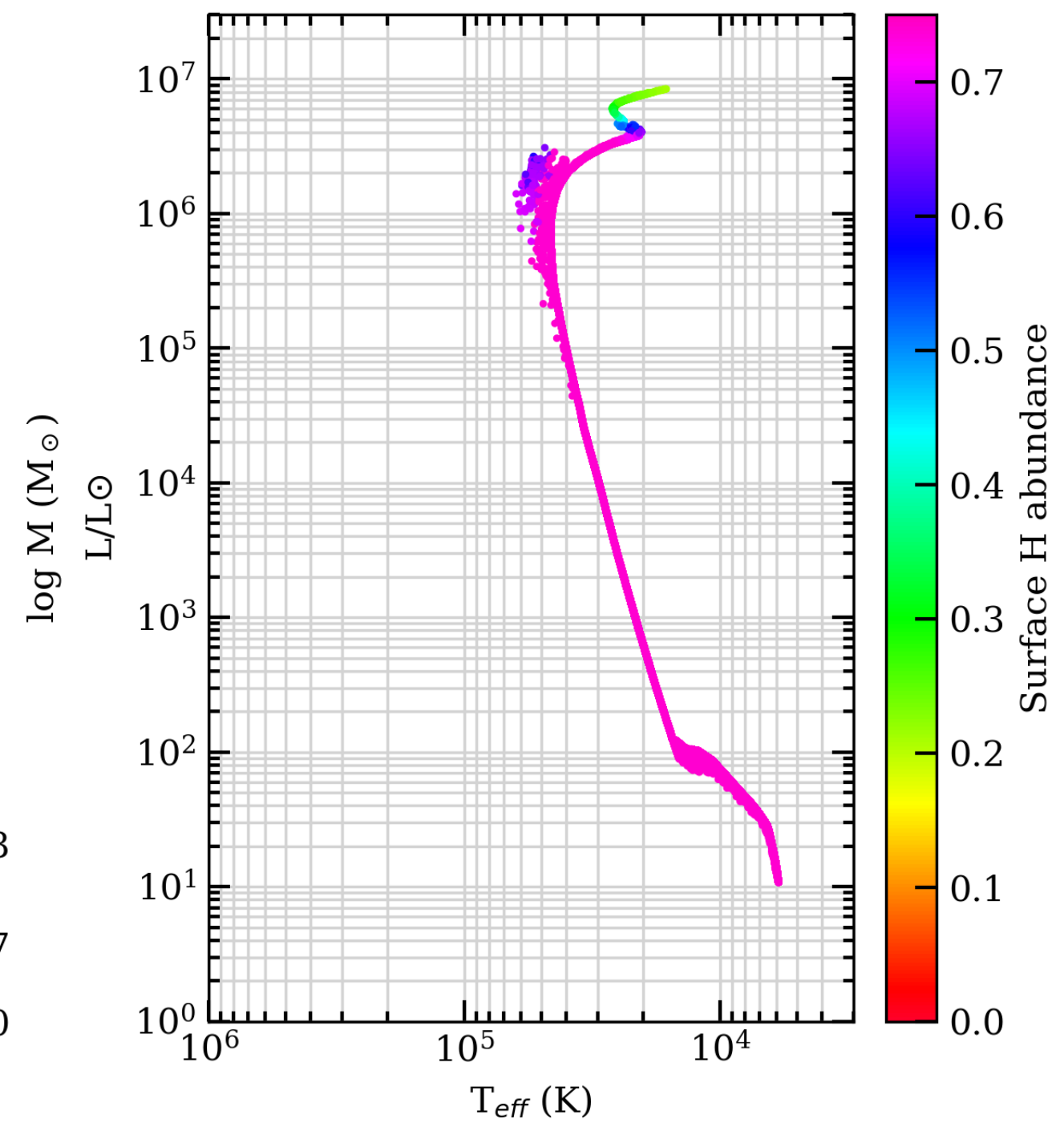
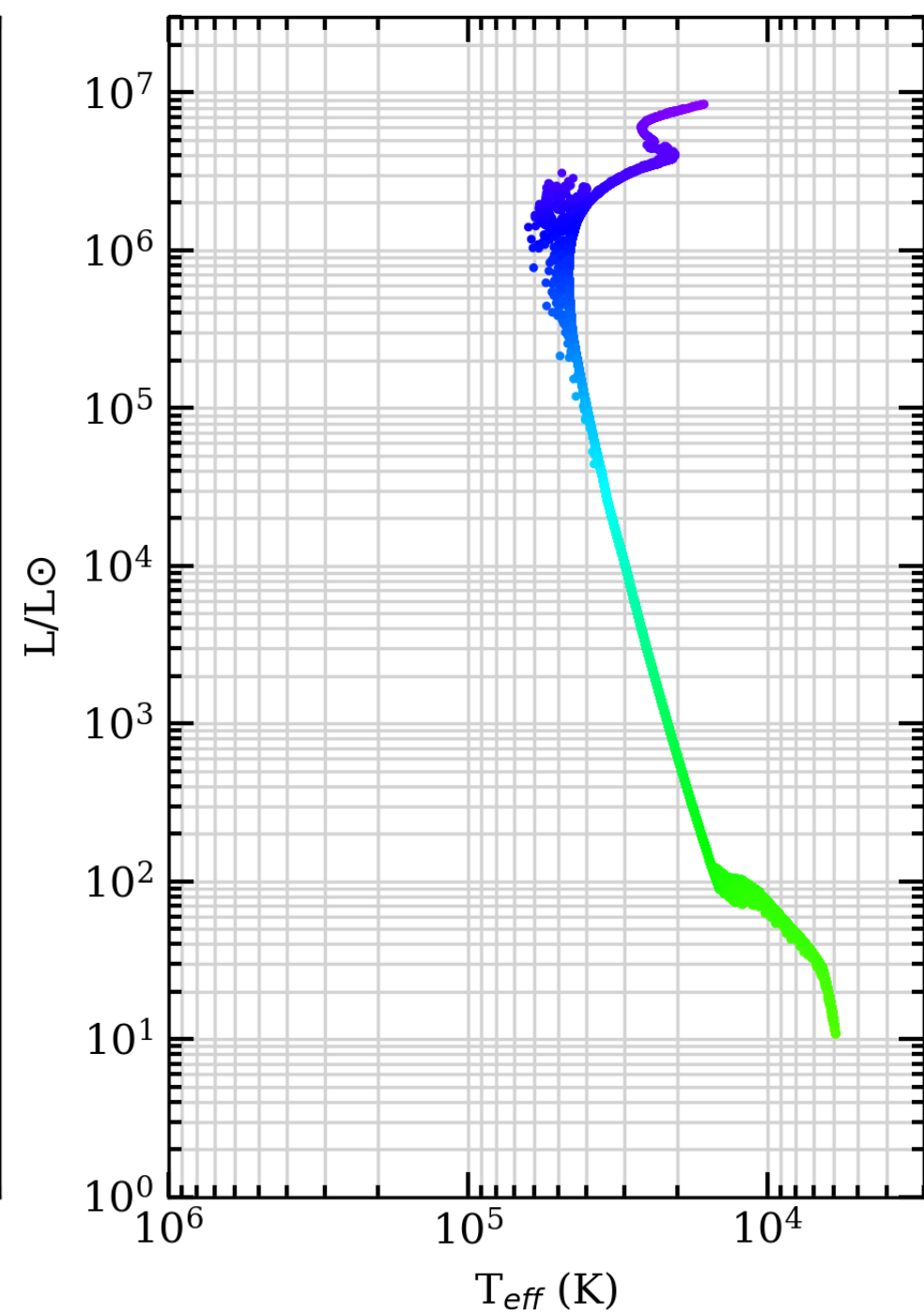
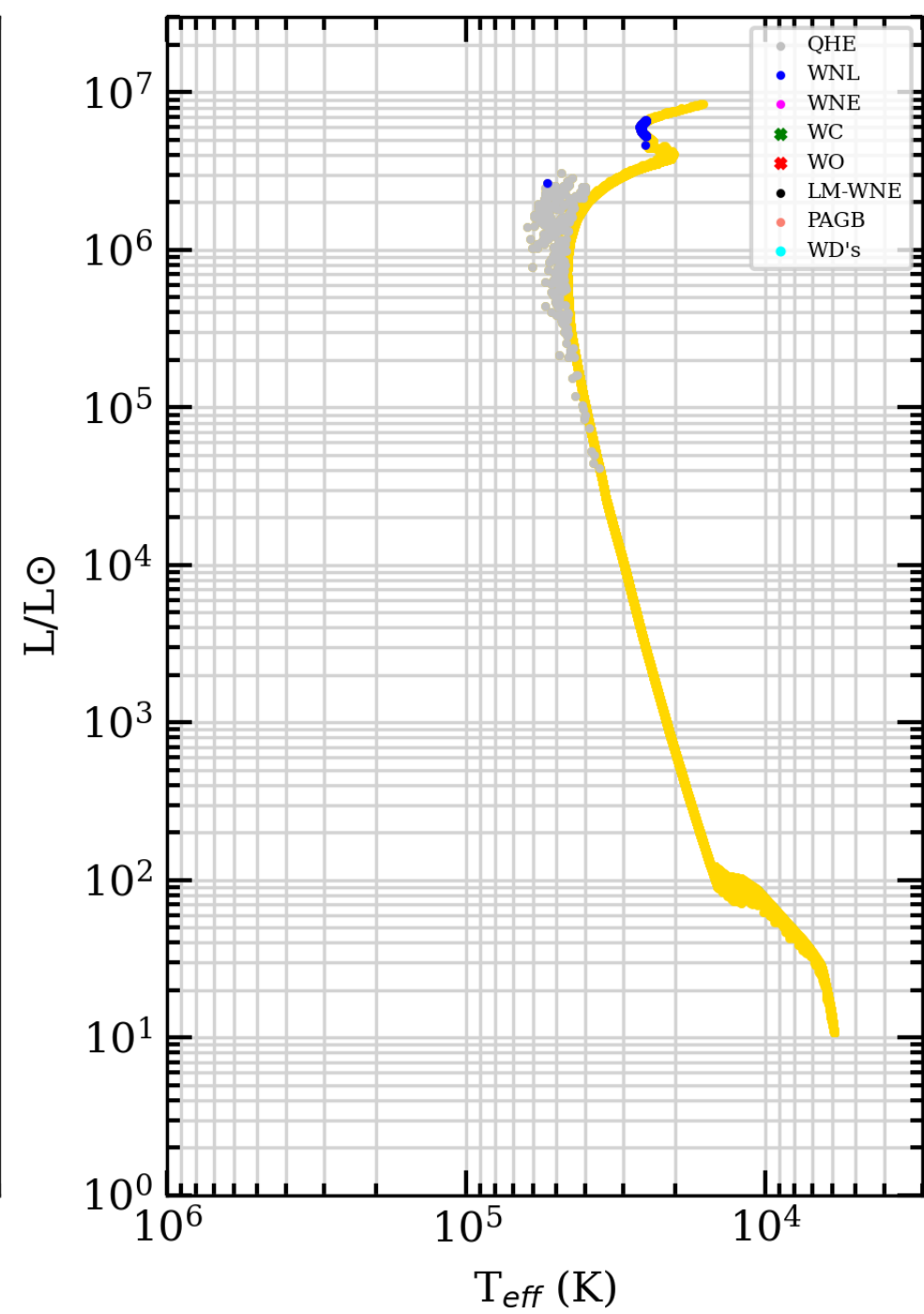
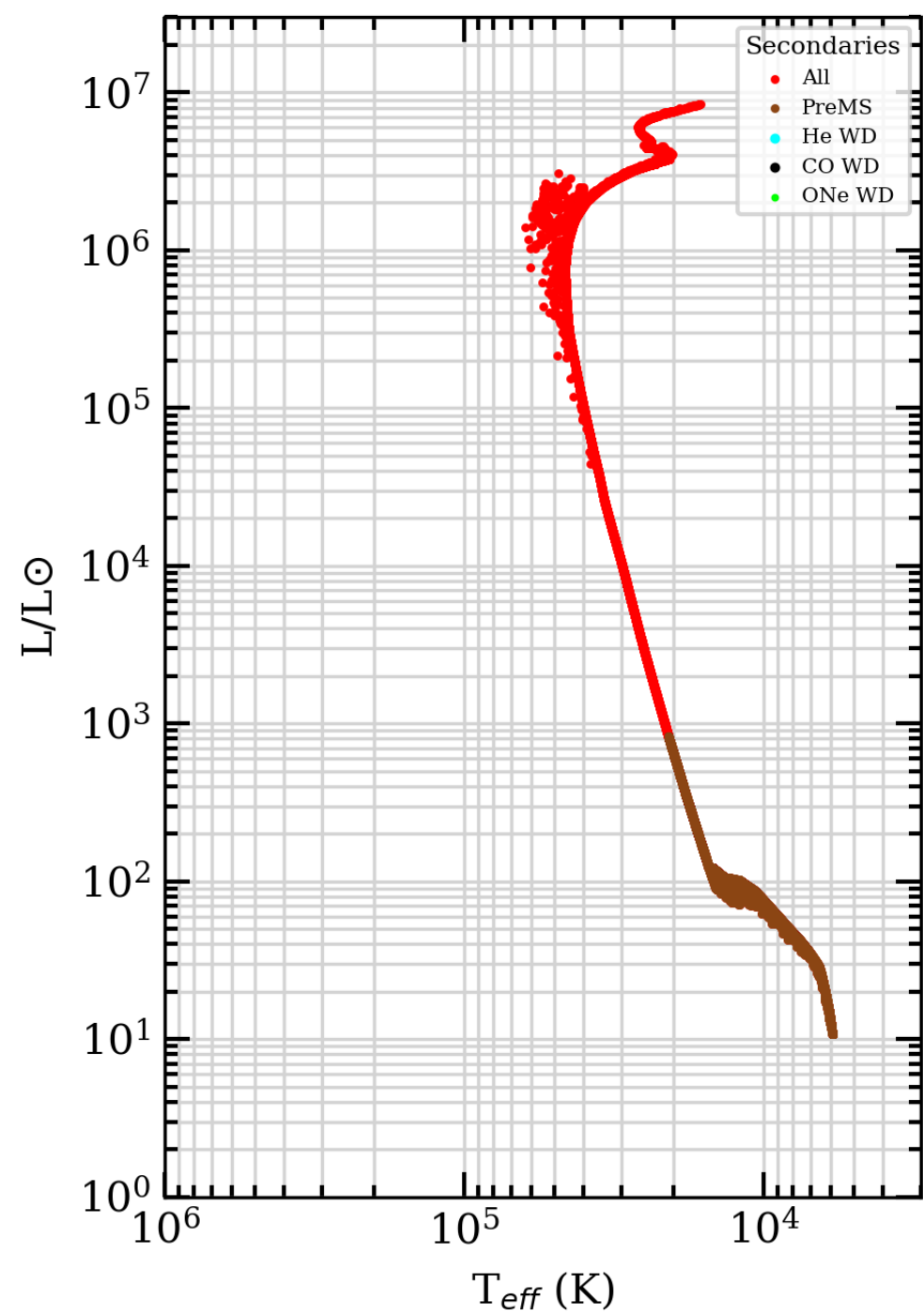
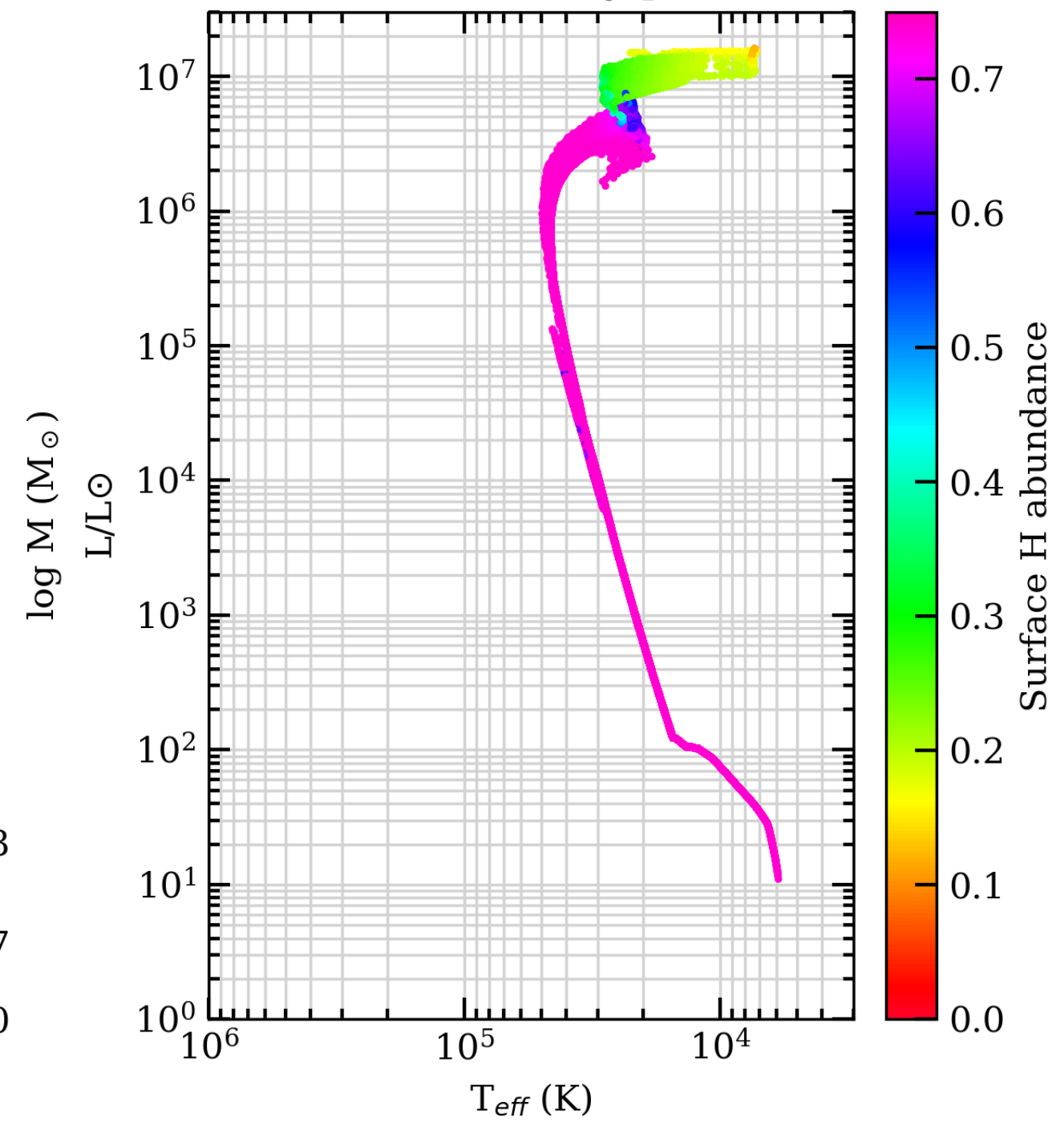
SEVN2.3 STD binary star tracks



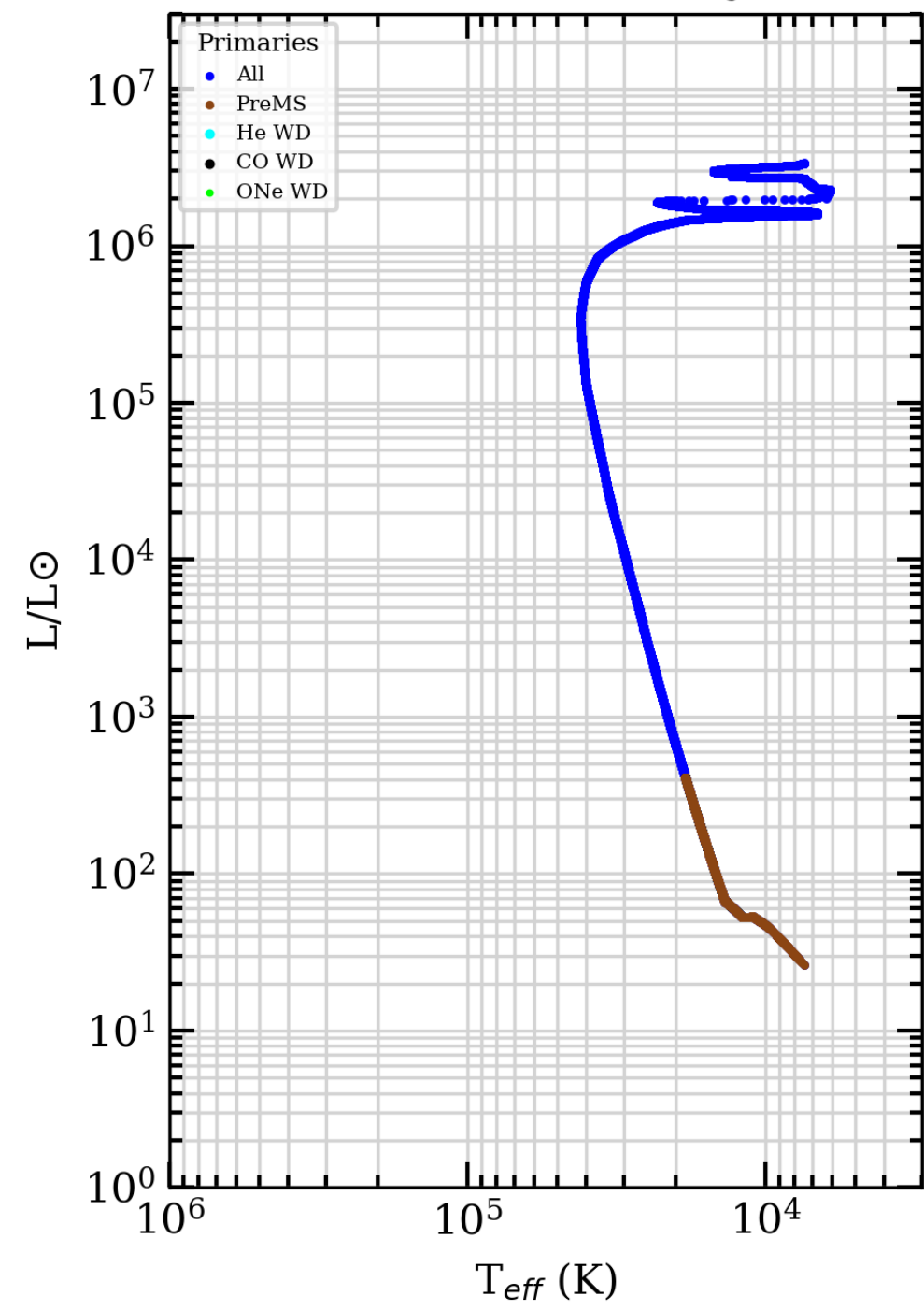
April 2023



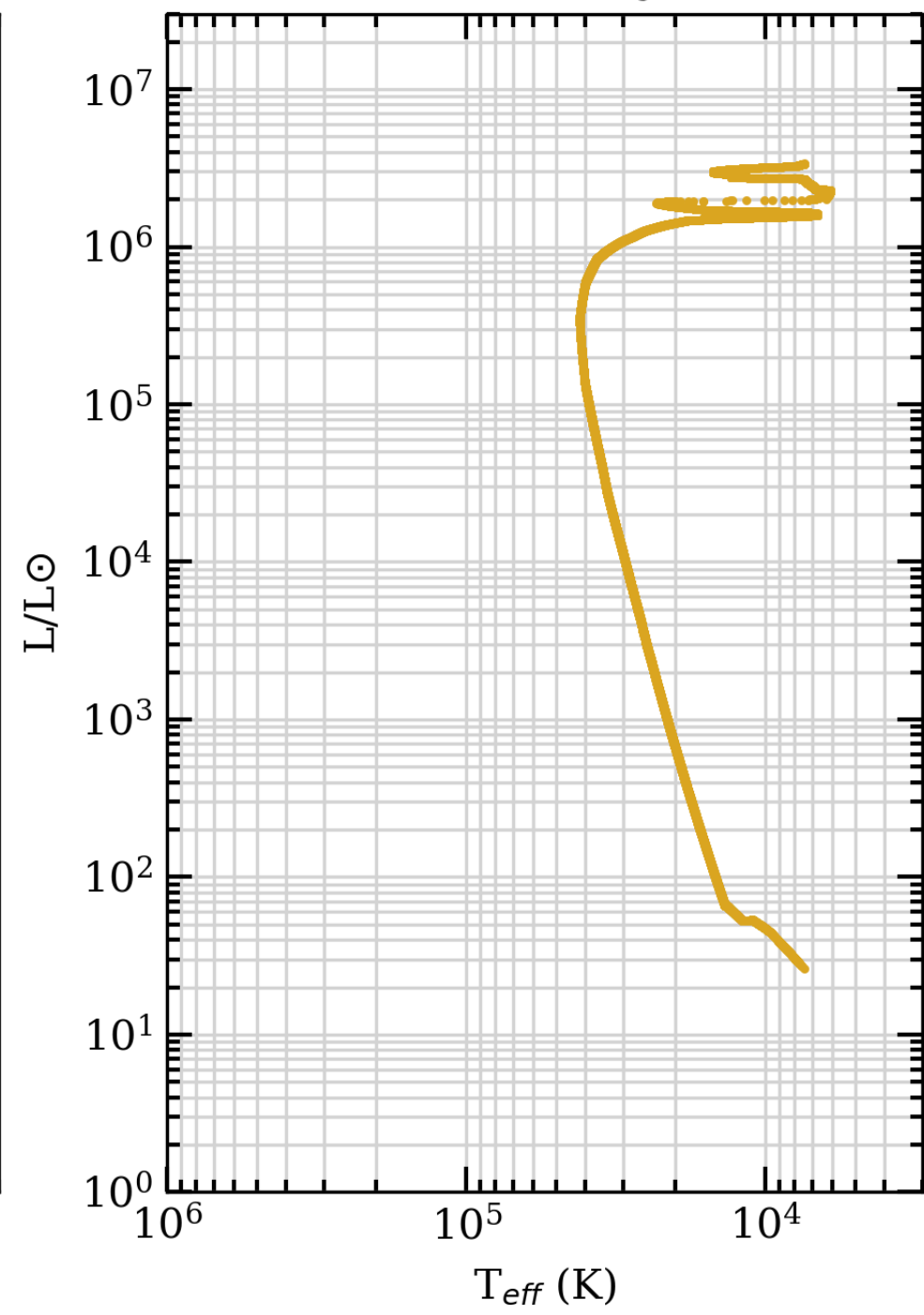
156250 binary pairs



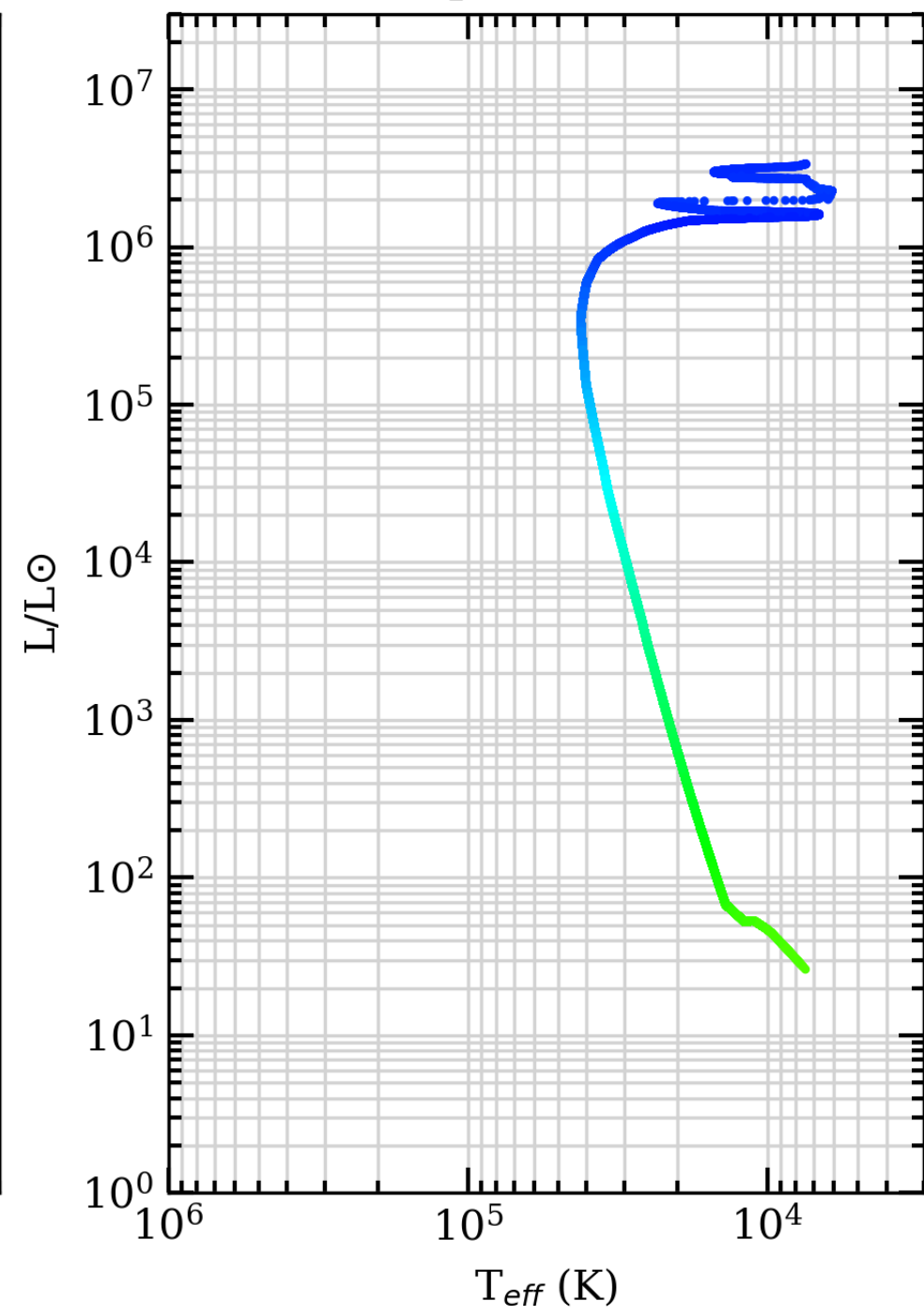
Z=0.004, t=3 Myr



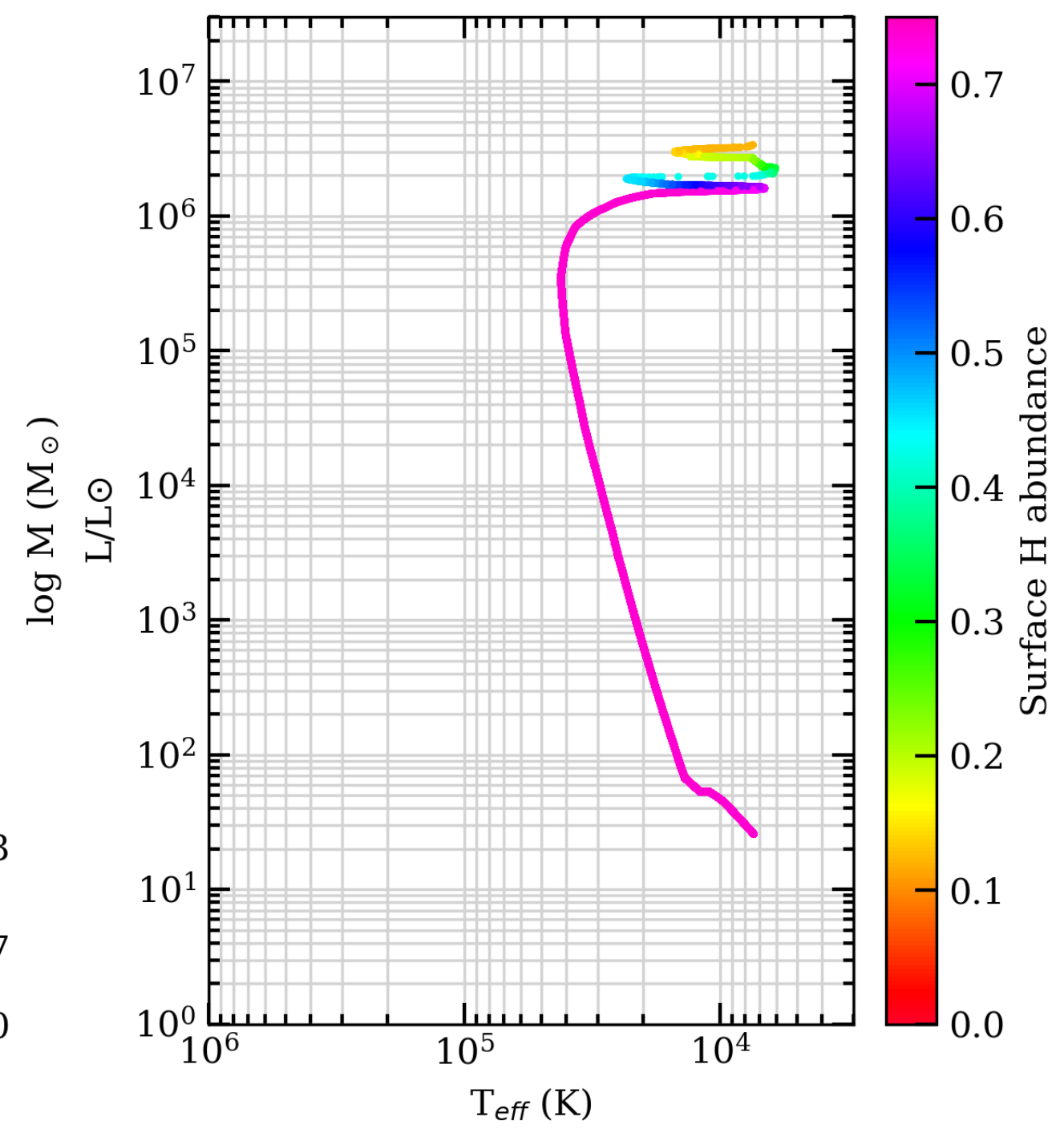
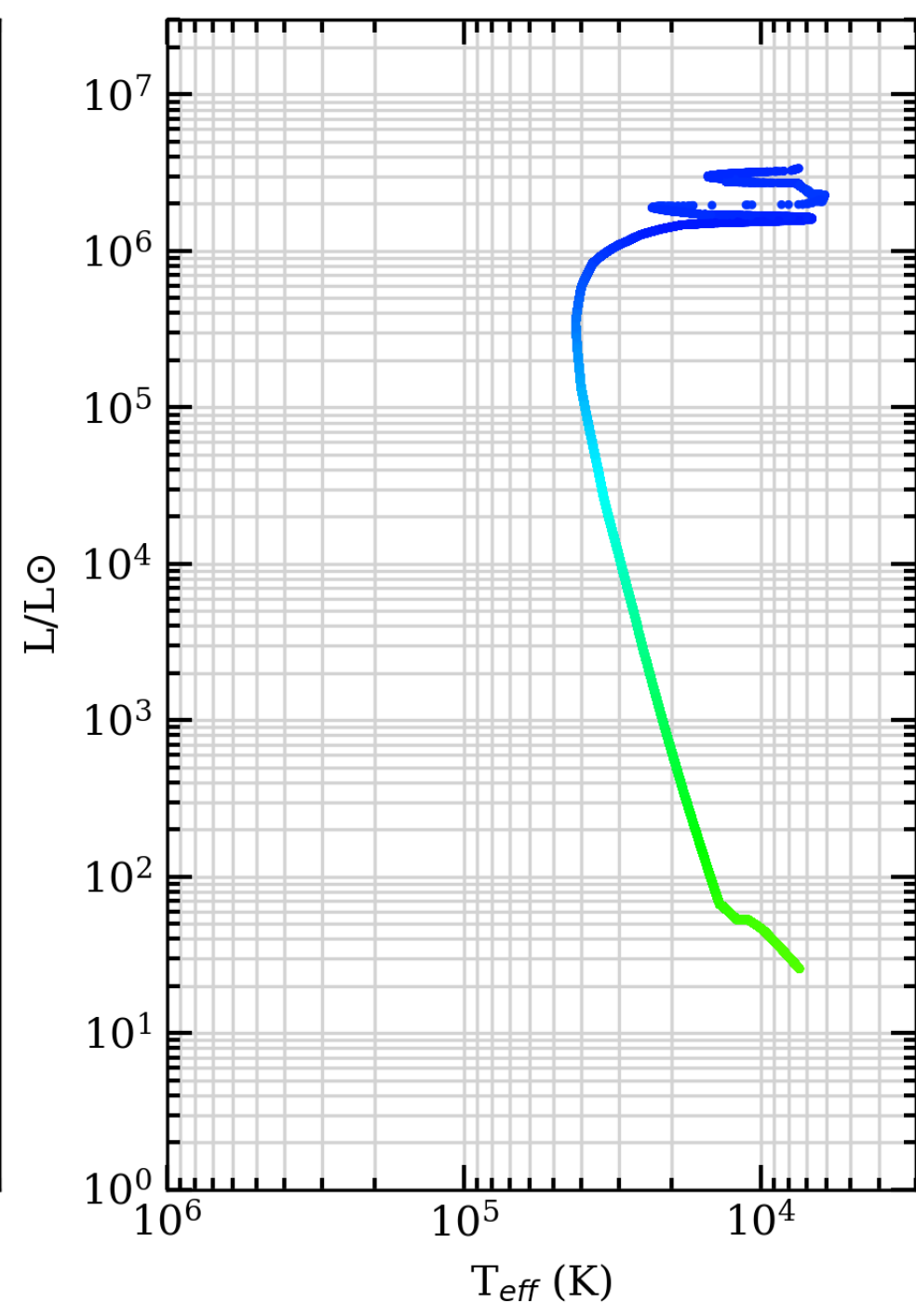
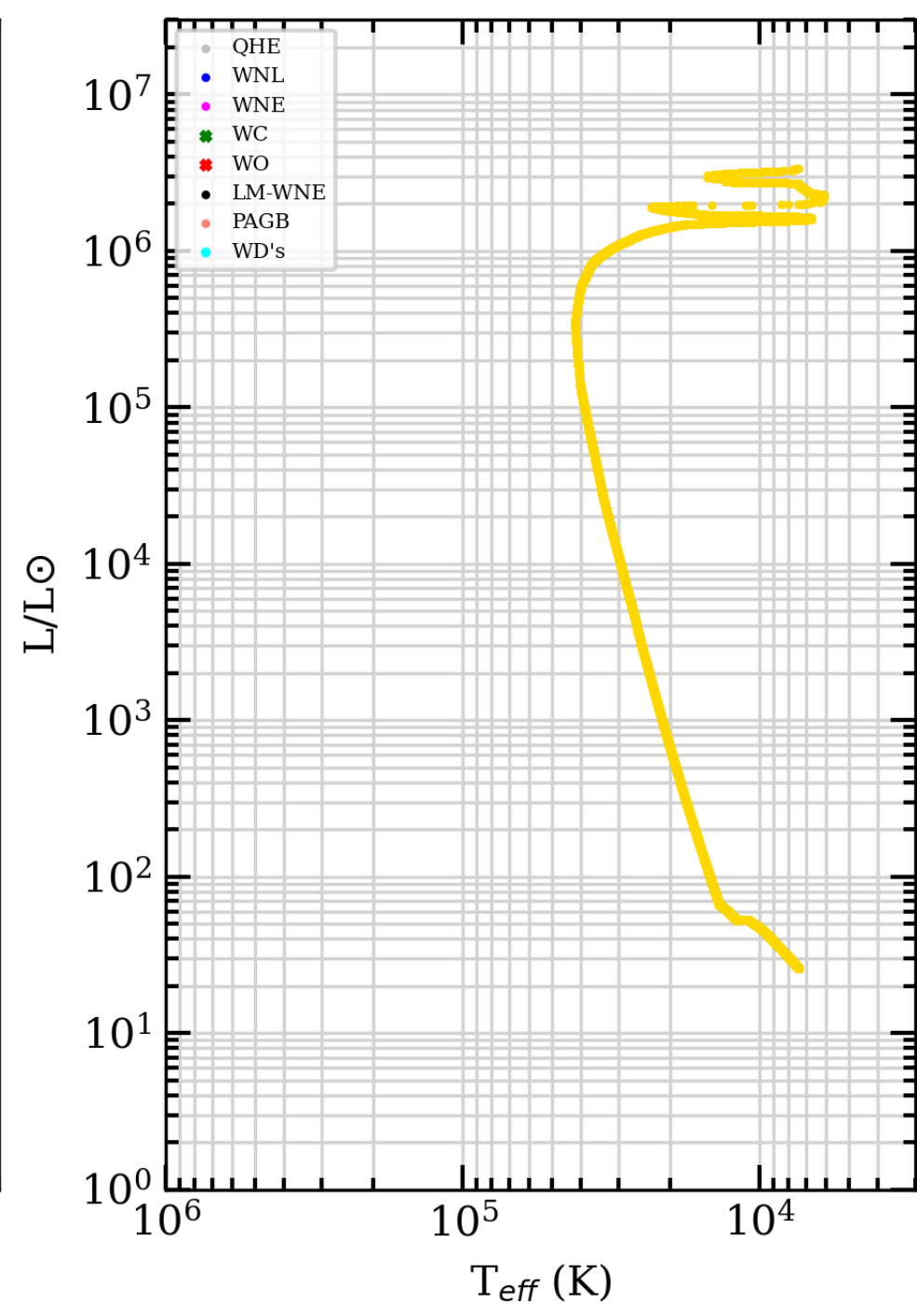
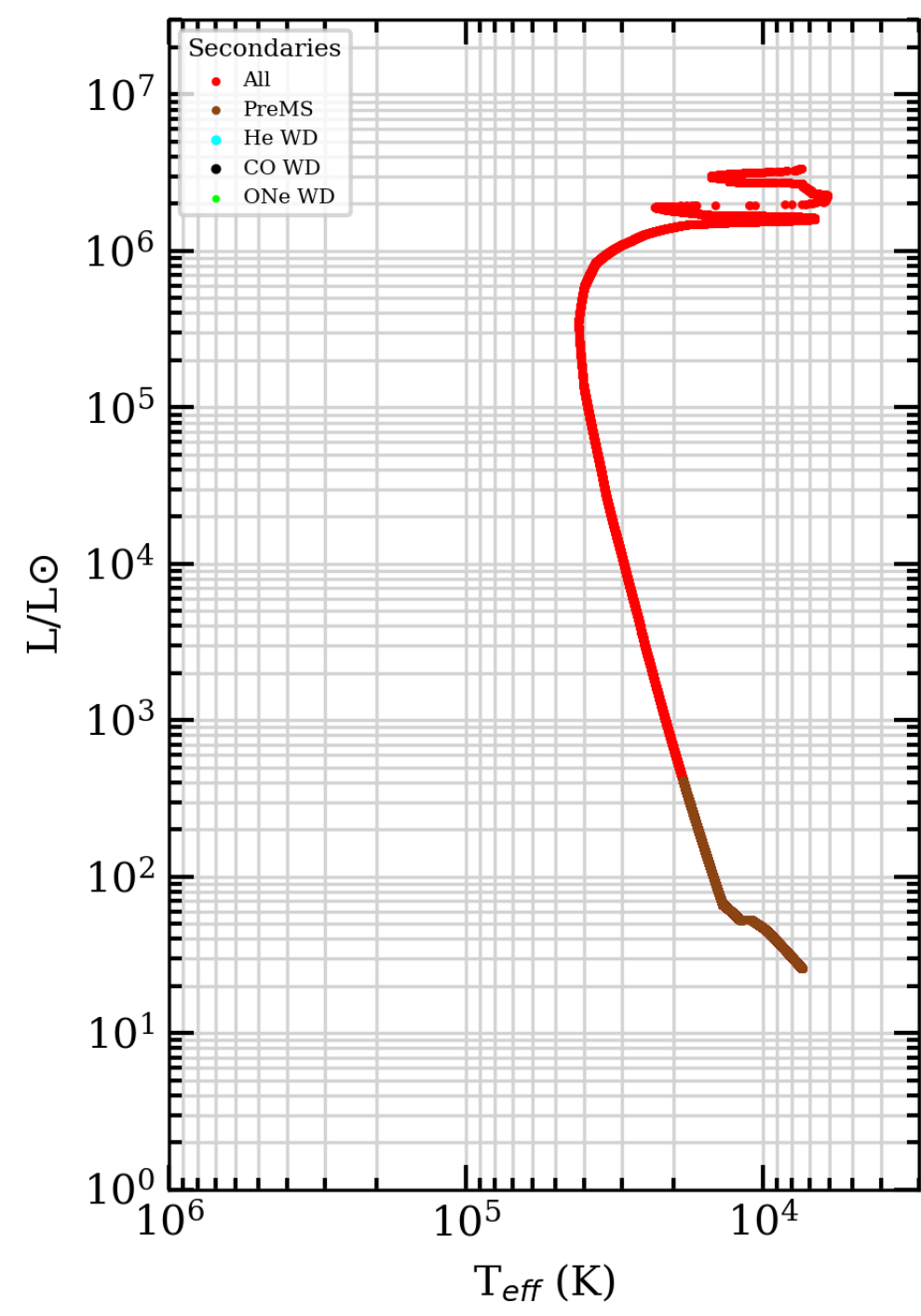
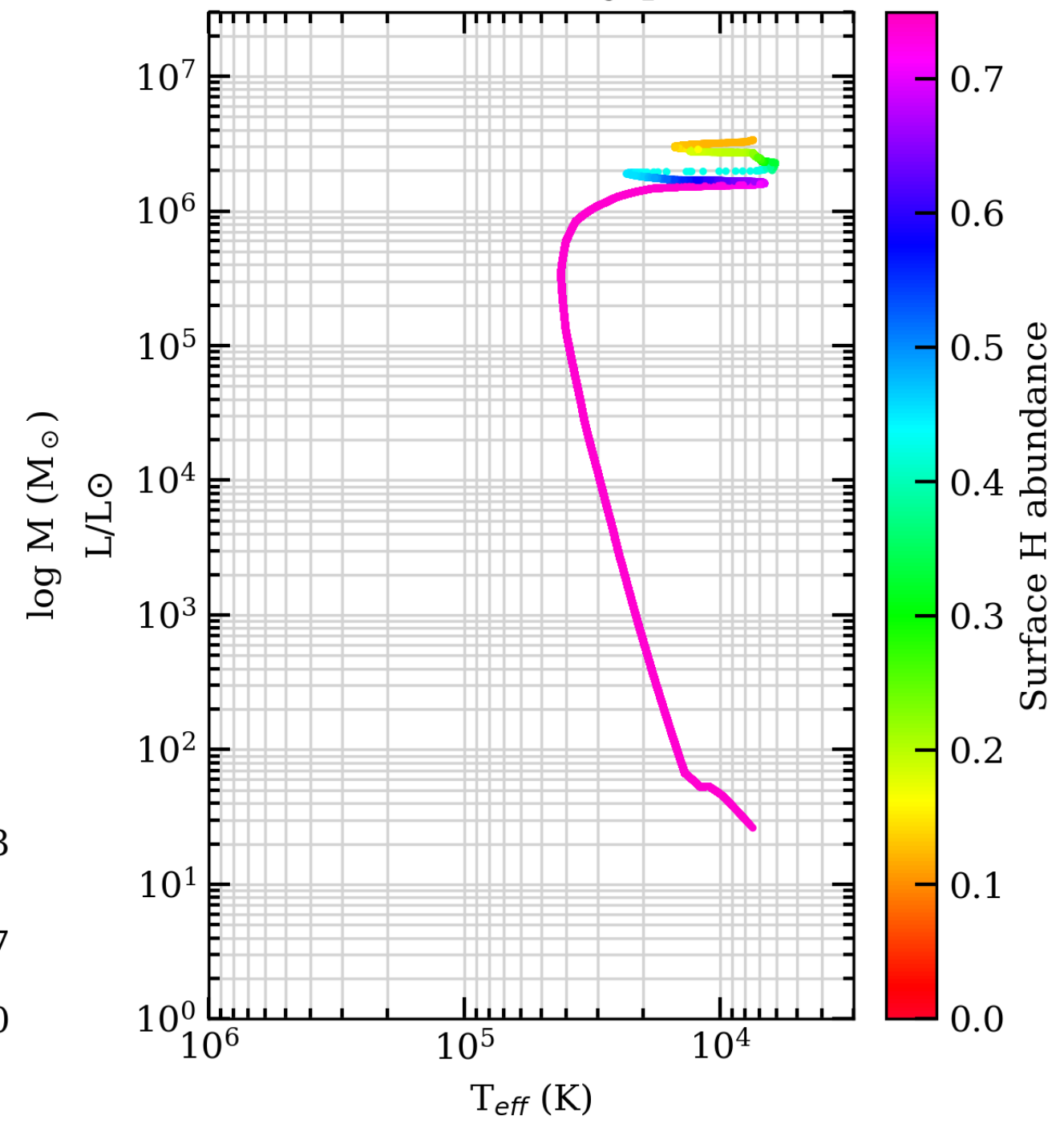
SEVN2.3 VLA binary star tracks



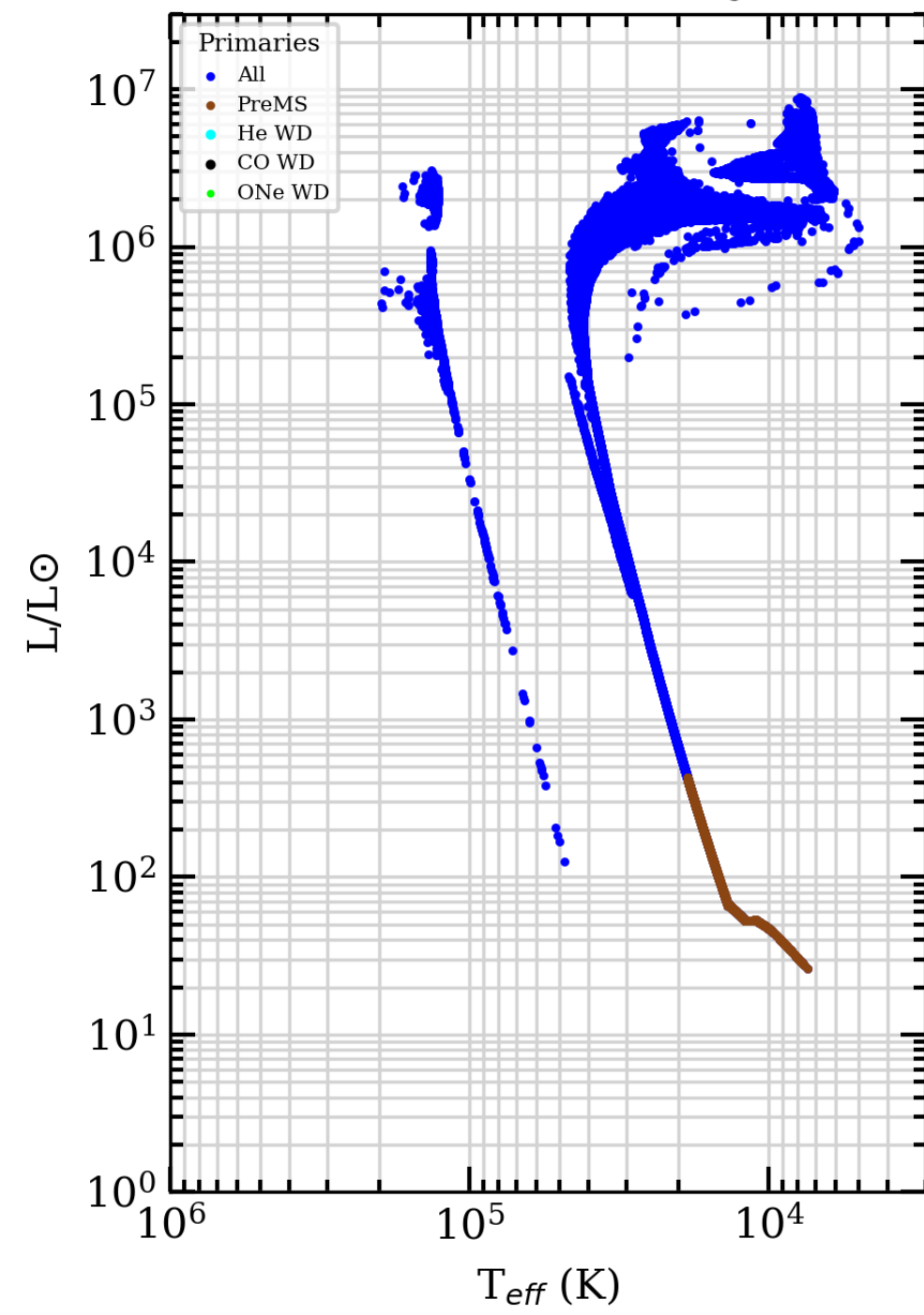
April 2023



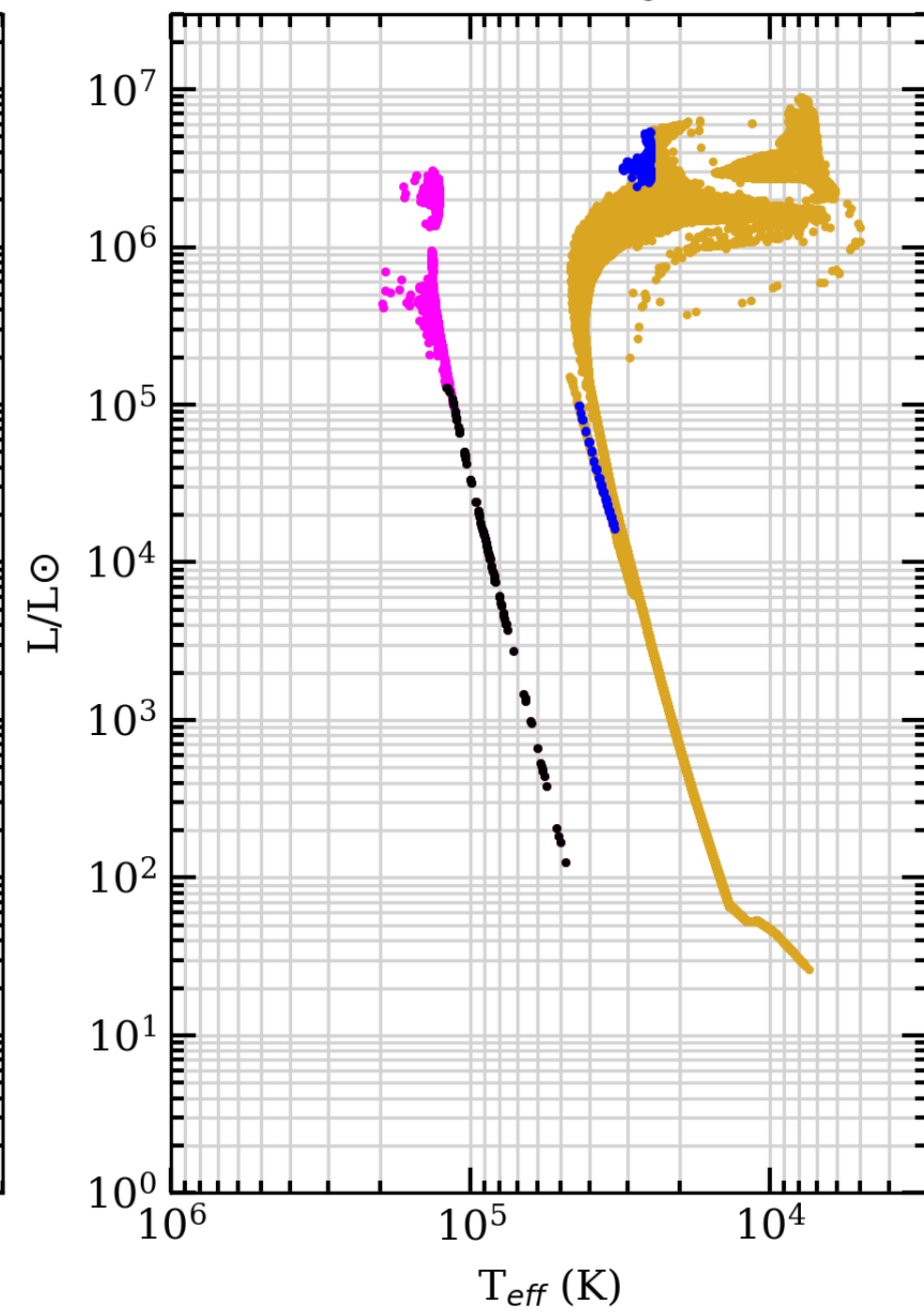
156250 binary pairs



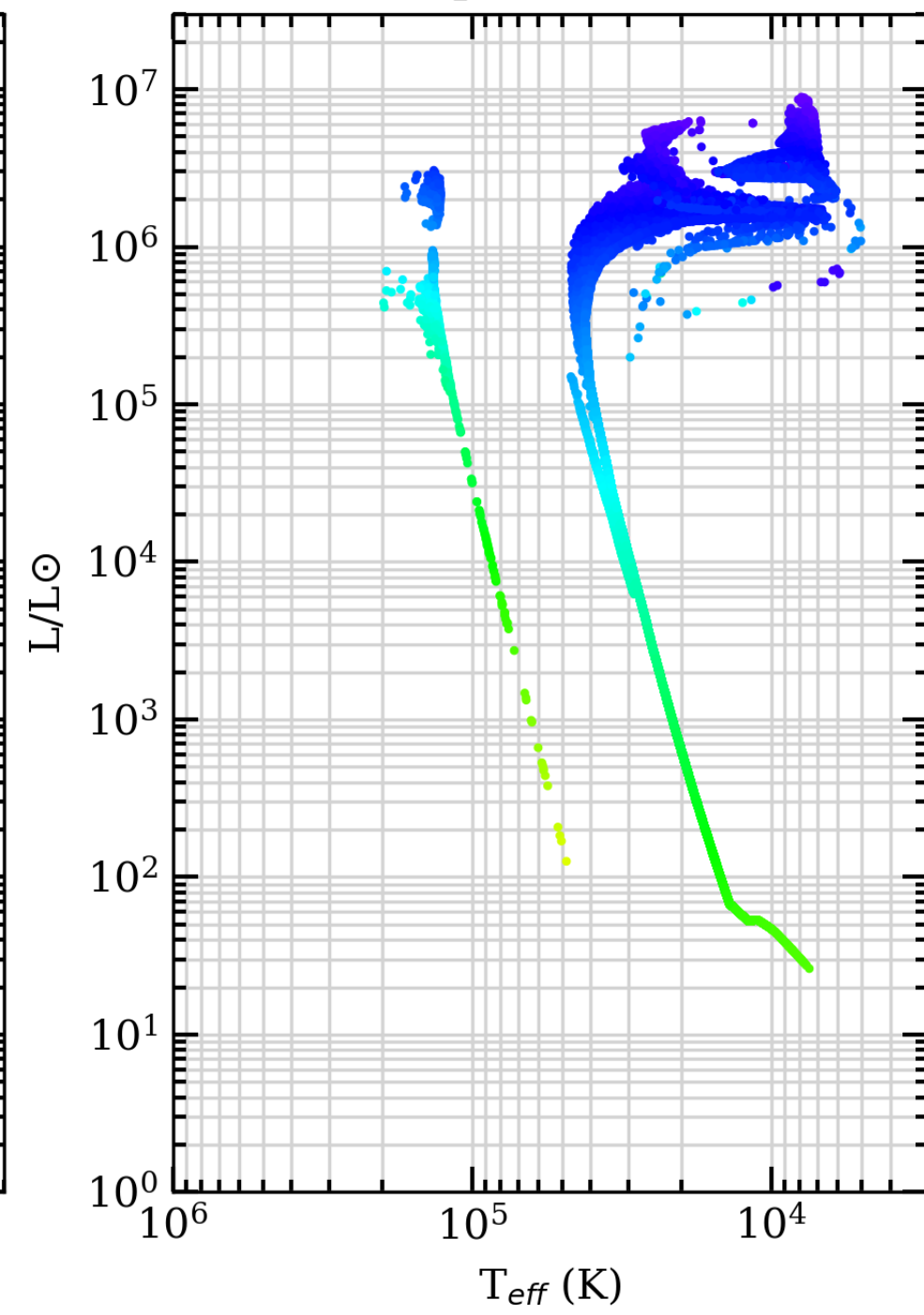
Z=0.004, t=3 Myr



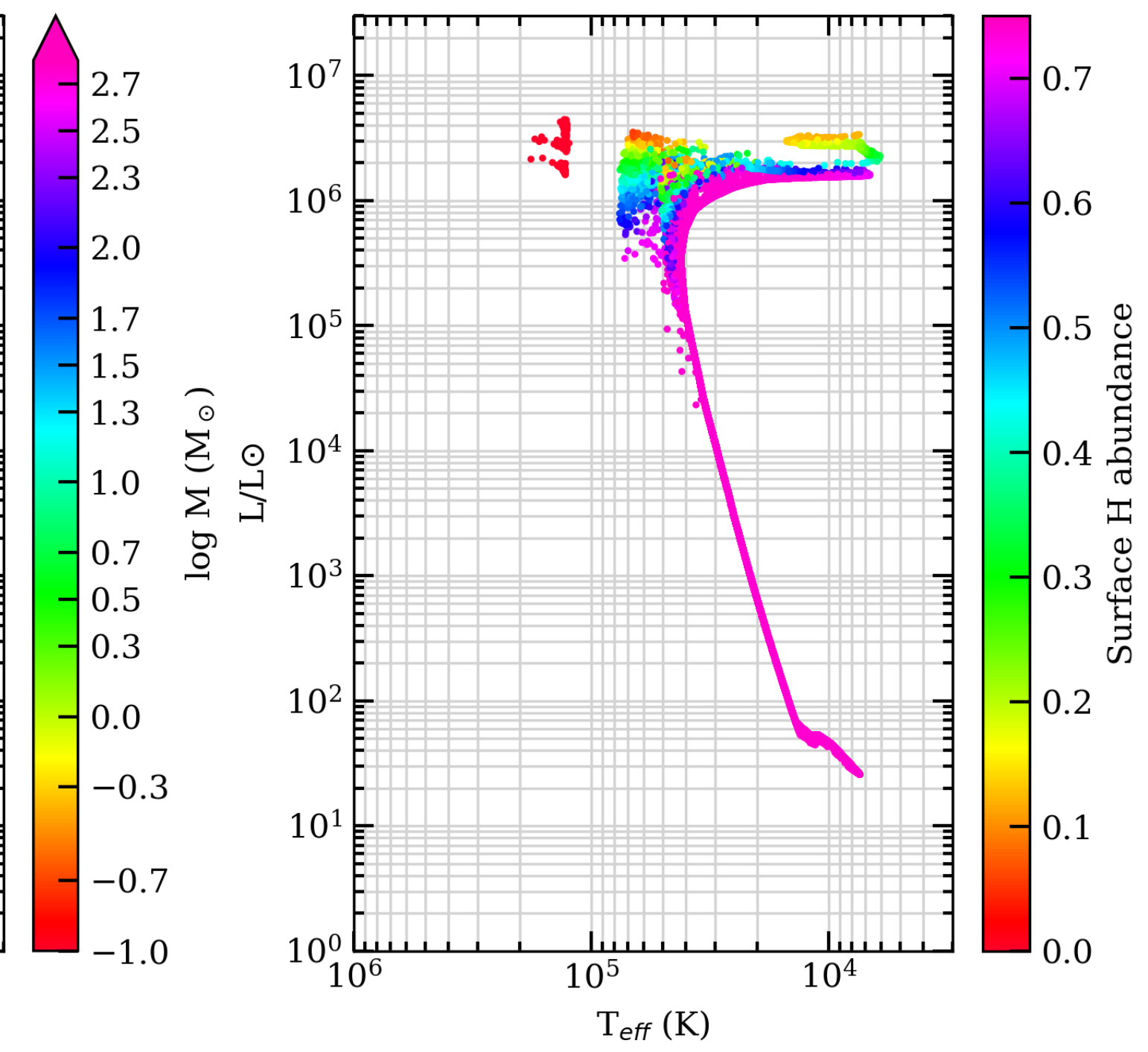
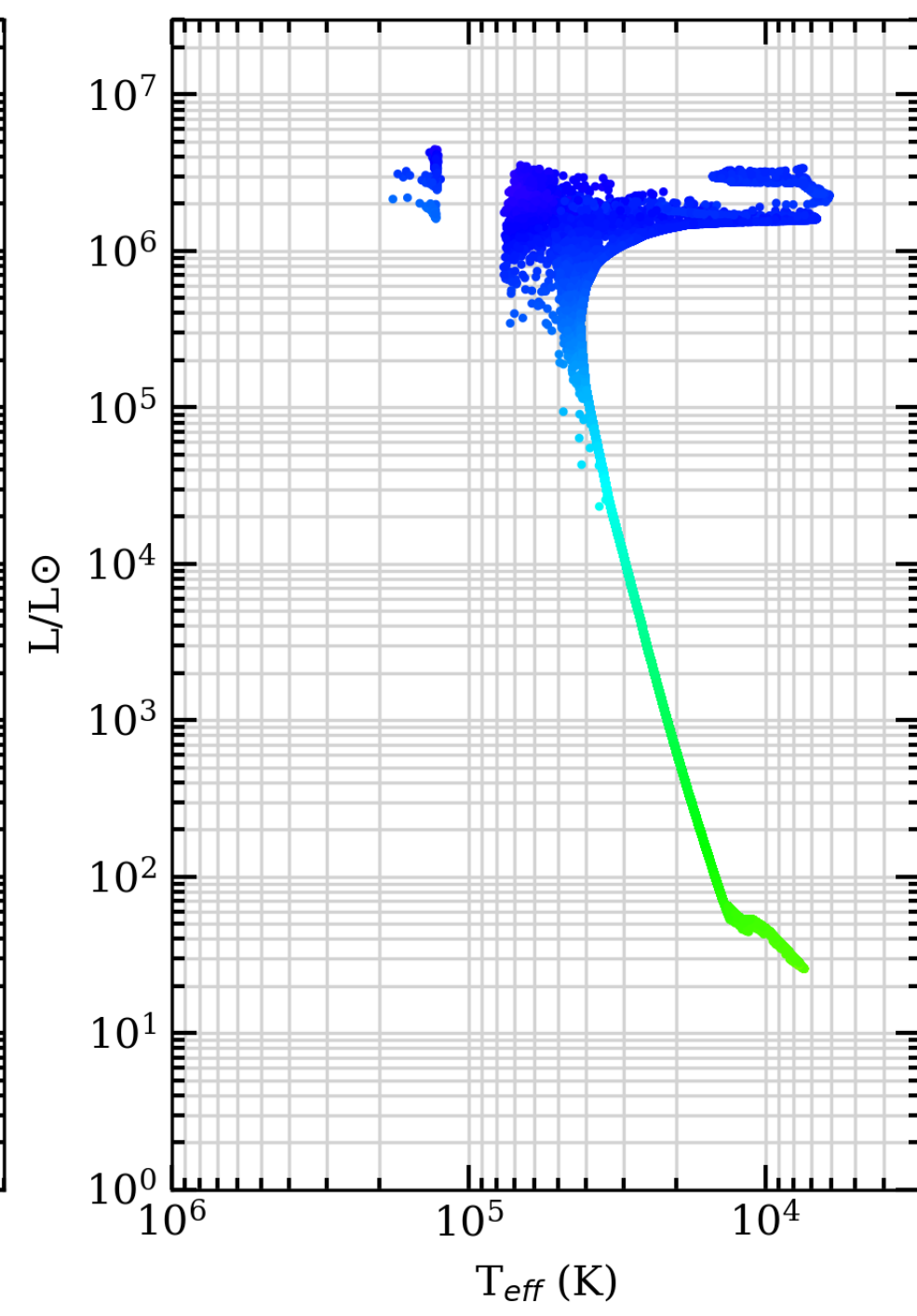
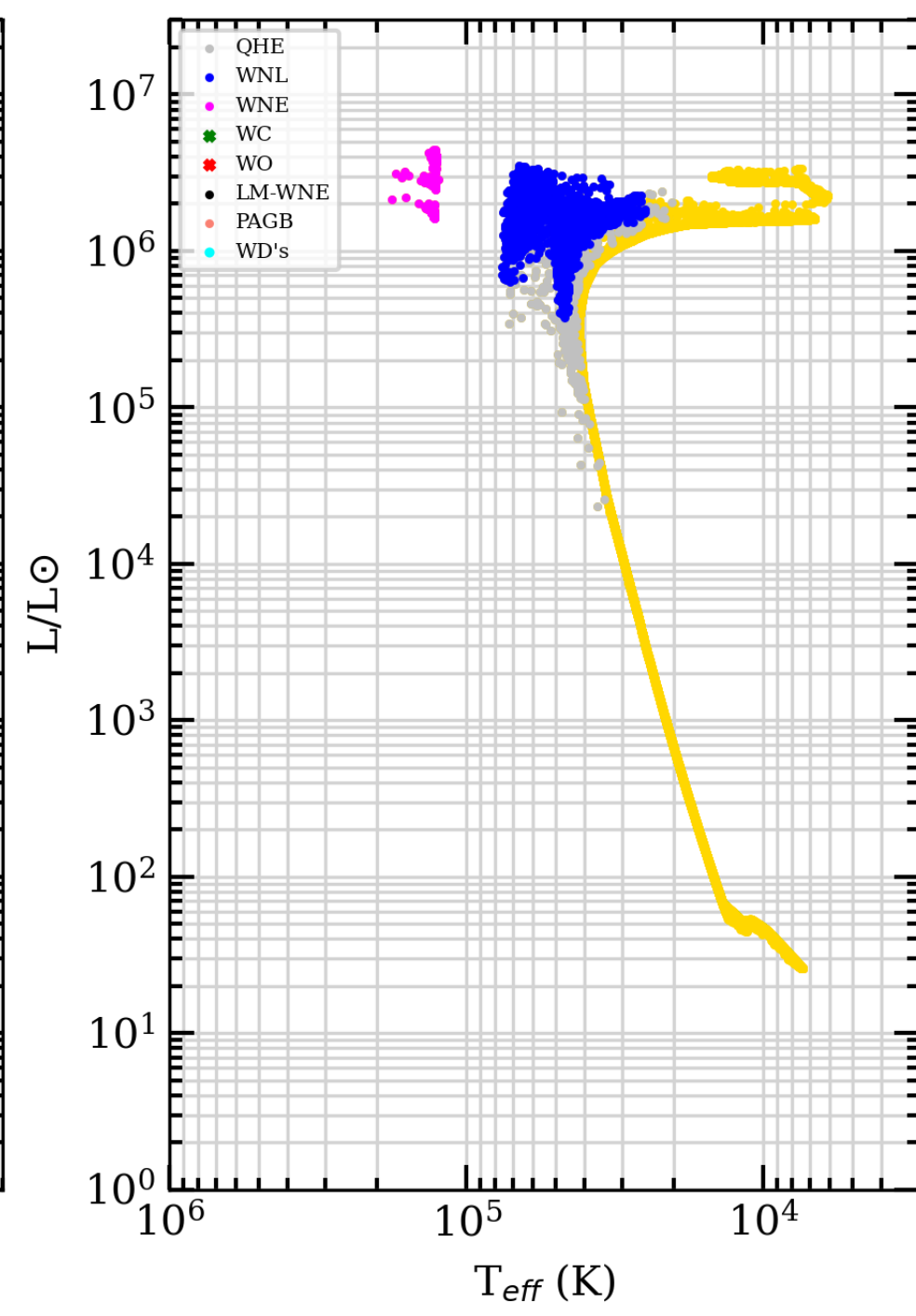
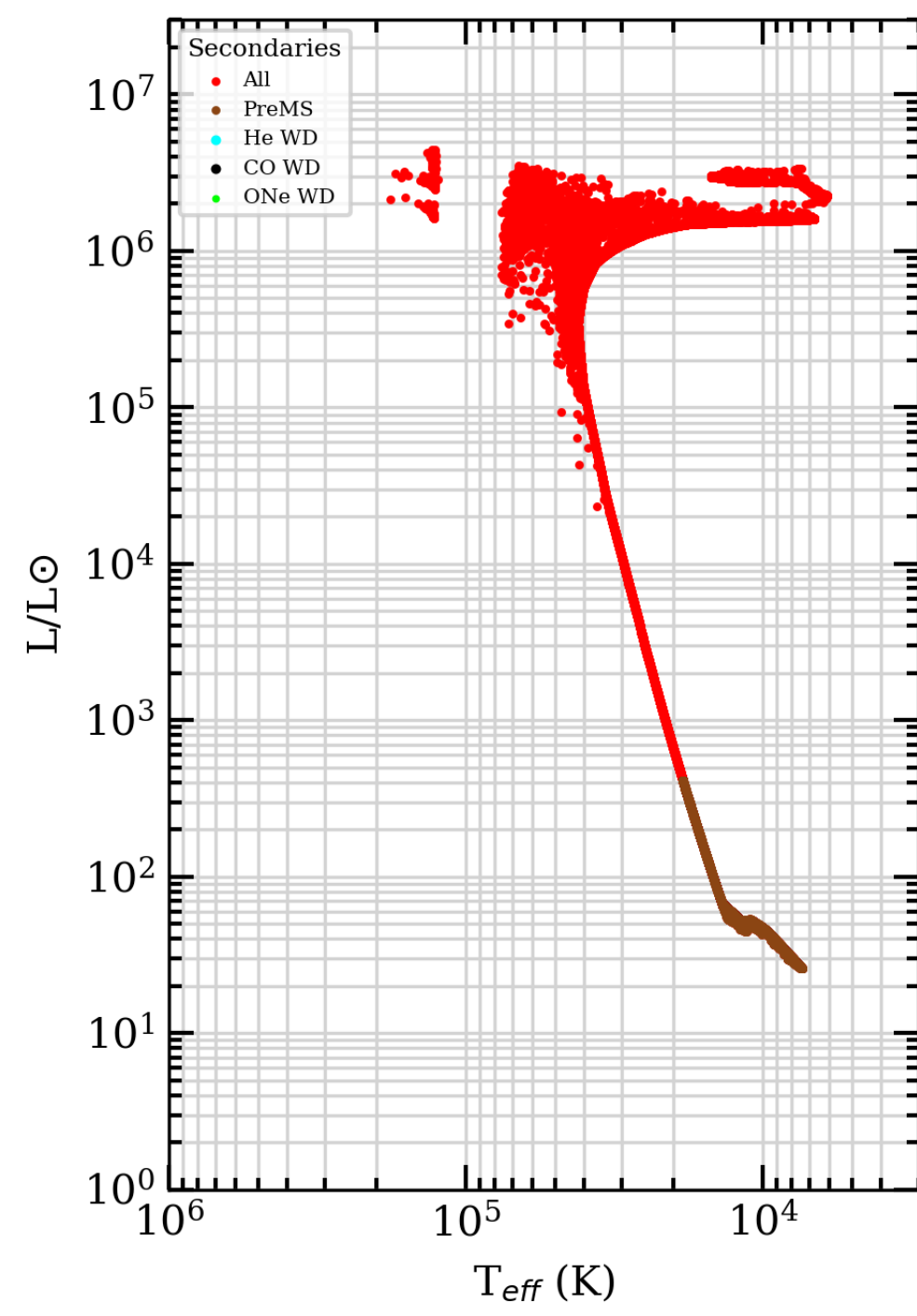
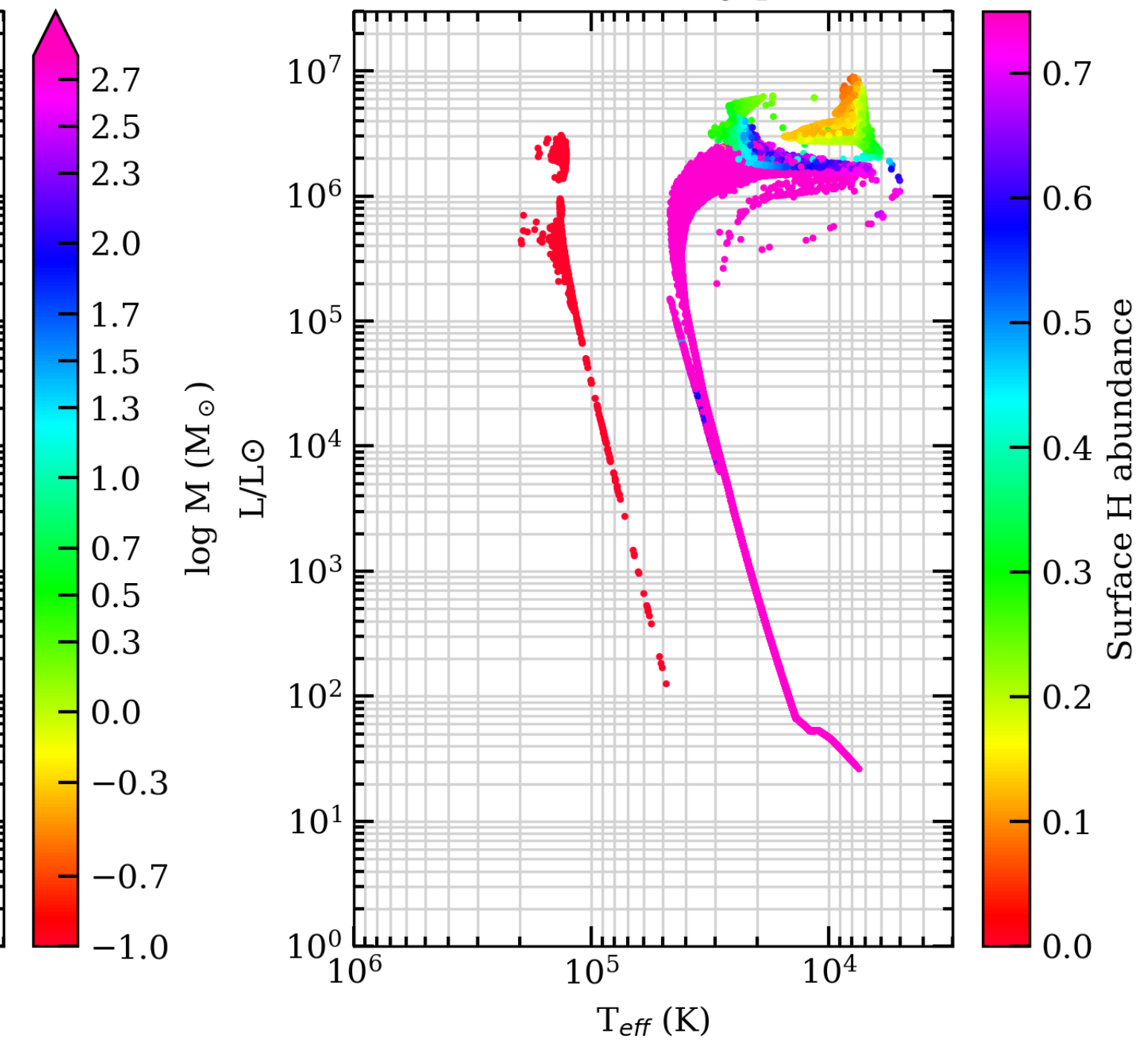
SEVN2.3 STD binary star tracks



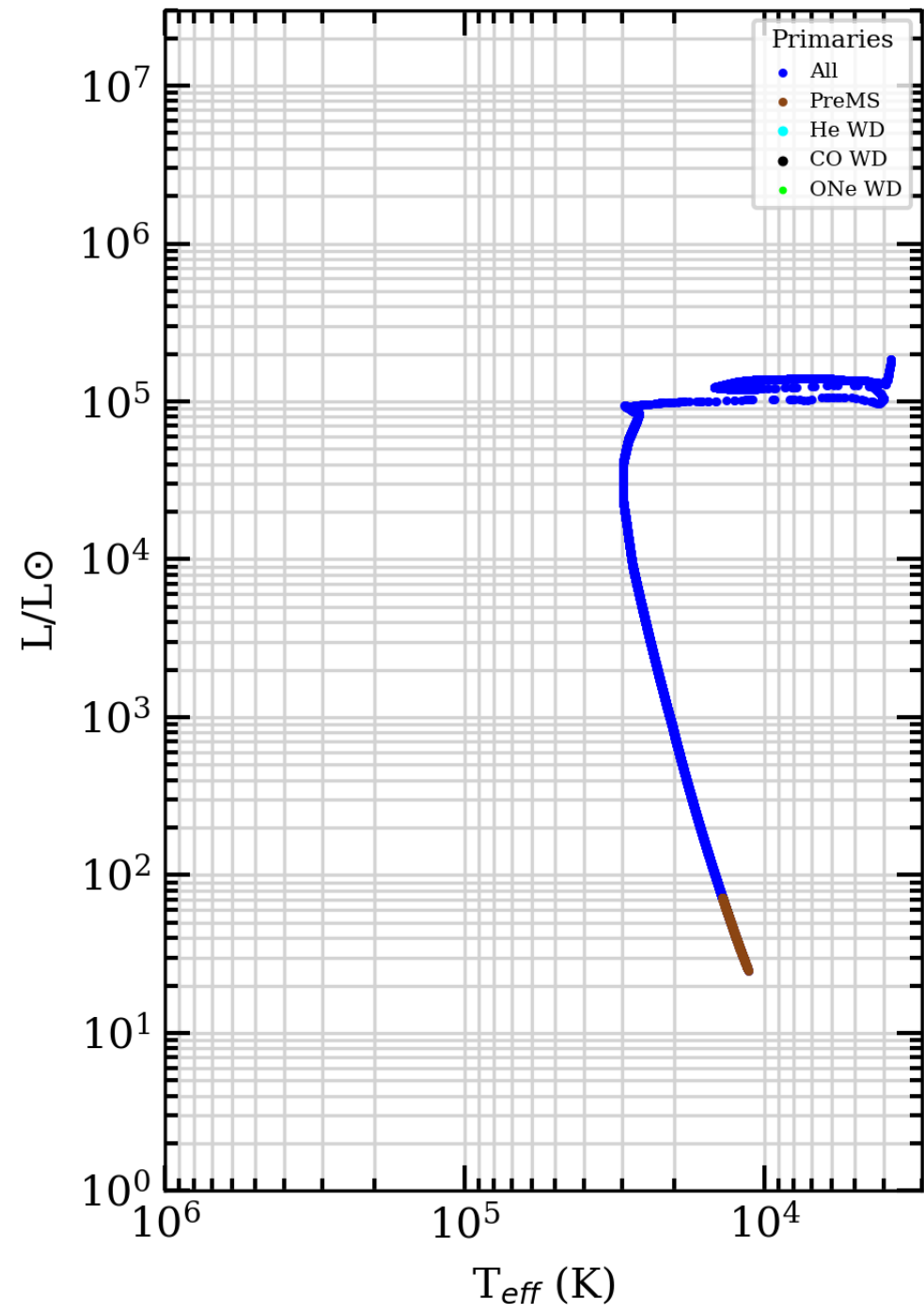
April 2023



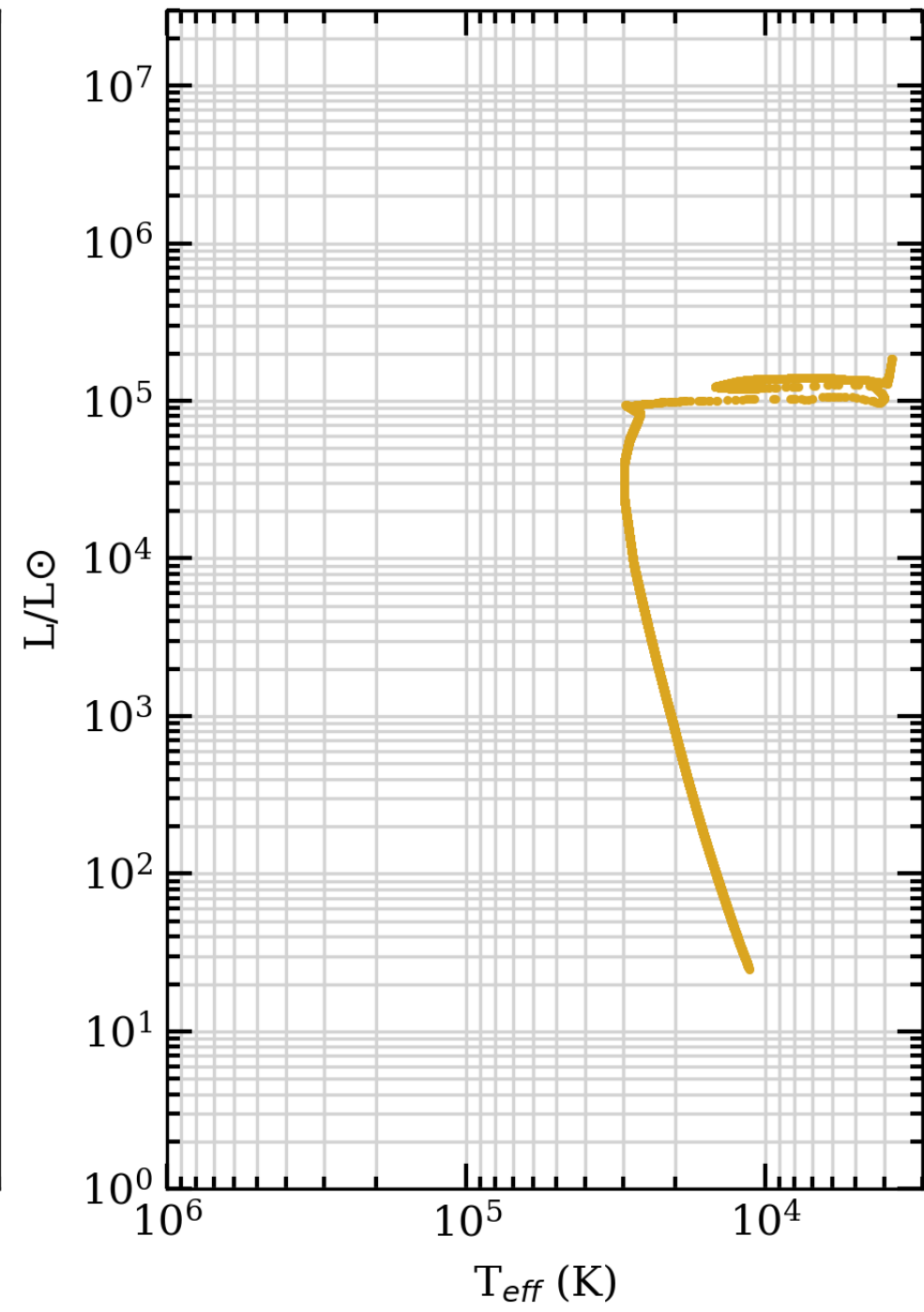
156250 binary pairs



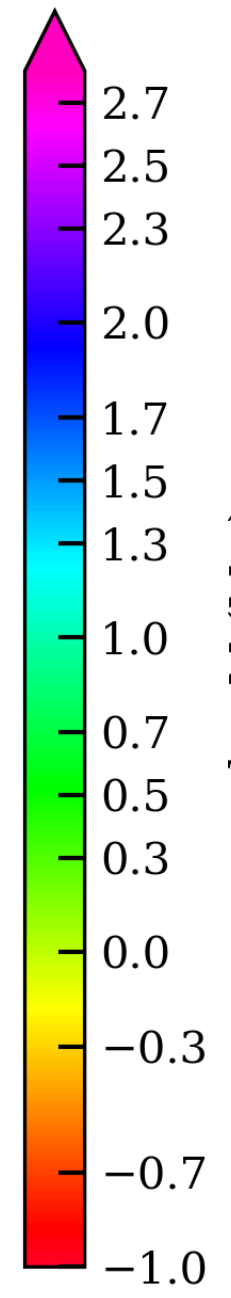
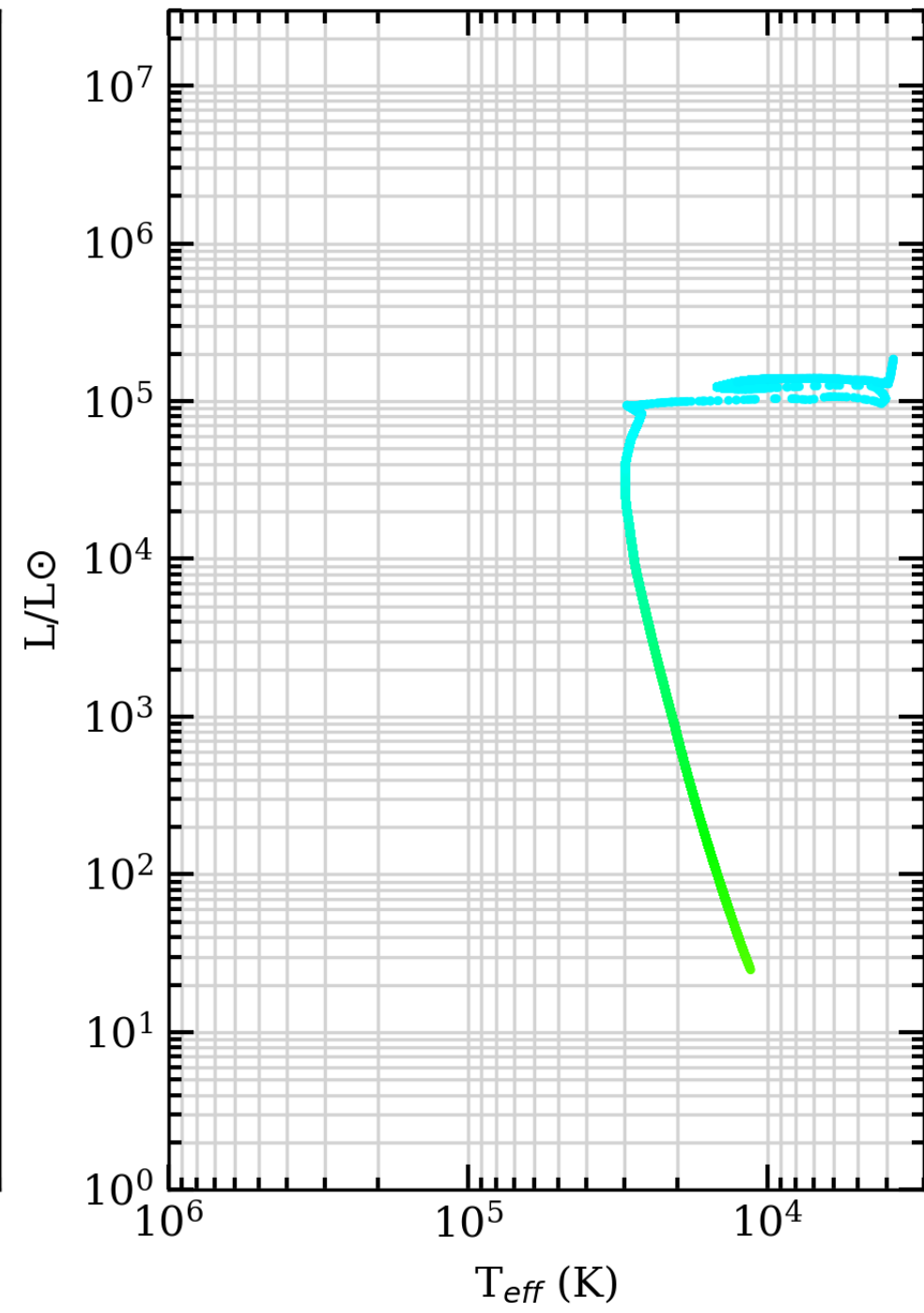
Z=0.004, t=10 Myr



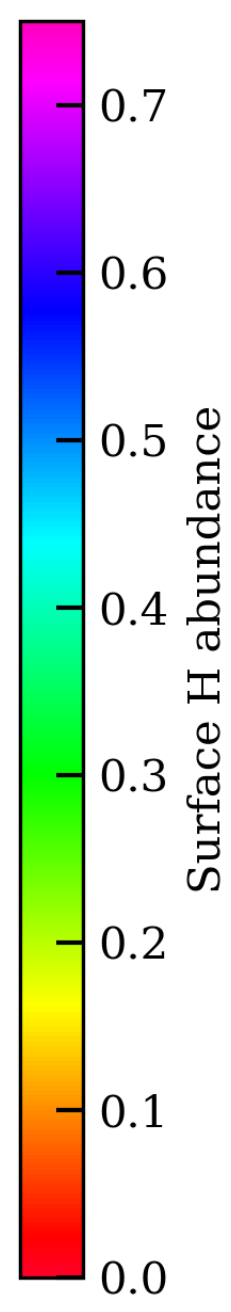
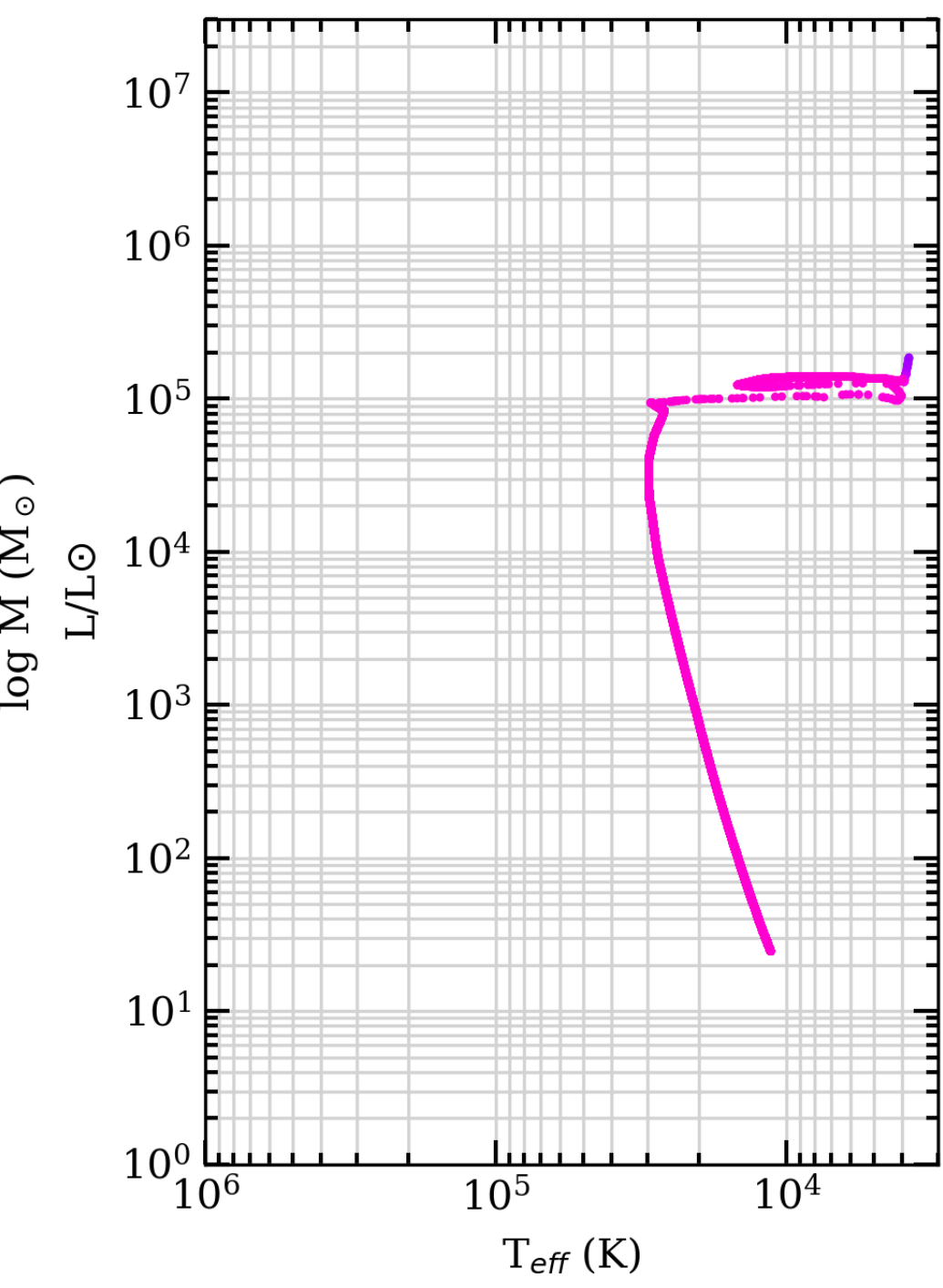
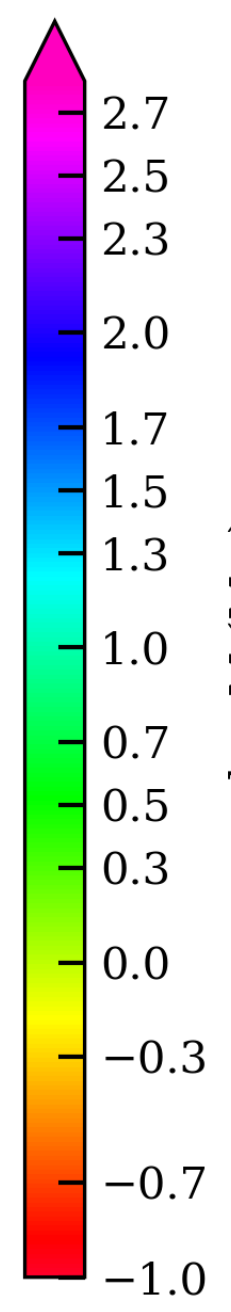
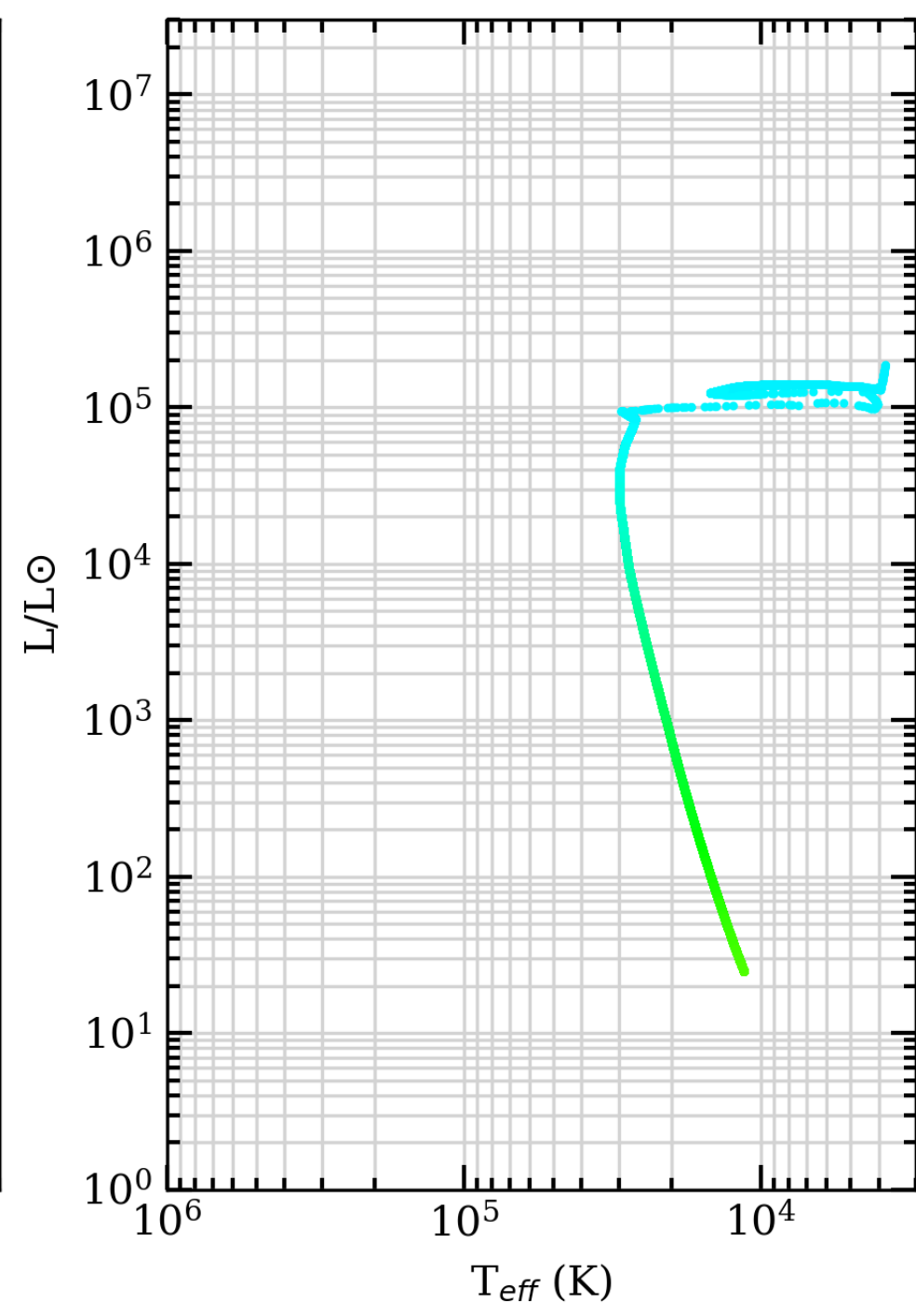
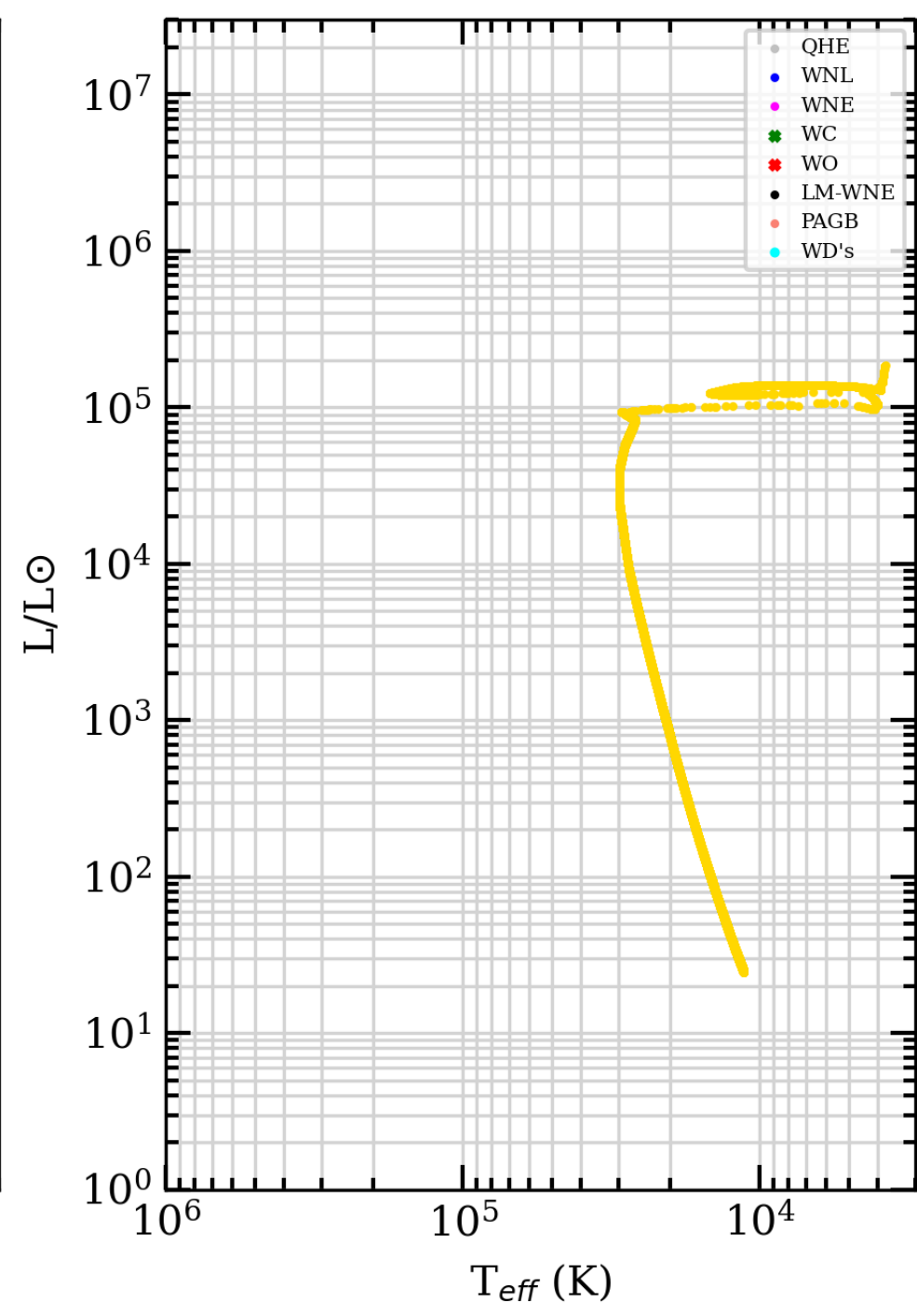
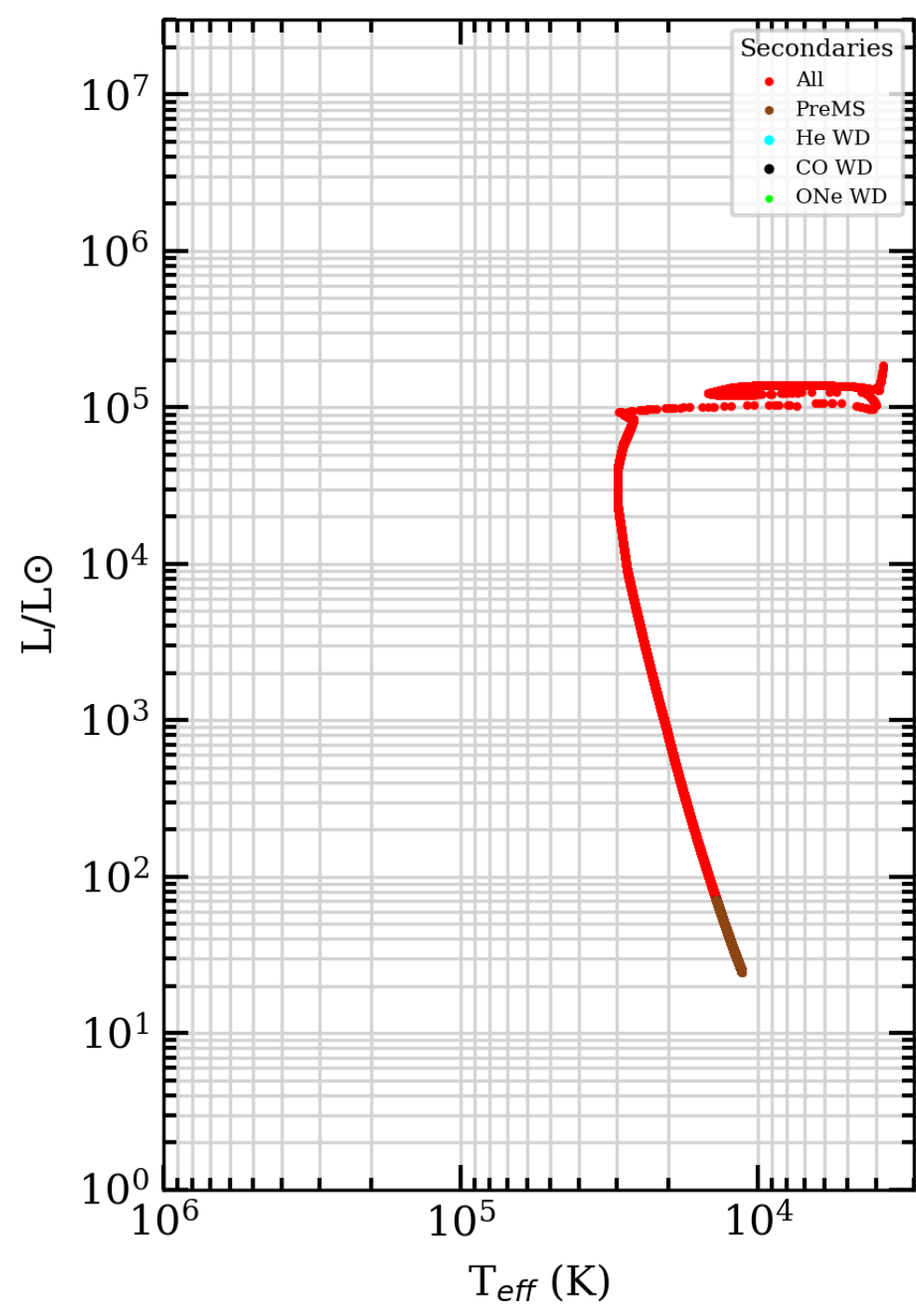
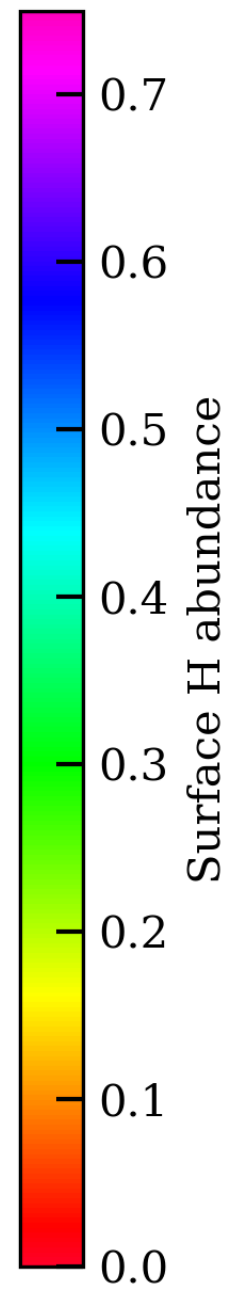
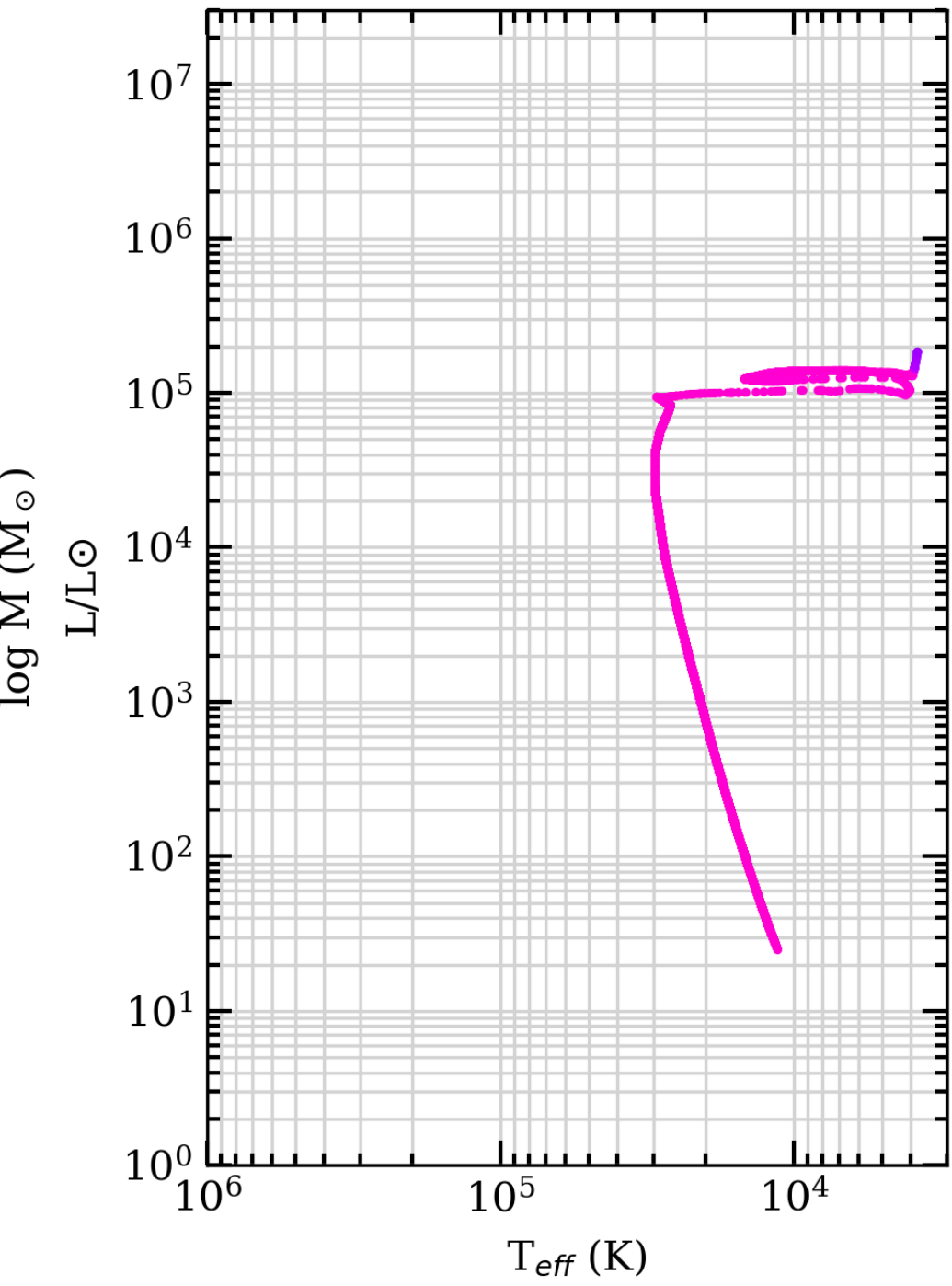
SEVN2.3 VLA binary star tracks



April 2023



156250 binary pairs

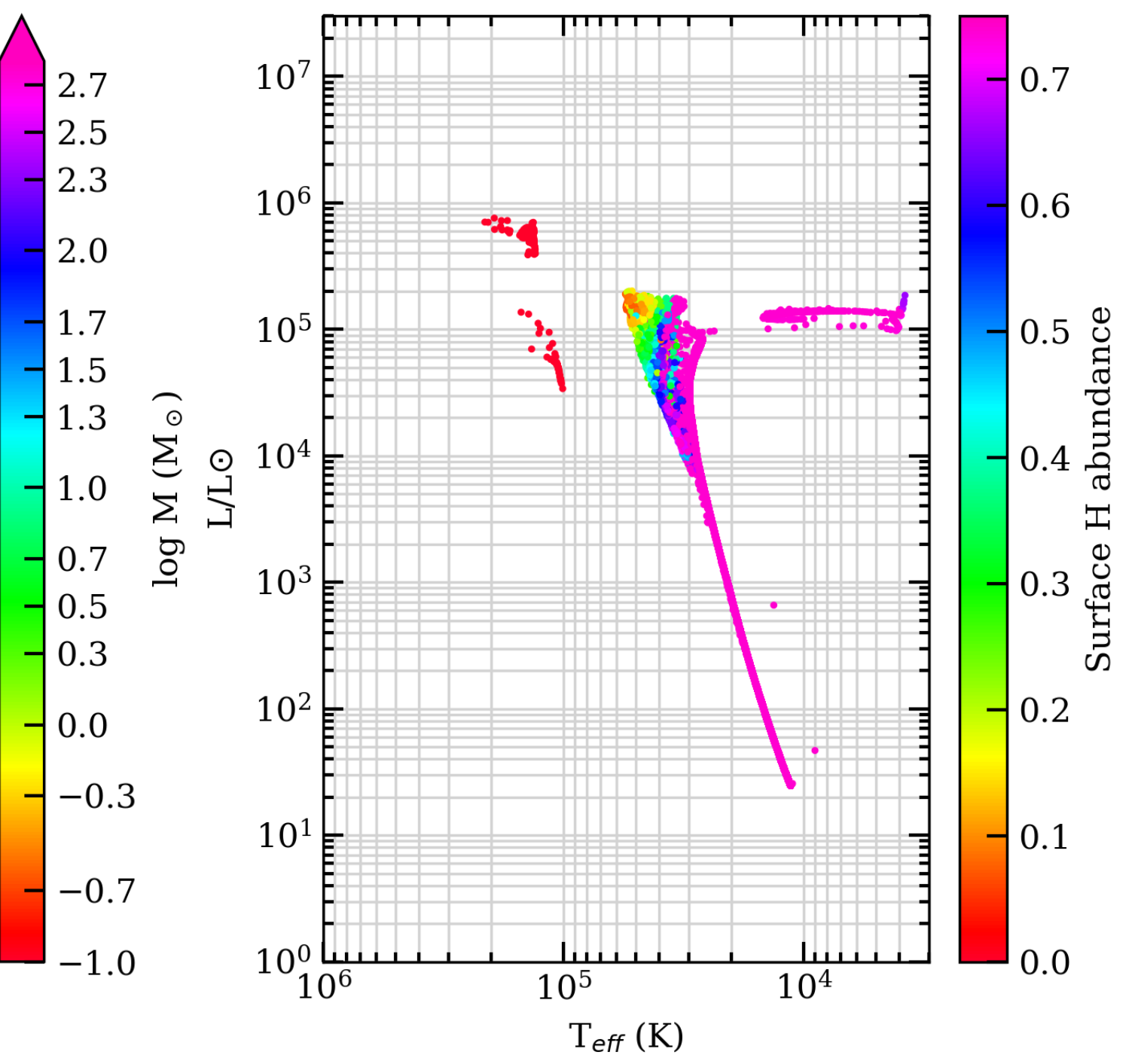
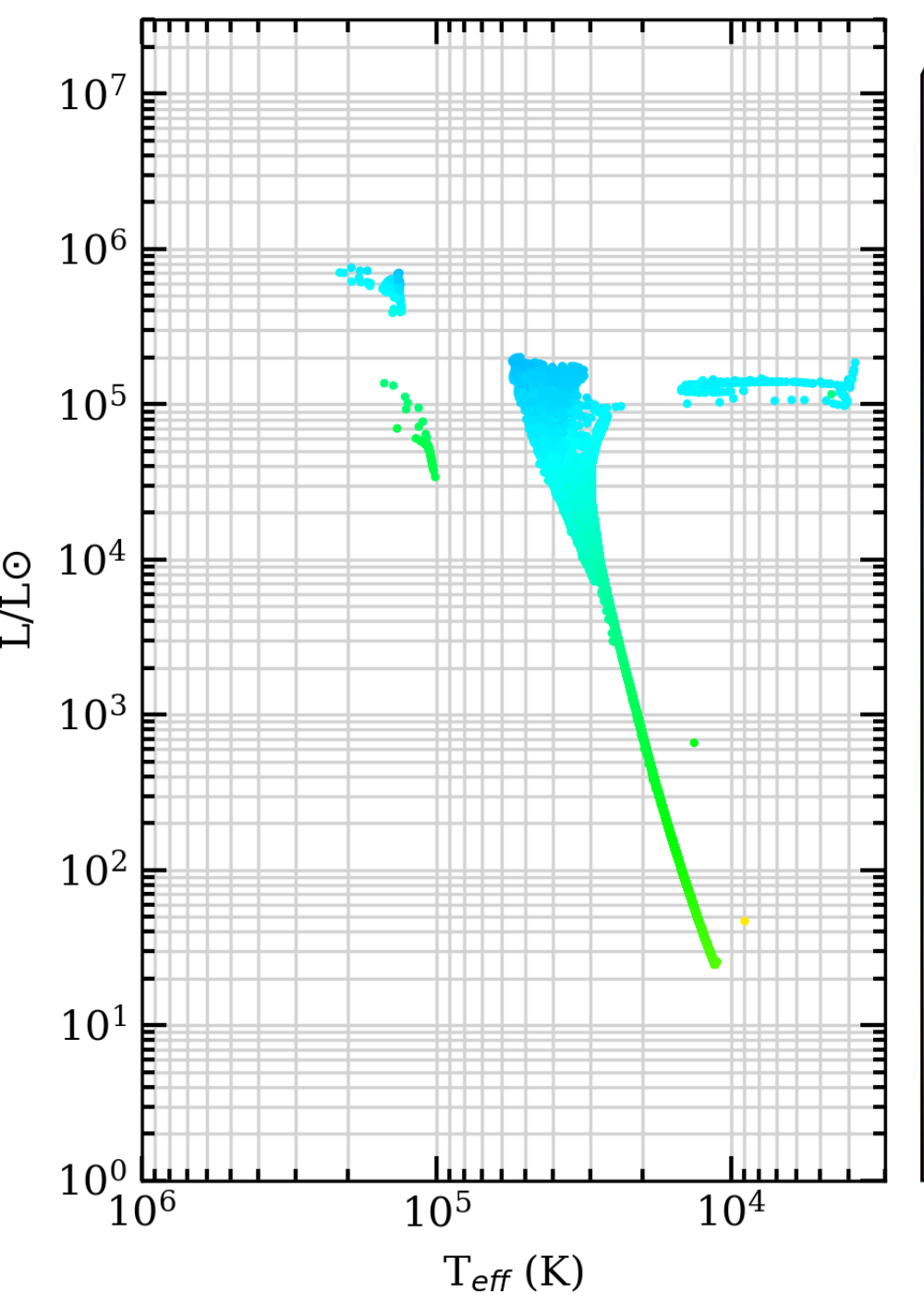
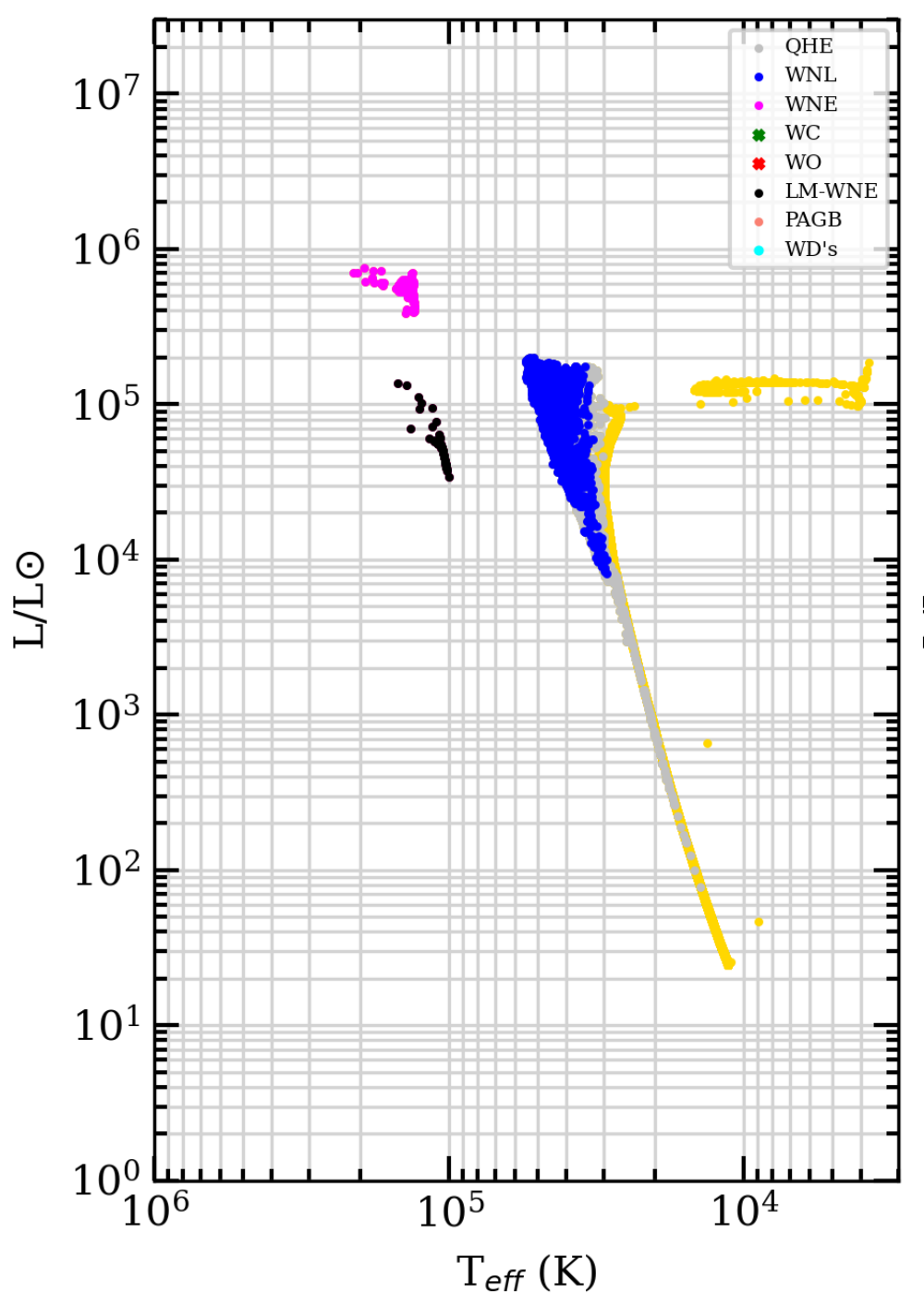
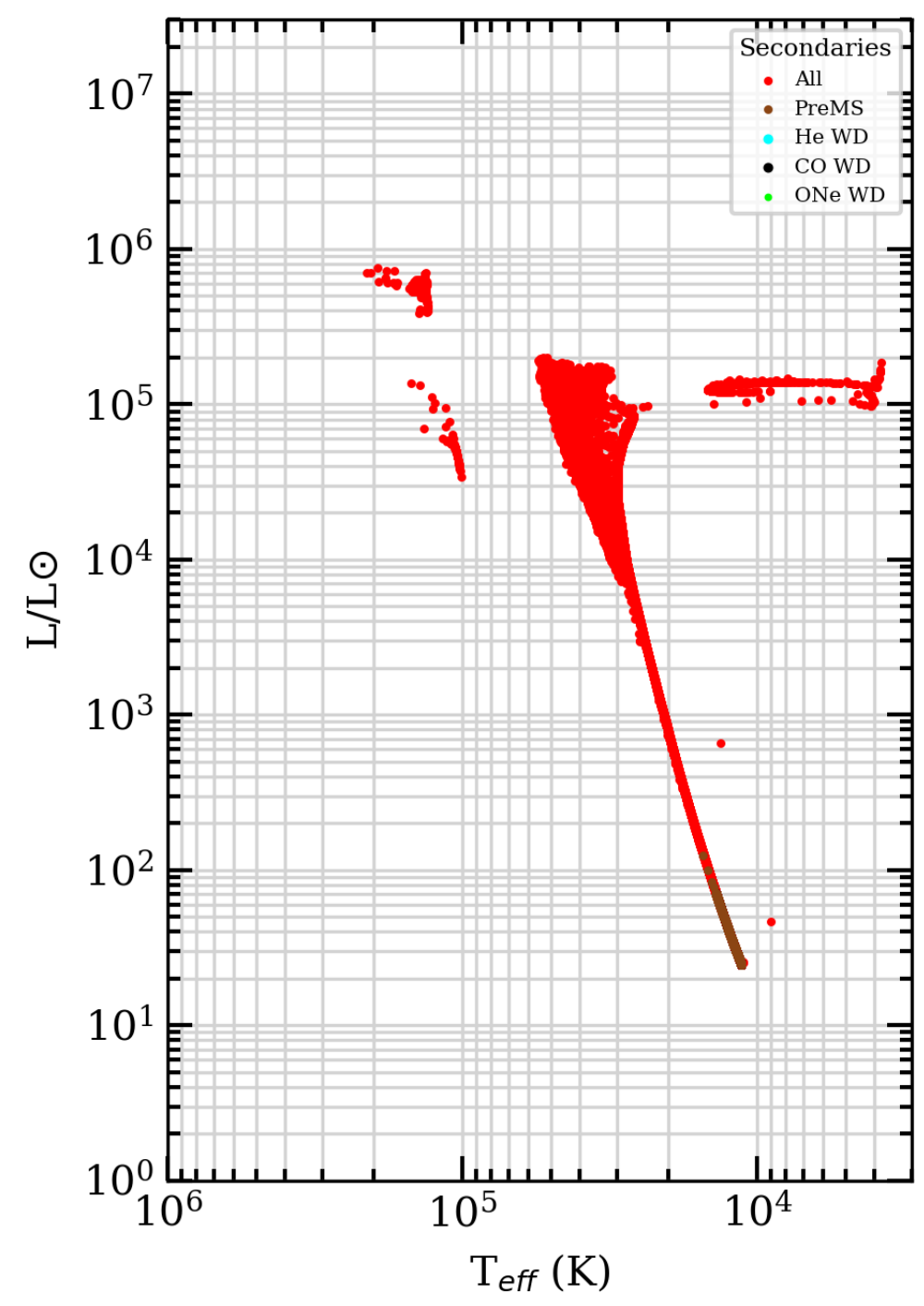
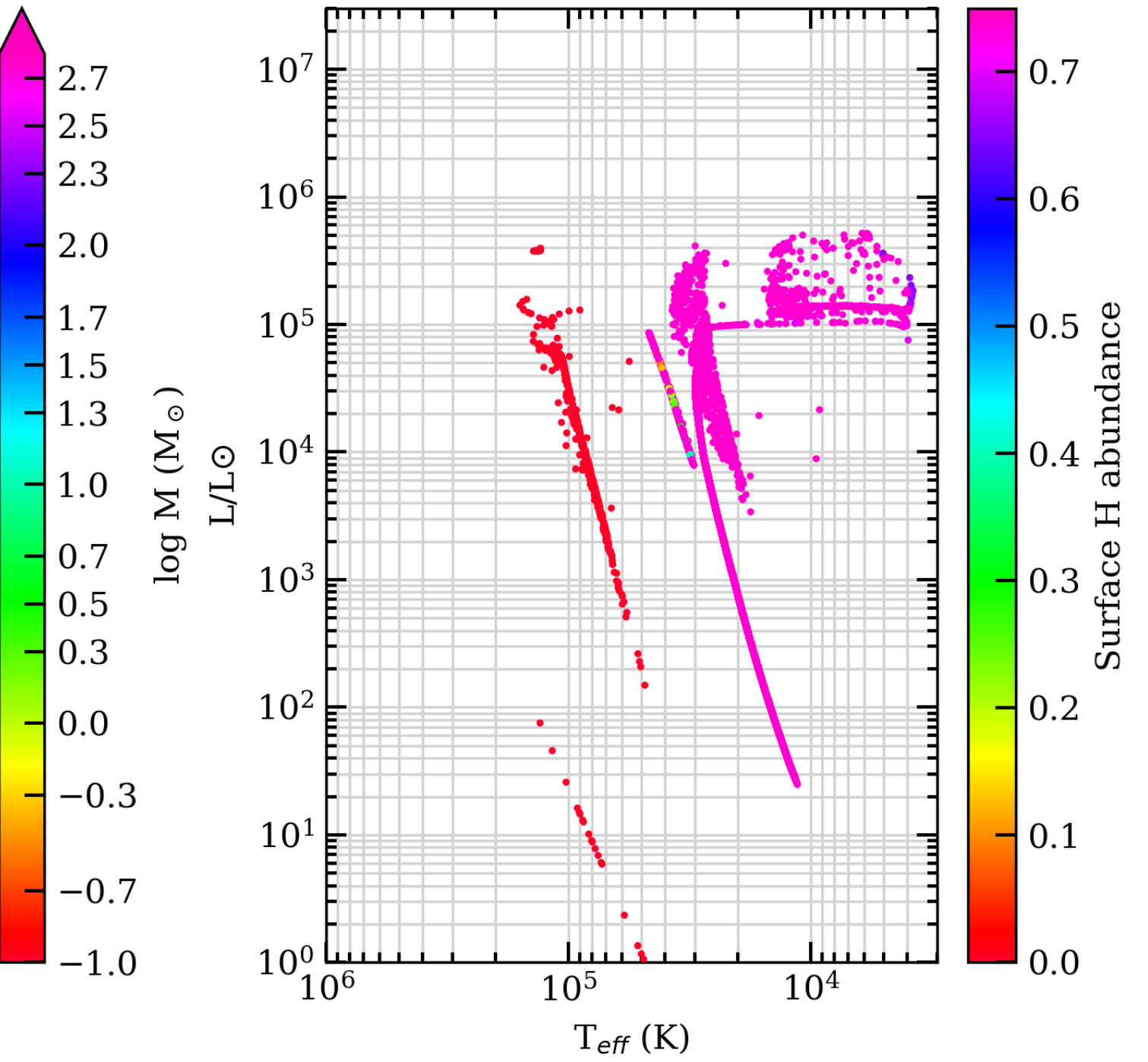
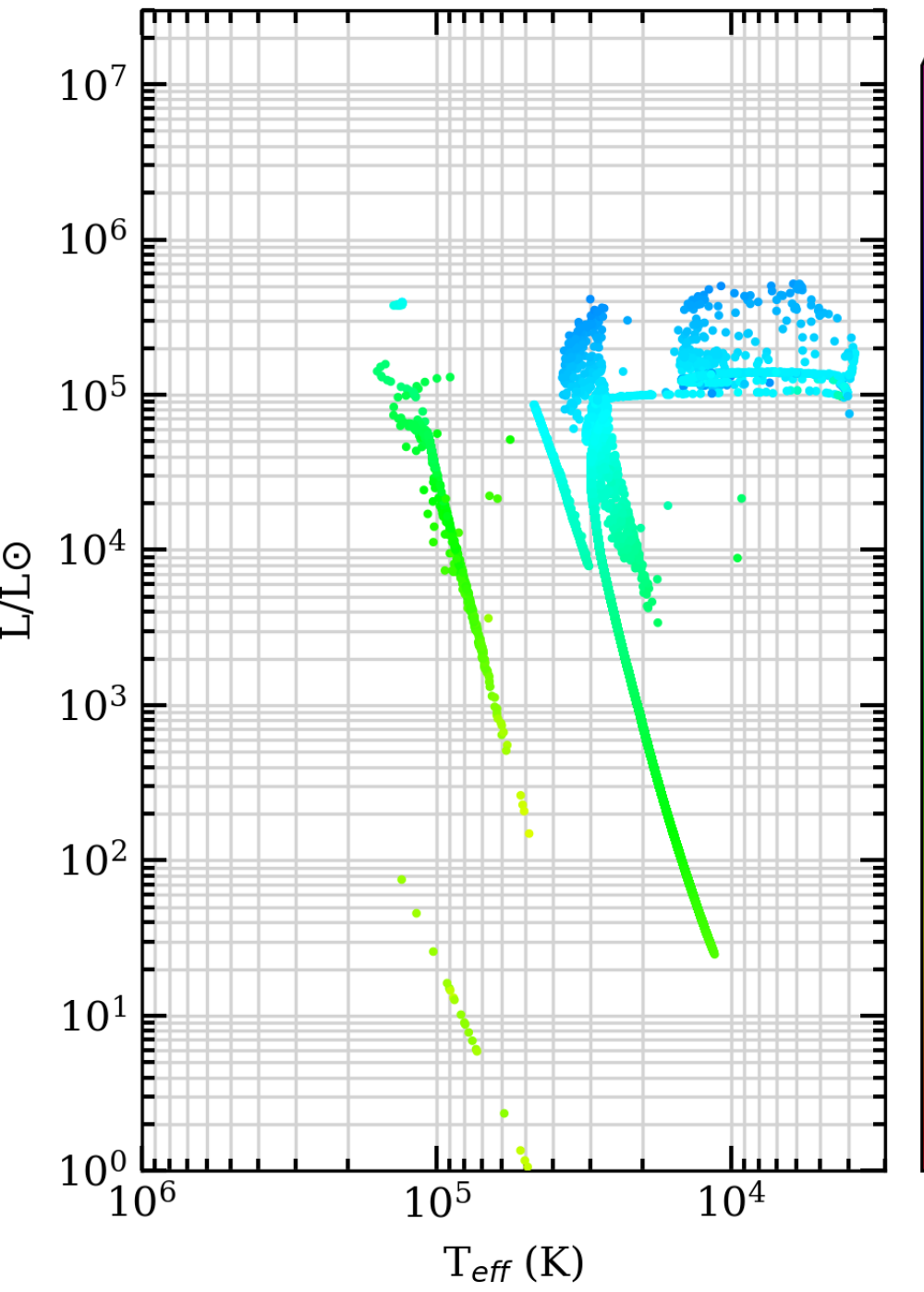
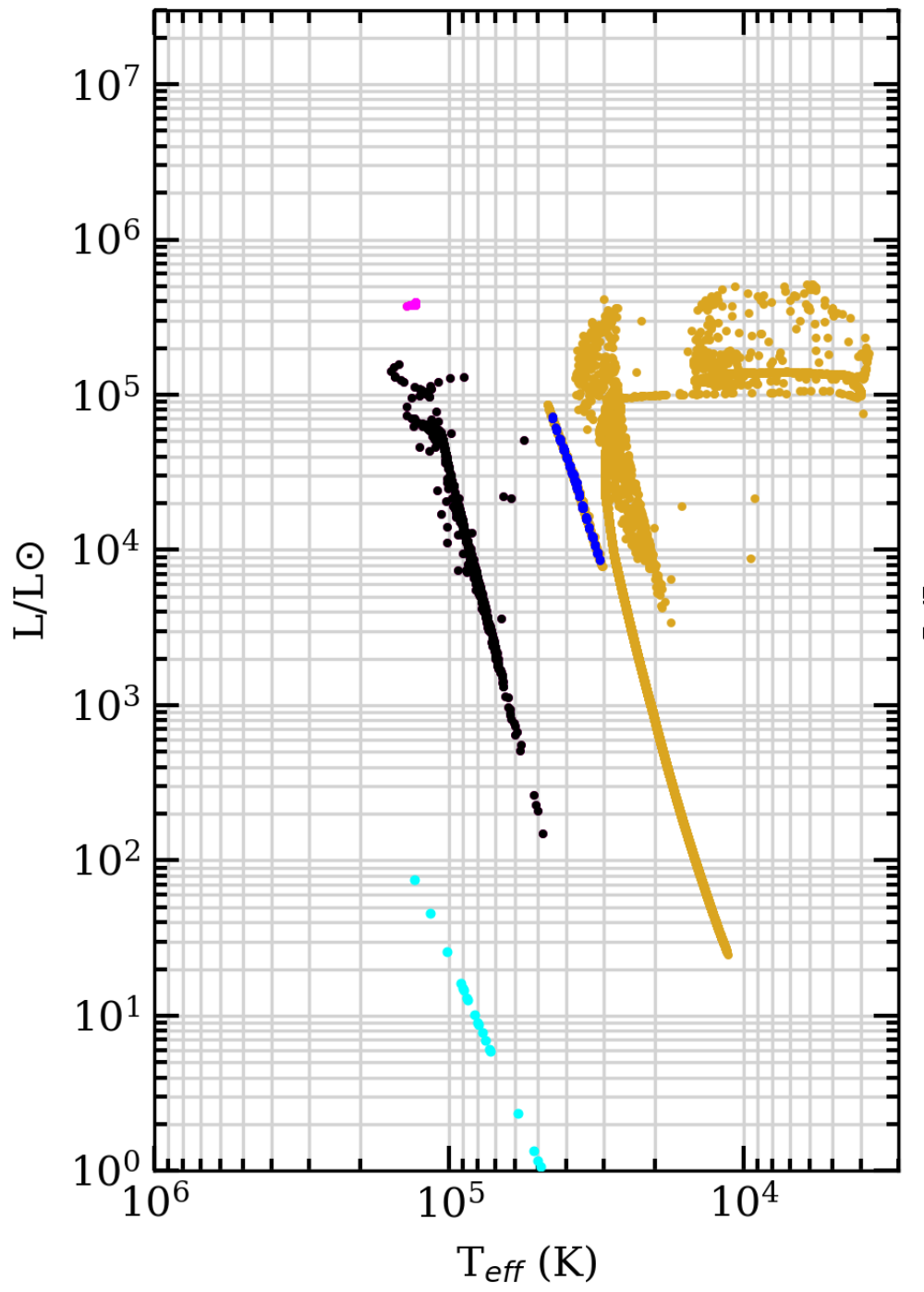
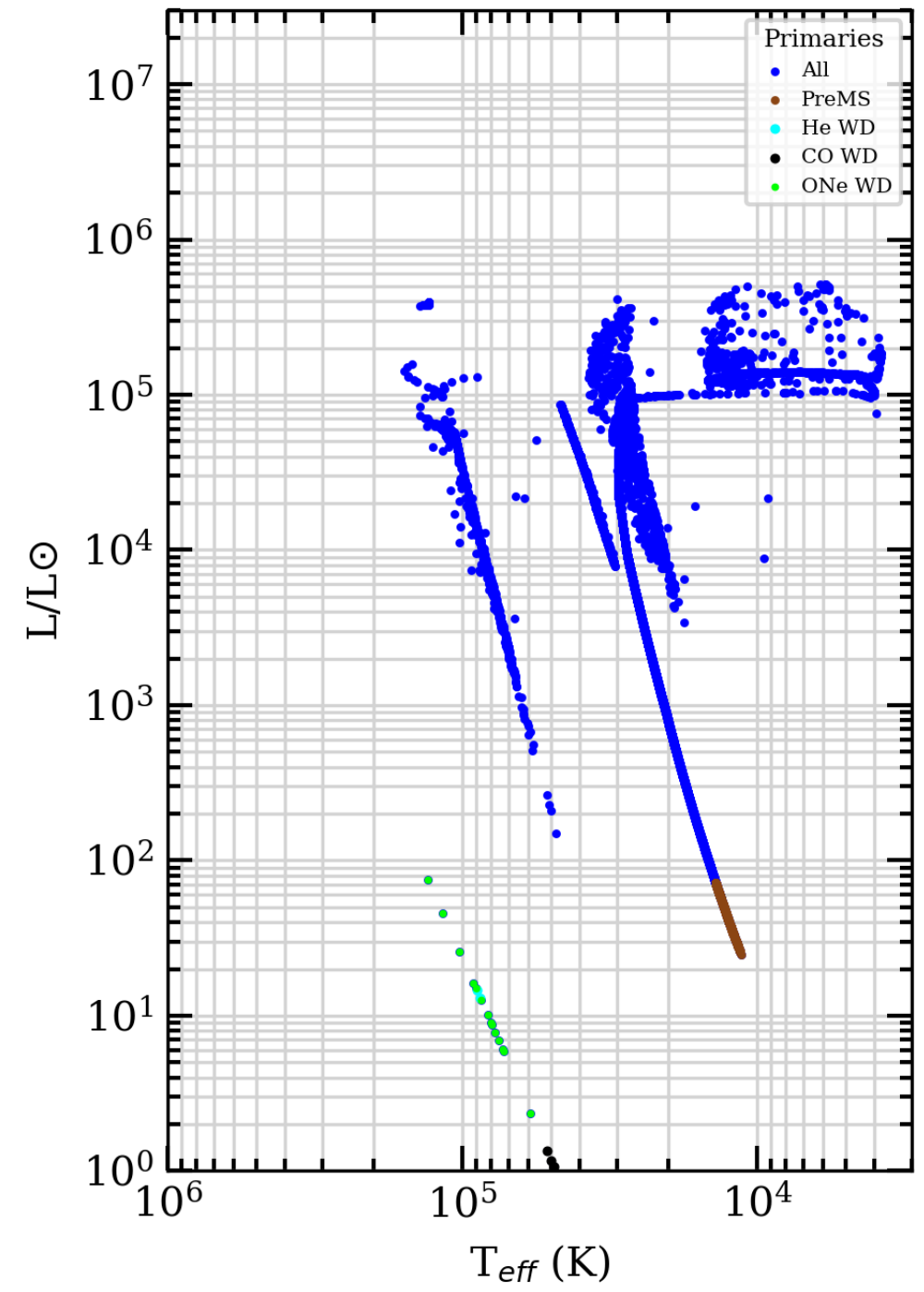


Z=0.004, t=10 Myr

SEVN2.3 STD binary star tracks

April 2023

156250 binary pairs

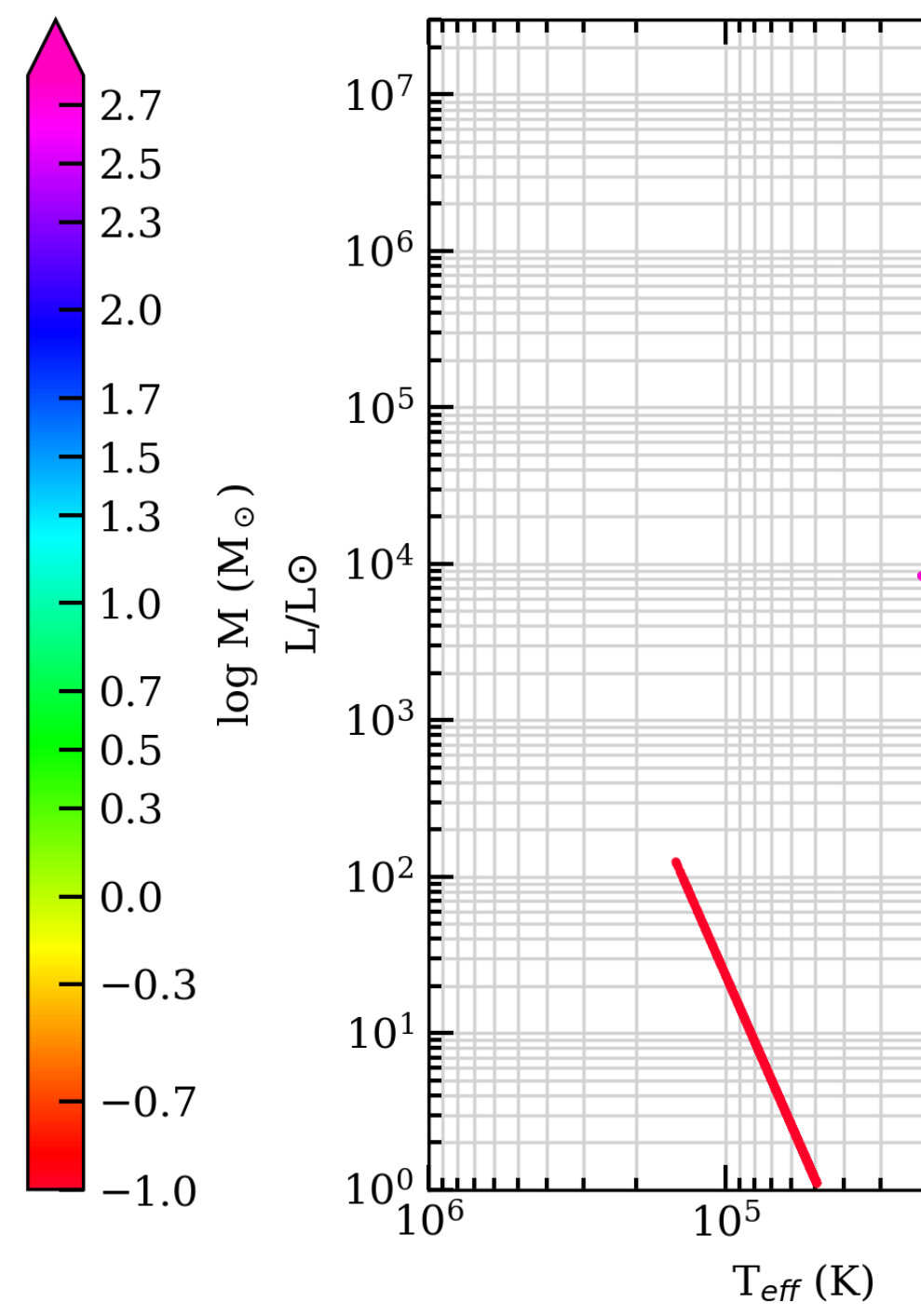
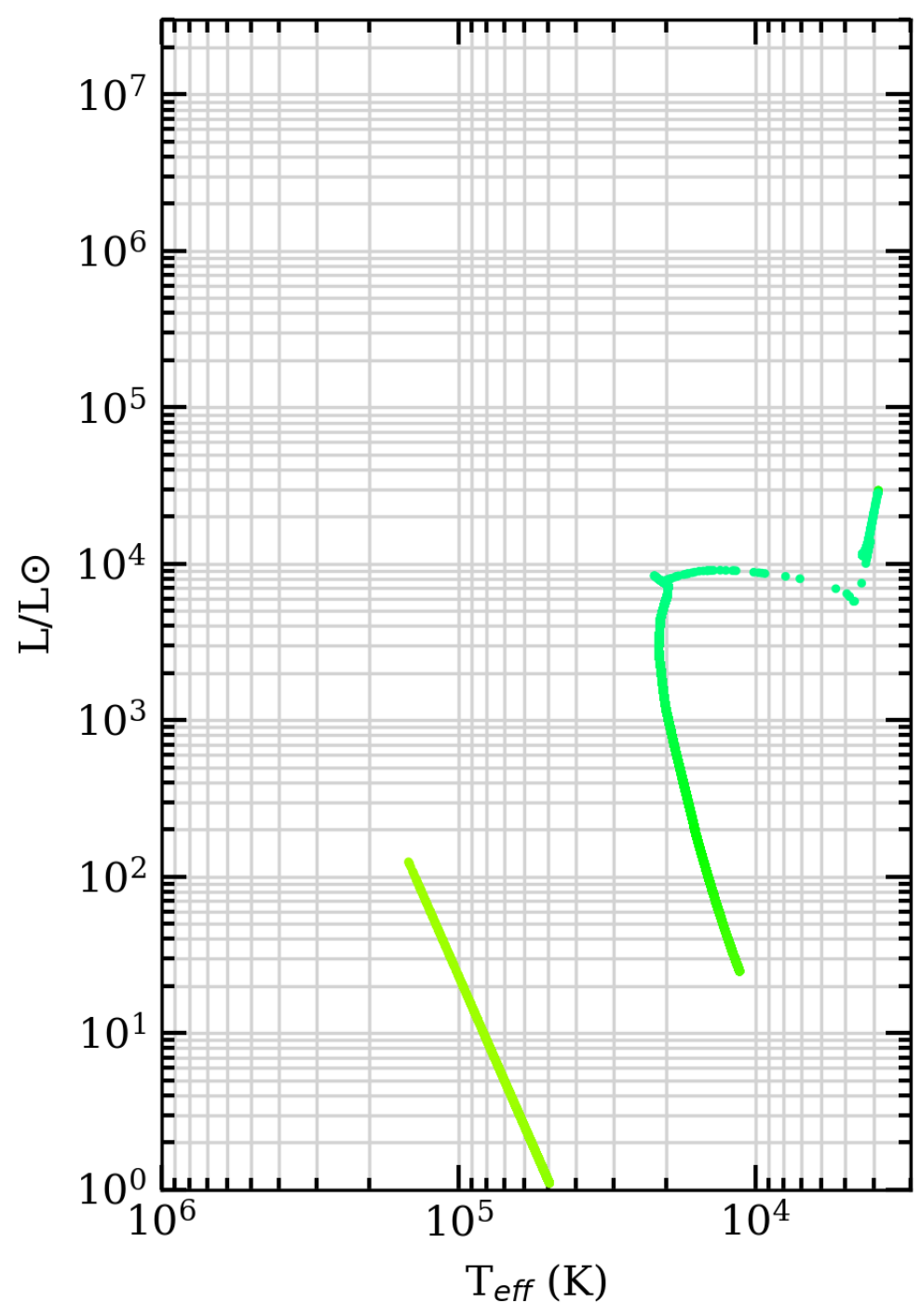
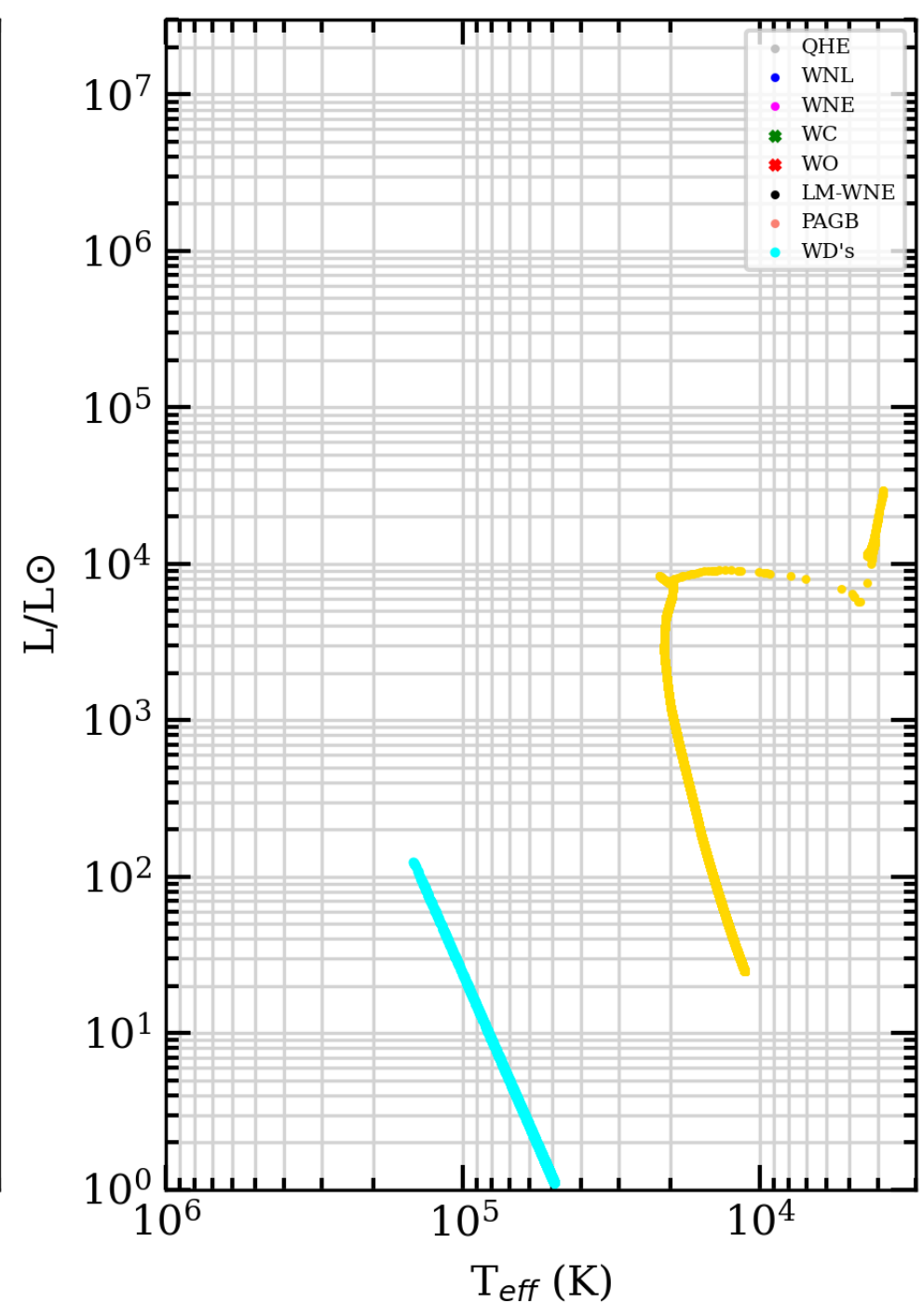
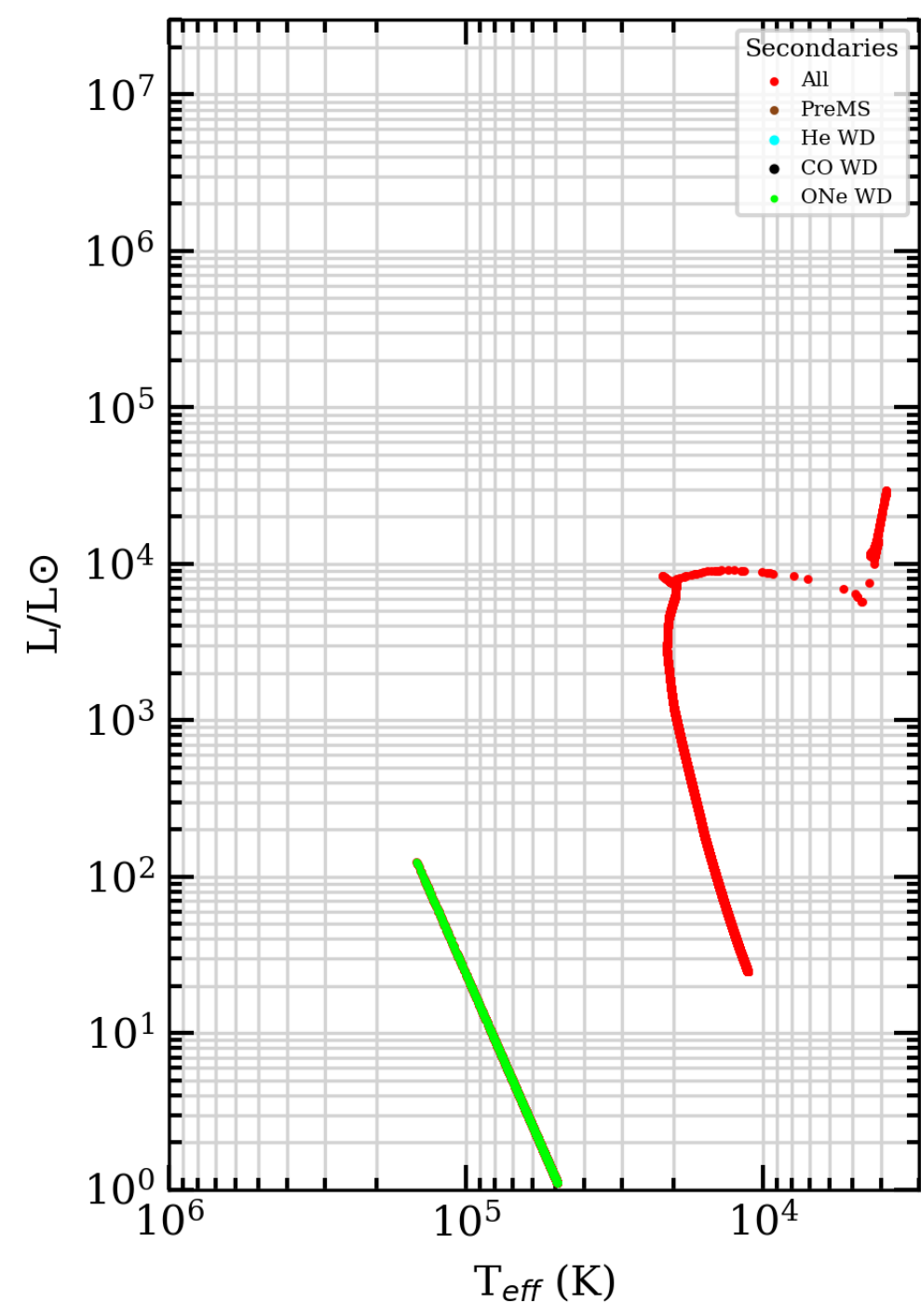
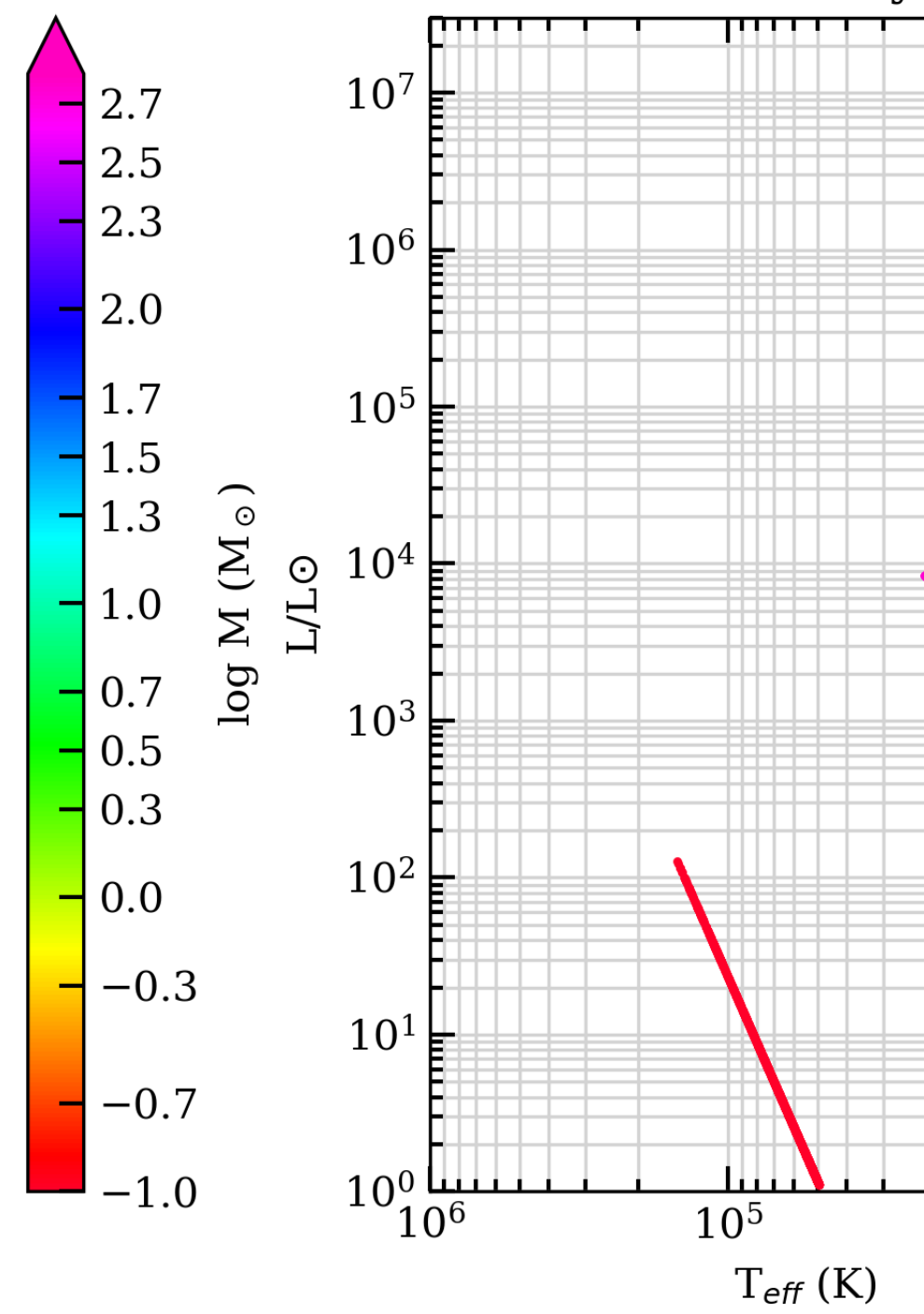
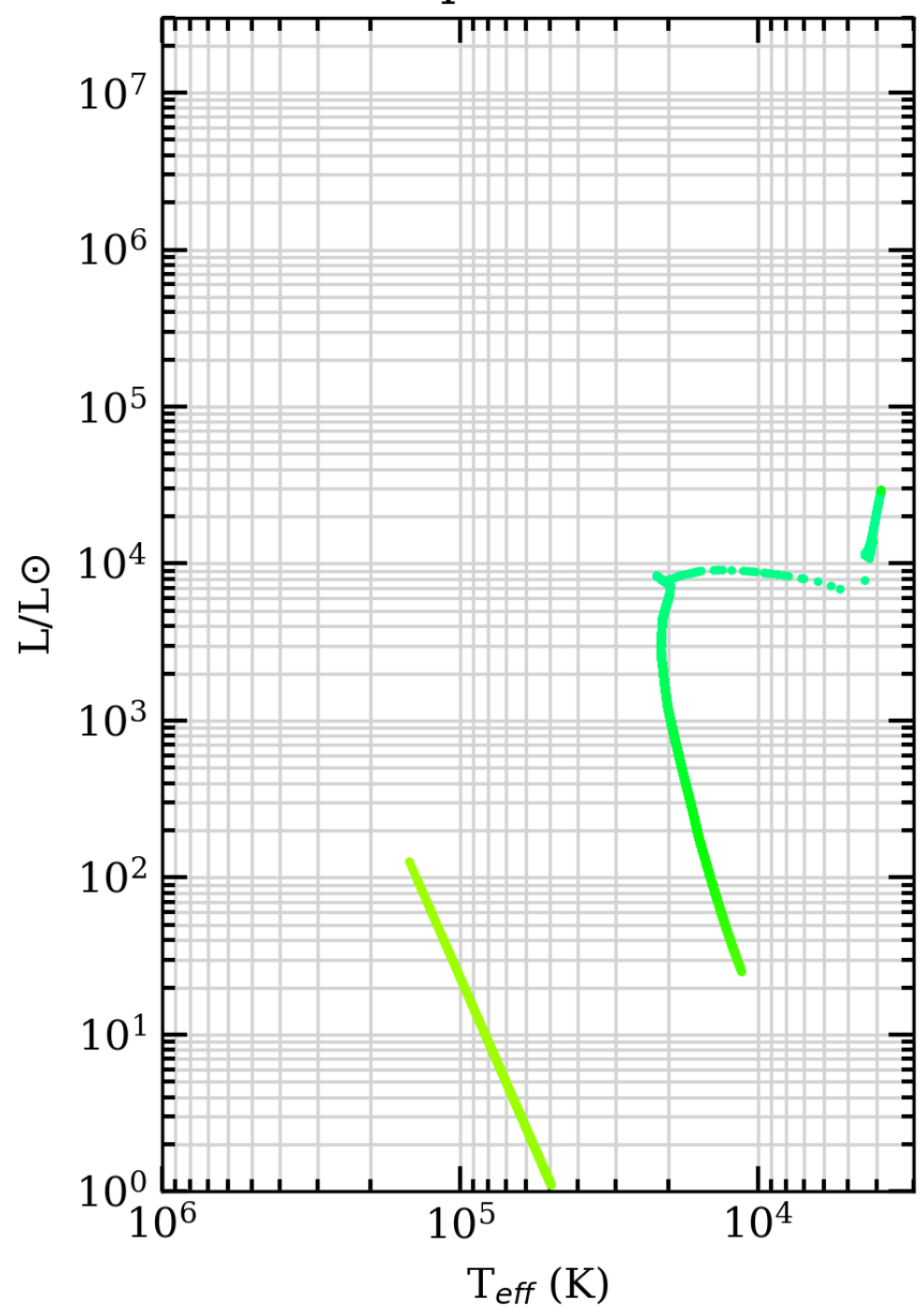
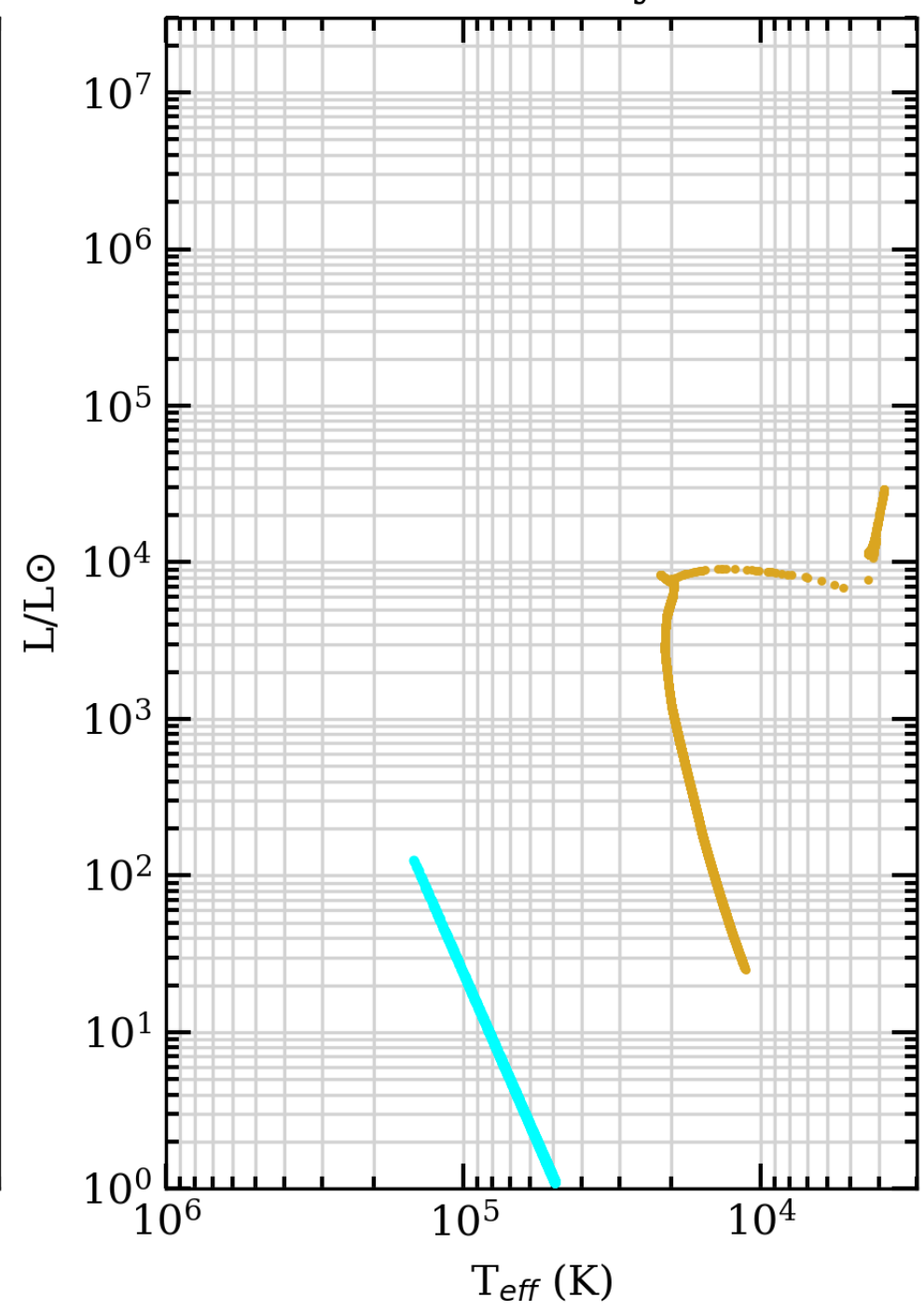
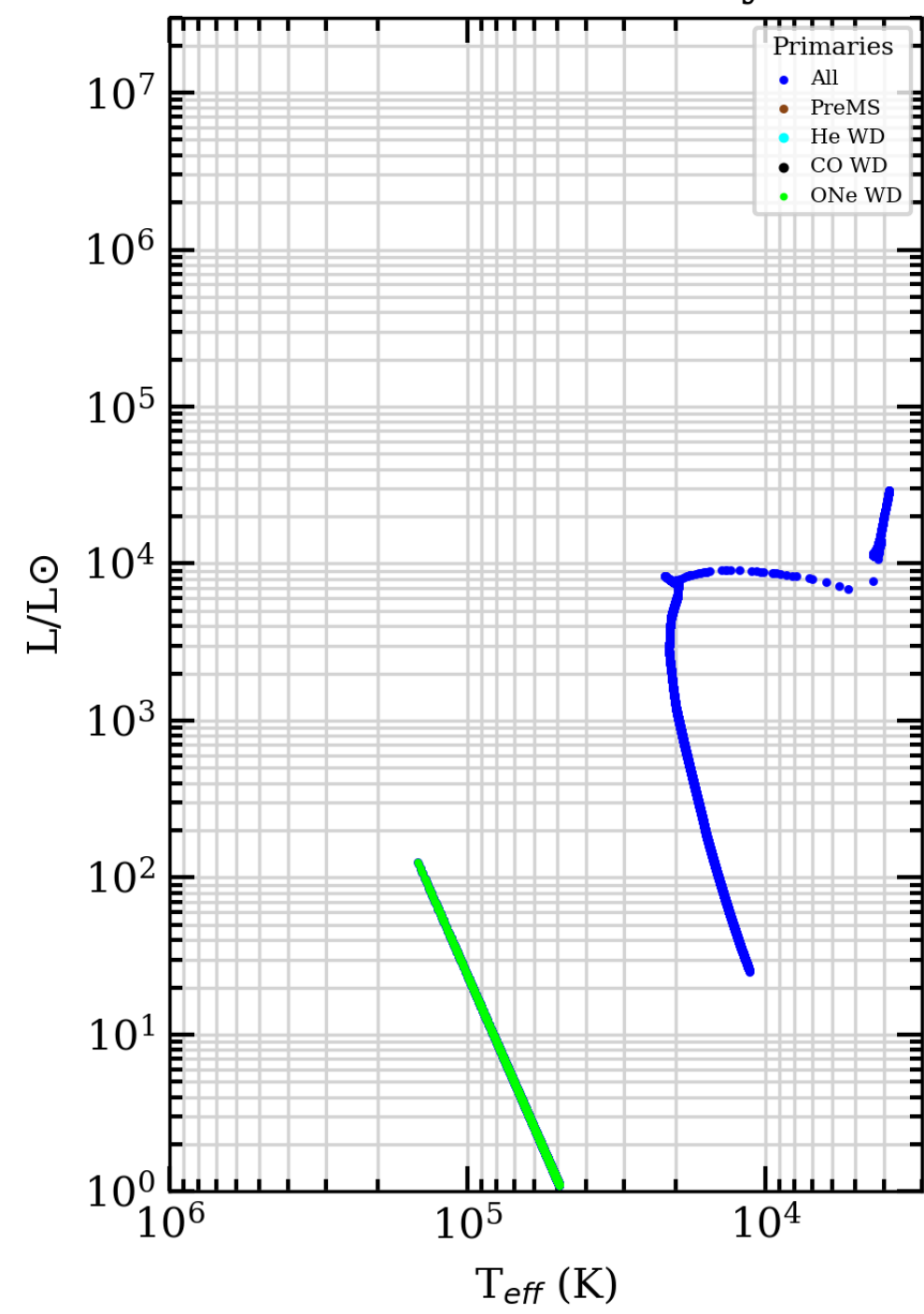


Z=0.004, t=35 Myr

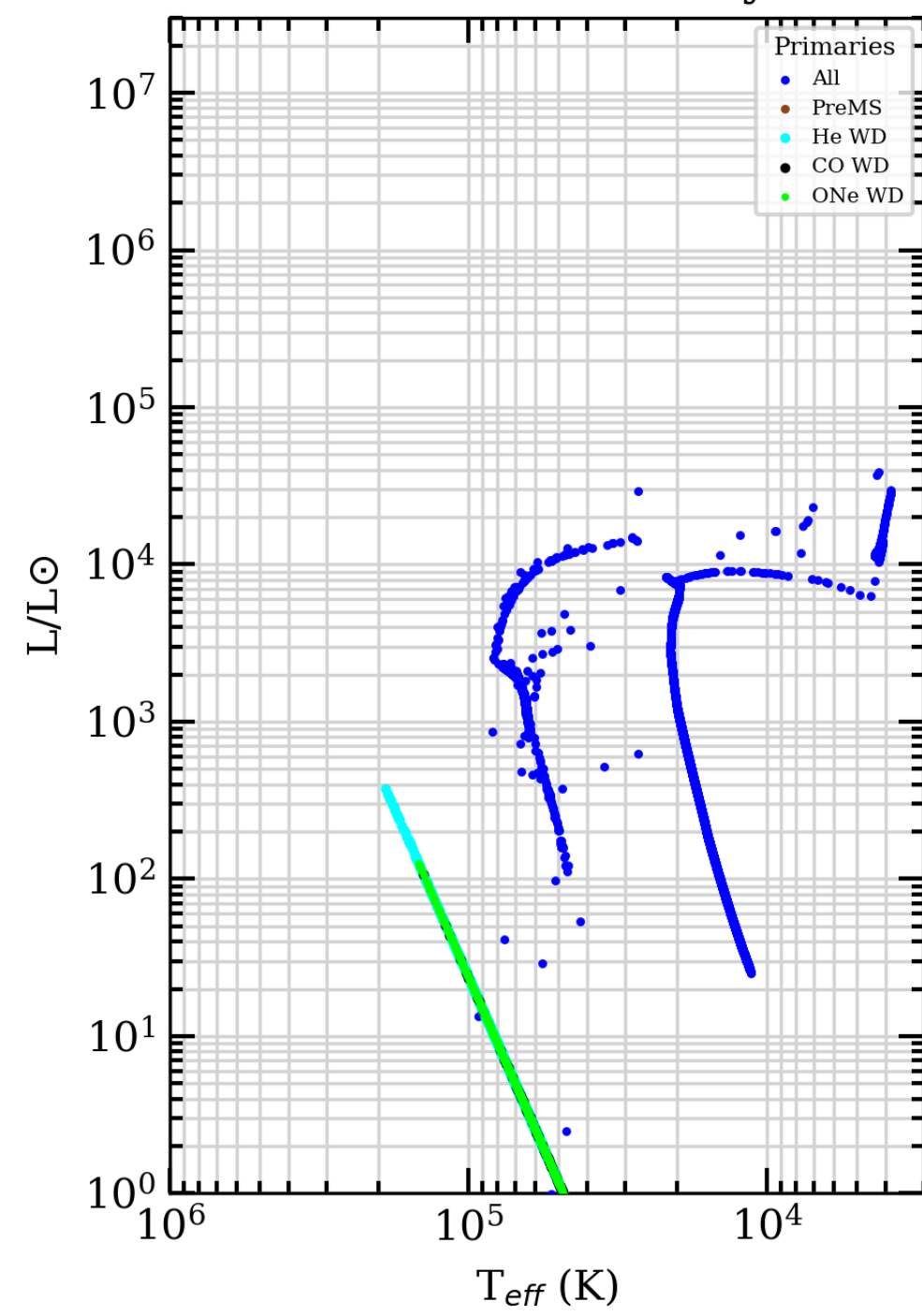
SEVN2.3 VLA binary star tracks

April 2023

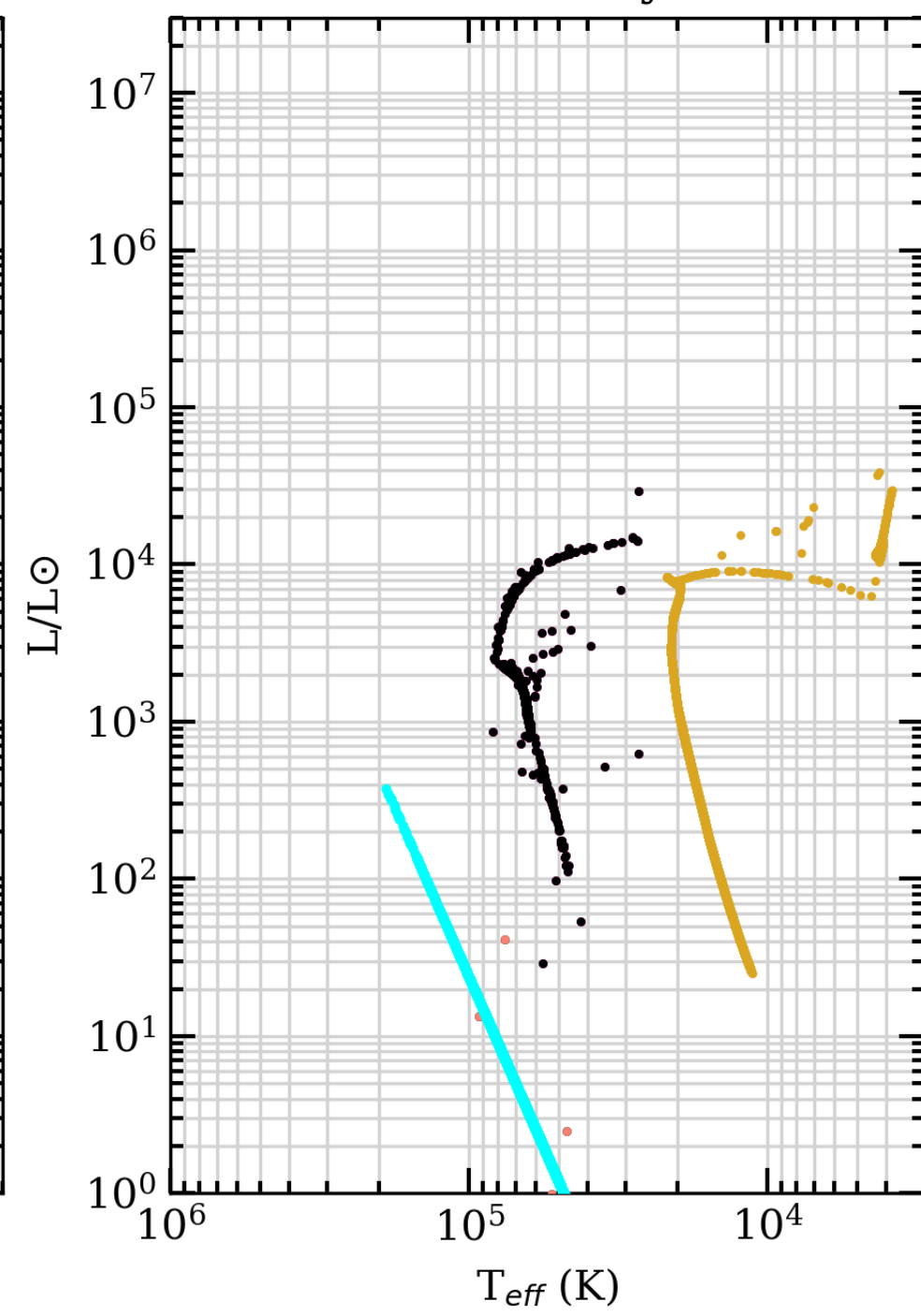
156250 binary pairs



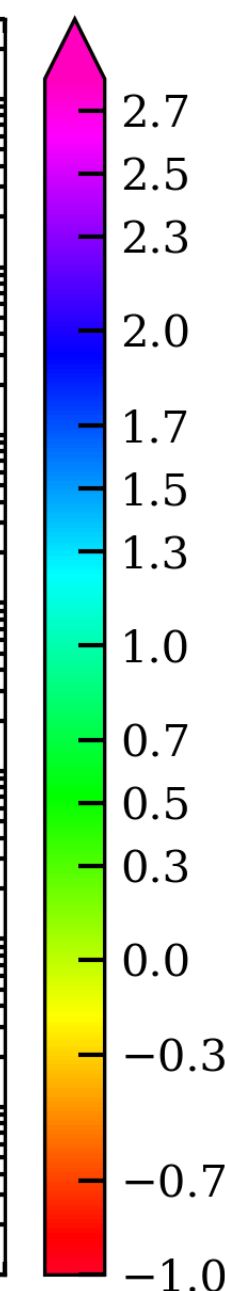
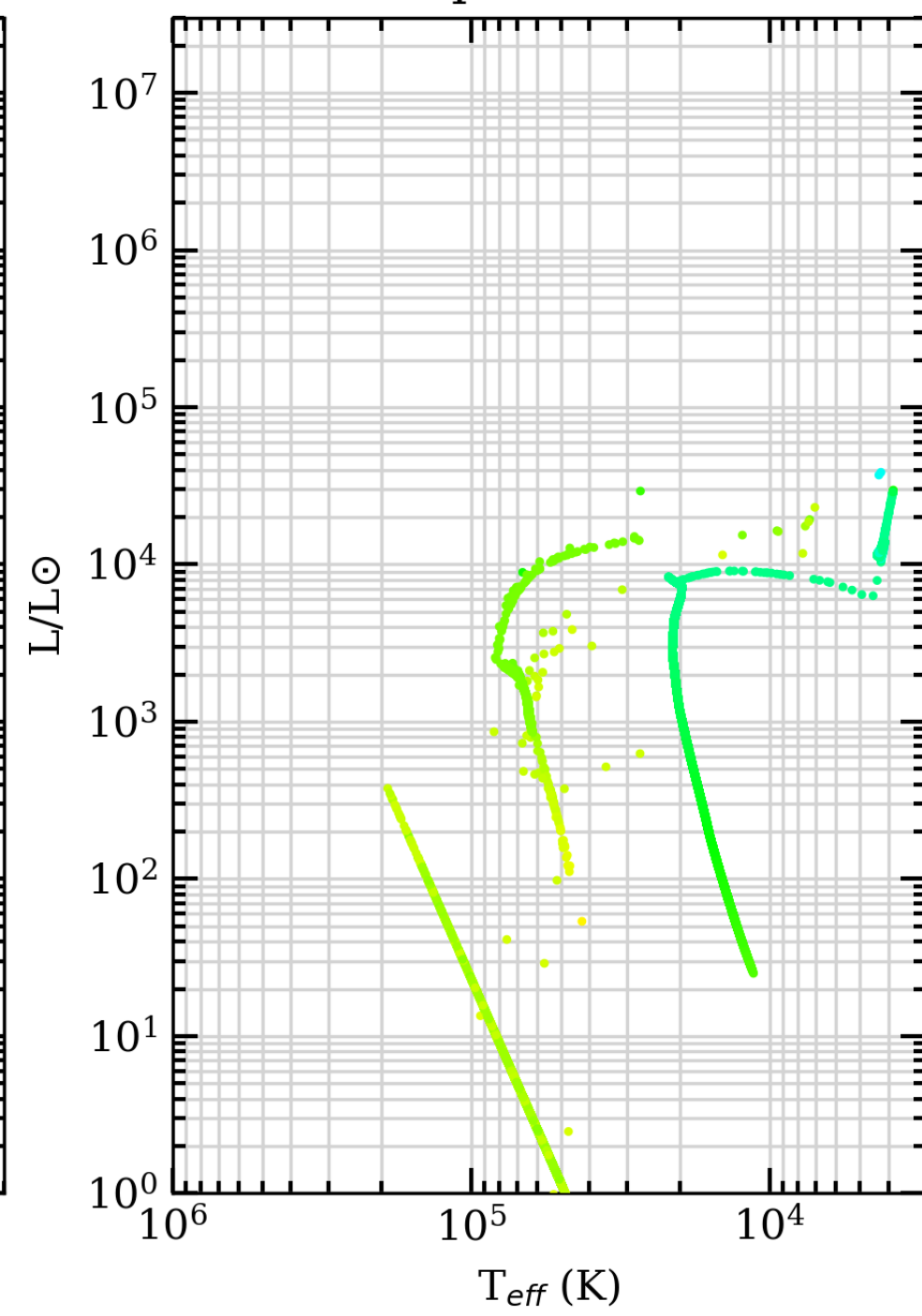
Z=0.004, t=35 Myr



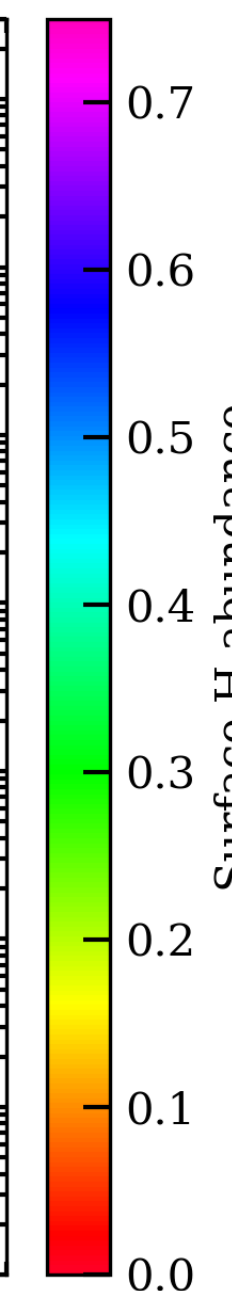
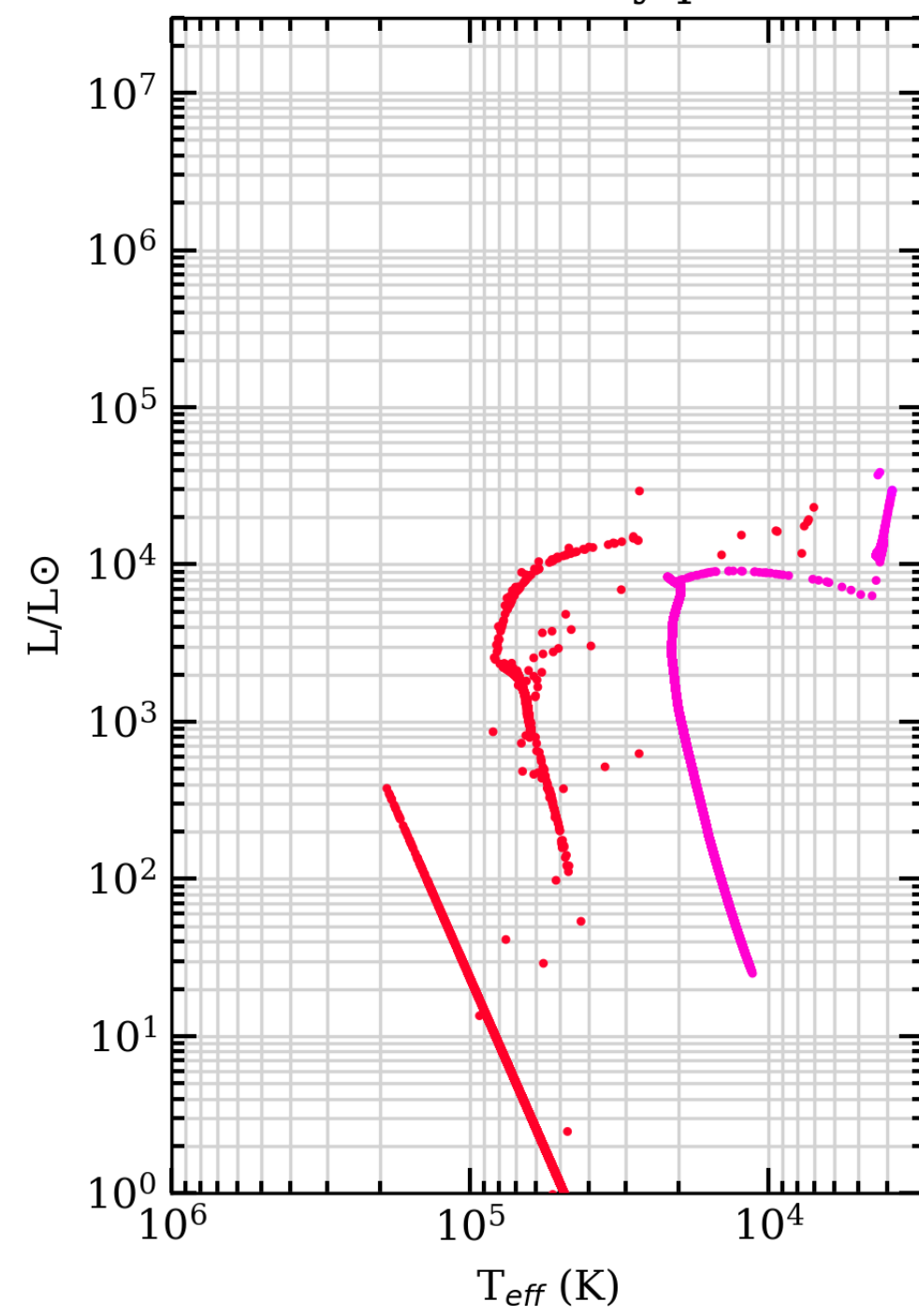
SEVN2.3 STD binary star tracks



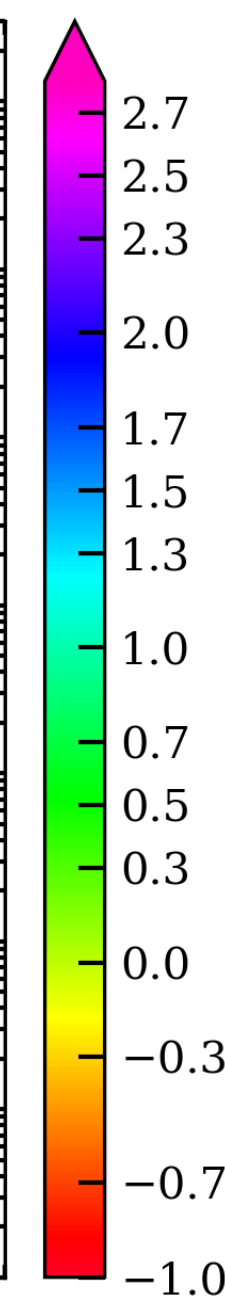
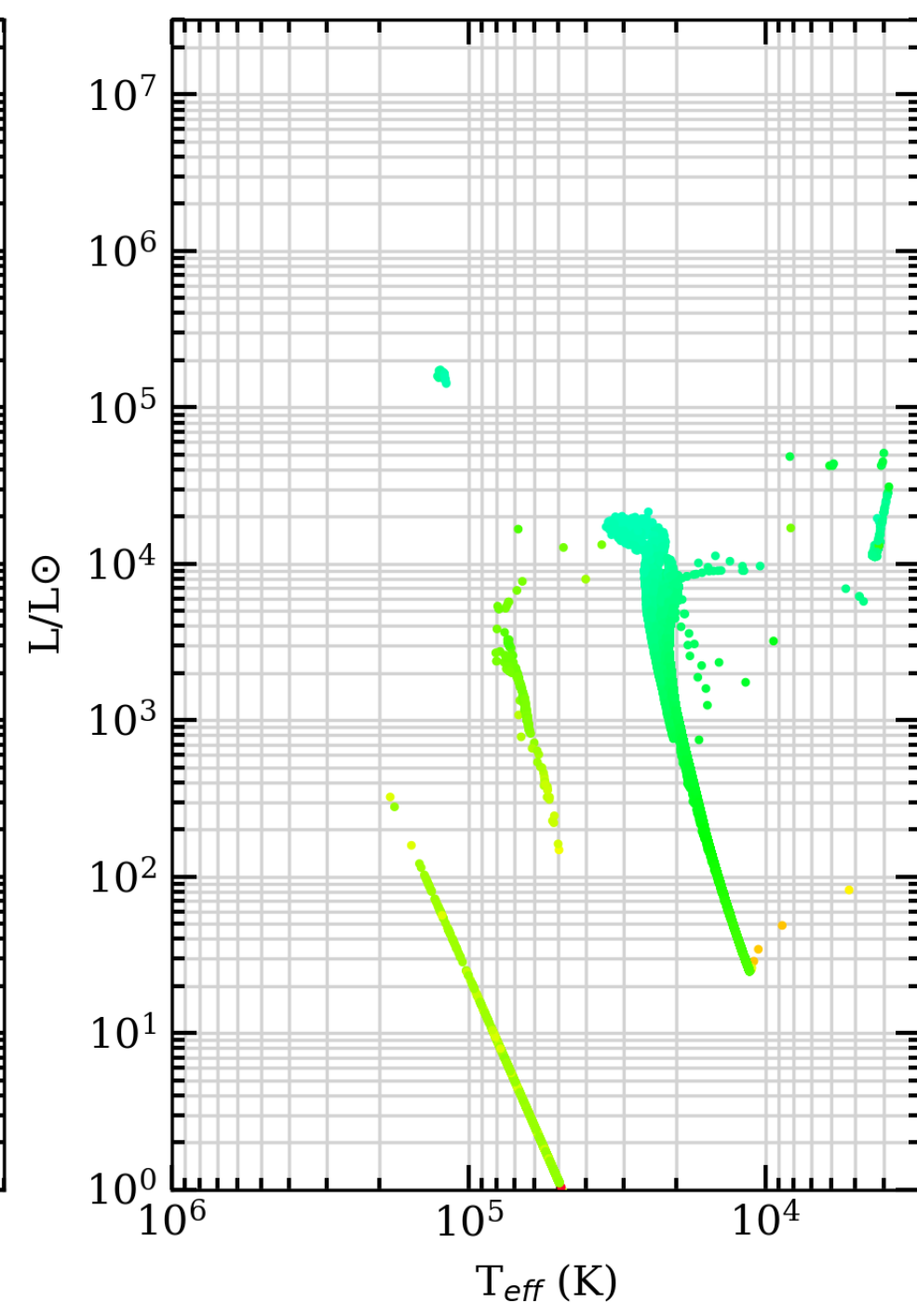
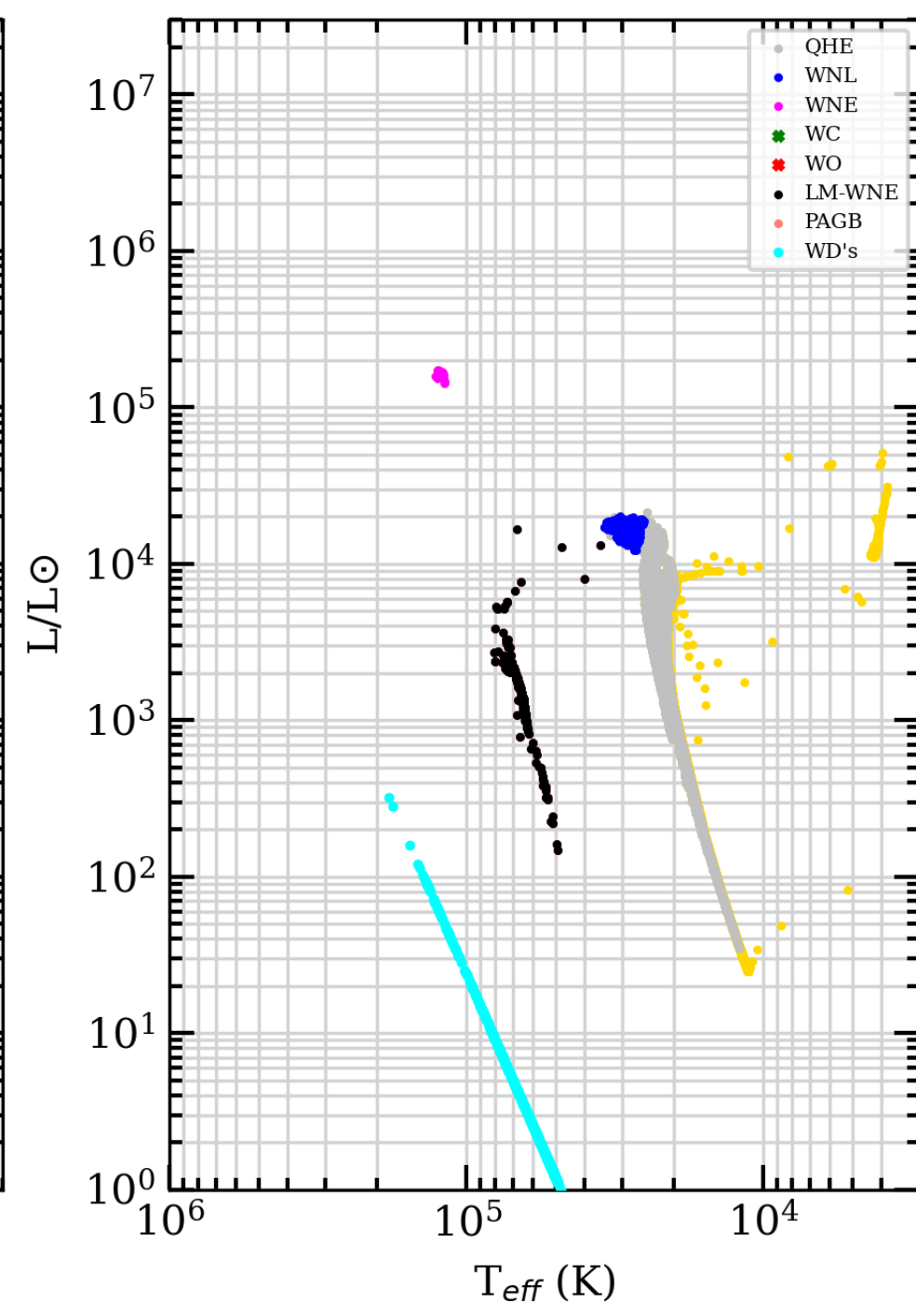
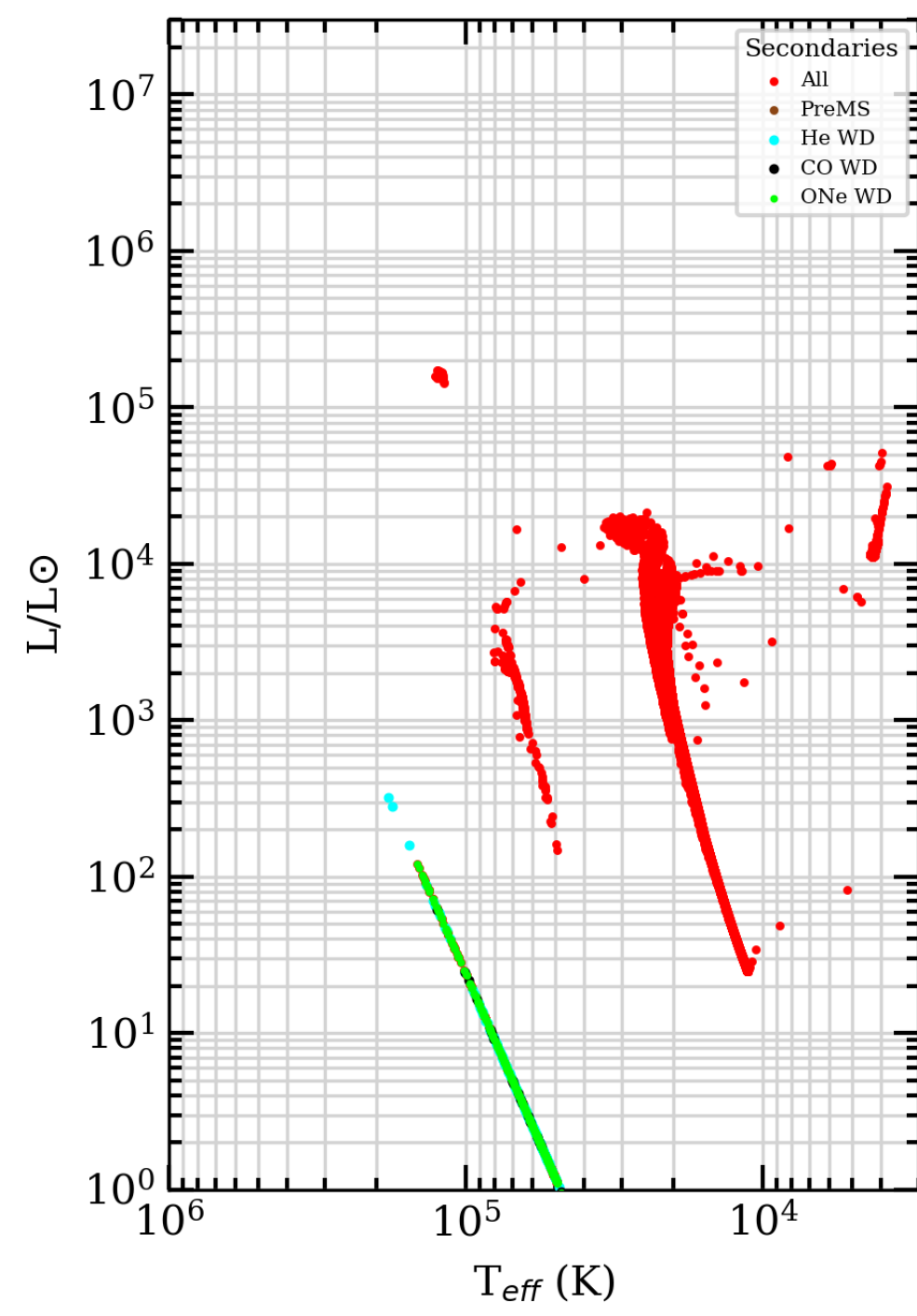
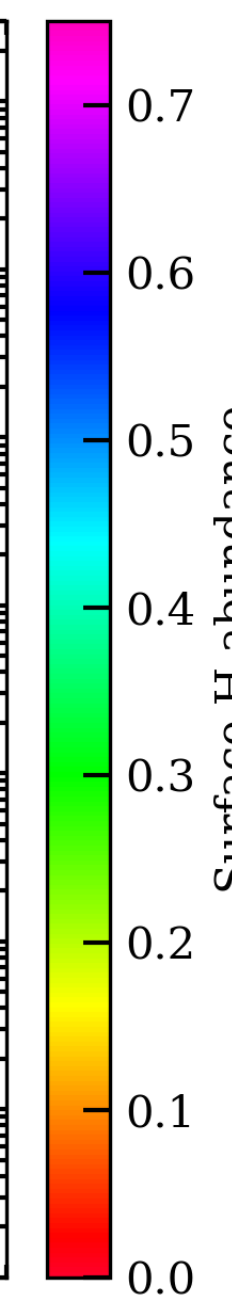
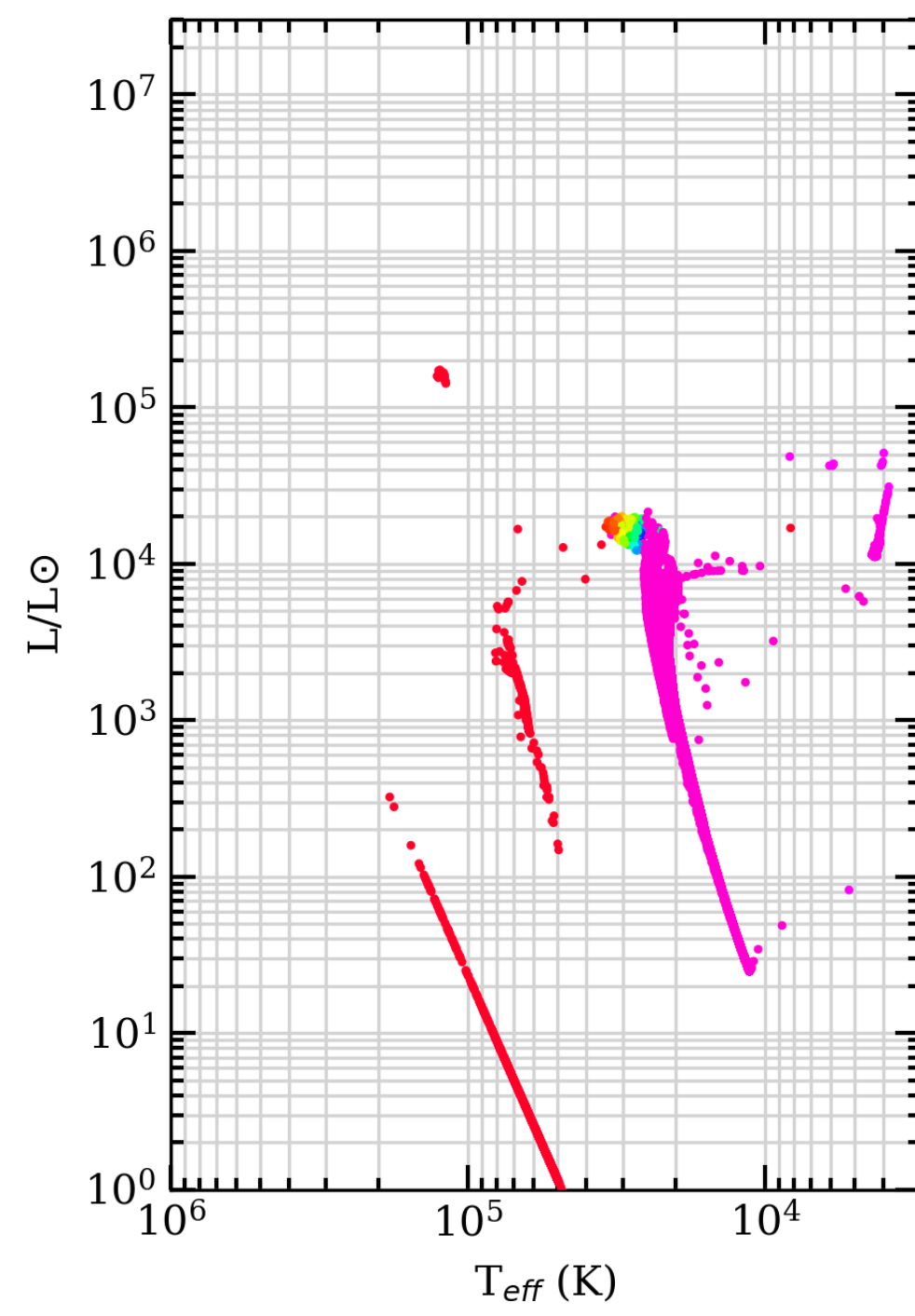
April 2023

log M ( $M_{\odot}$ )

156250 binary pairs

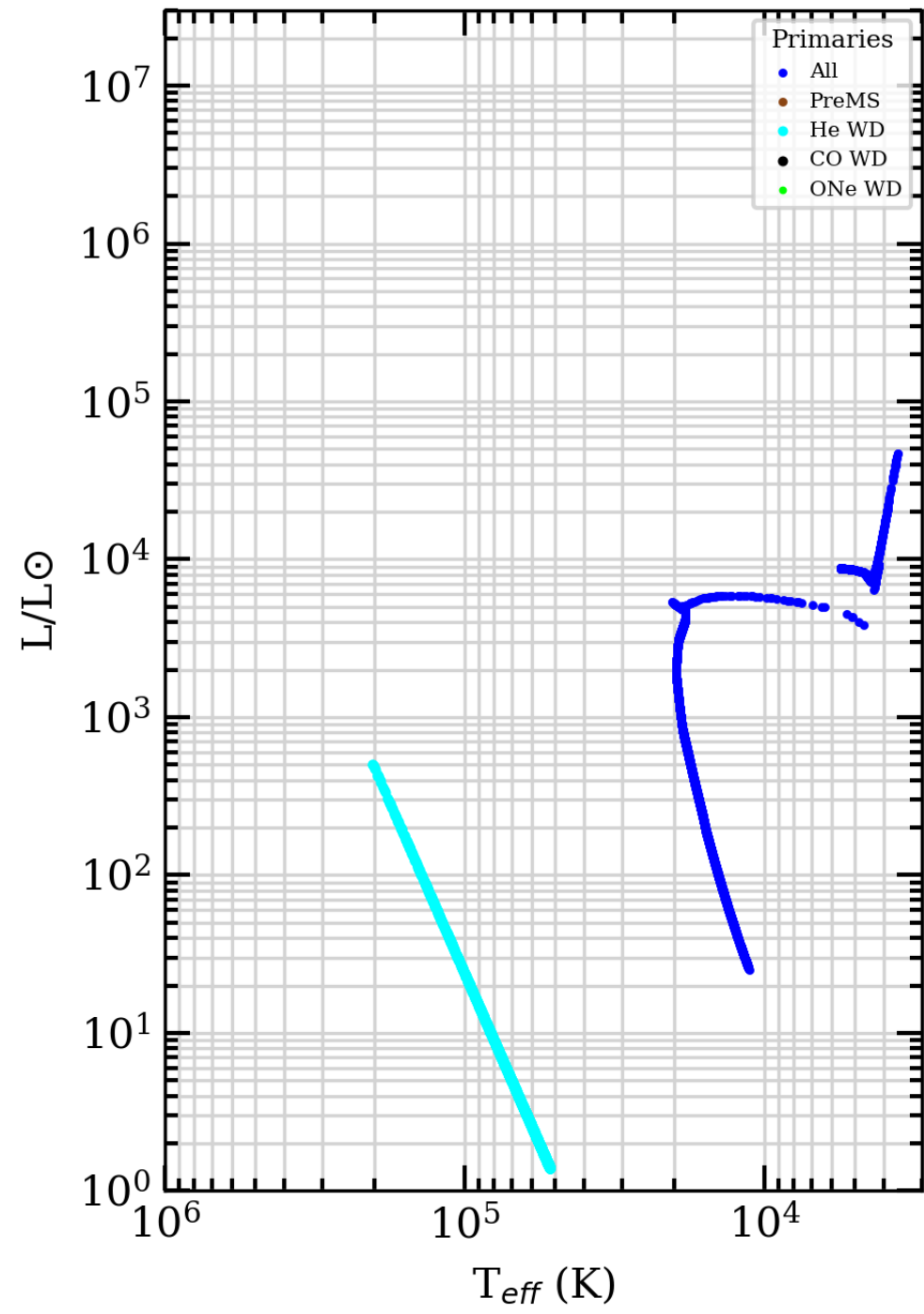


Surface H abundance

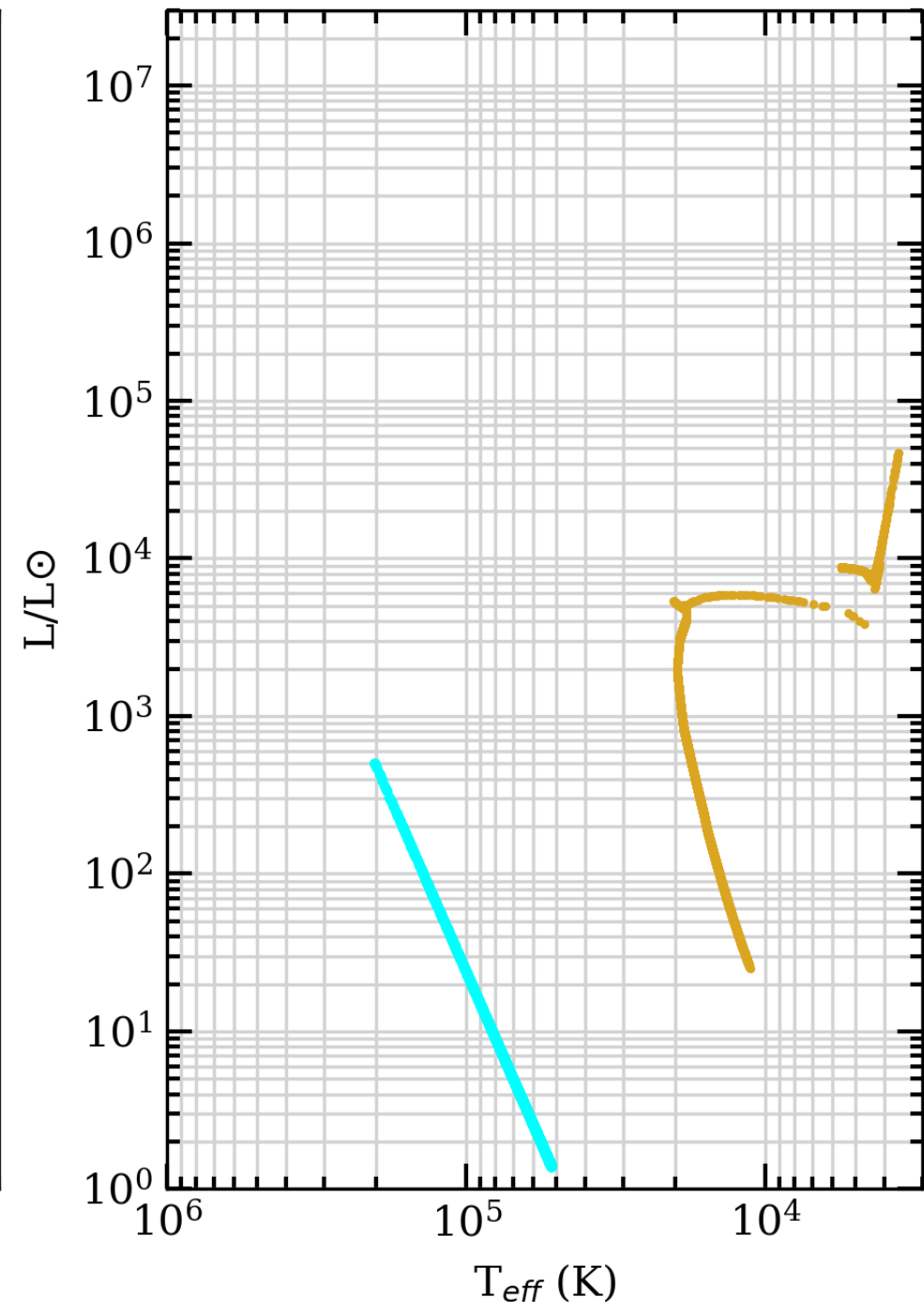
log M ( $M_{\odot}$ )

Surface H abundance

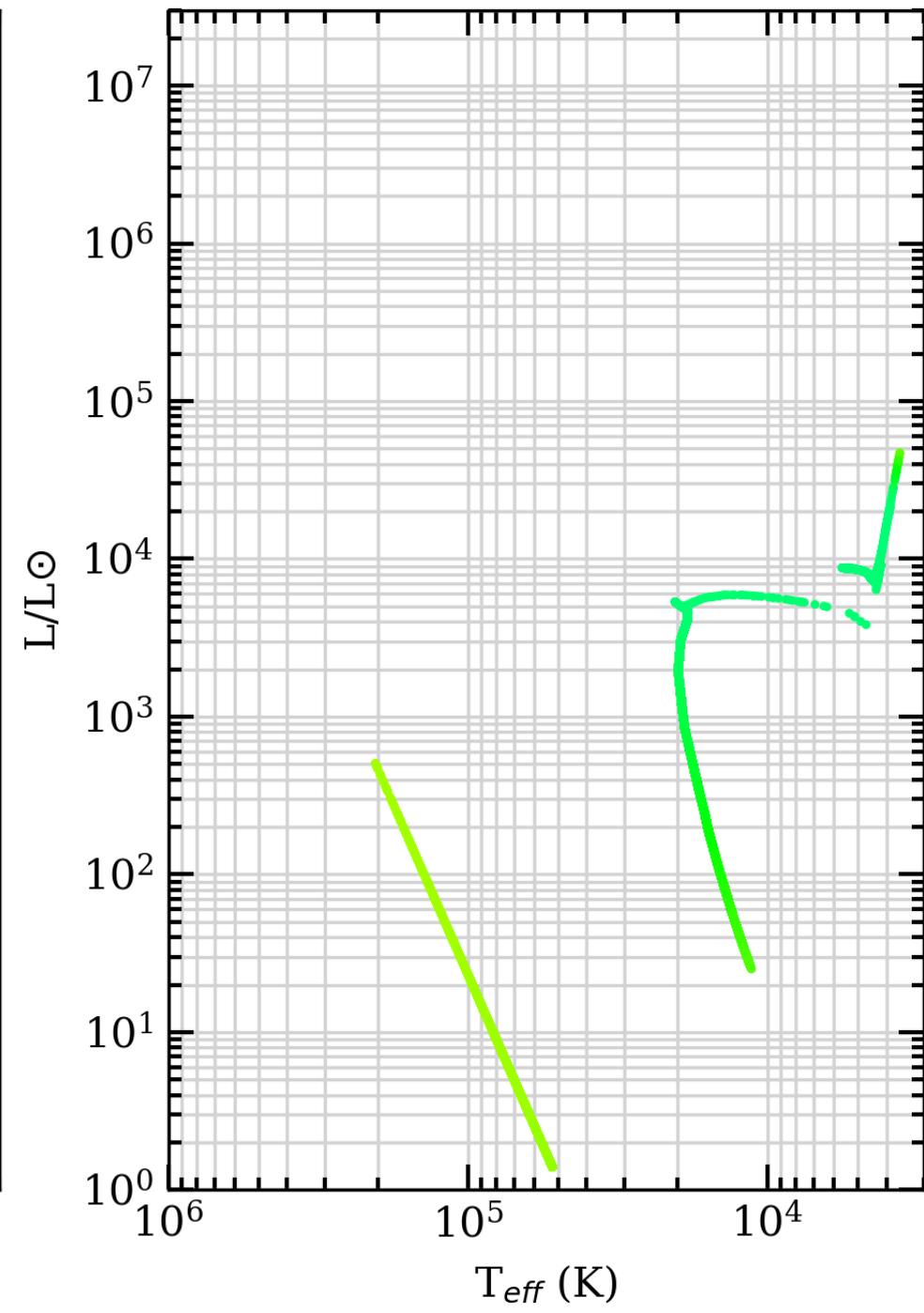
Z=0.004, t=45 Myr



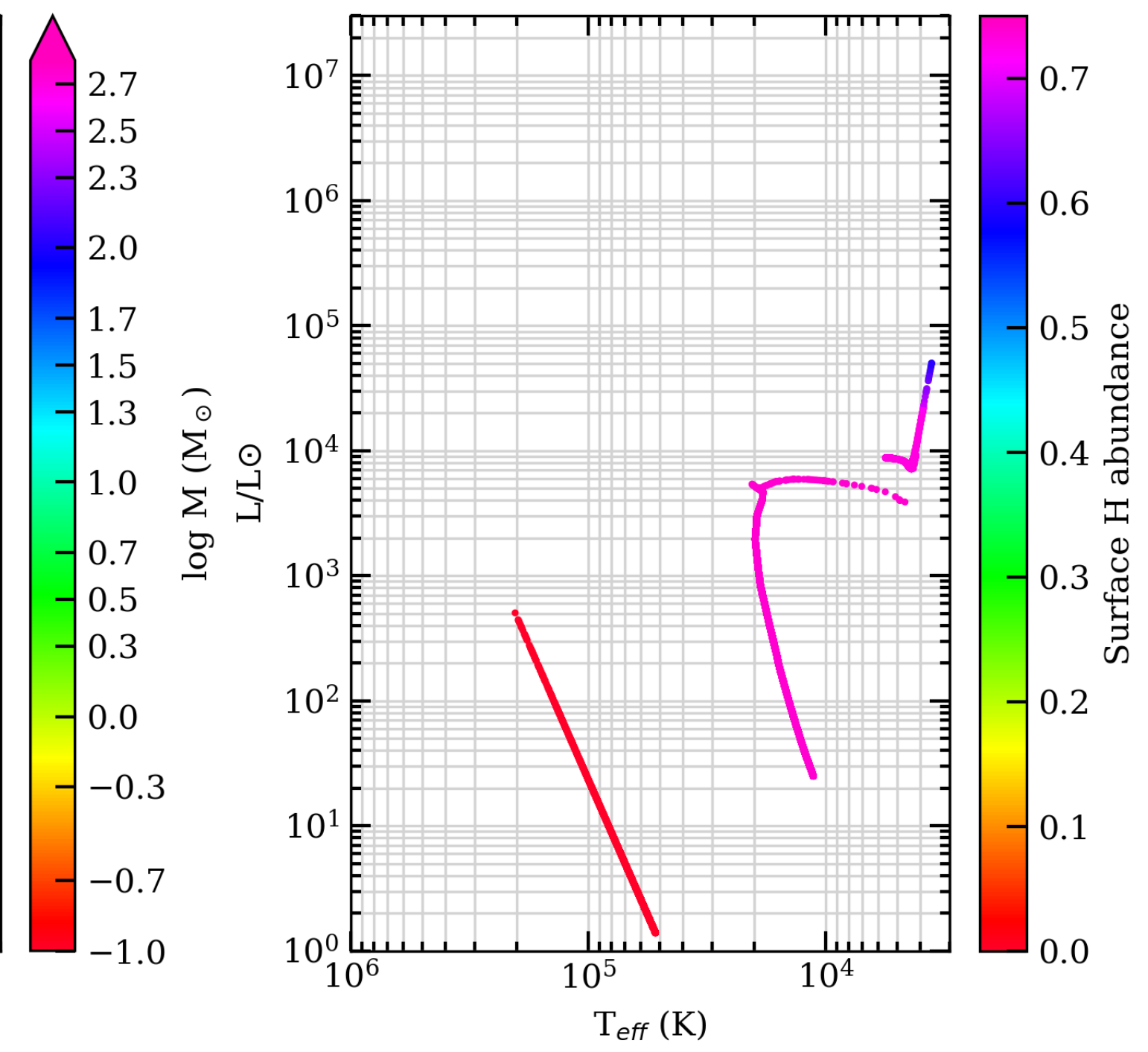
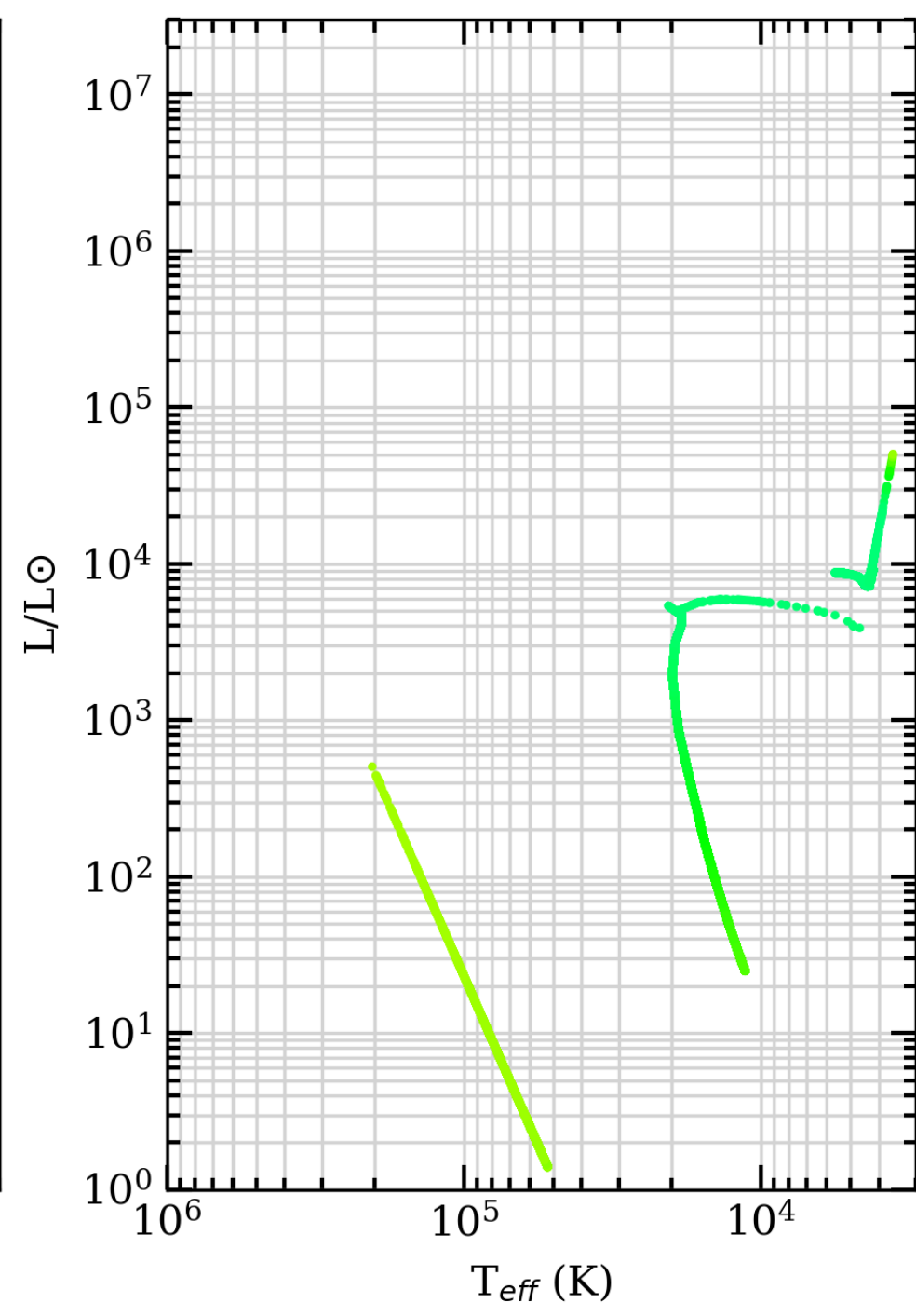
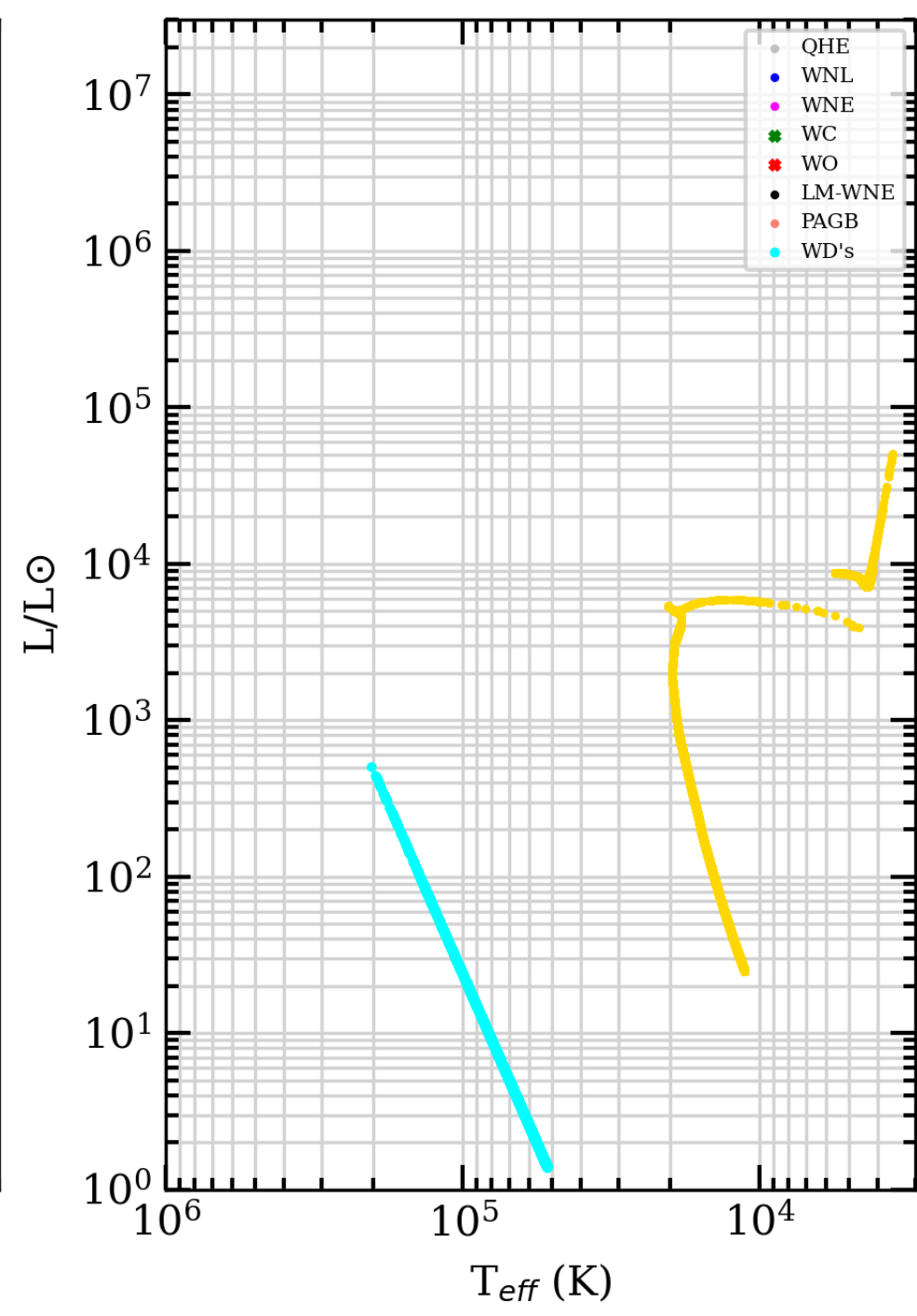
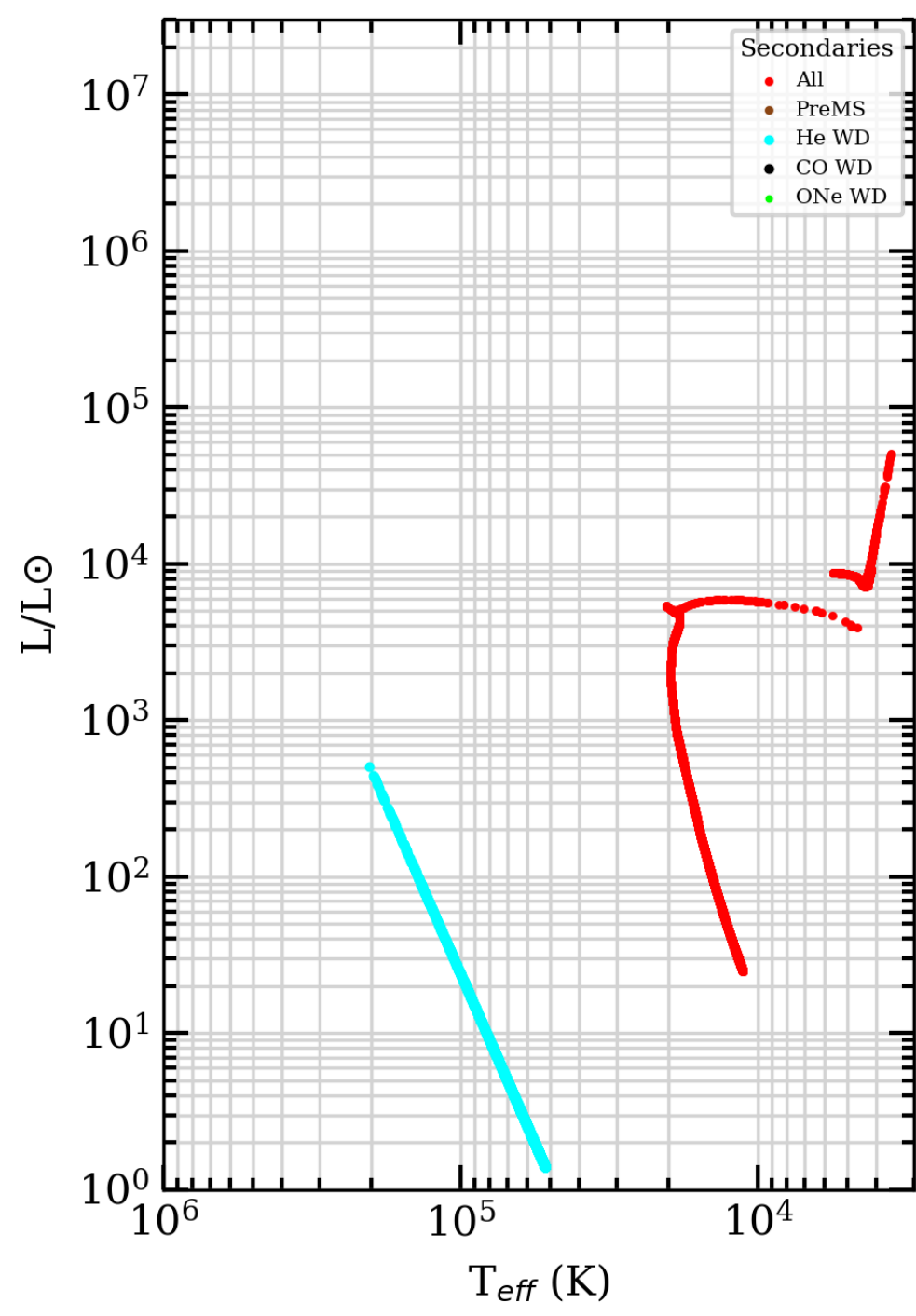
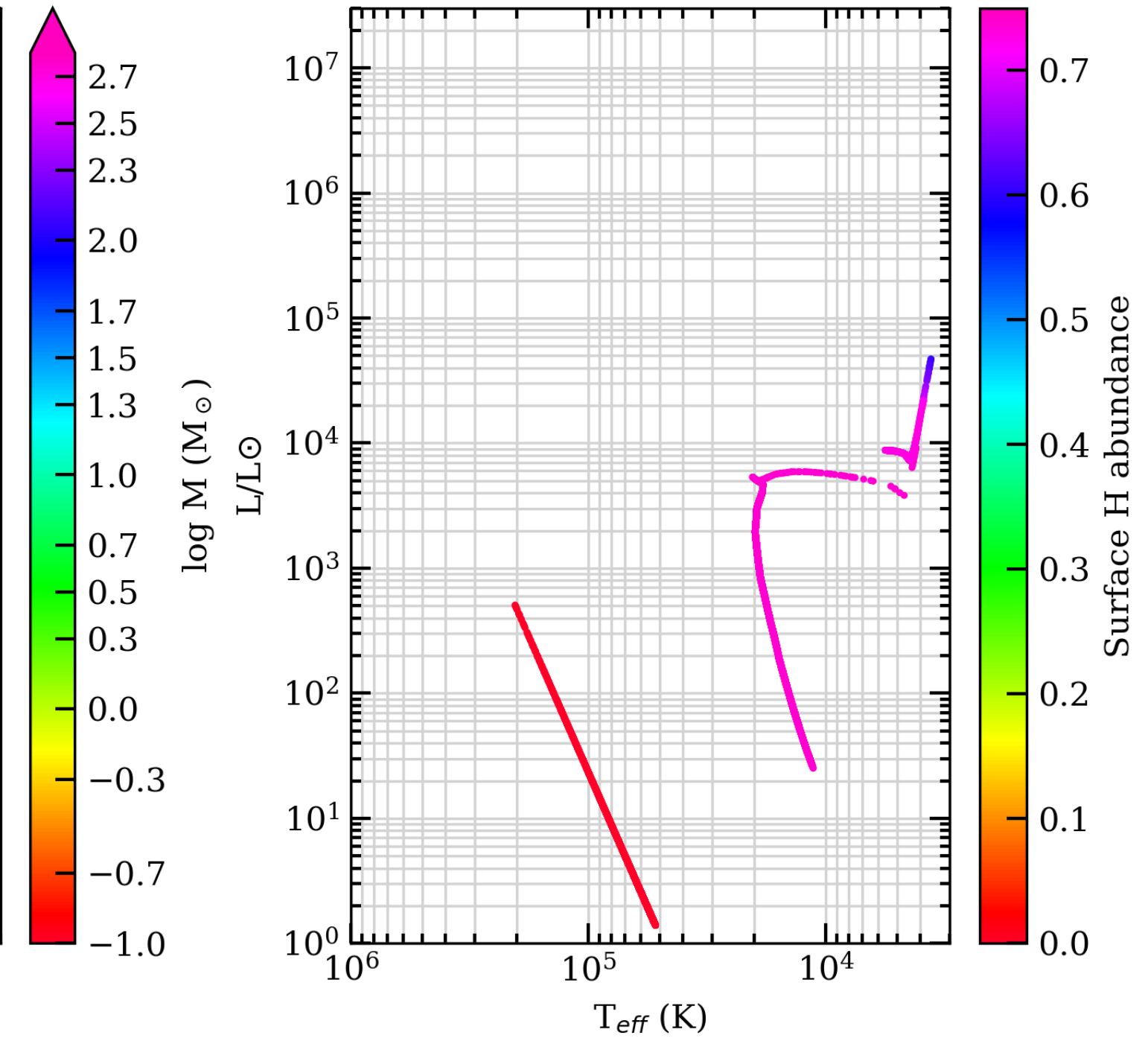
SEVN2.3 VLA binary star tracks



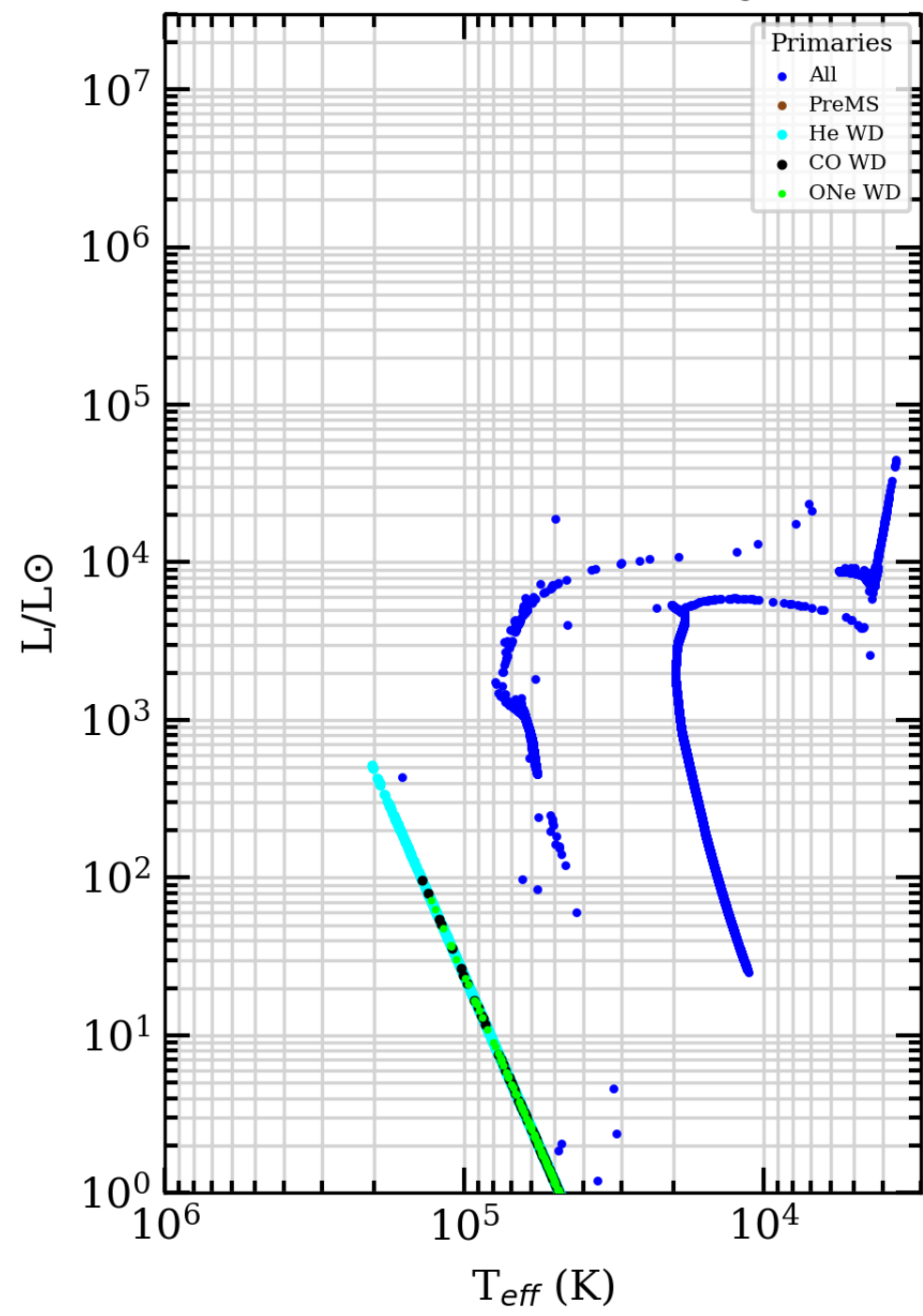
April 2023



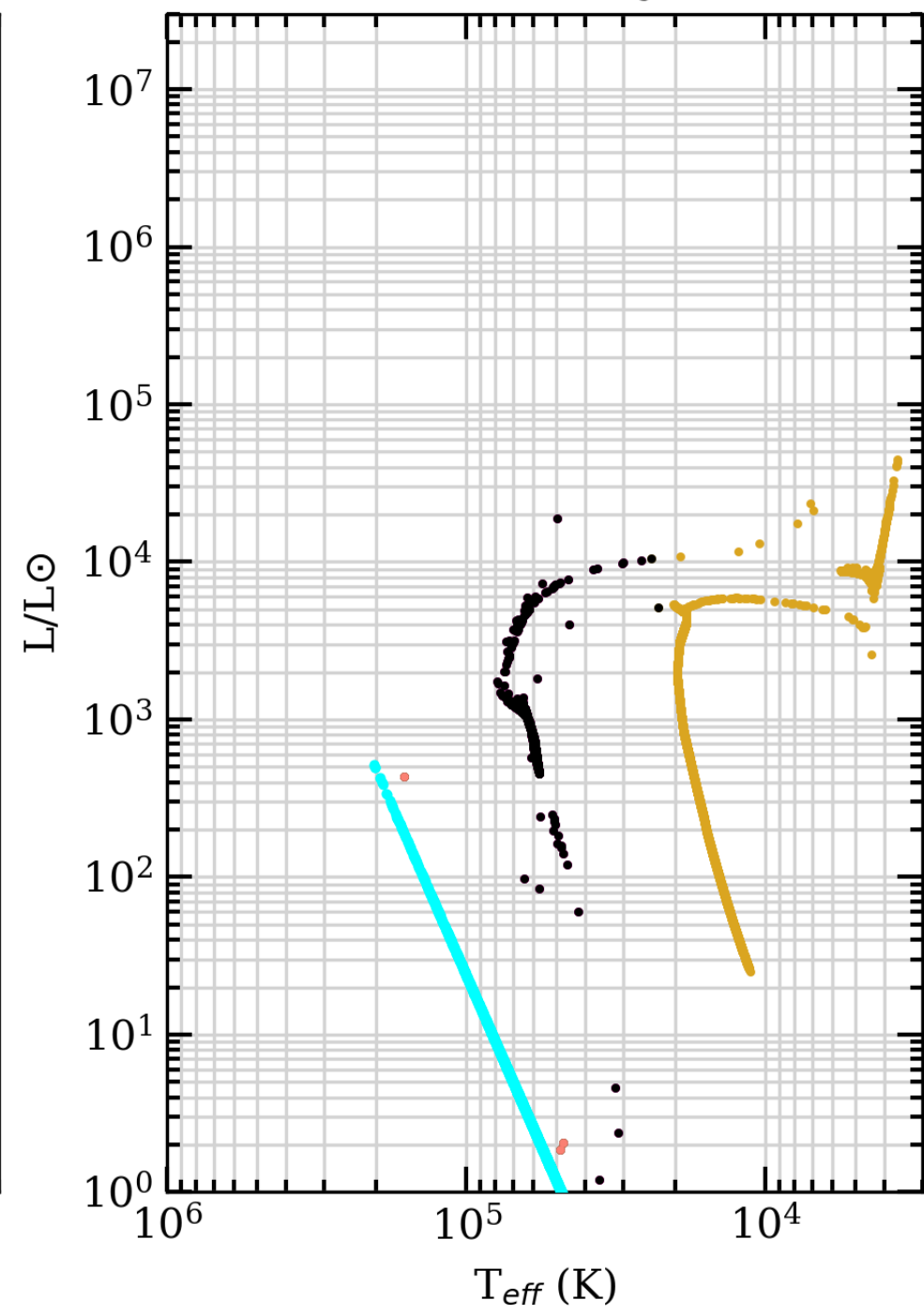
156250 binary pairs



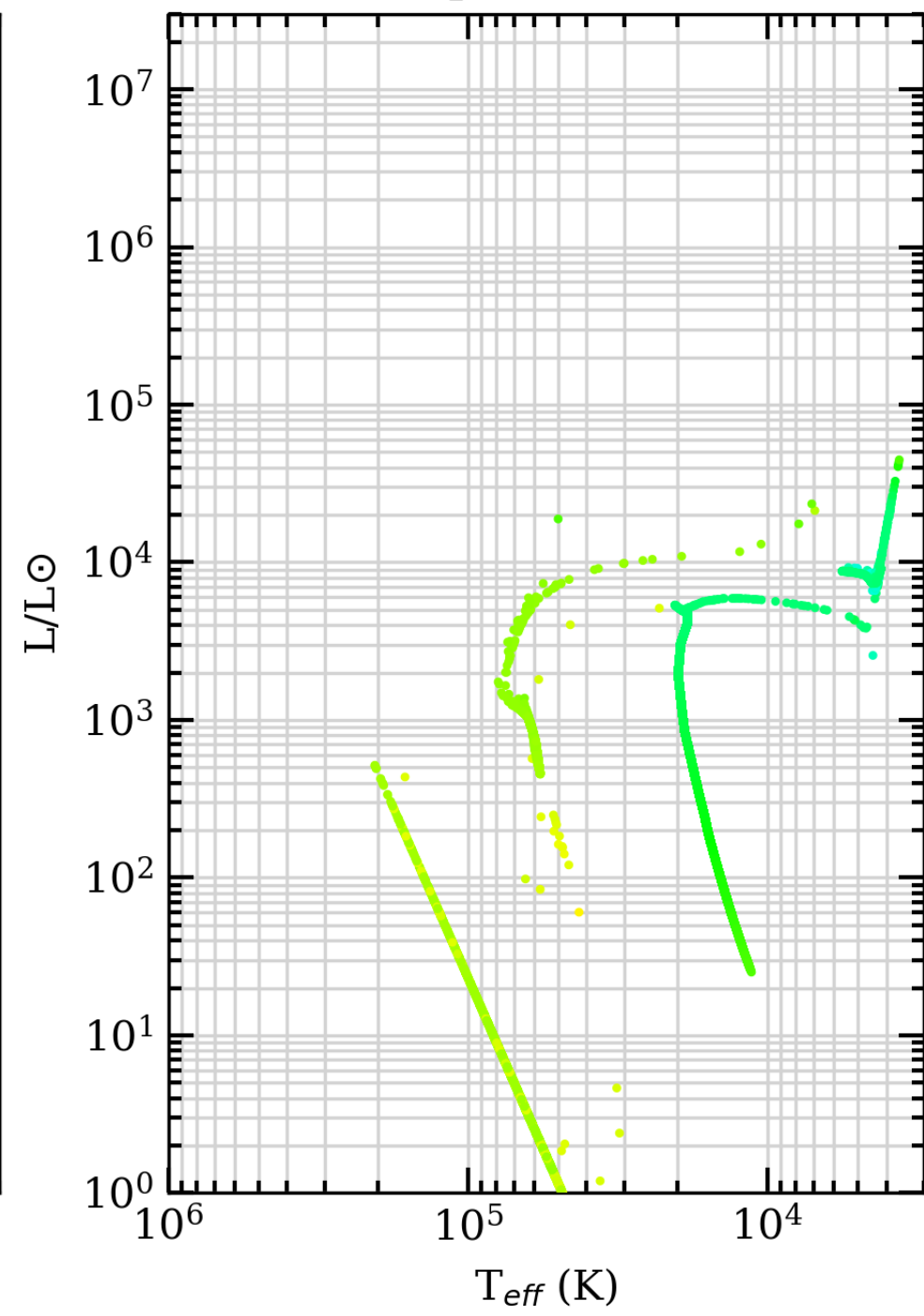
Z=0.004, t=45 Myr



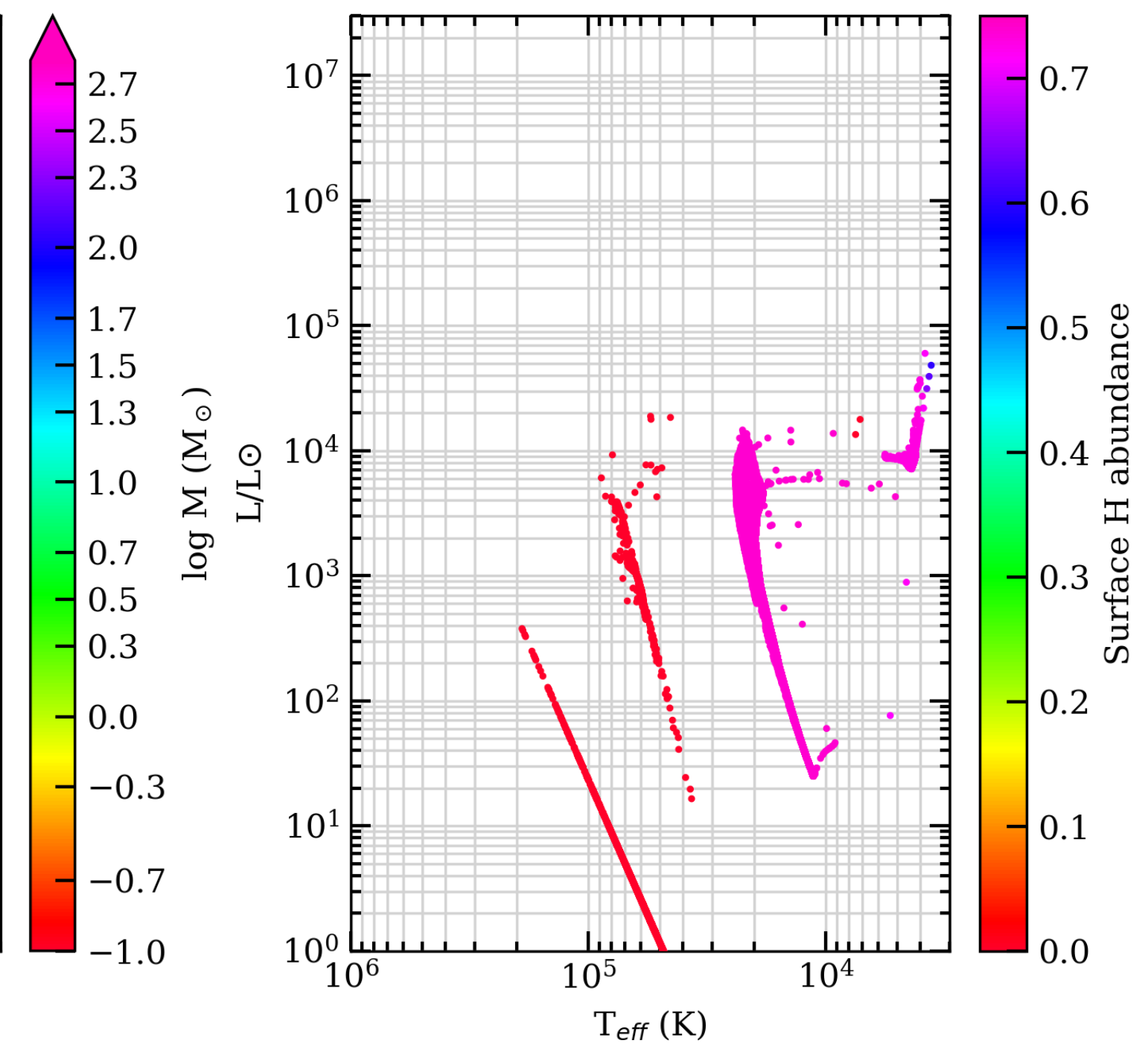
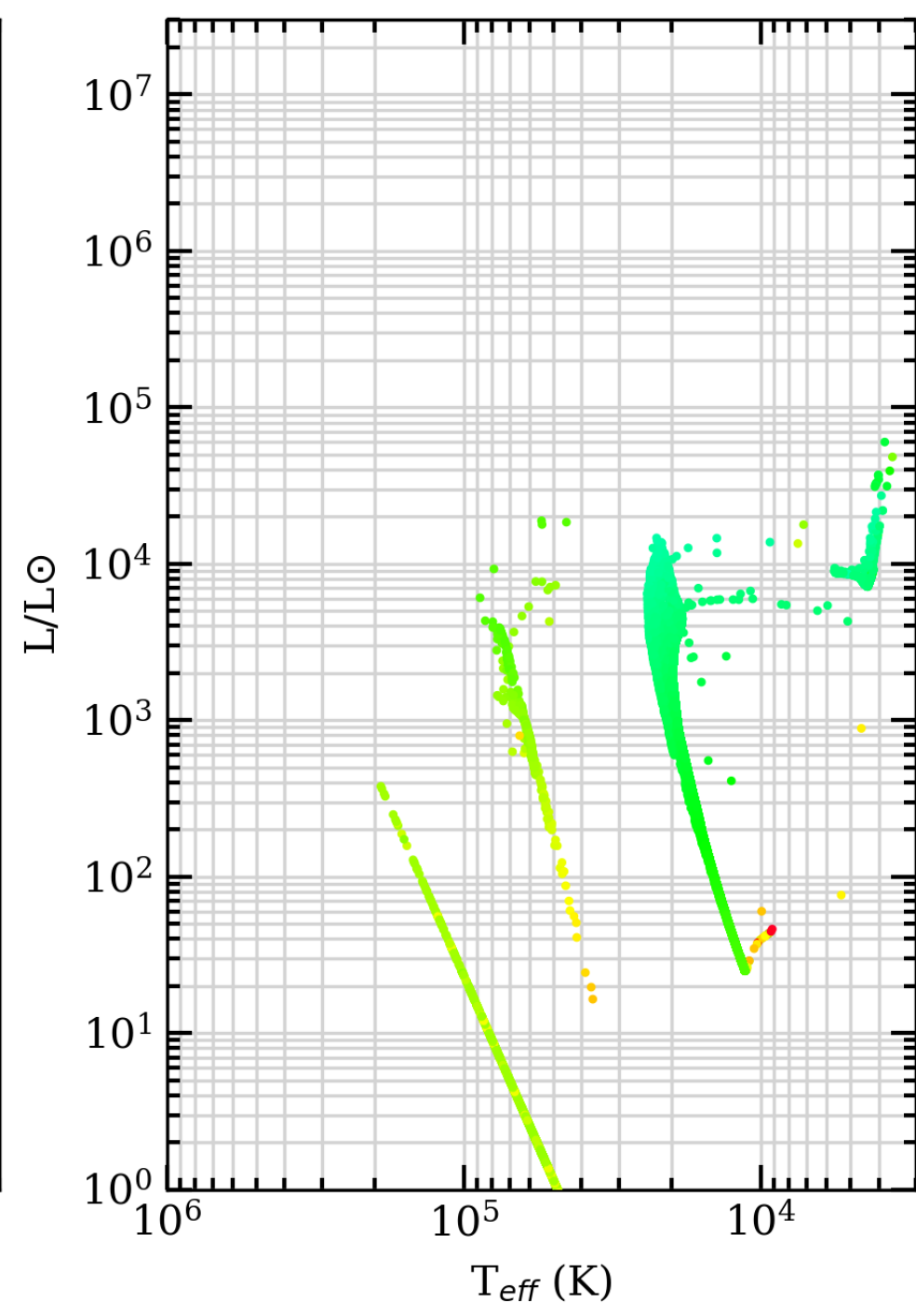
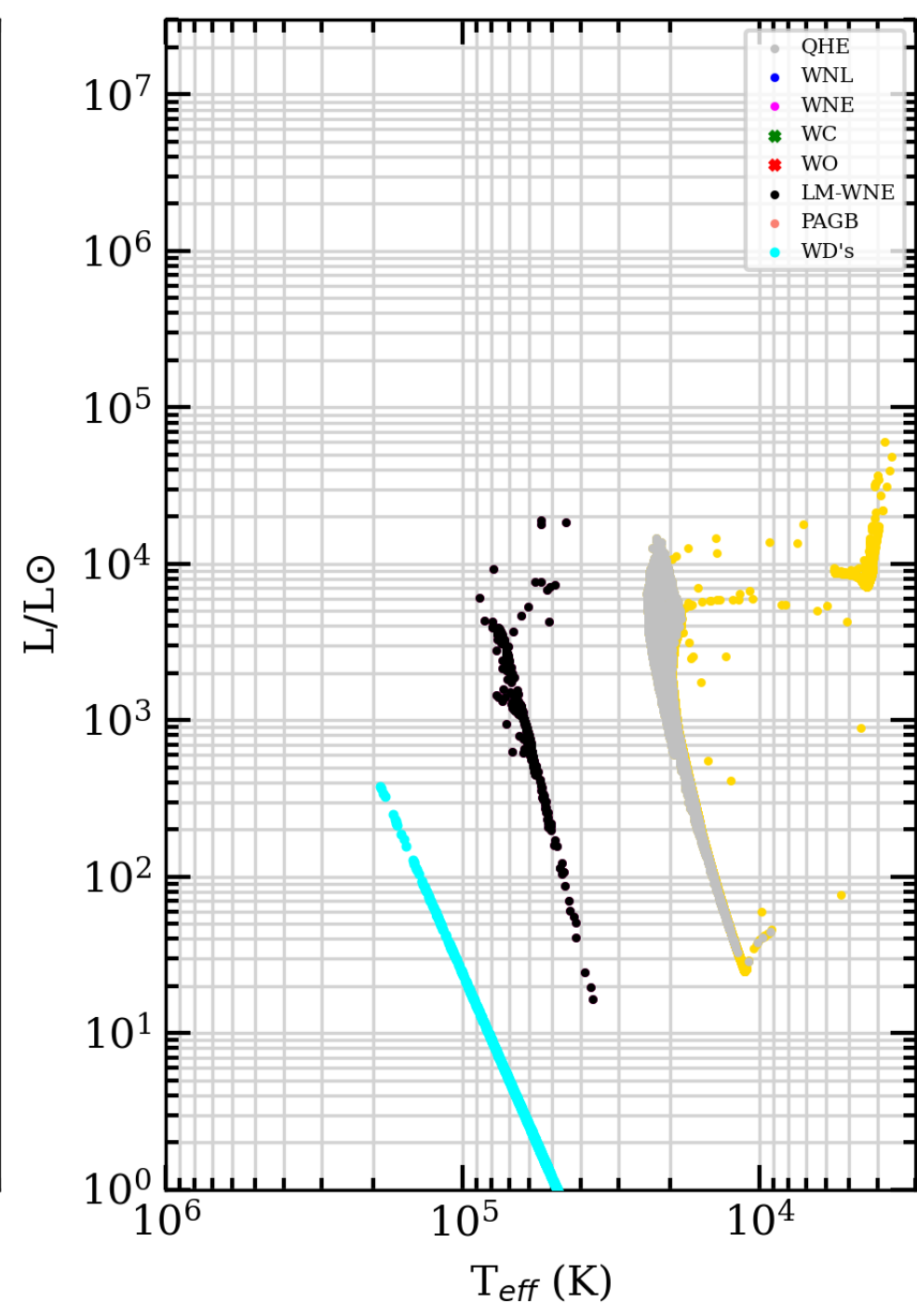
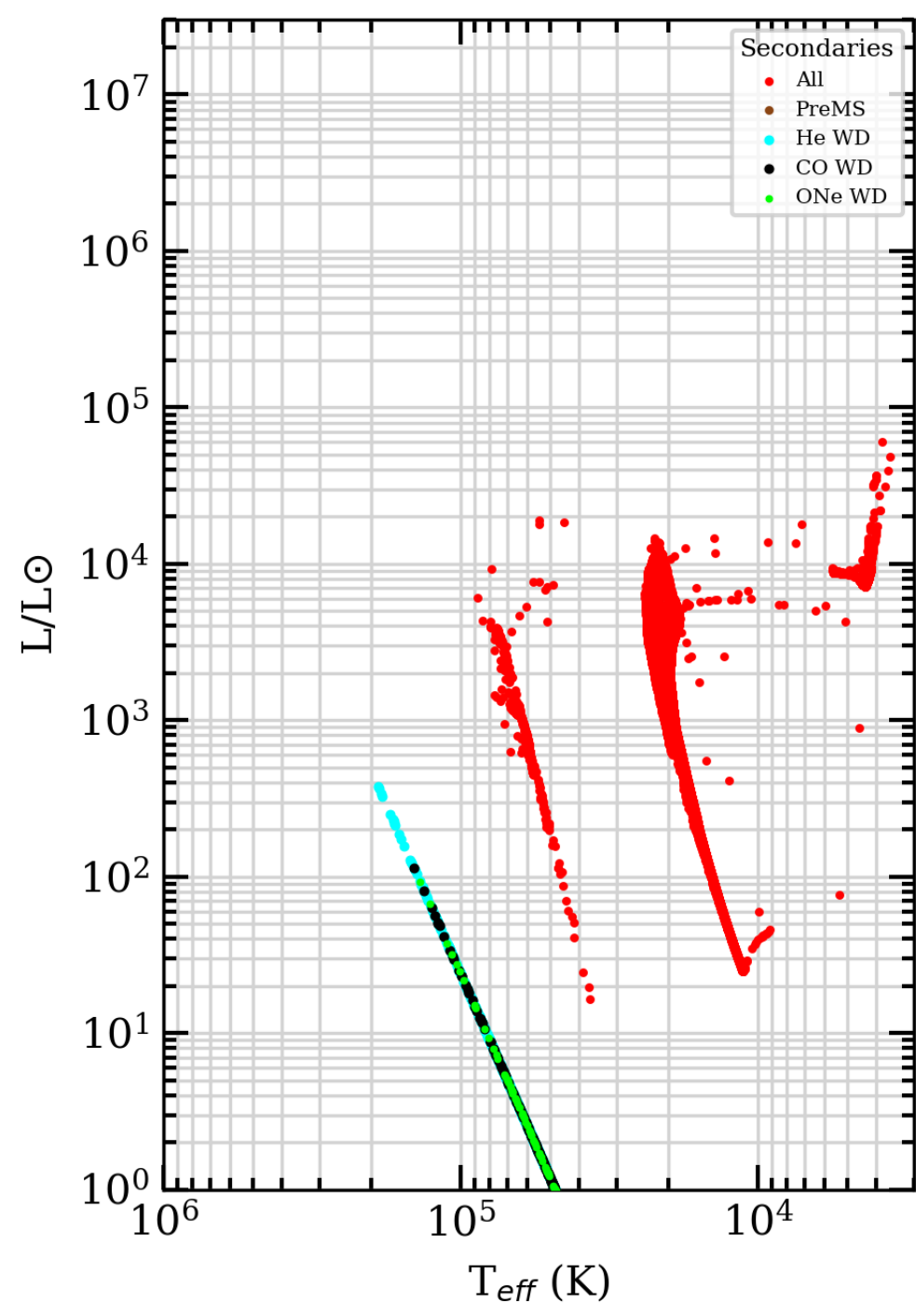
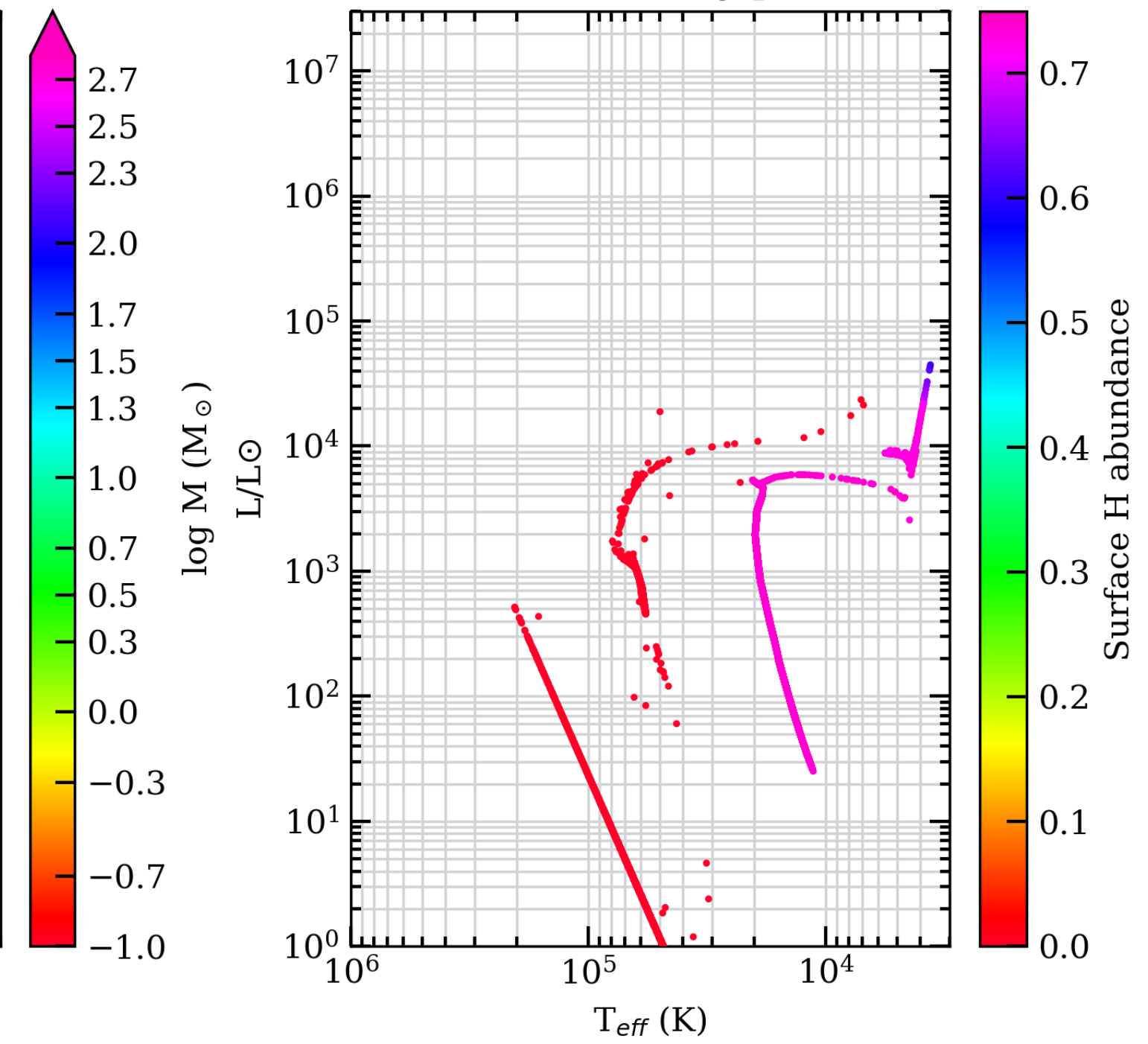
SEVN2.3 STD binary star tracks



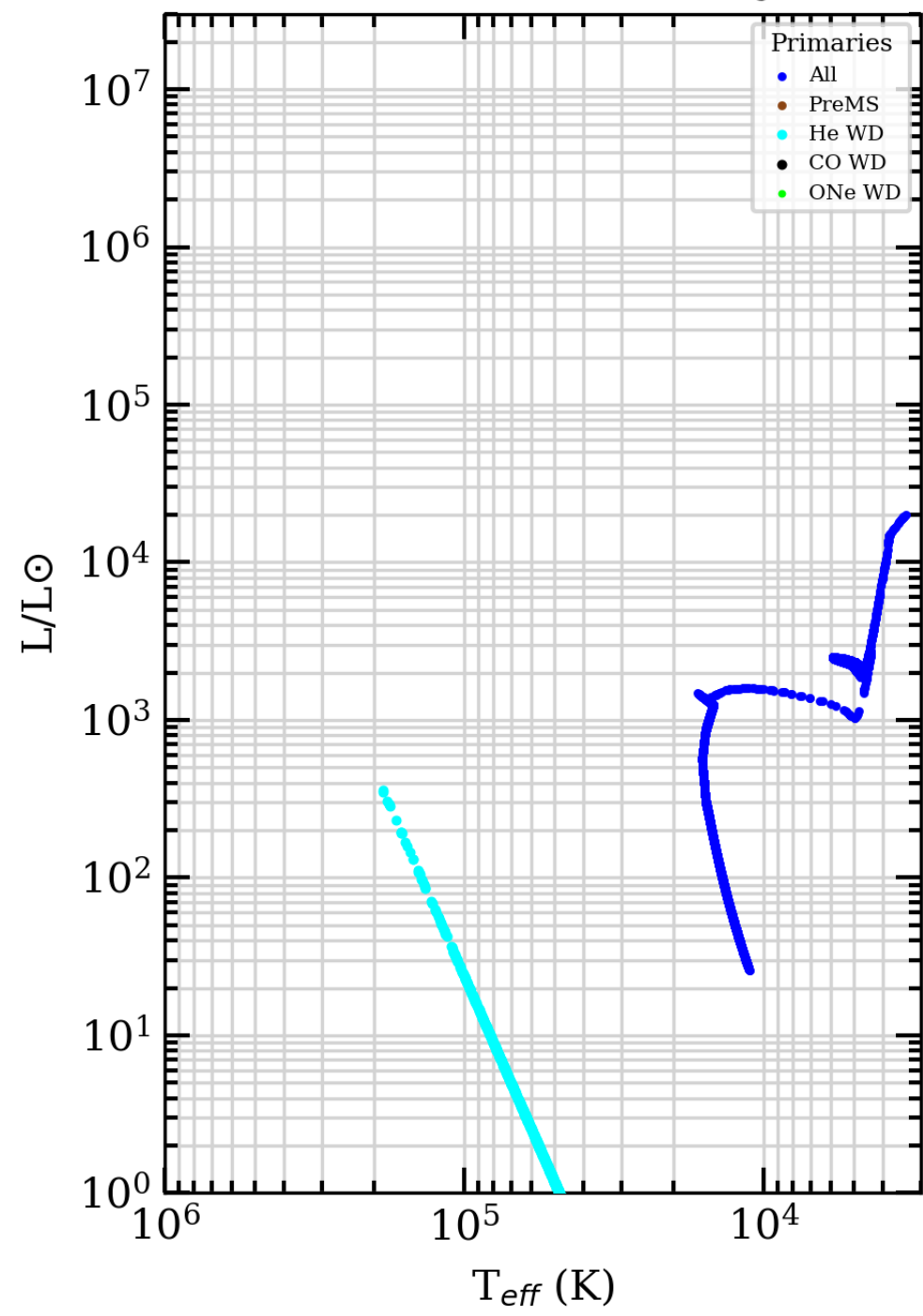
April 2023



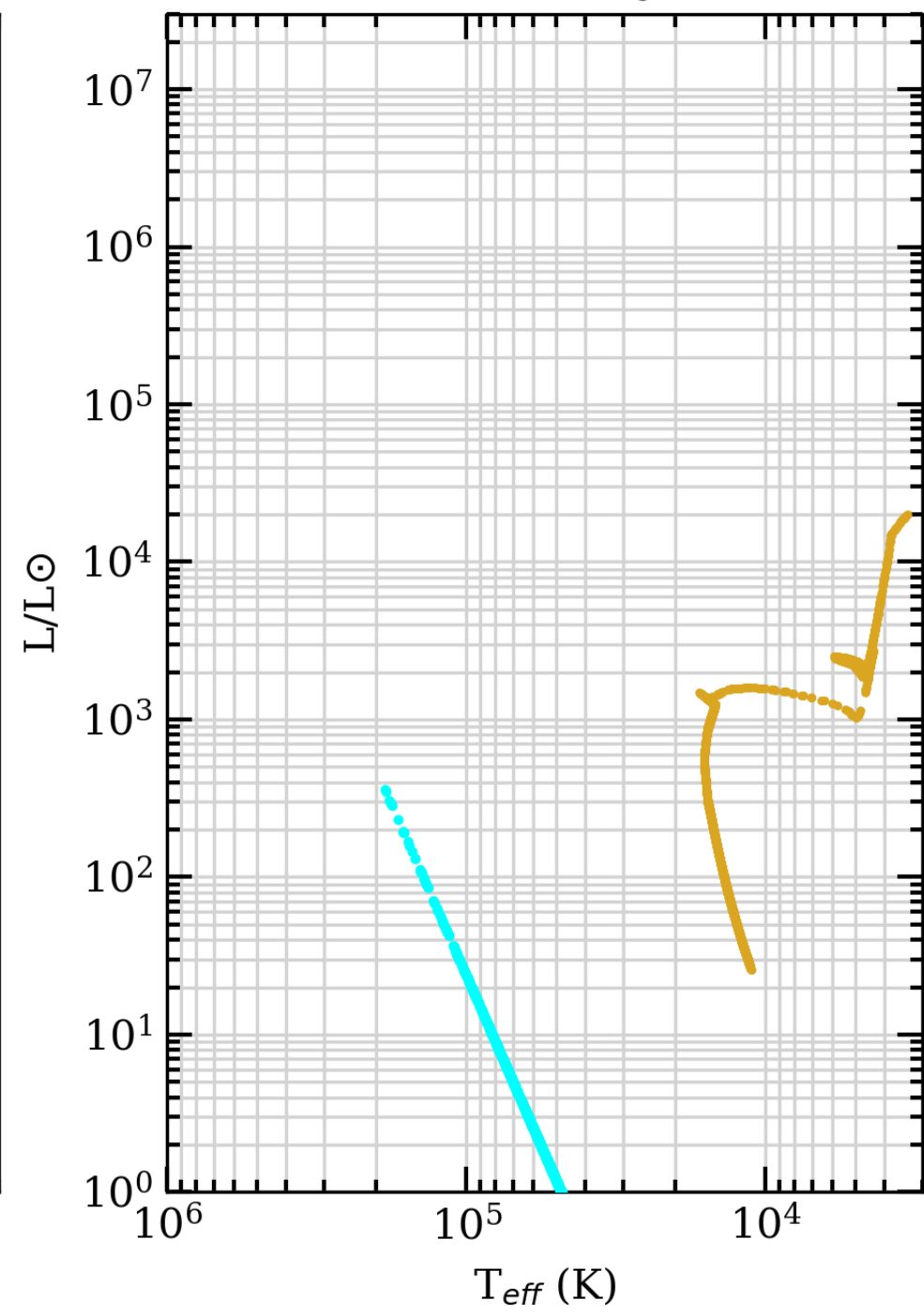
156250 binary pairs



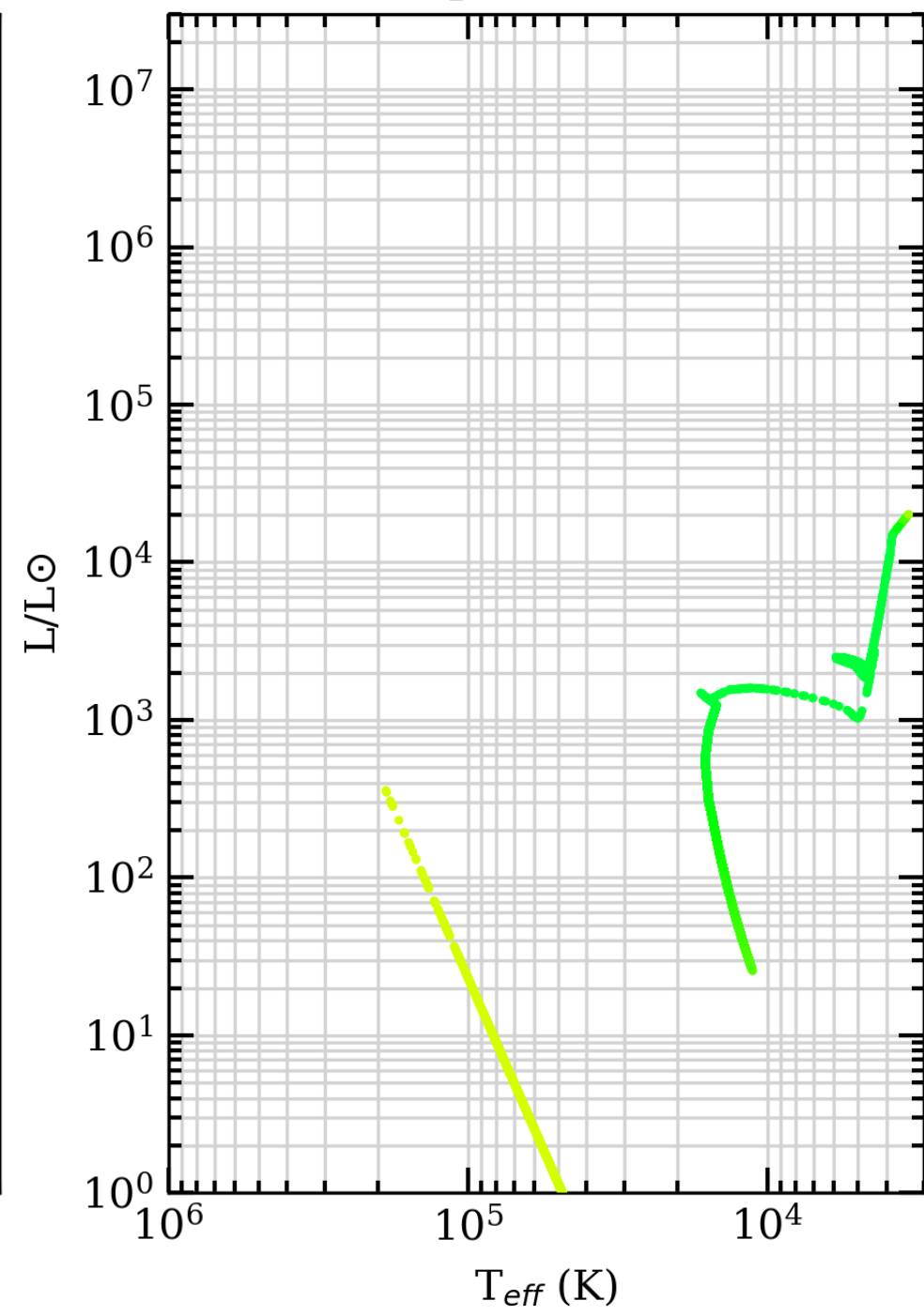
Z=0.004, t=100 Myr



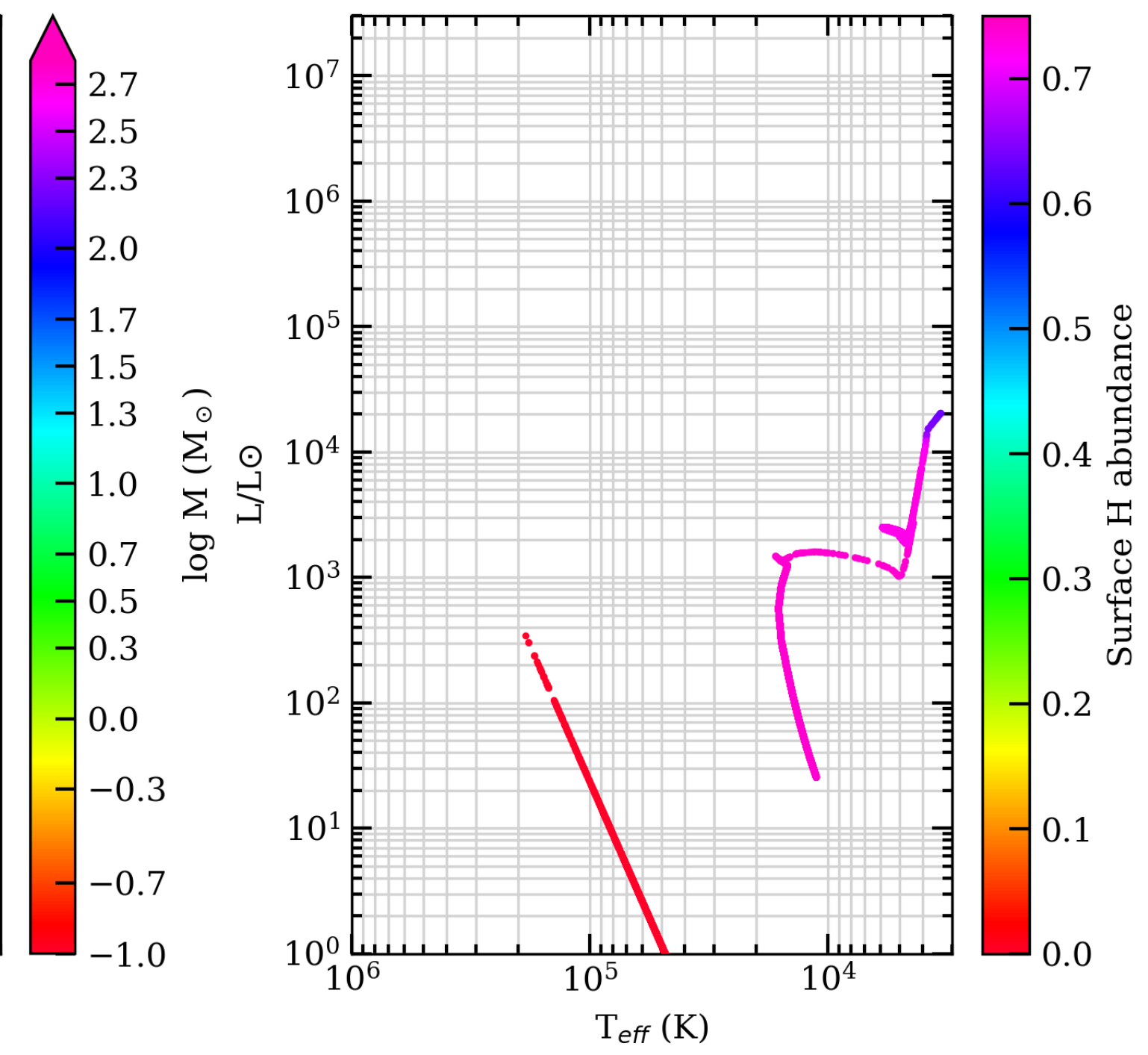
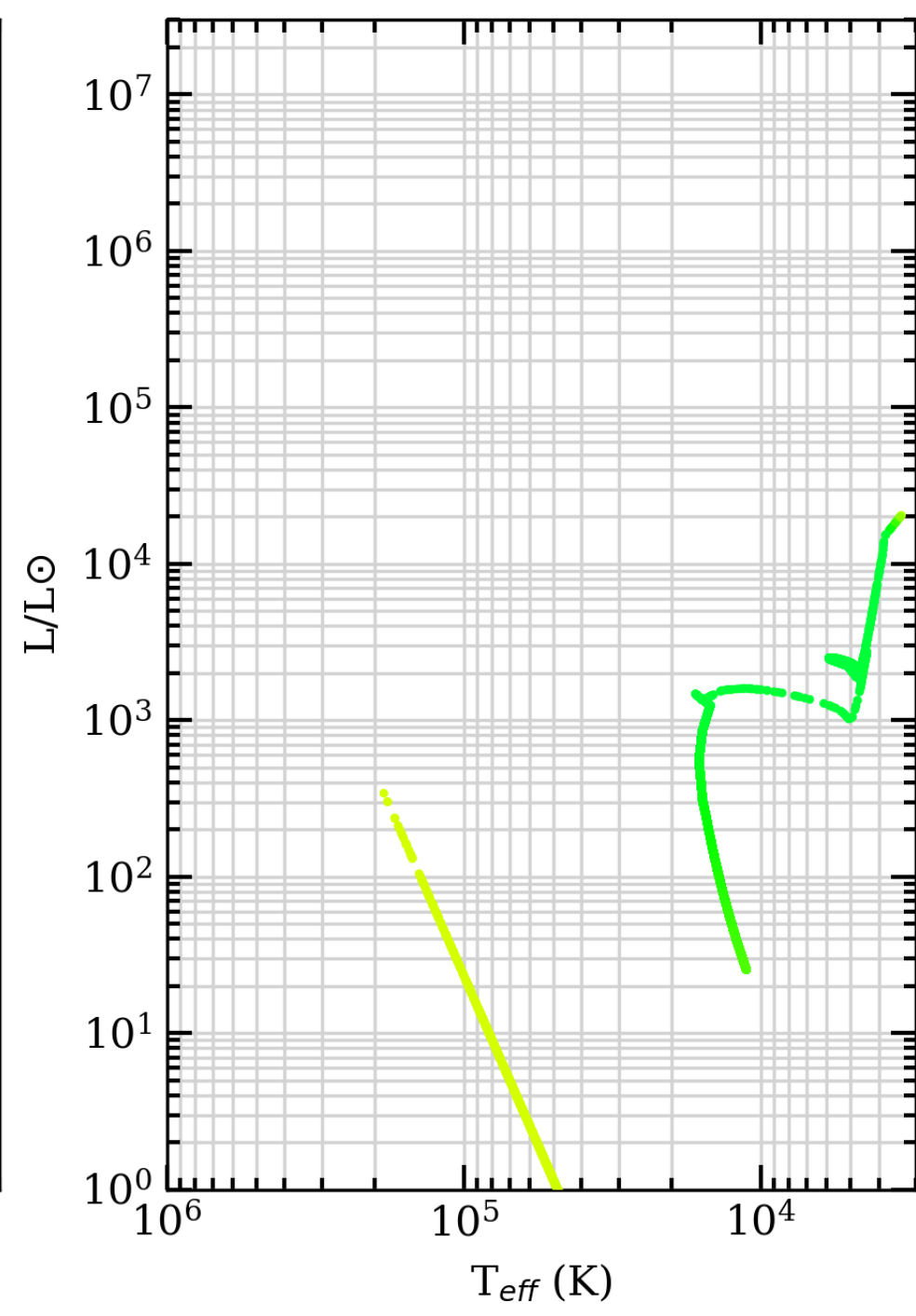
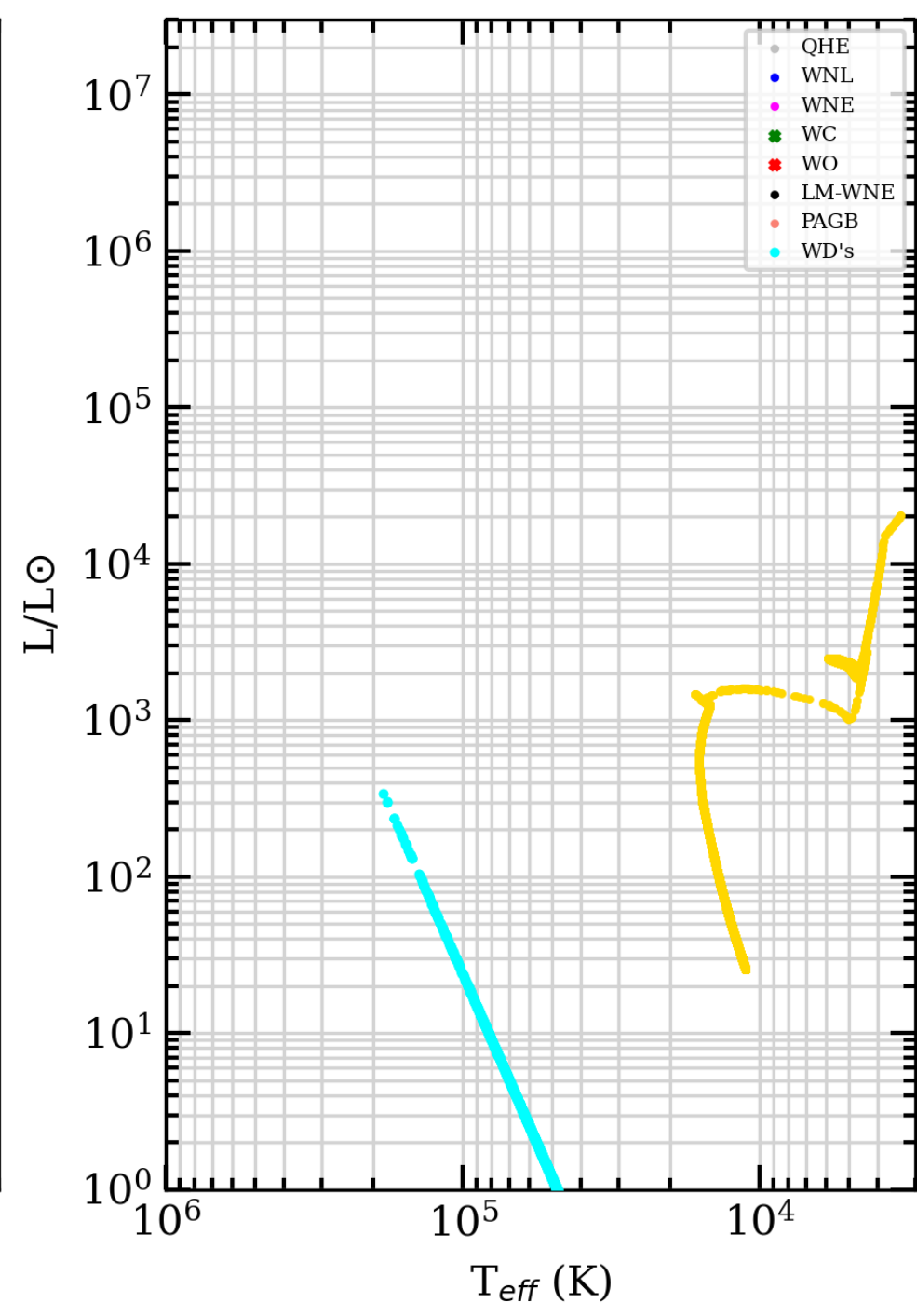
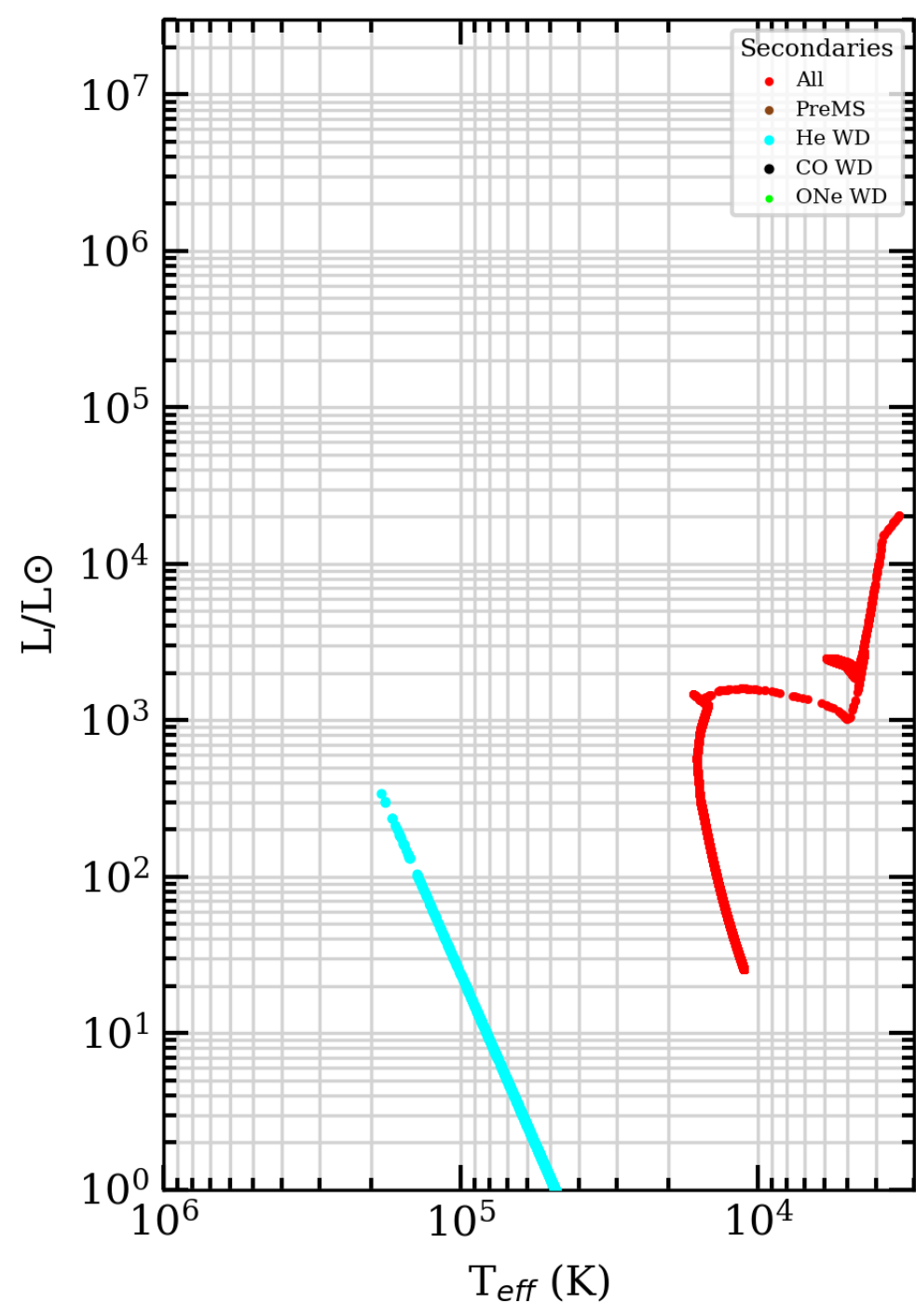
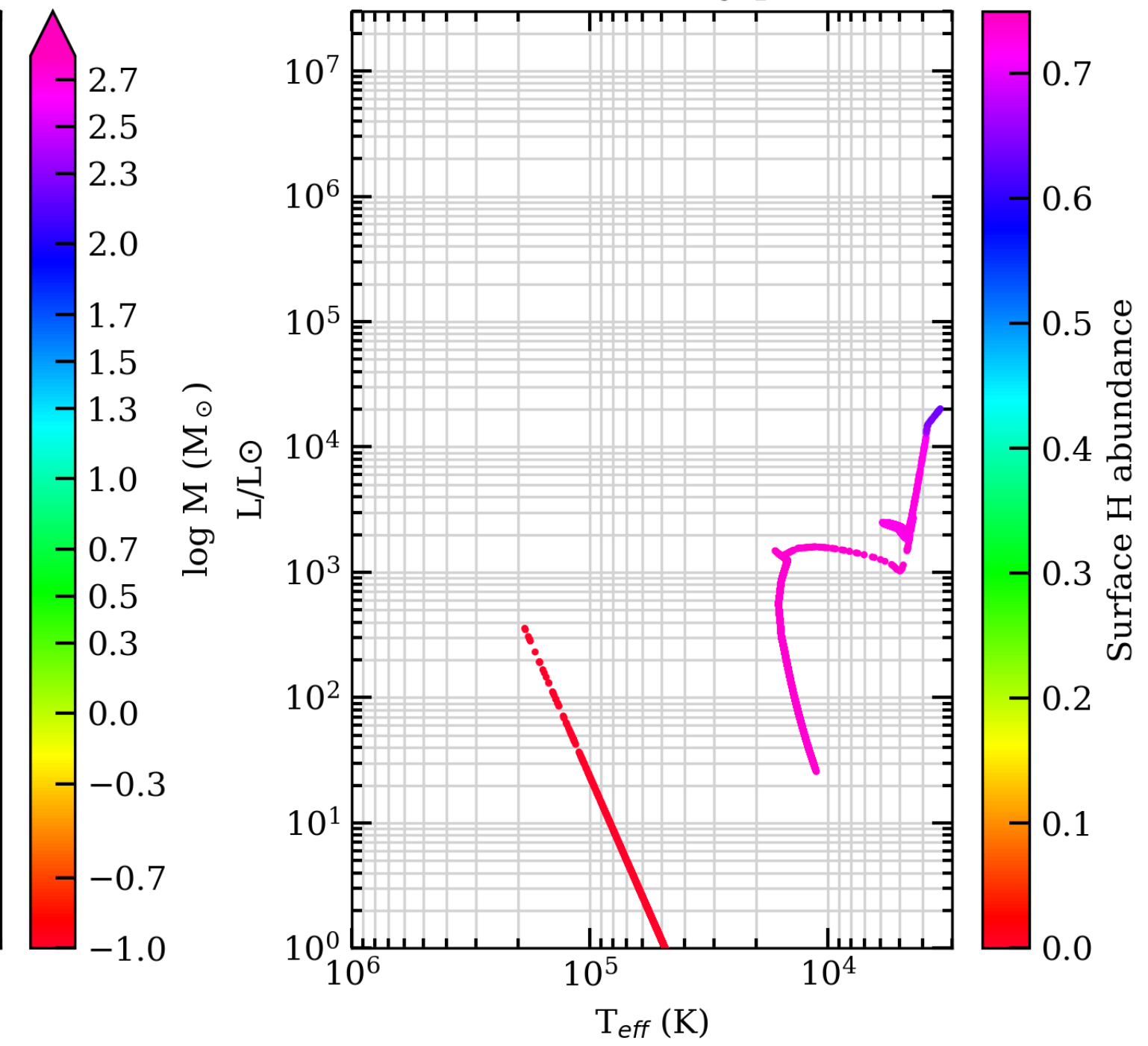
SEVN2.3 VLA binary star tracks



April 2023



156250 binary pairs

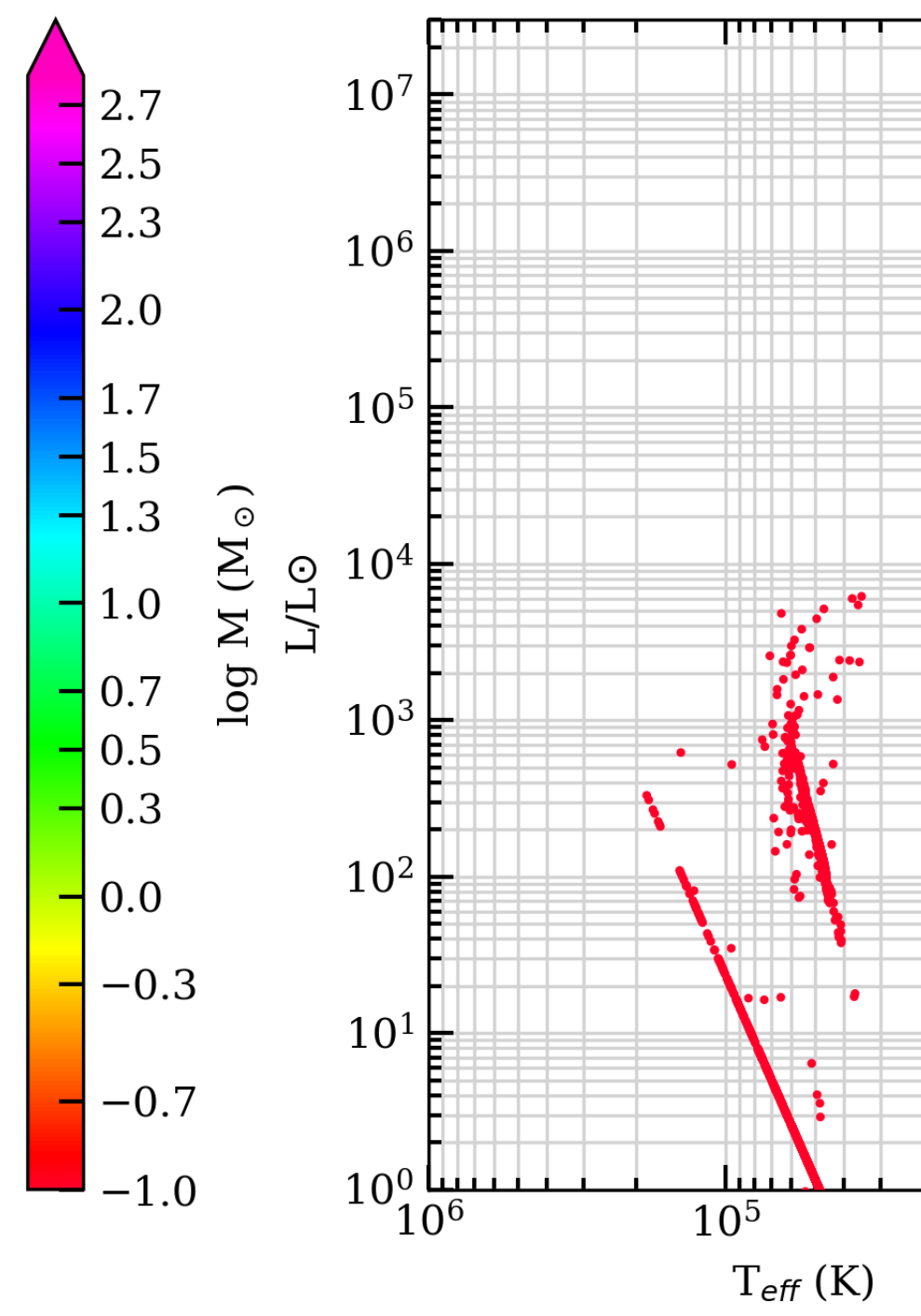
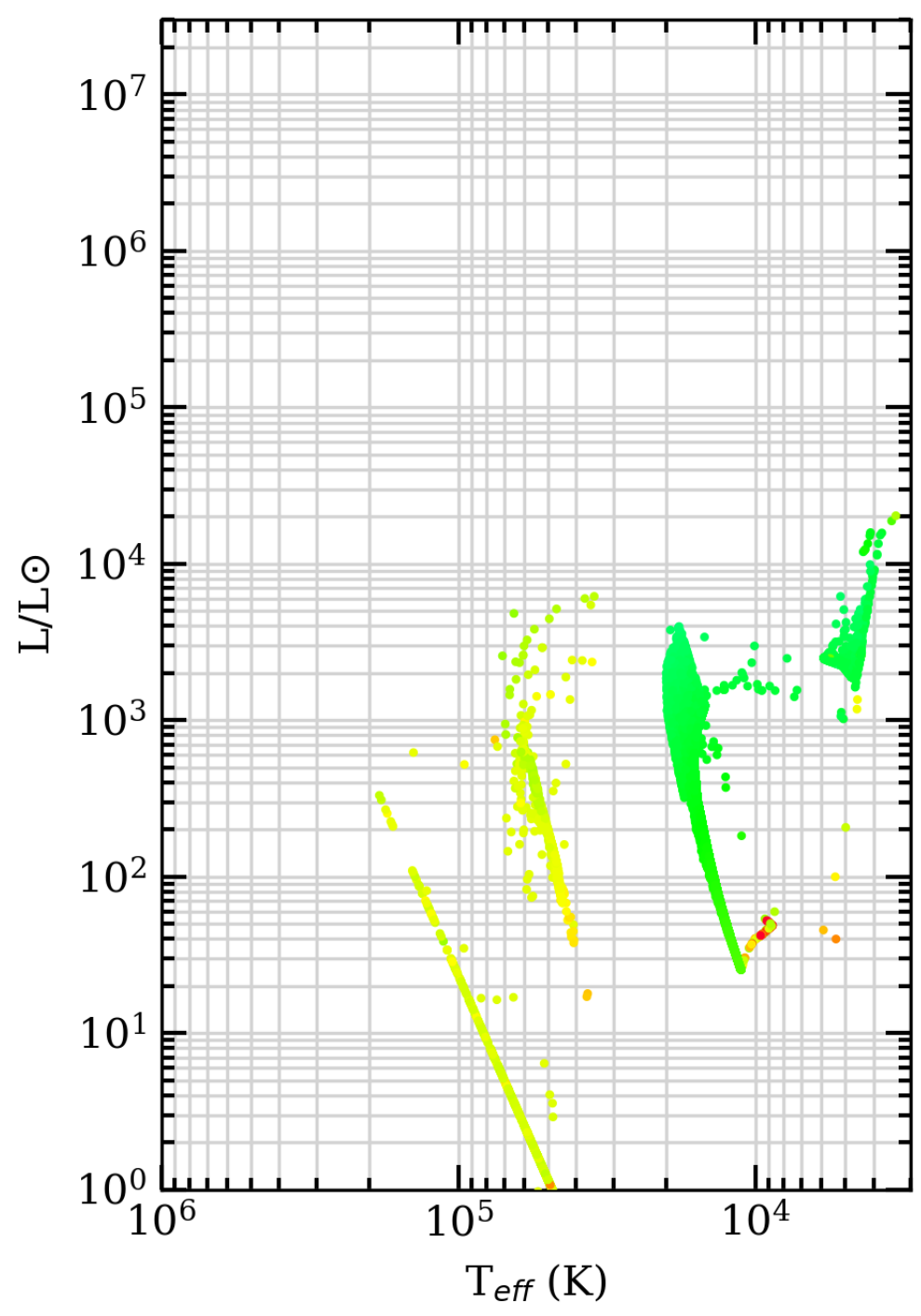
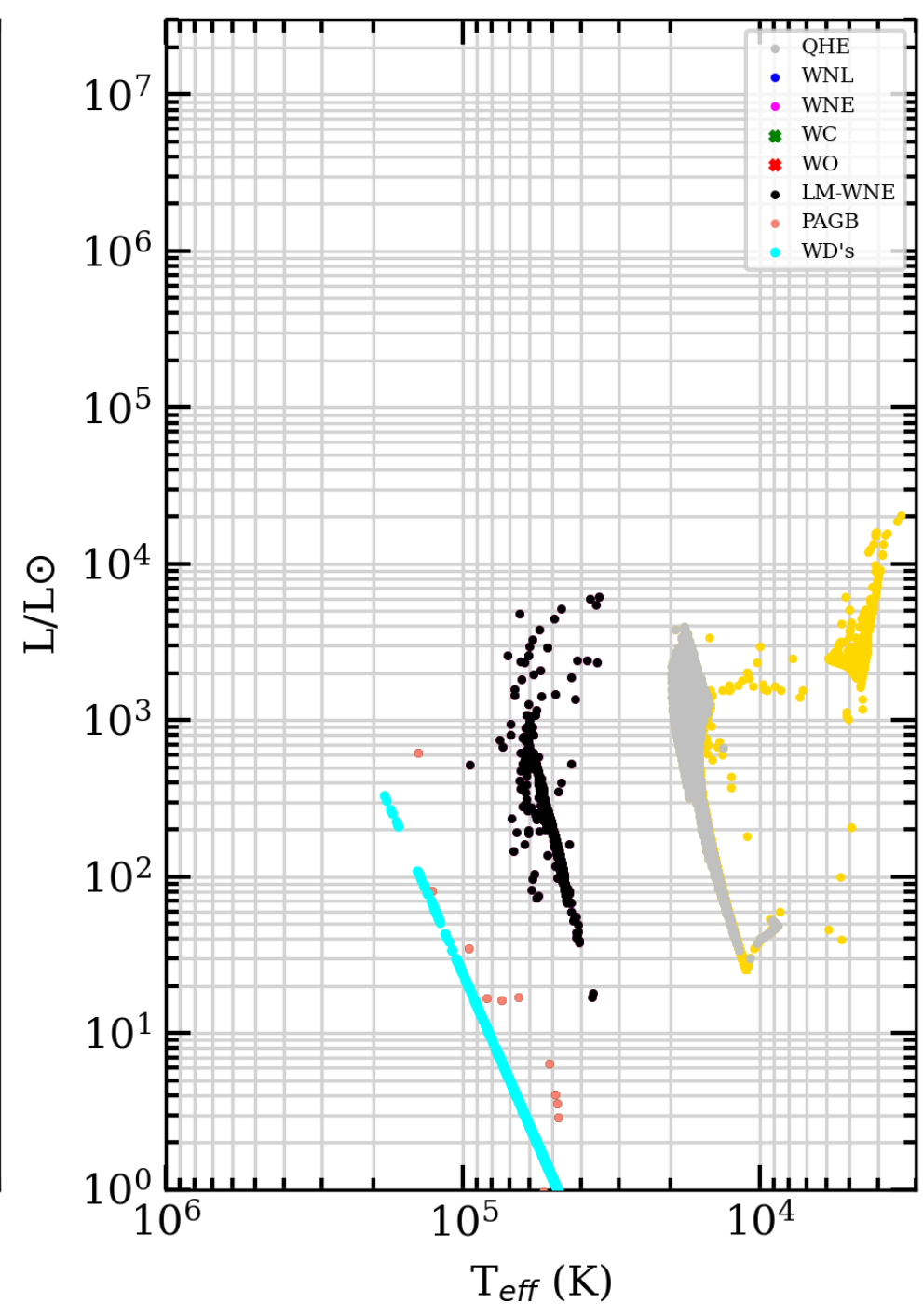
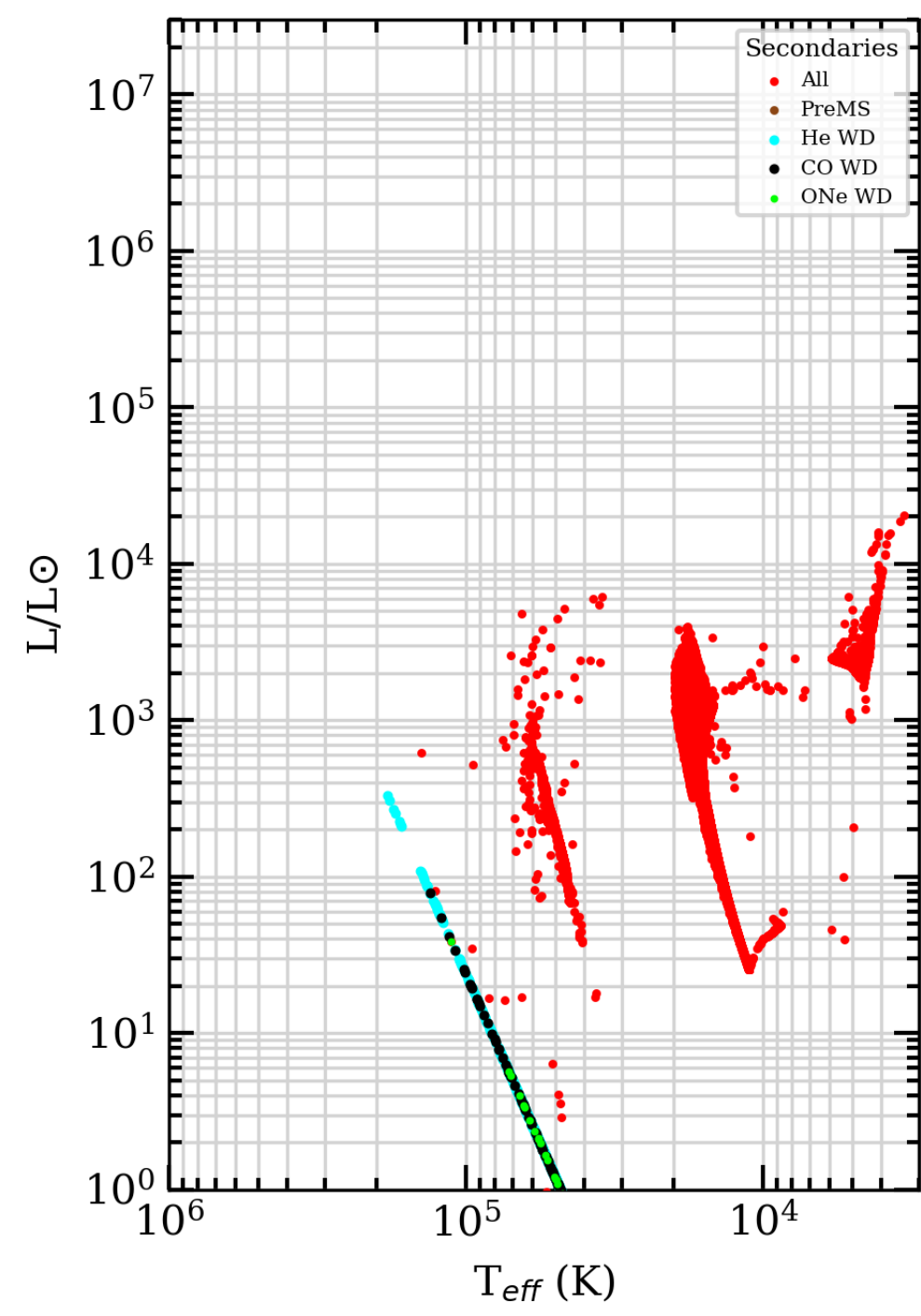
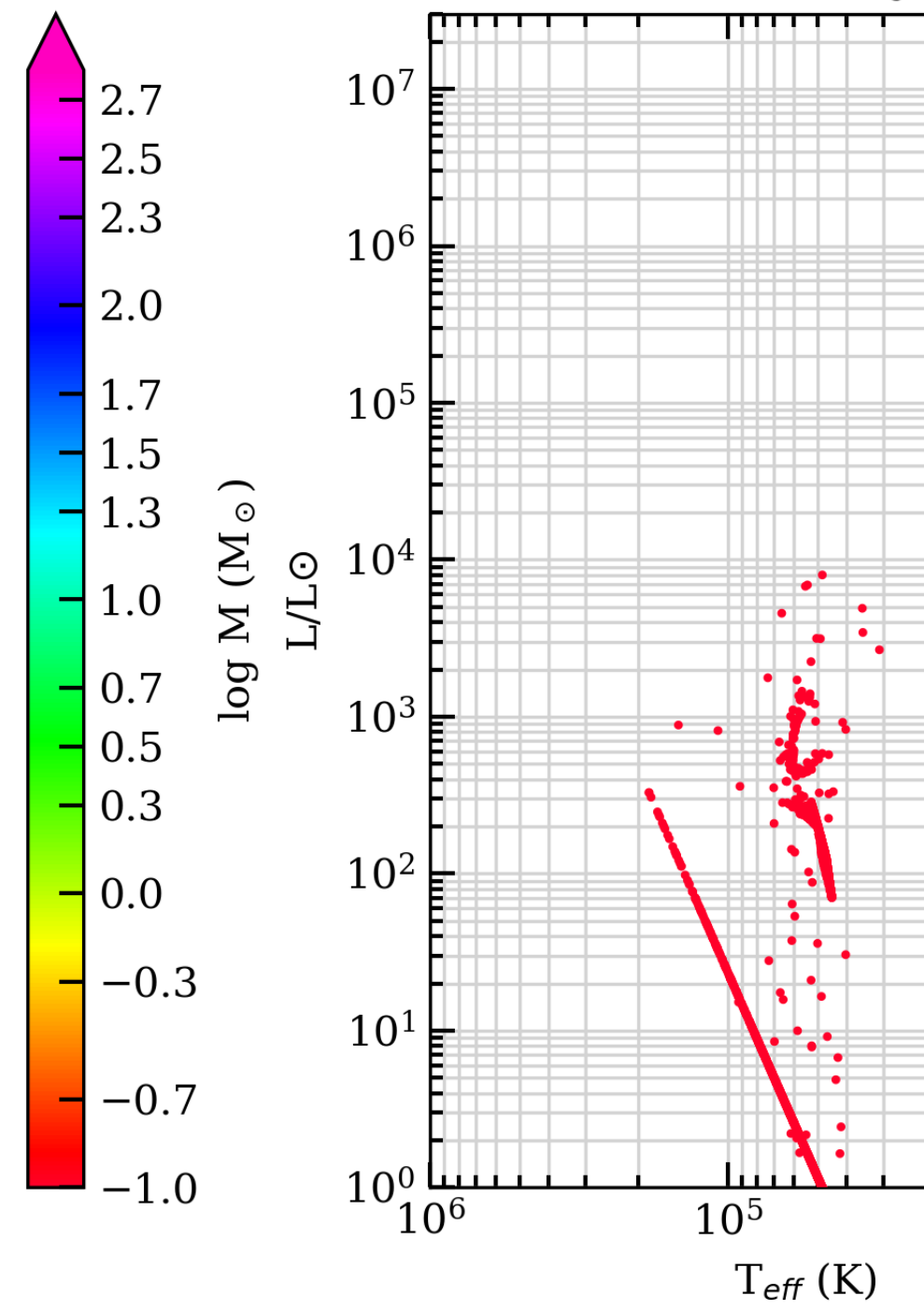
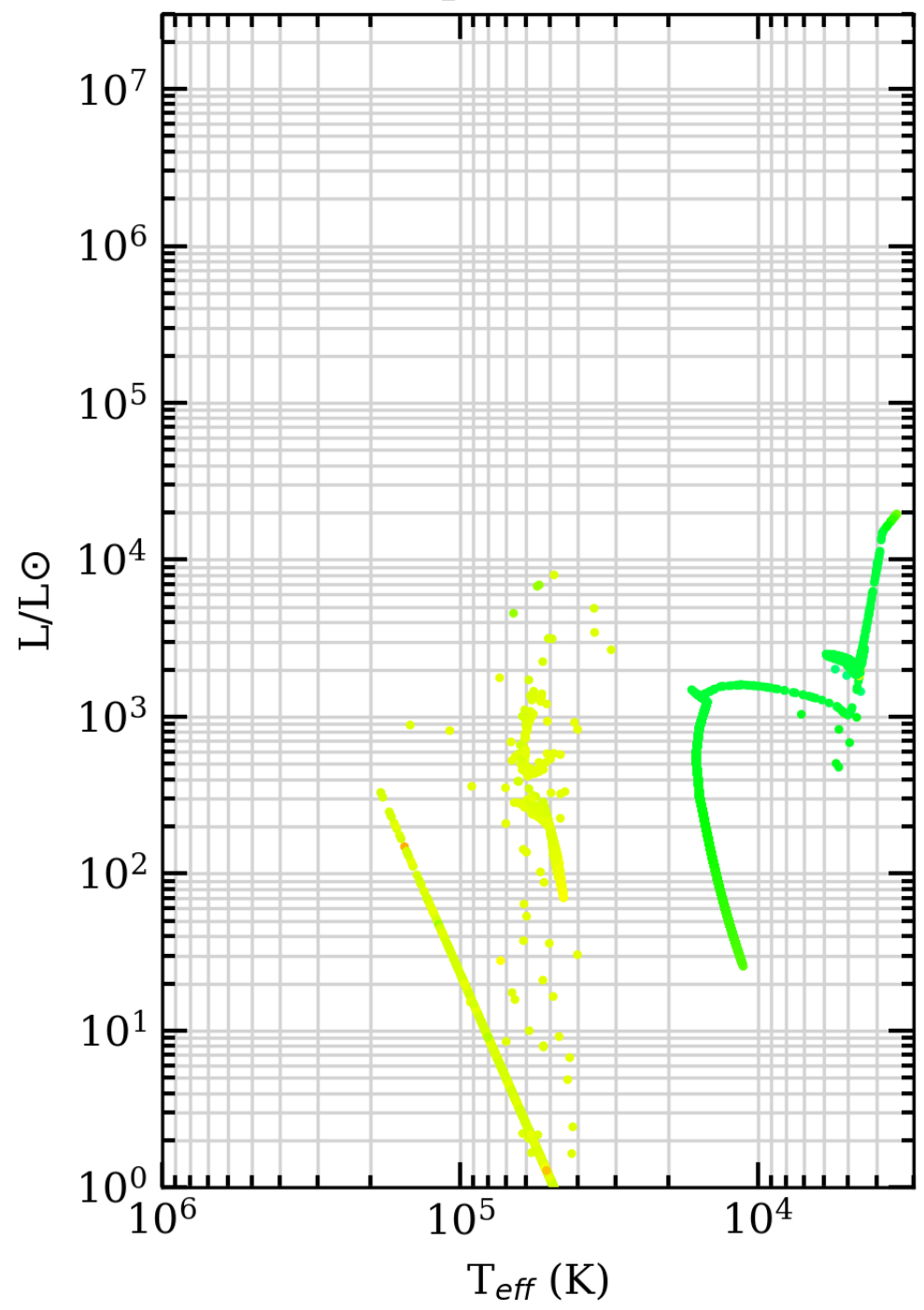
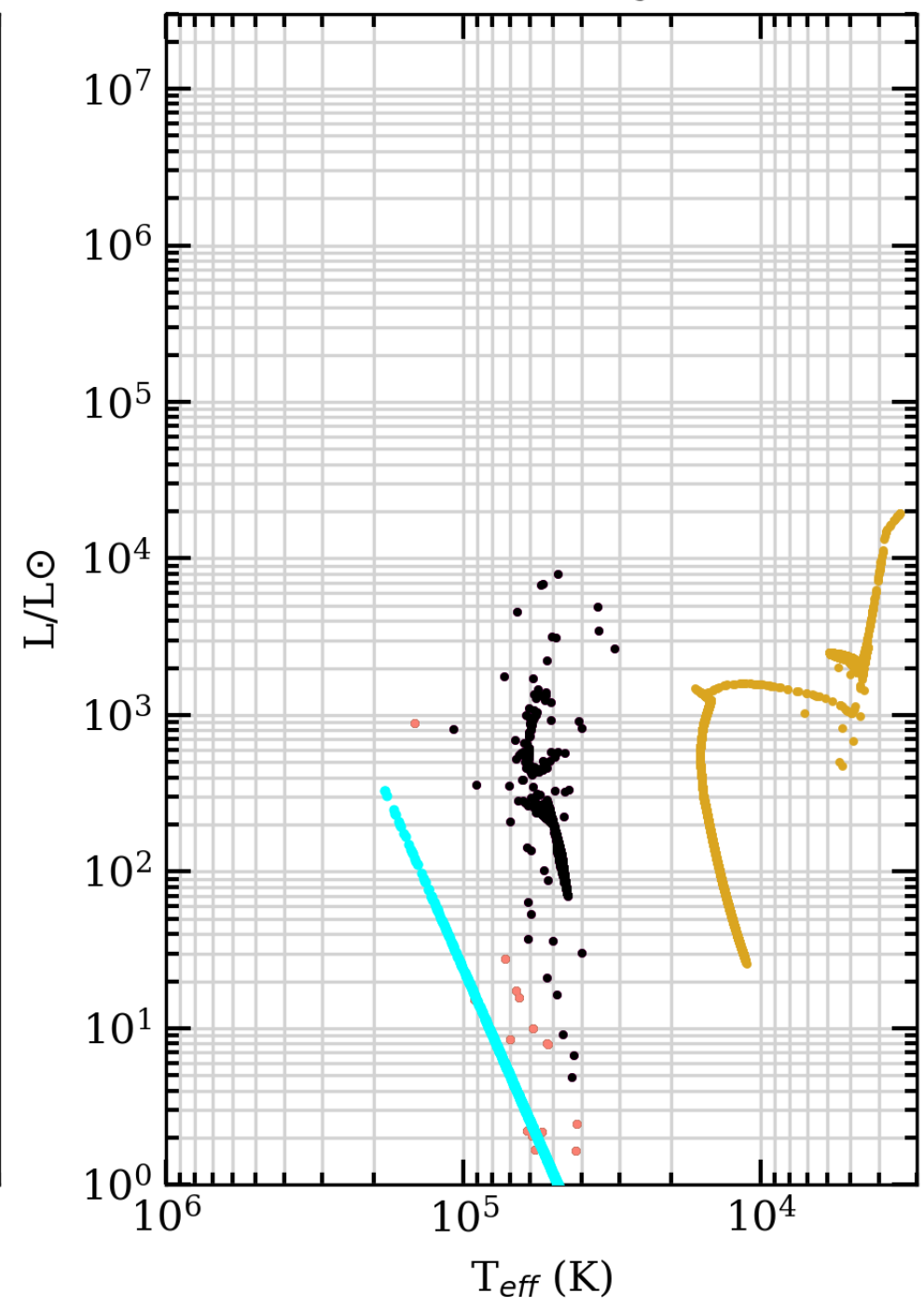
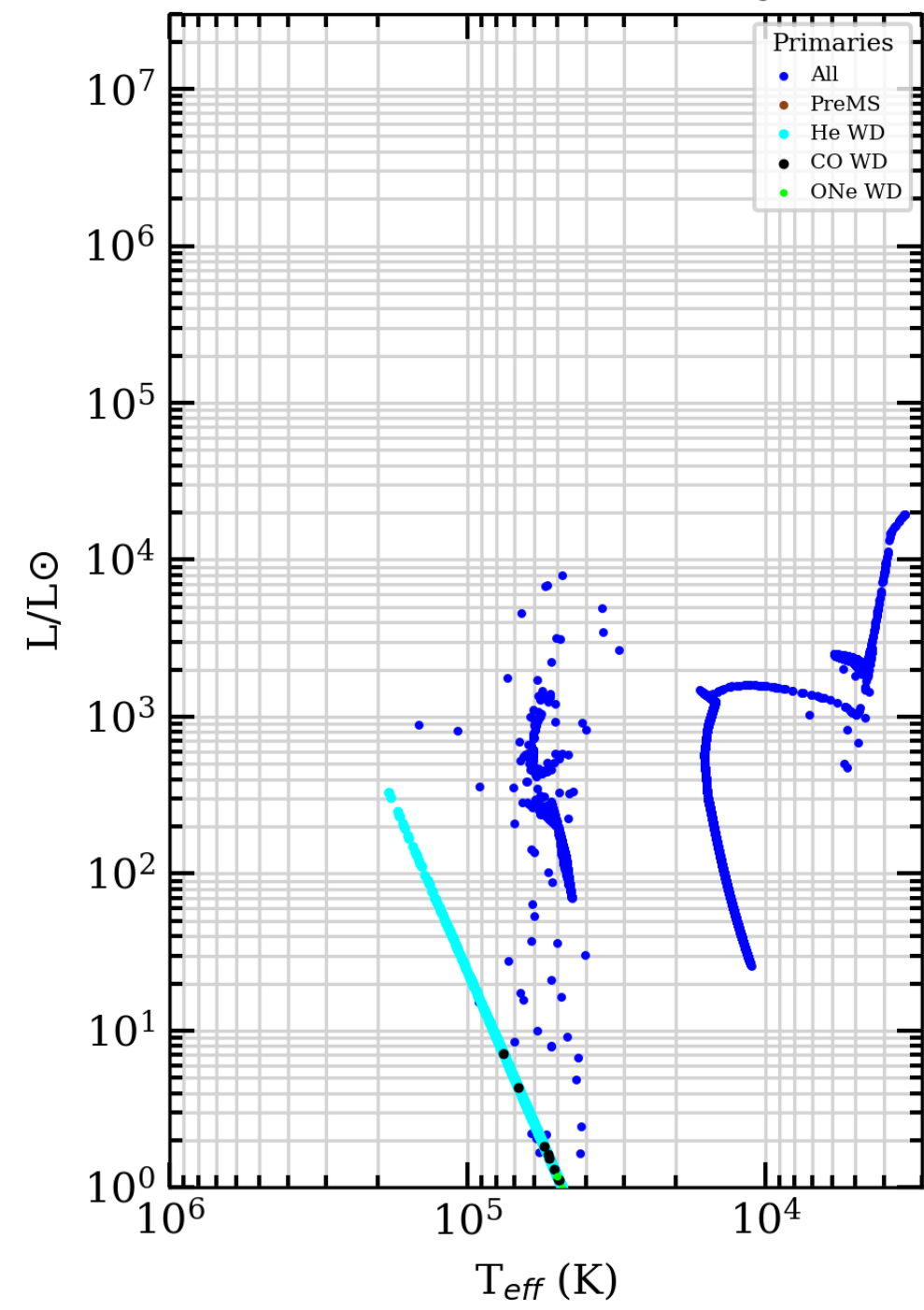


Z=0.004, t=100 Myr

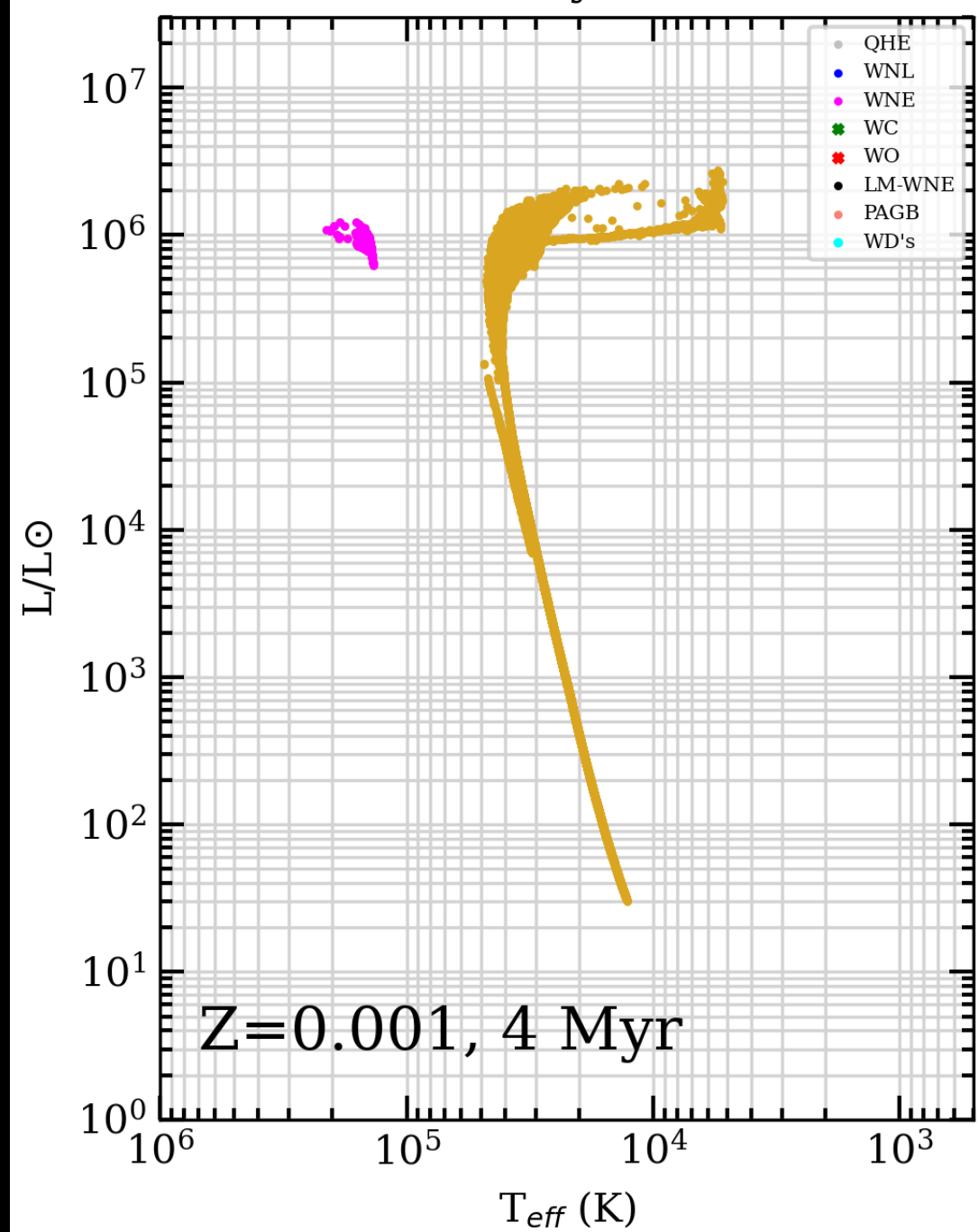
SEVN2.3 STD binary star tracks

April 2023

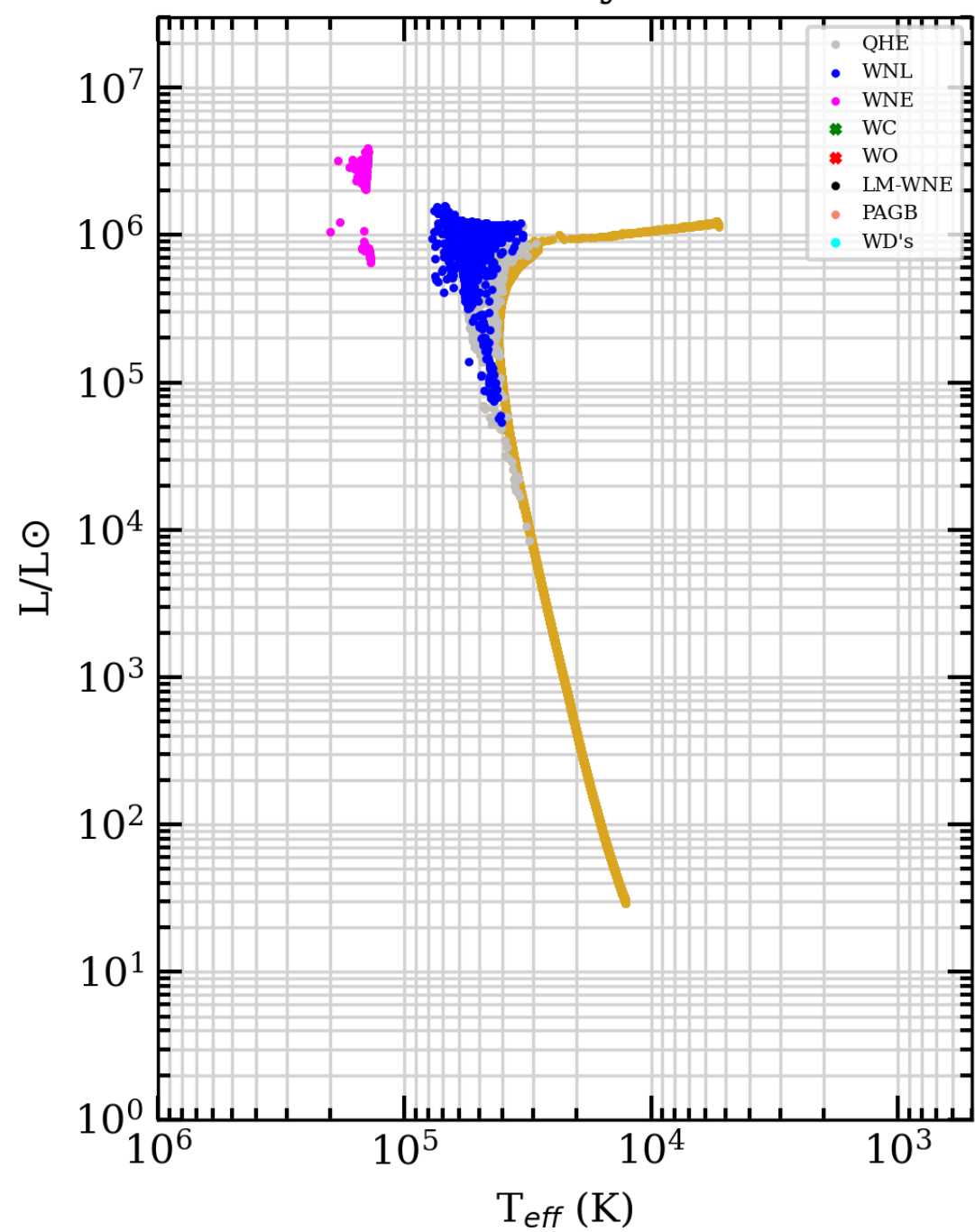
156250 binary pairs



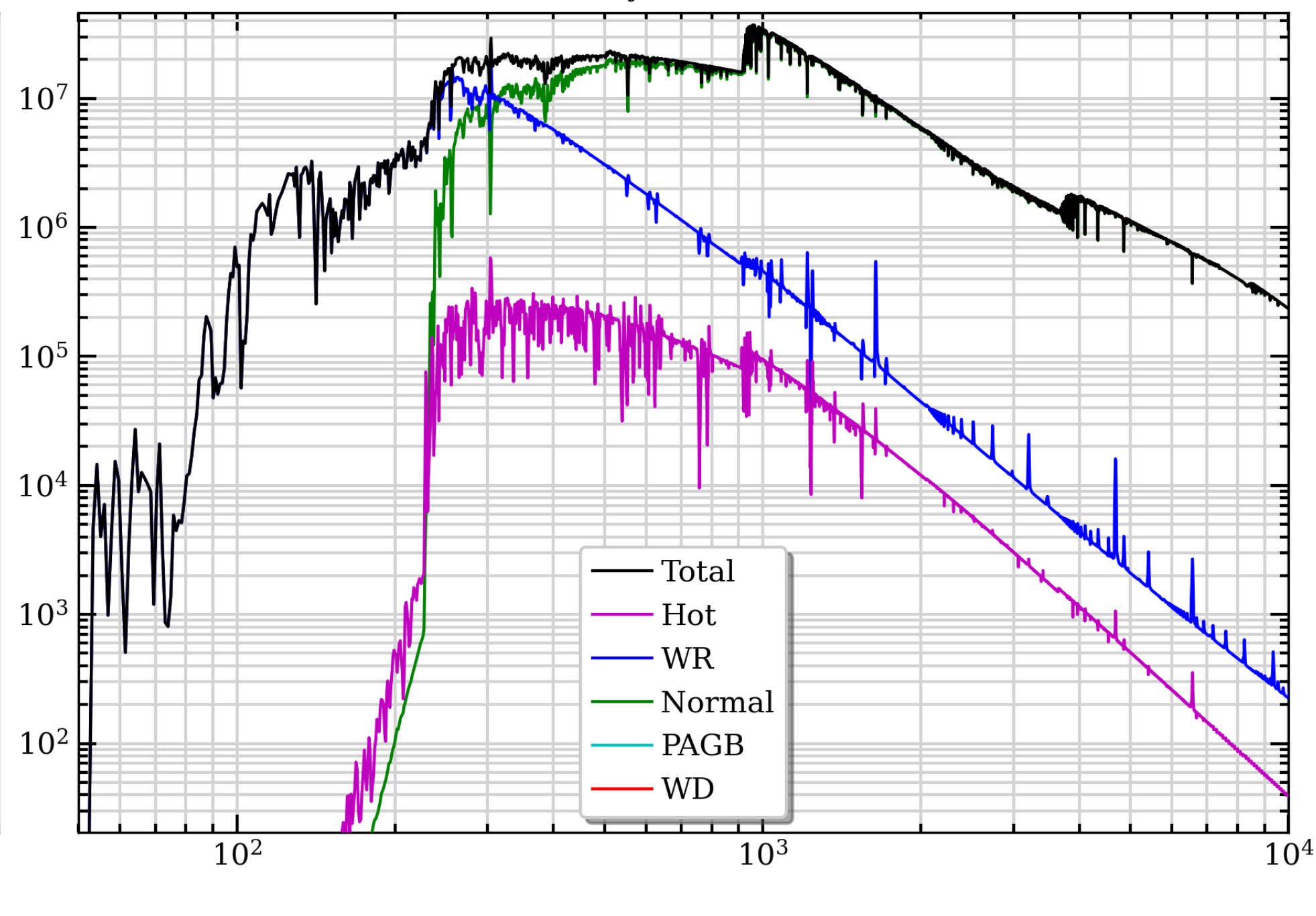
Primary stars



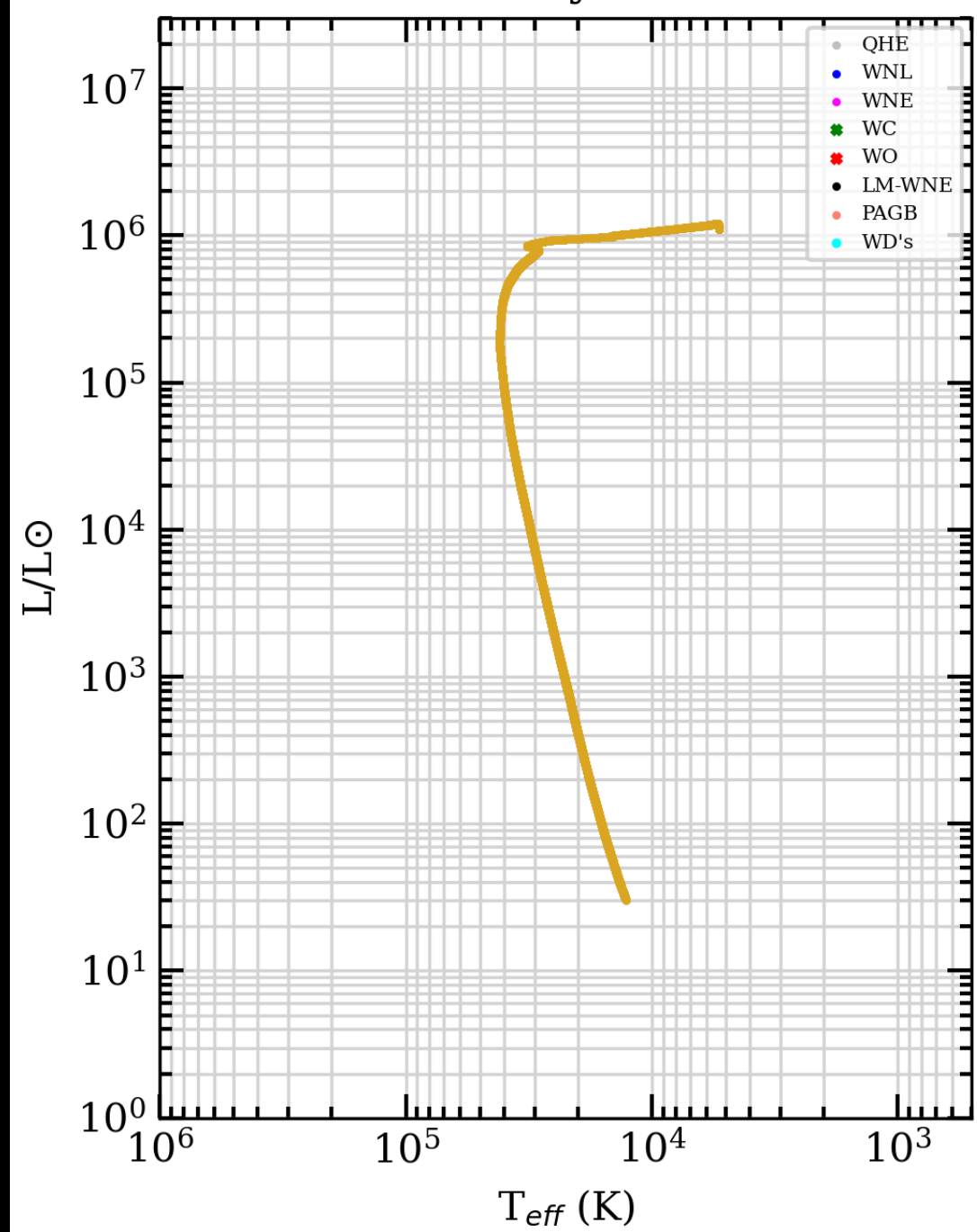
Secondary stars



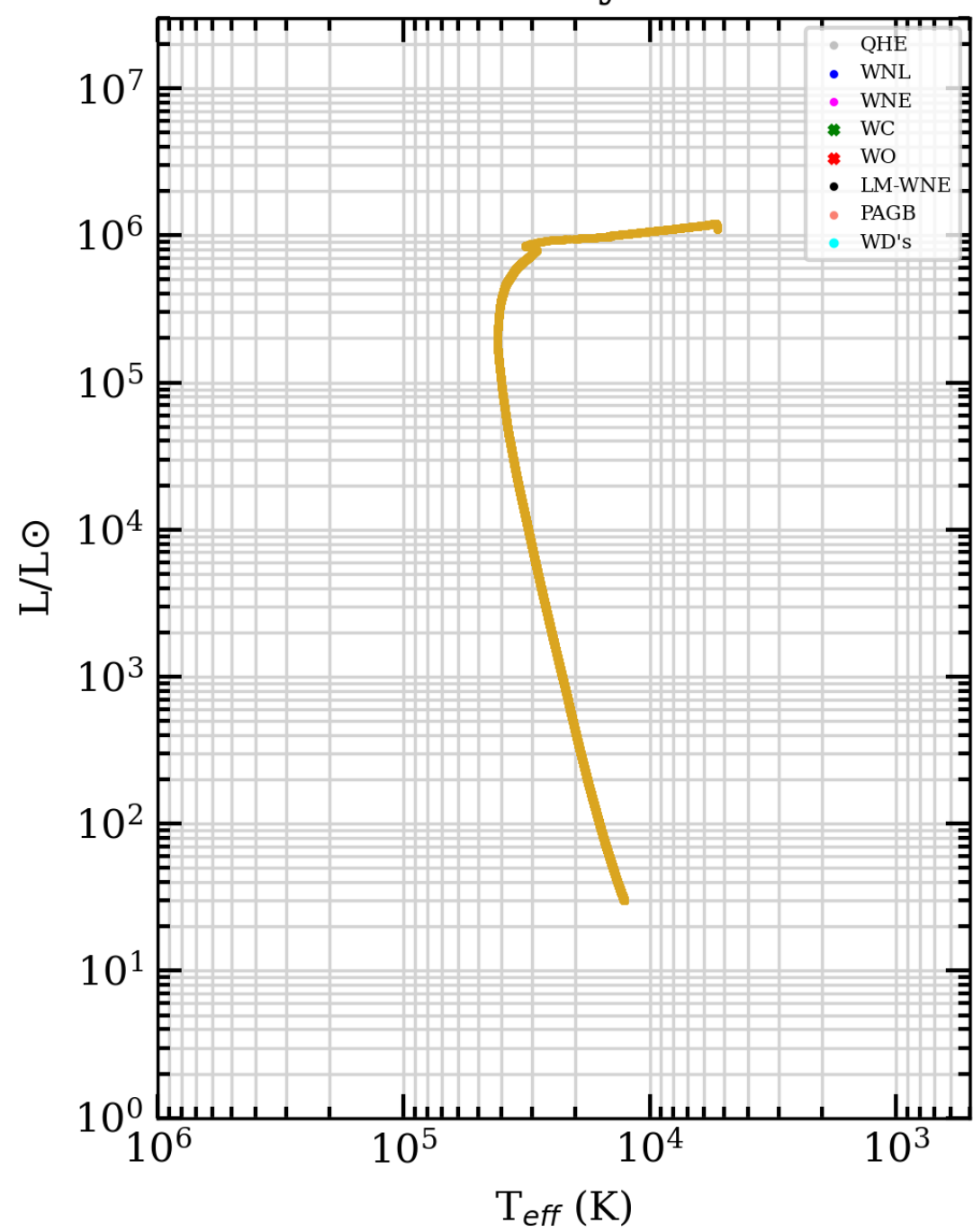
4 Myr, Binaries



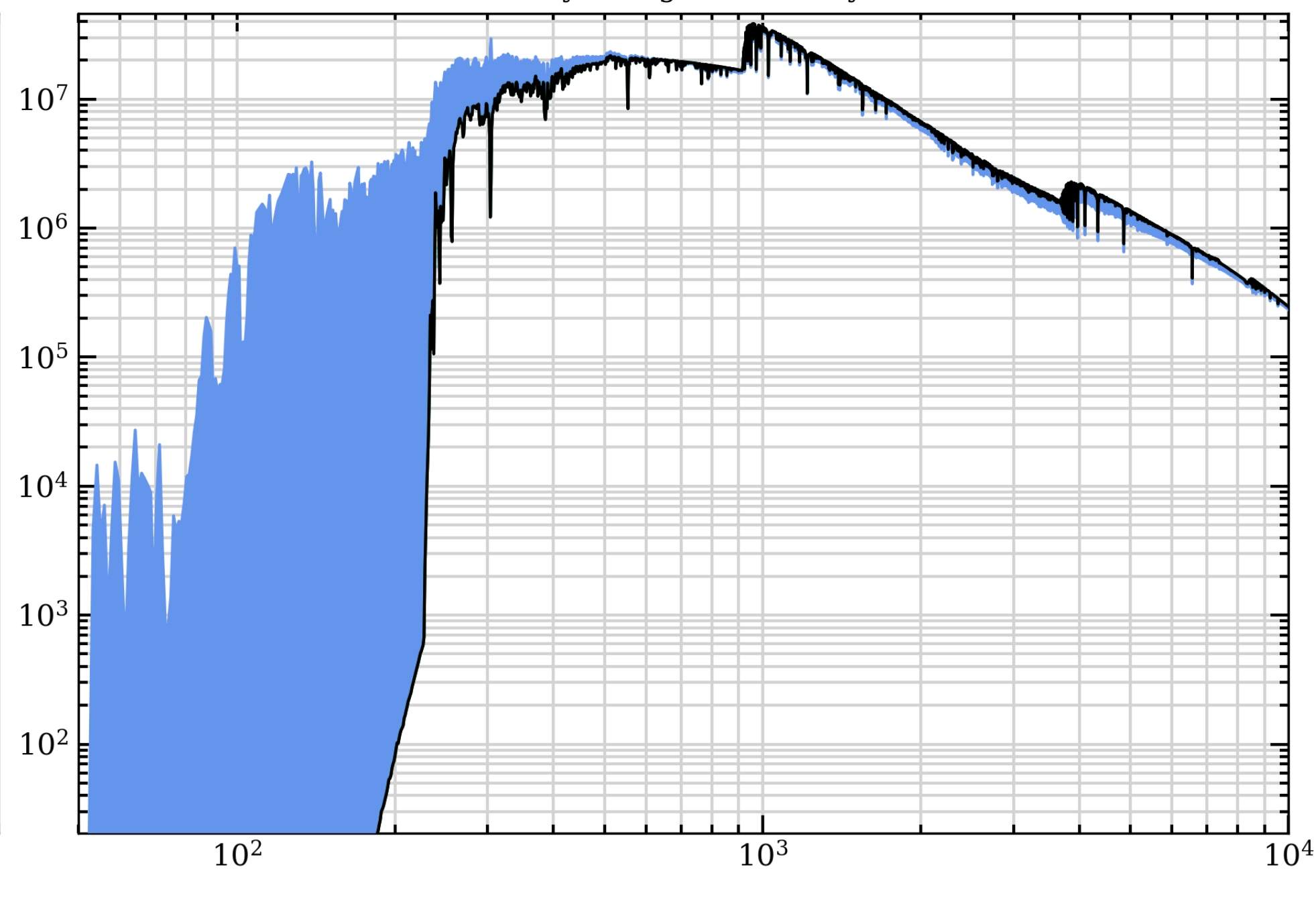
Primary stars

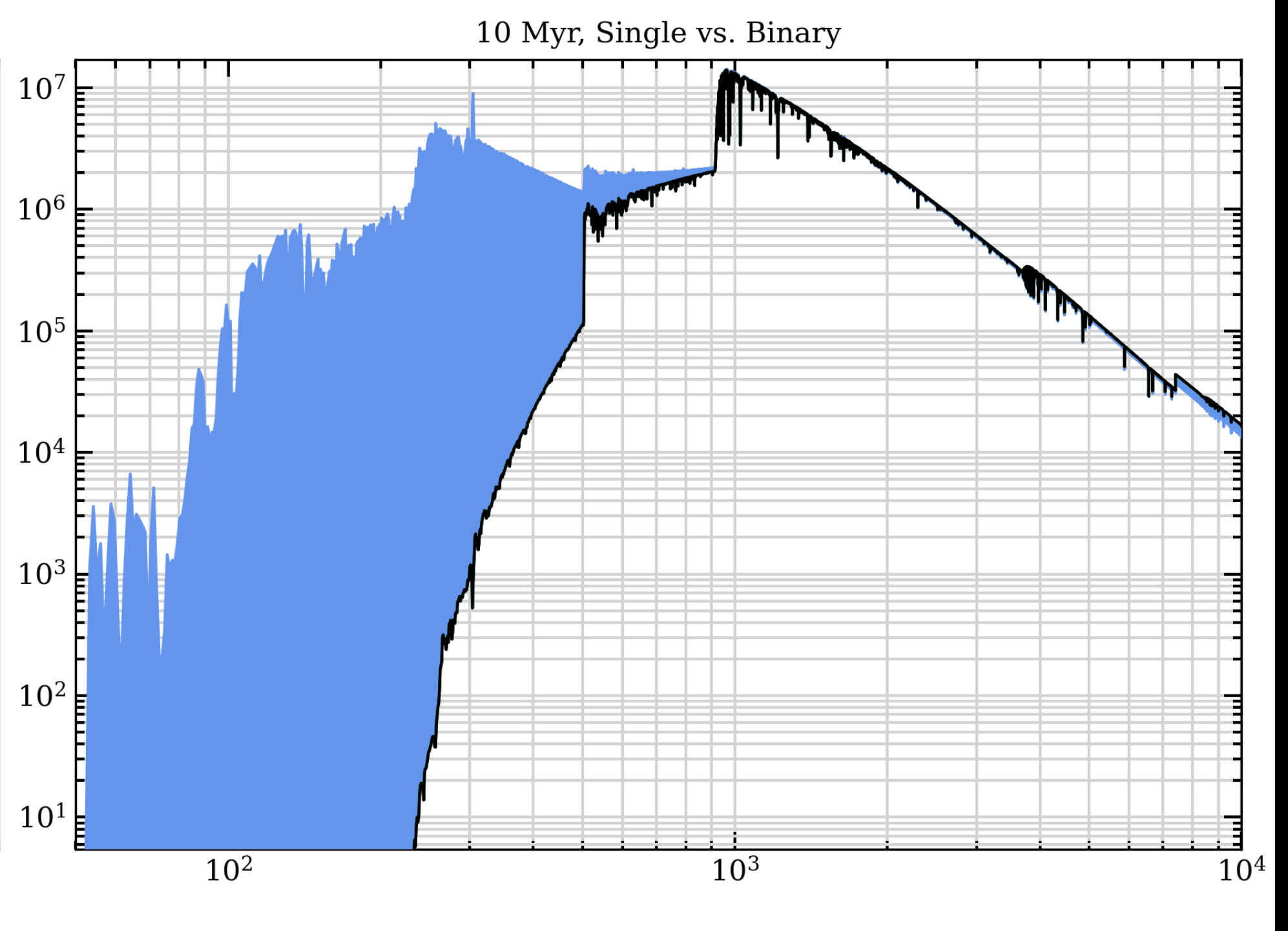
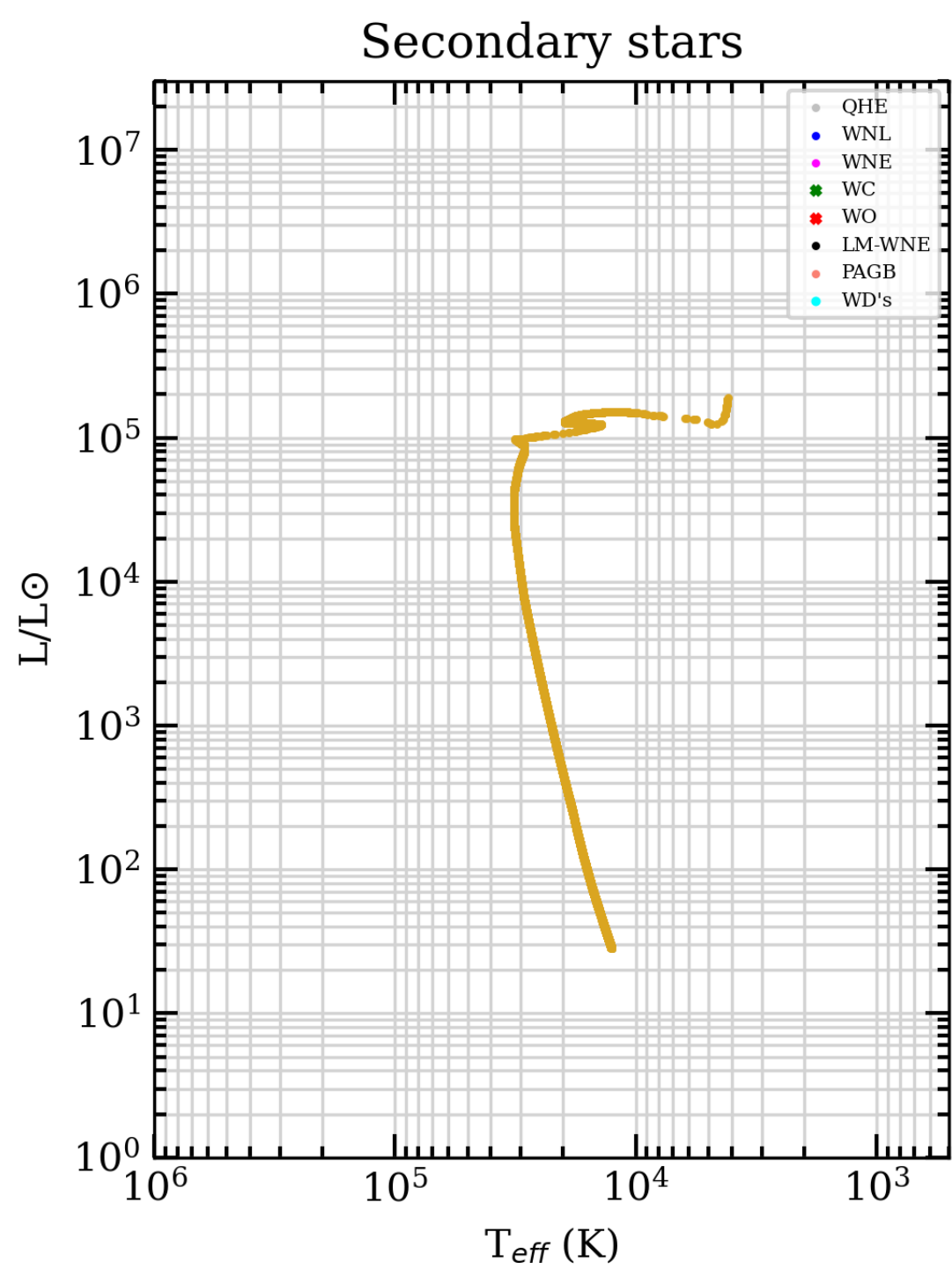
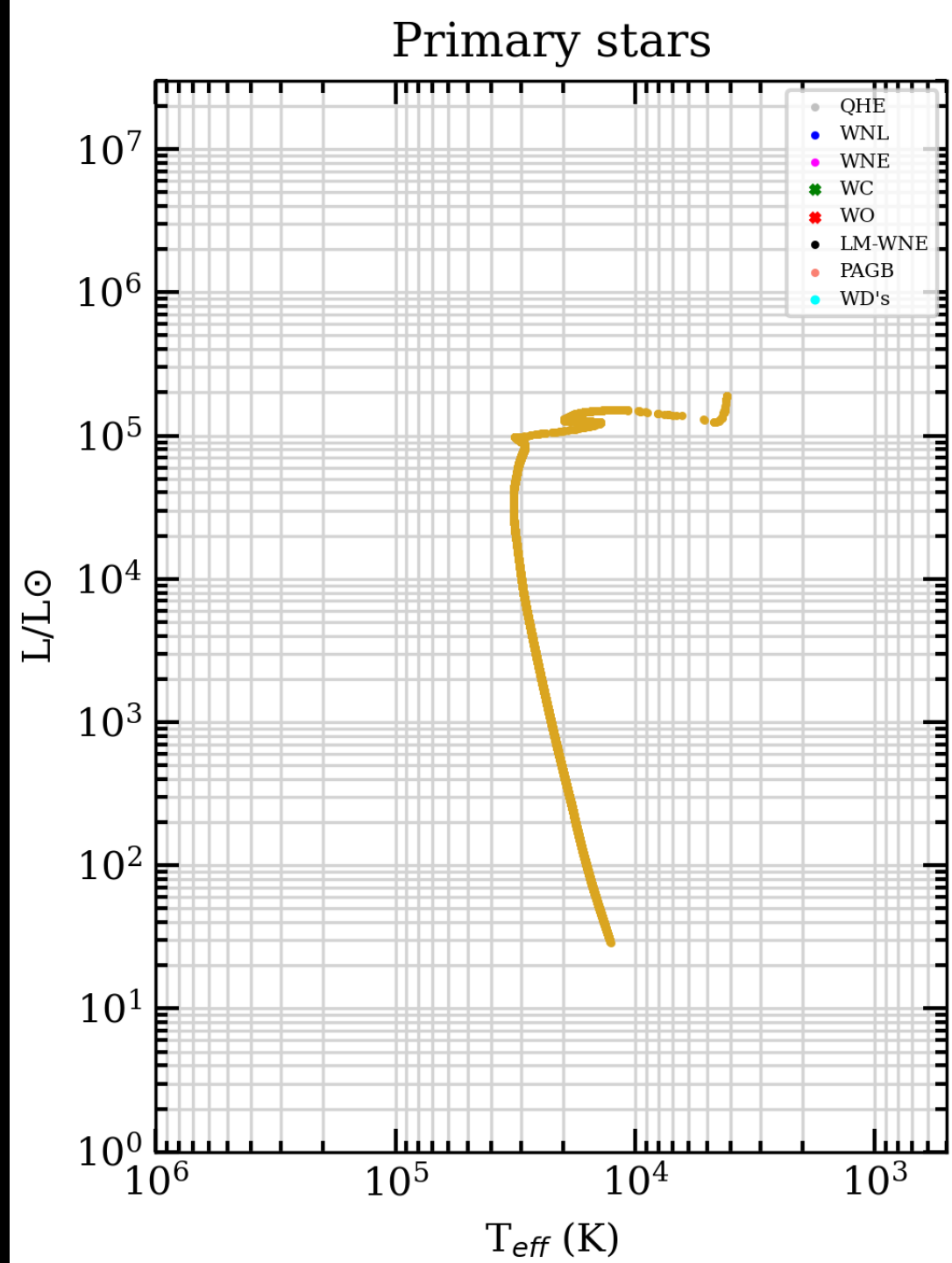
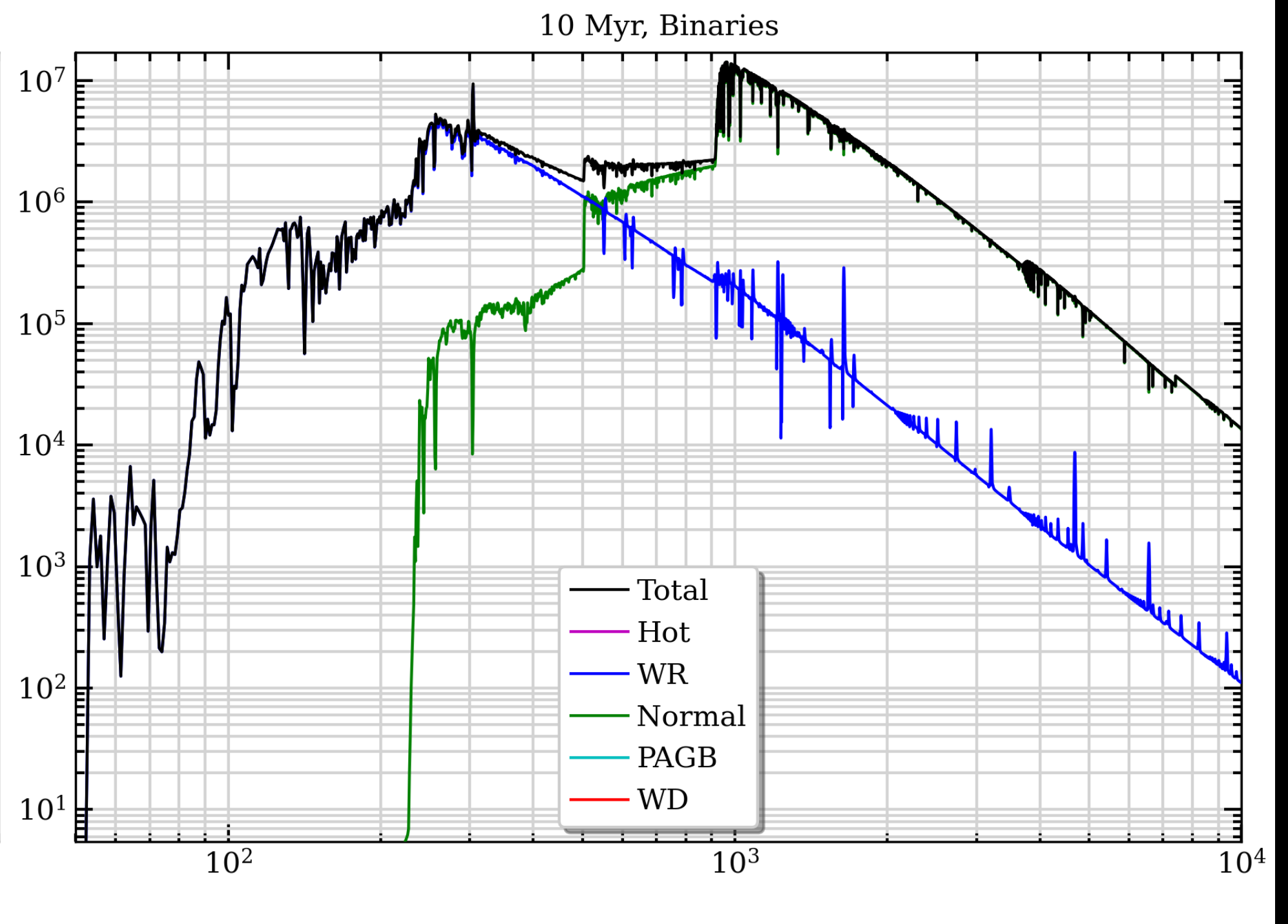
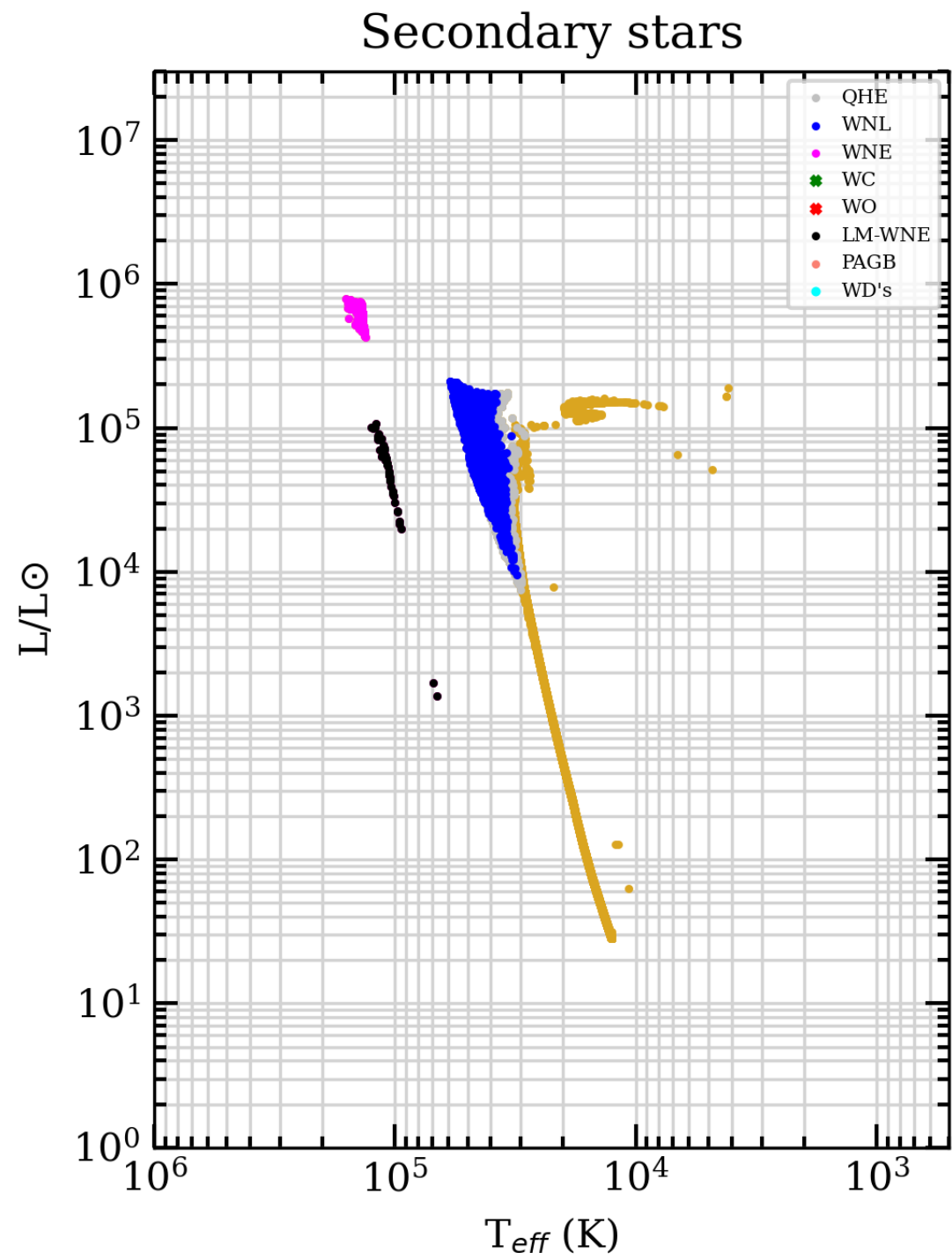
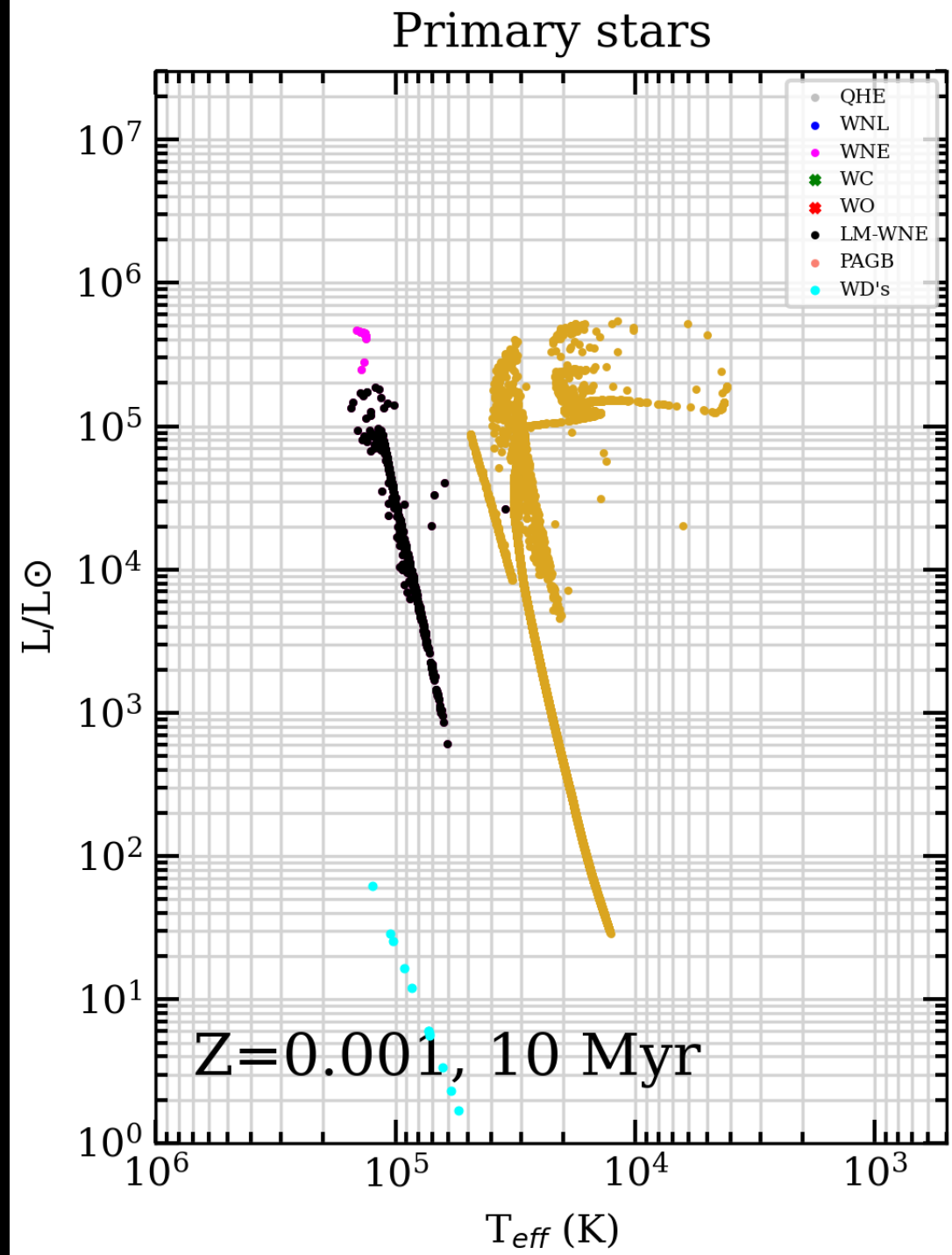


Secondary stars

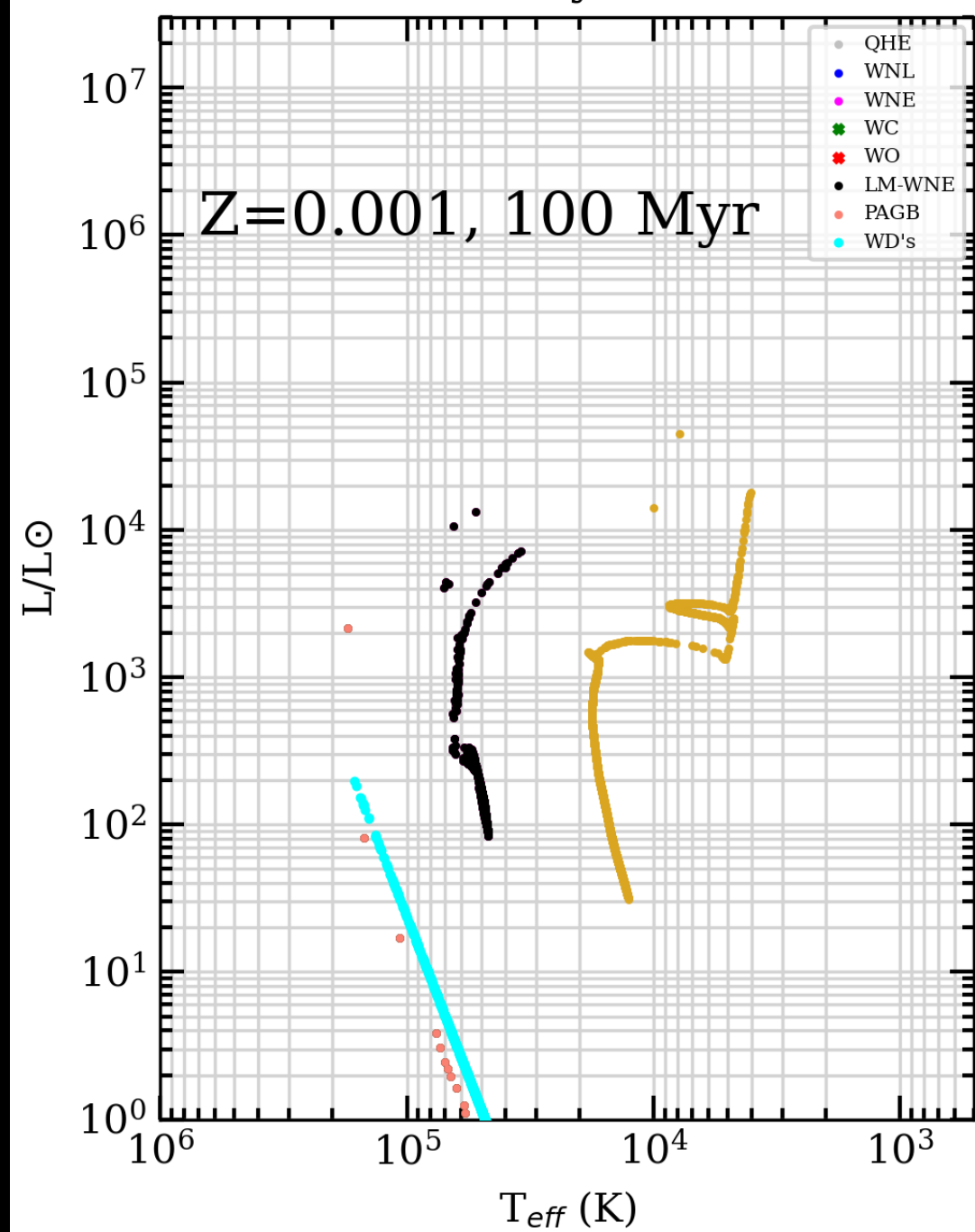


4 Myr, Single vs. Binary

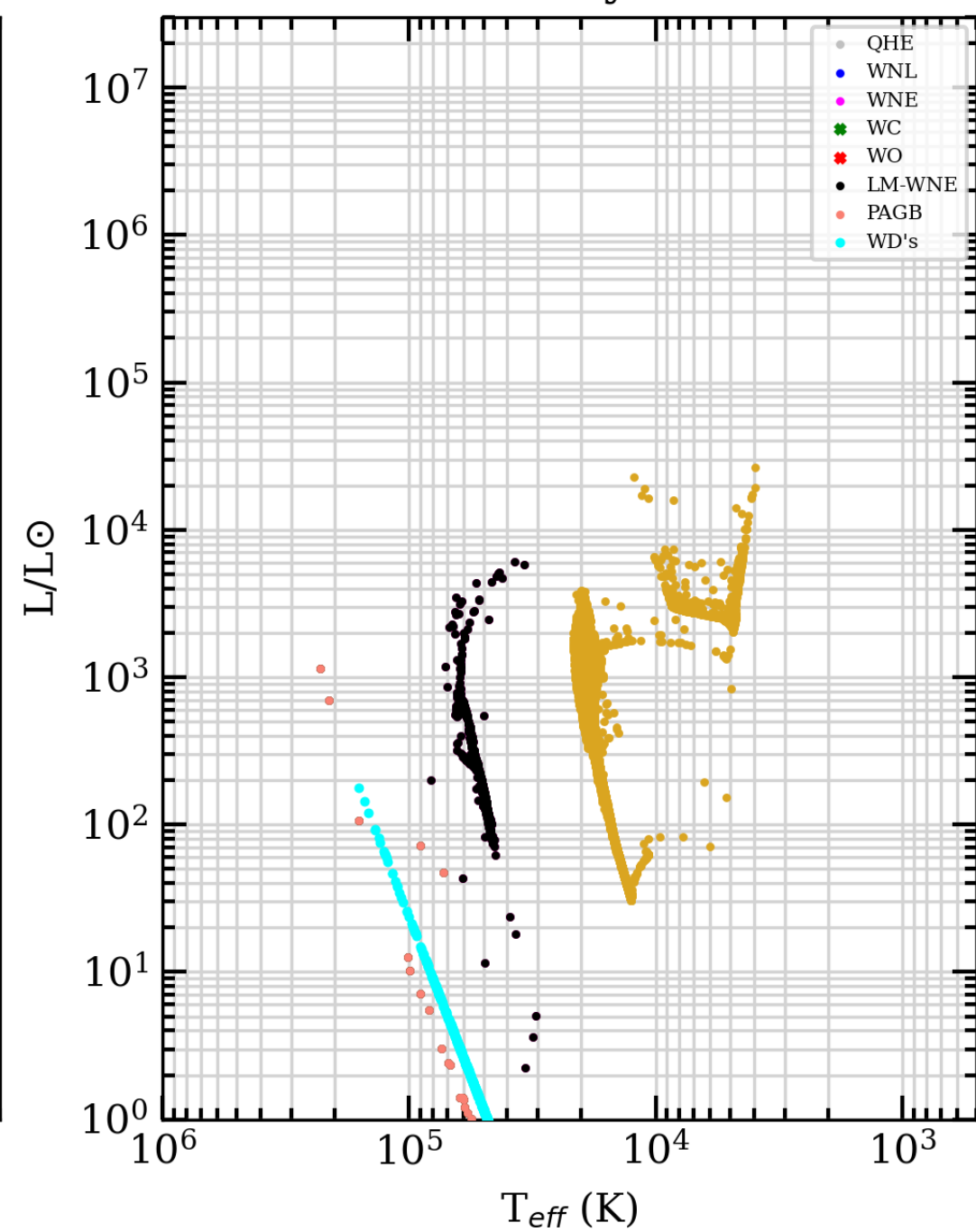




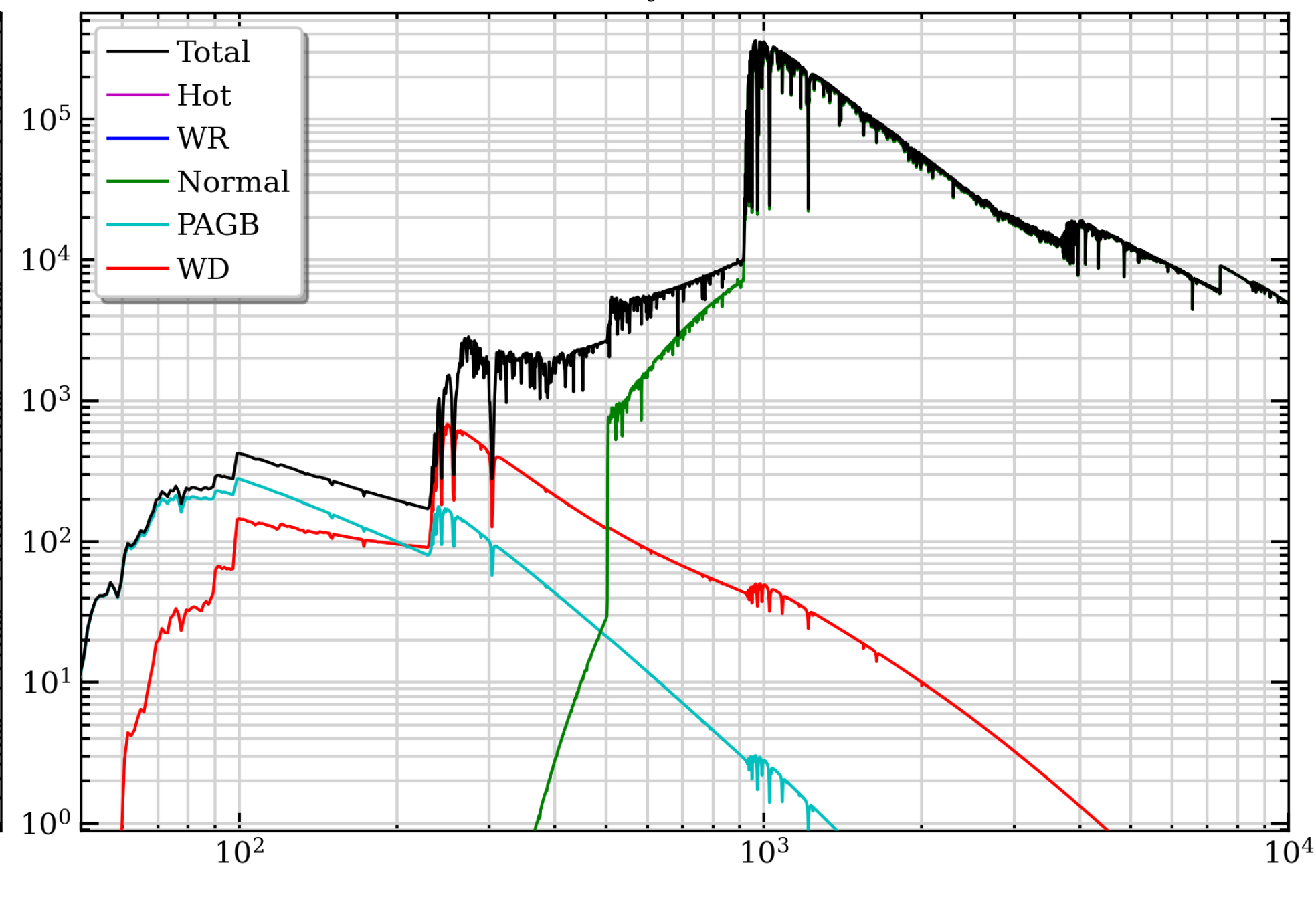
Primary stars



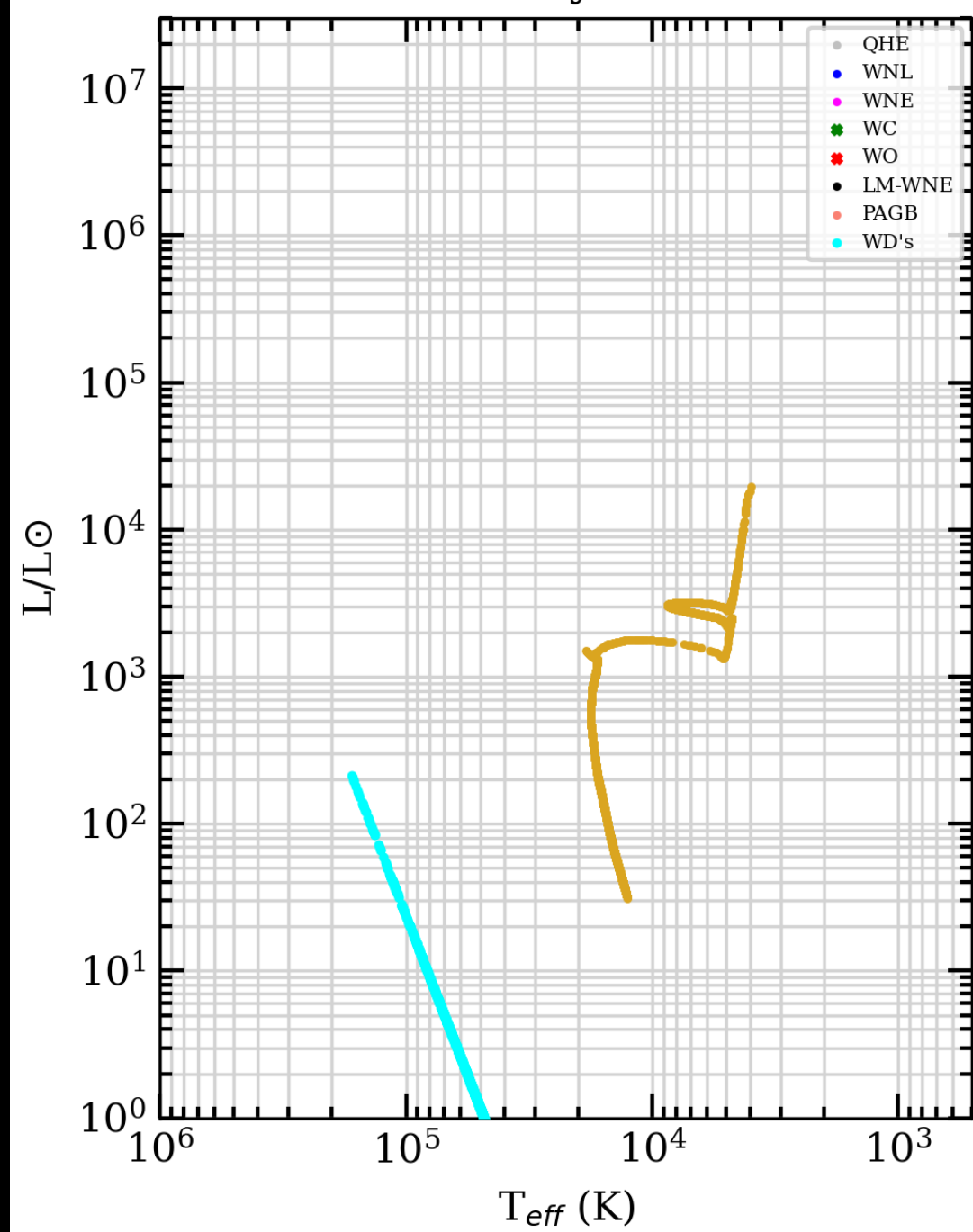
Secondary stars



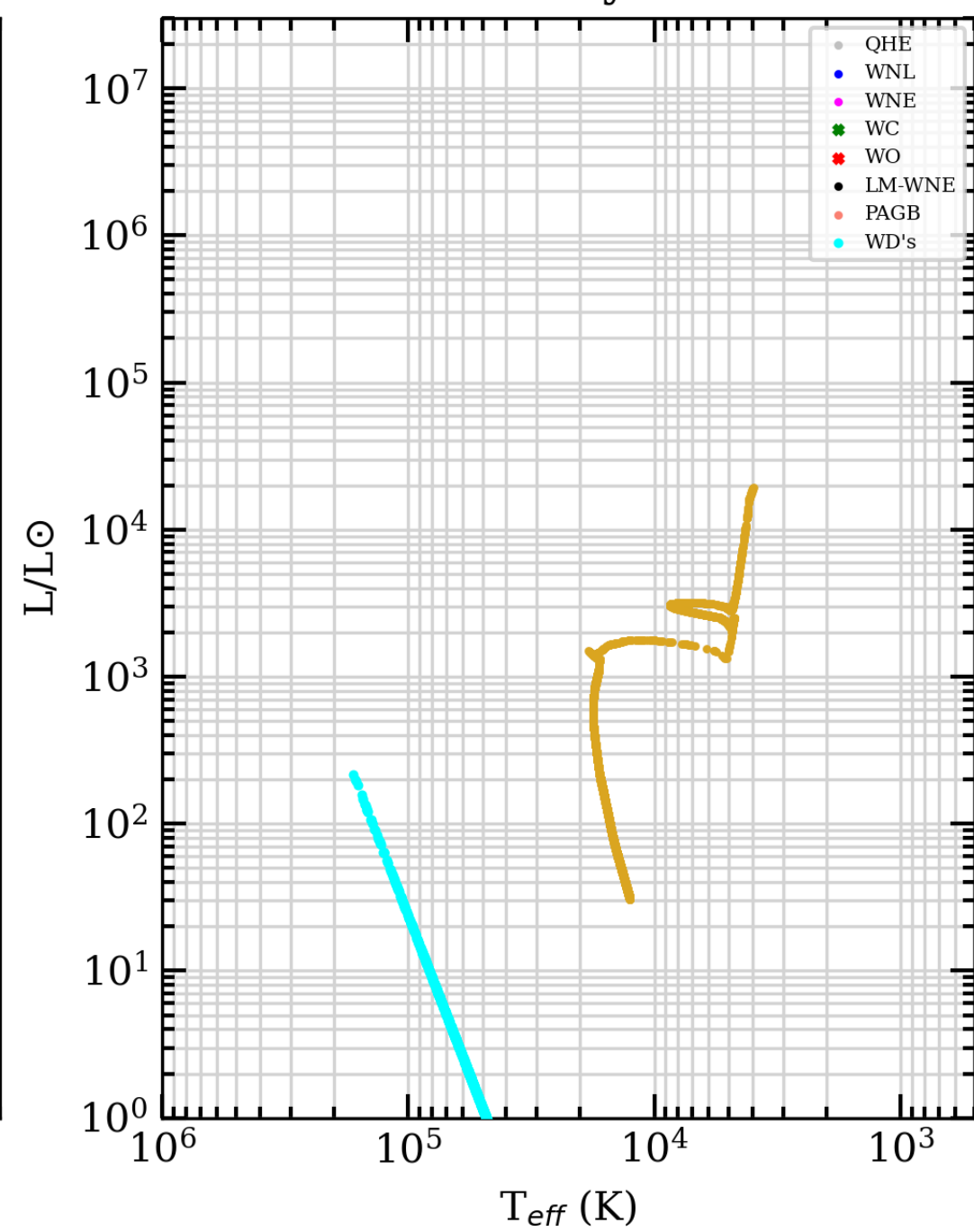
100 Myr, Binaries



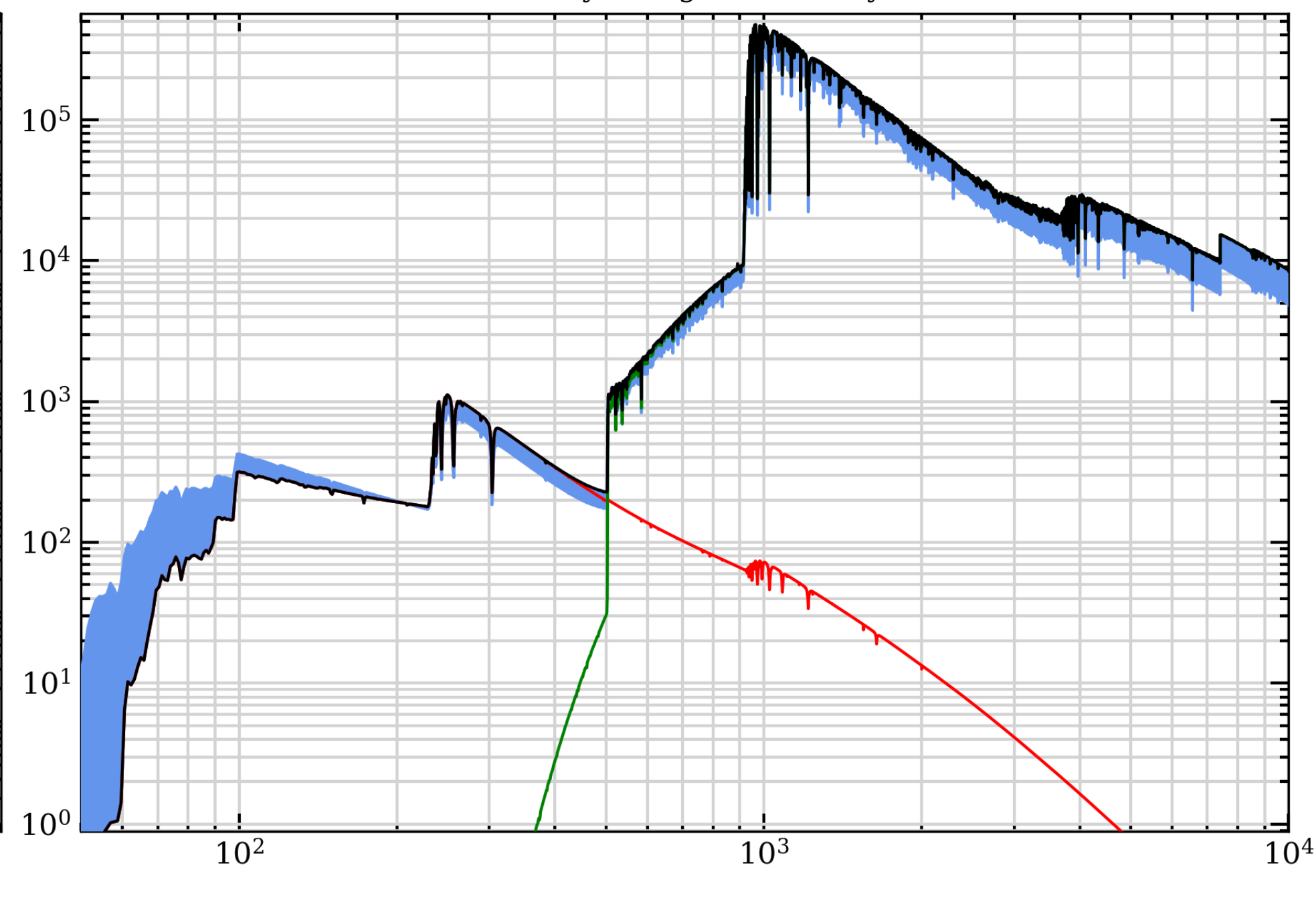
Primary stars

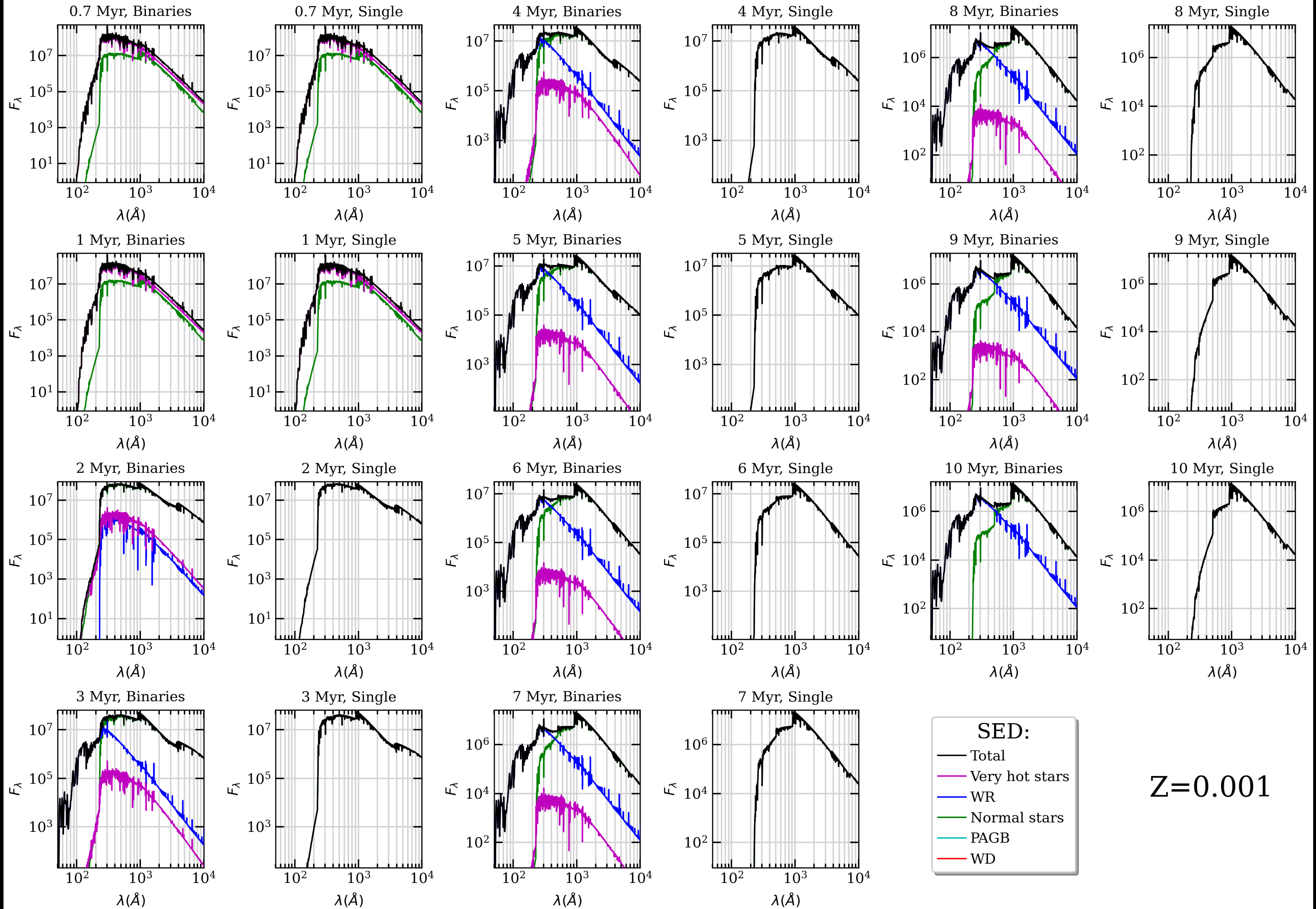


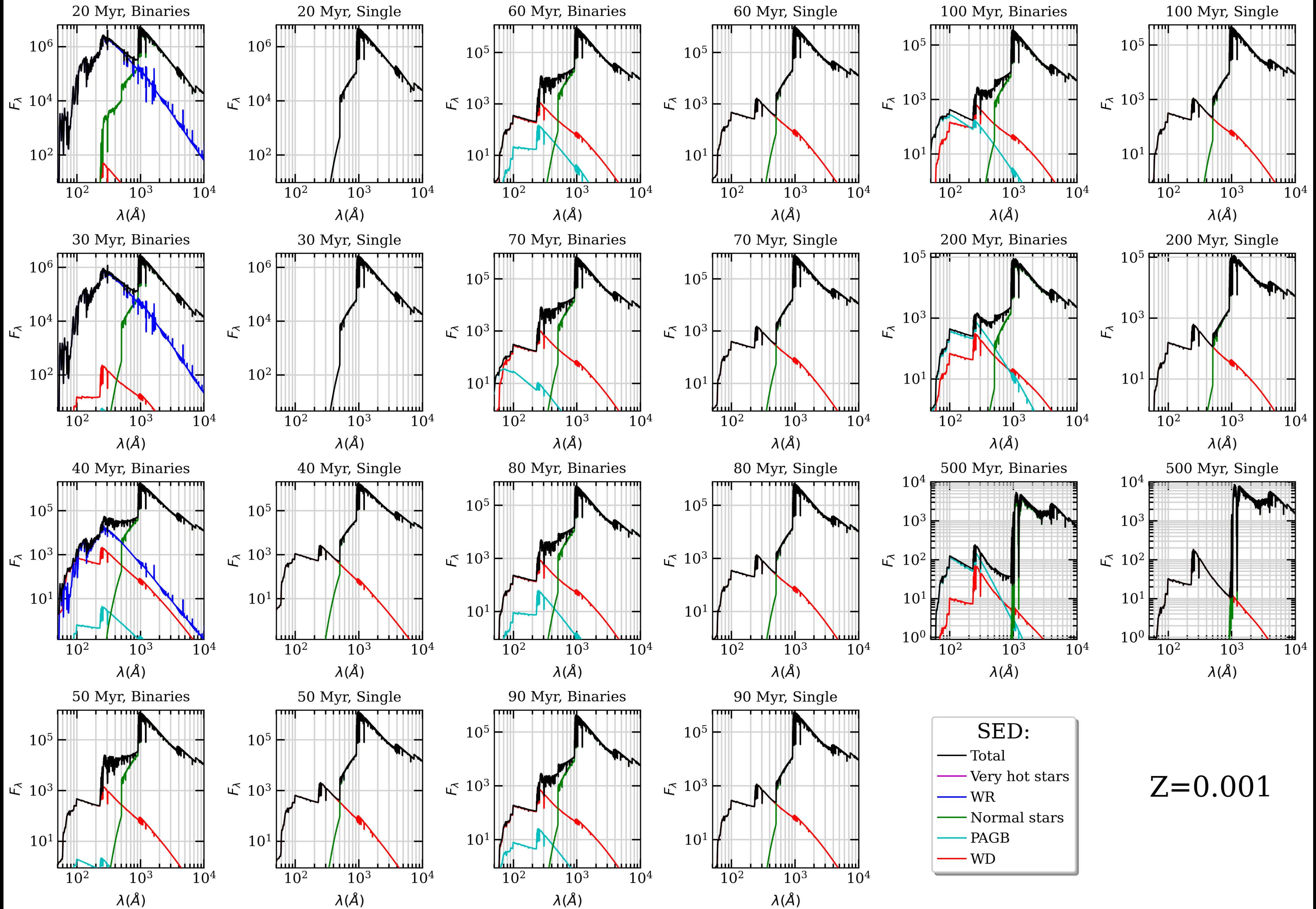
Secondary stars



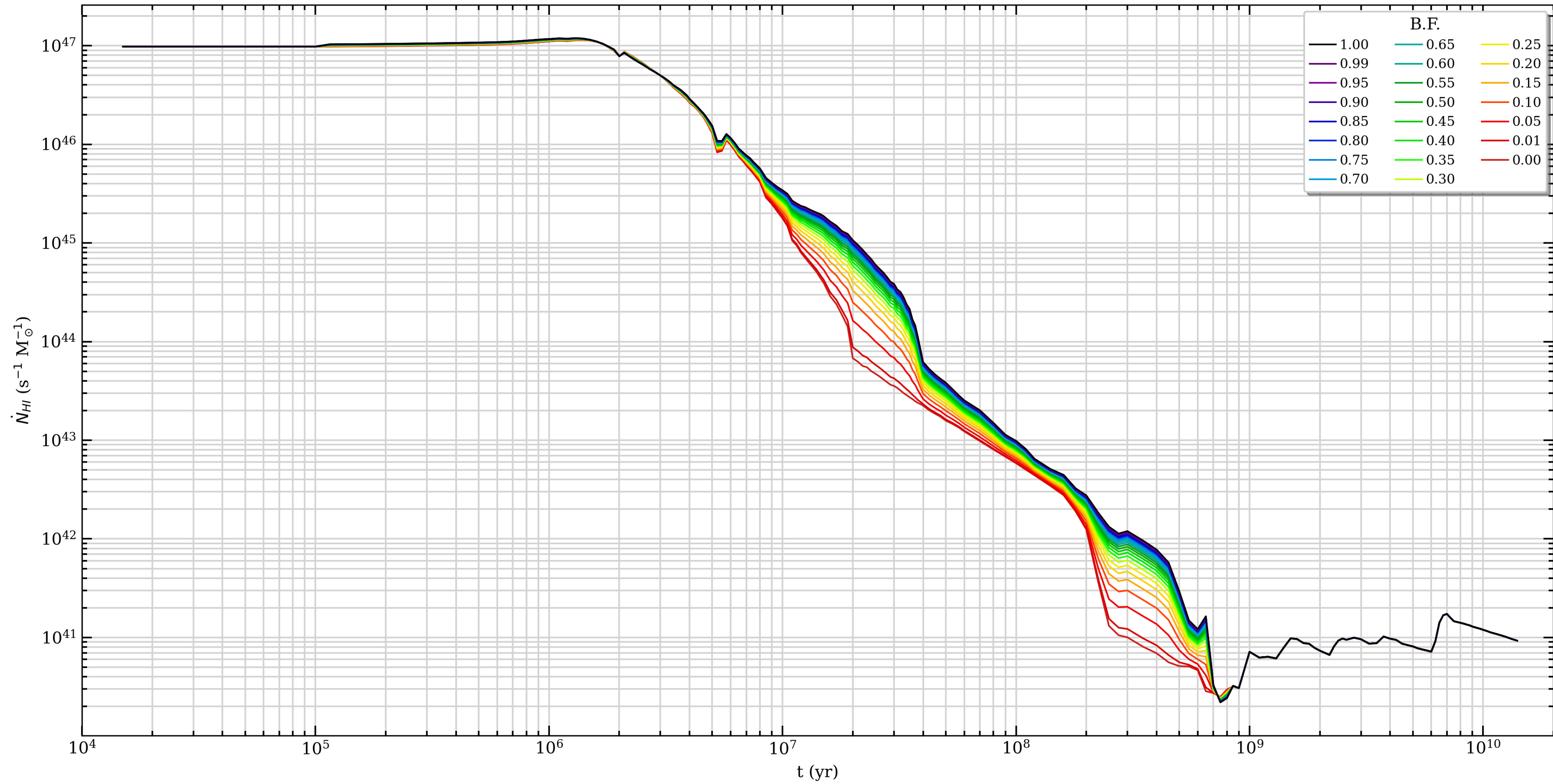
100 Myr, Single vs. Binary



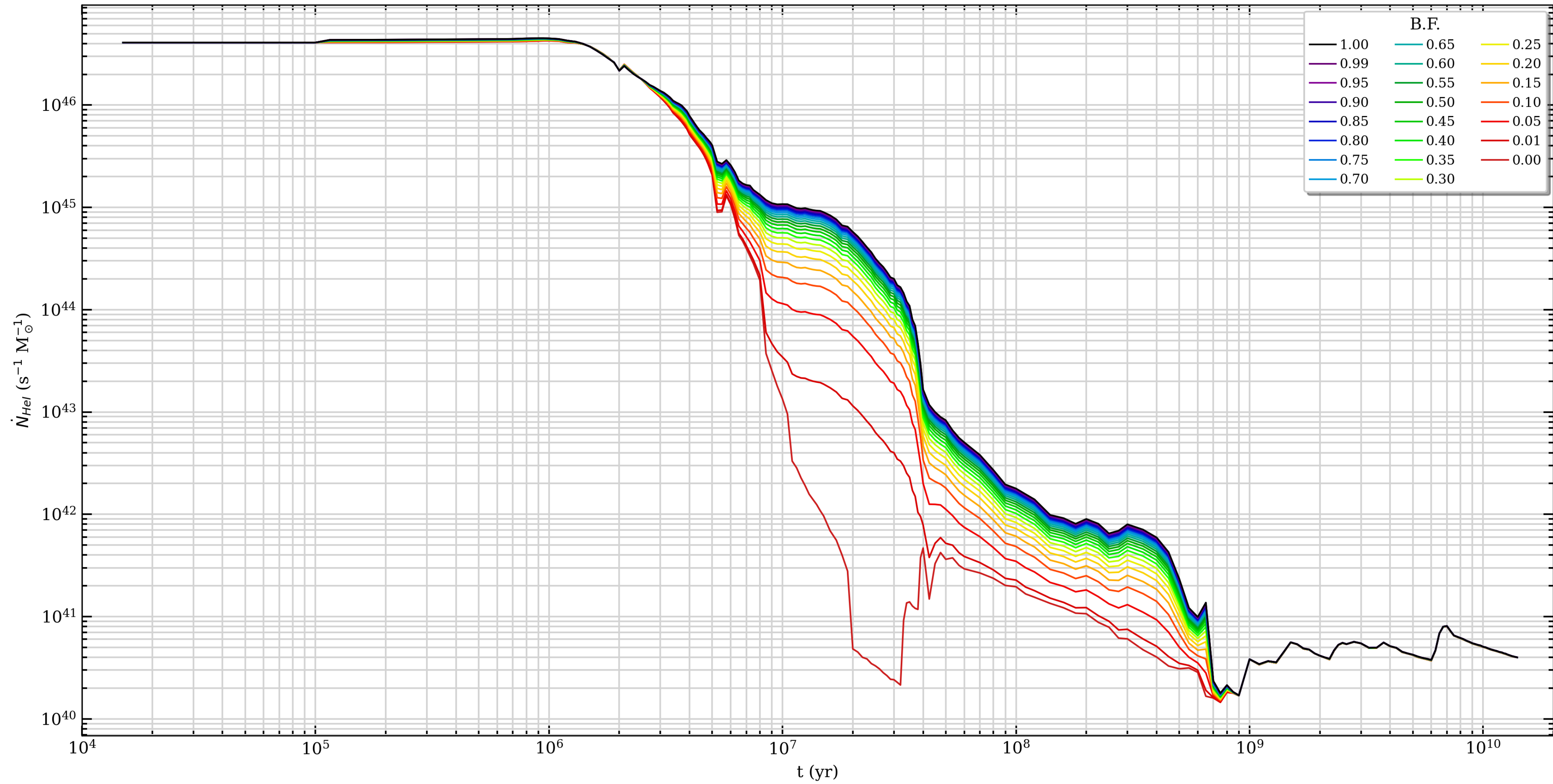




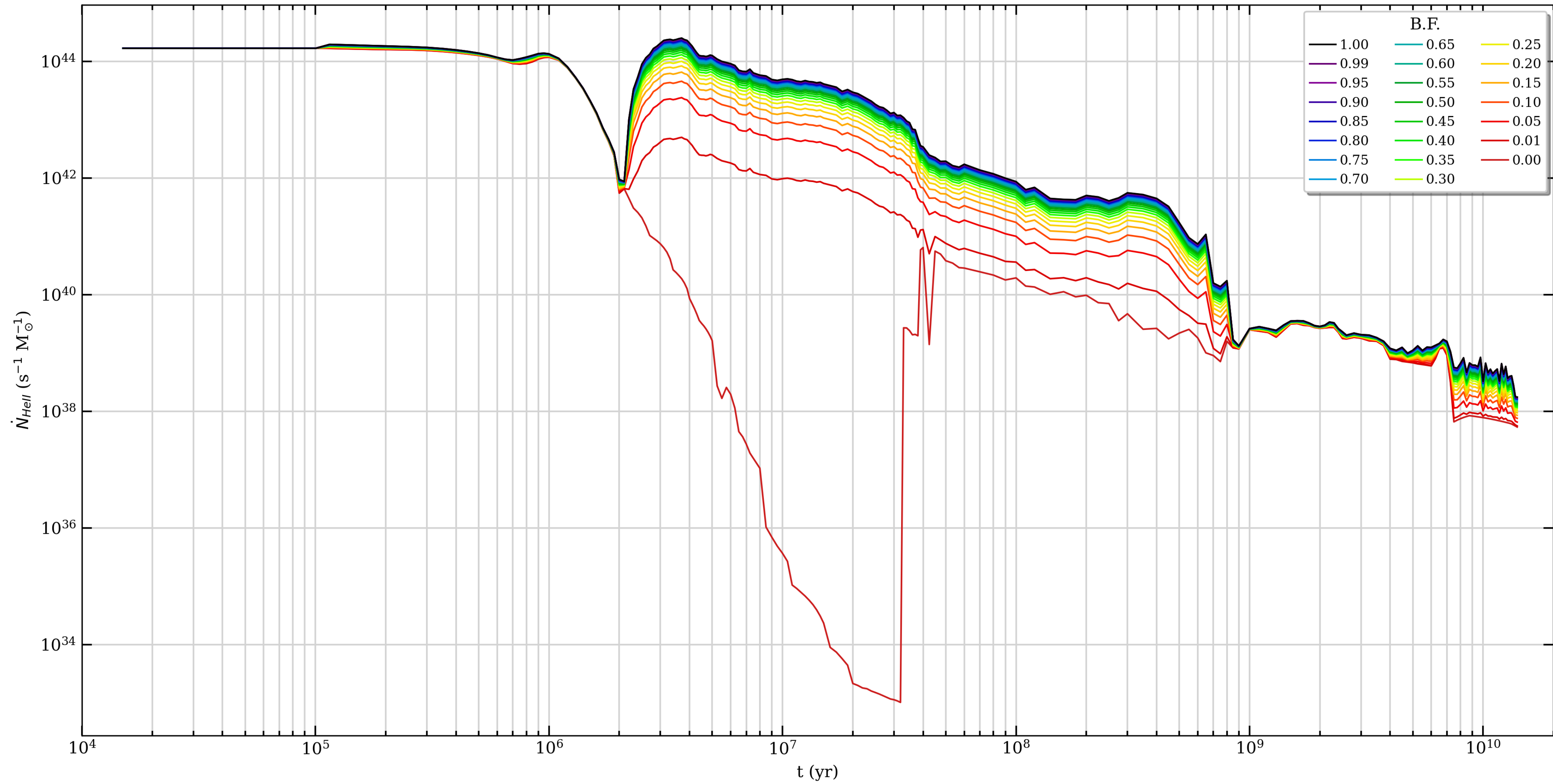
GALSEVN 2024 SSP models, various Binary Fractions,  $Z=0.001$ , Chabrier IMF,  $M_{UP}=300 M_{\odot}$

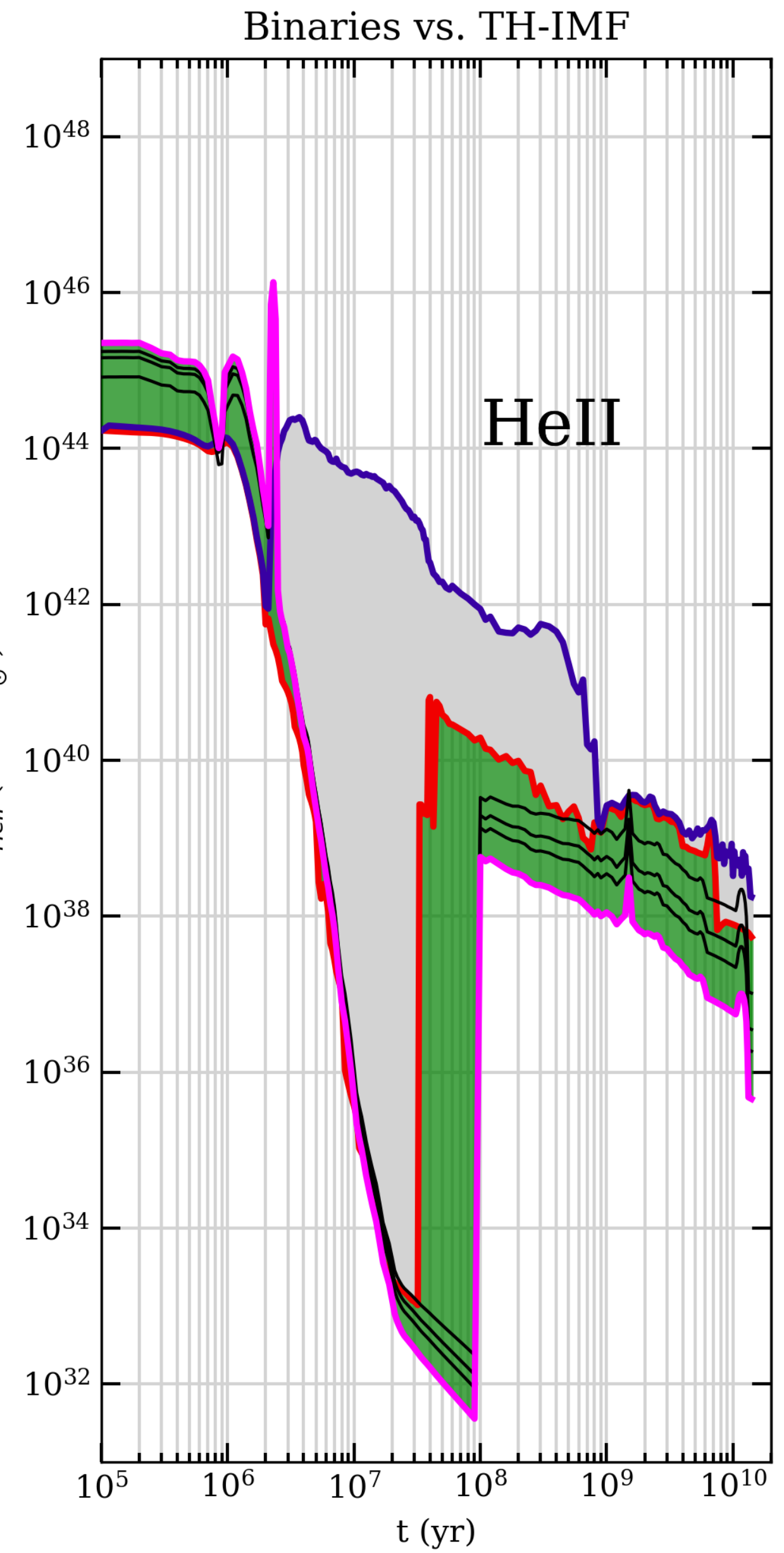
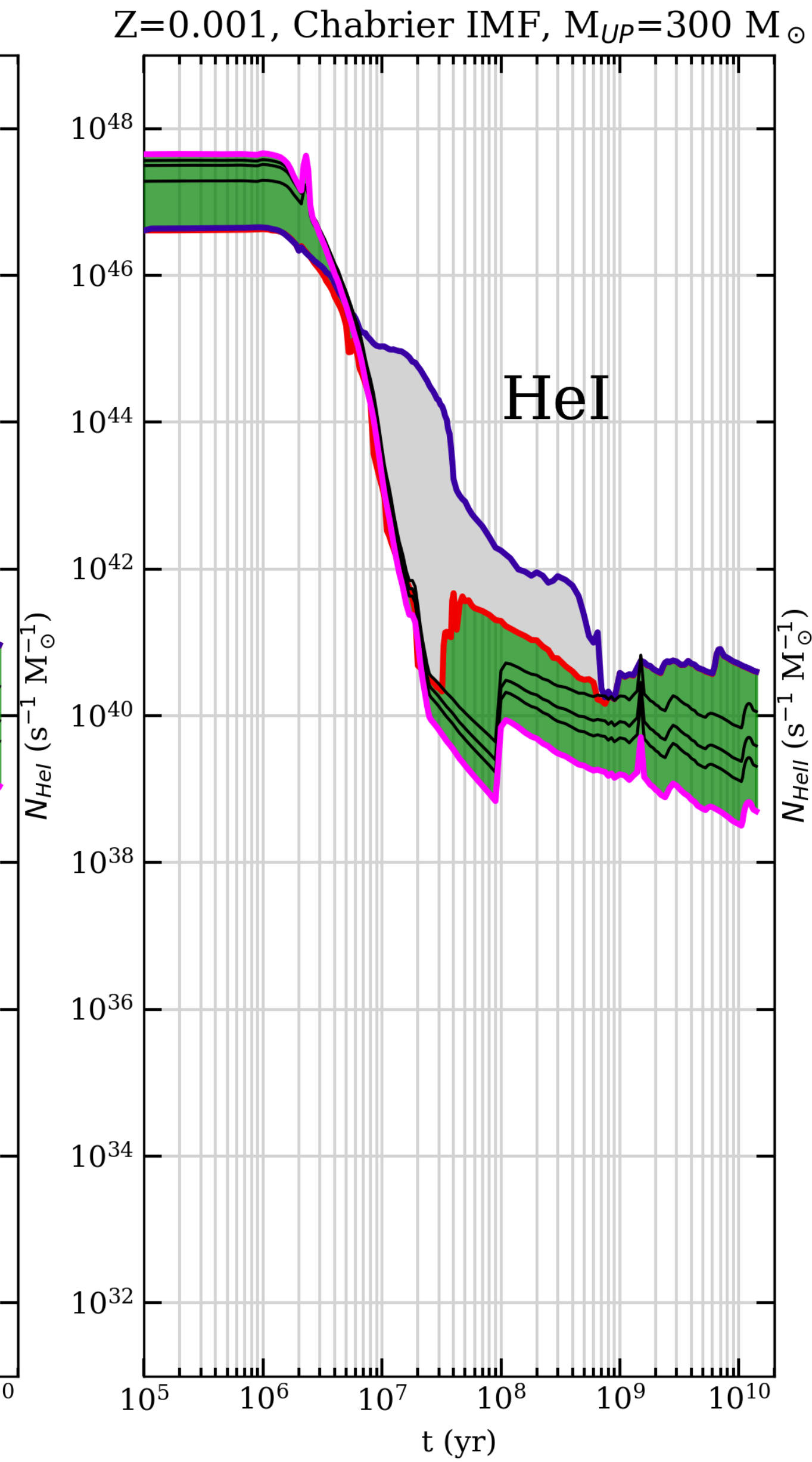
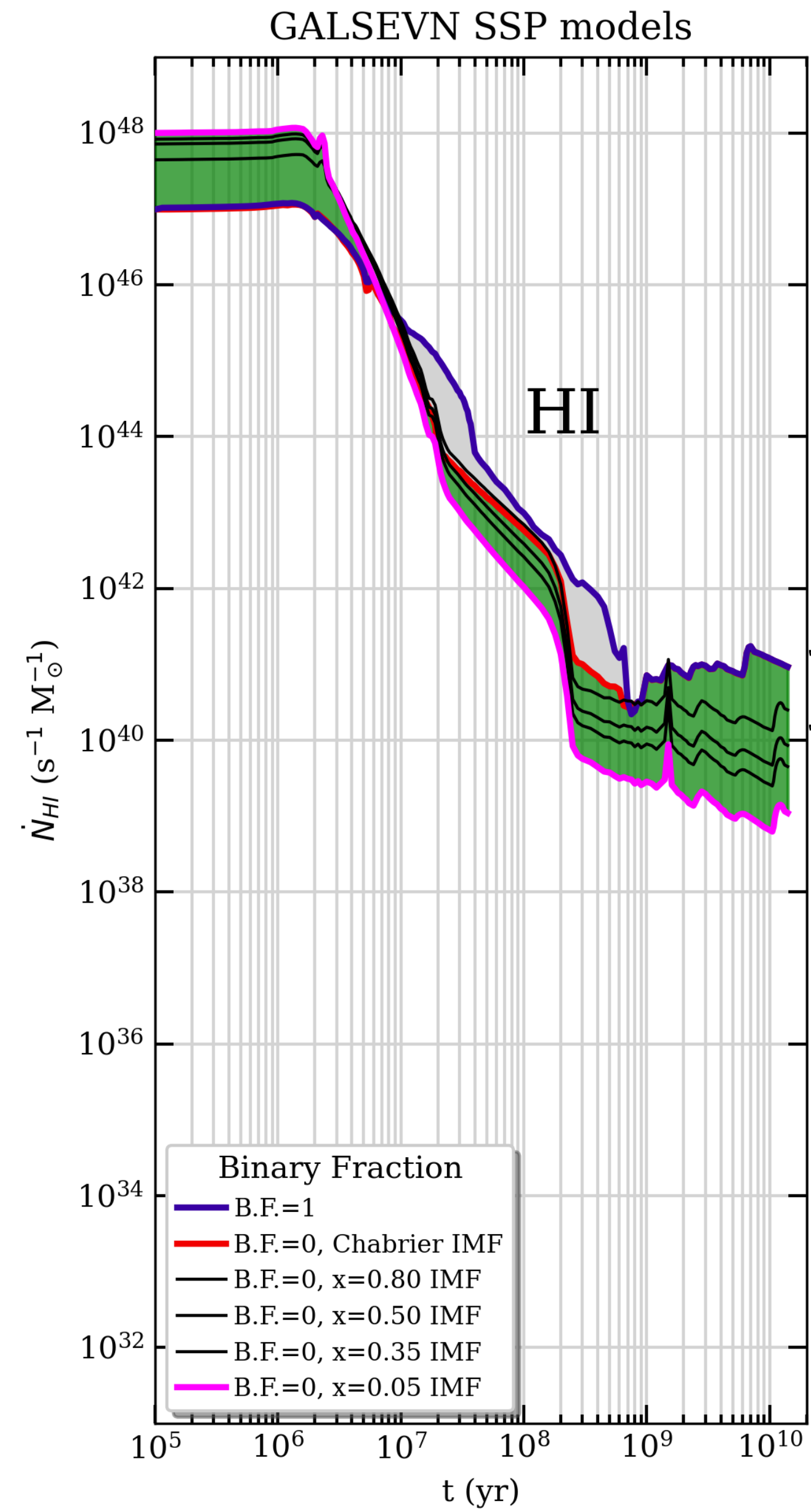


GALSEVN 2024 SSP models, various Binary Fractions,  $Z=0.001$ , Chabrier IMF,  $M_{UP}=300 M_{\odot}$

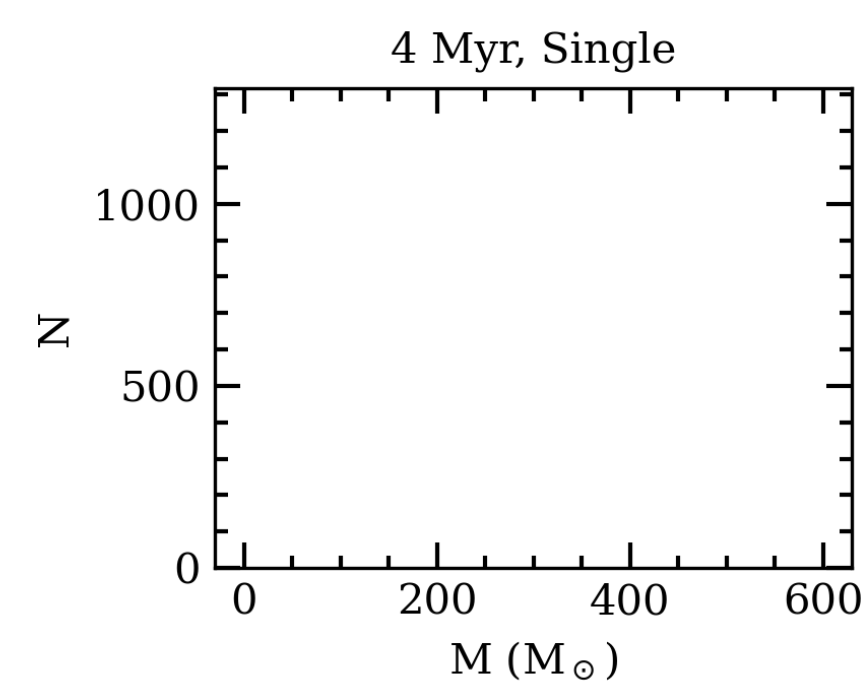
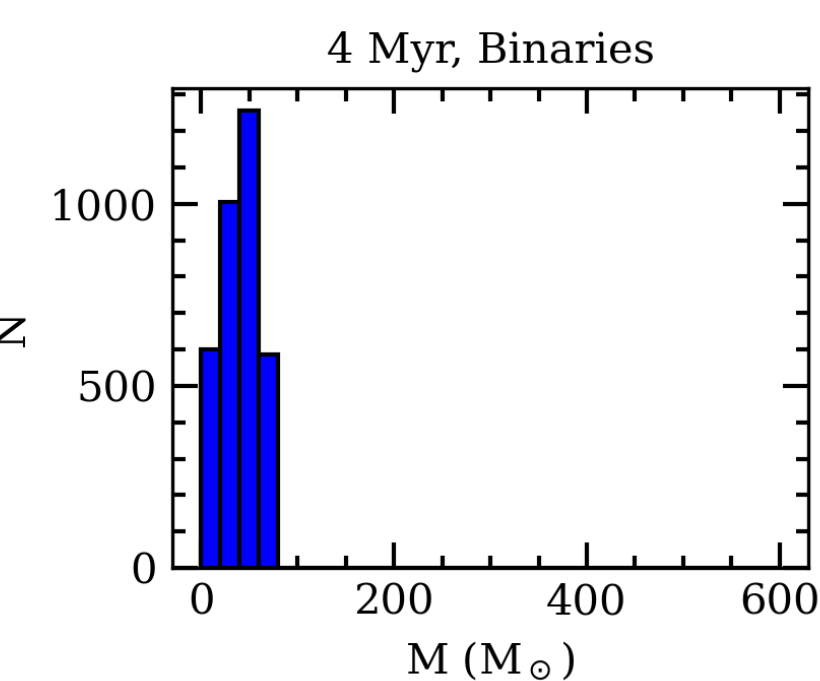
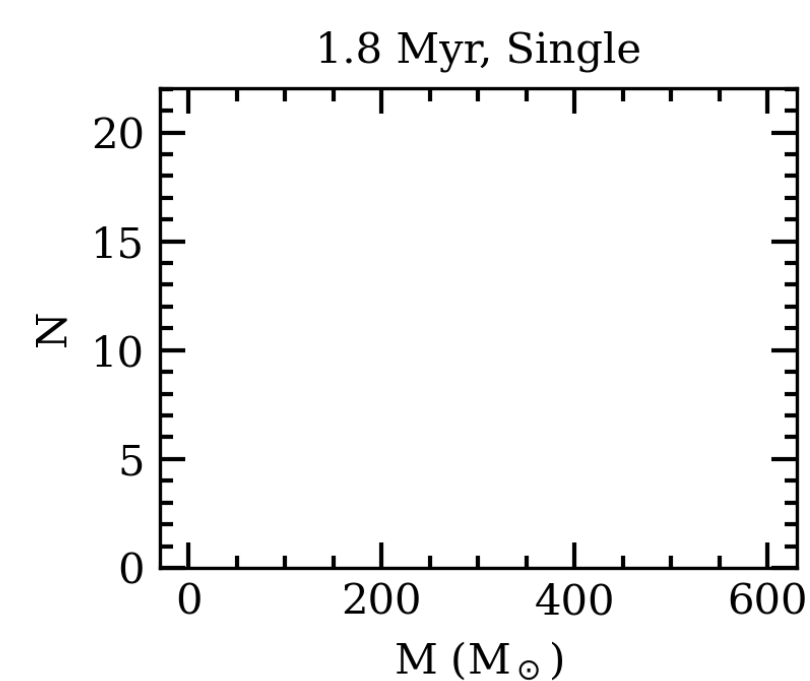
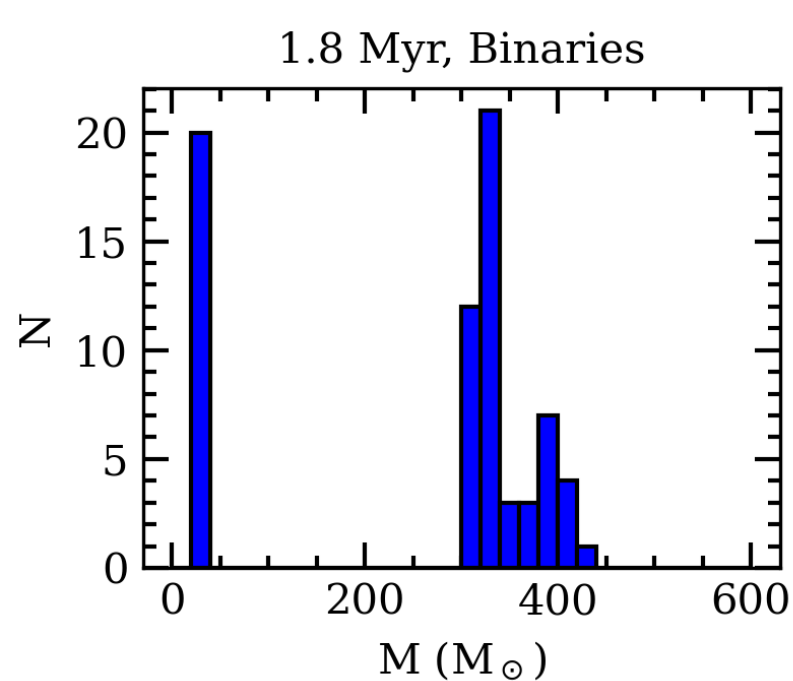
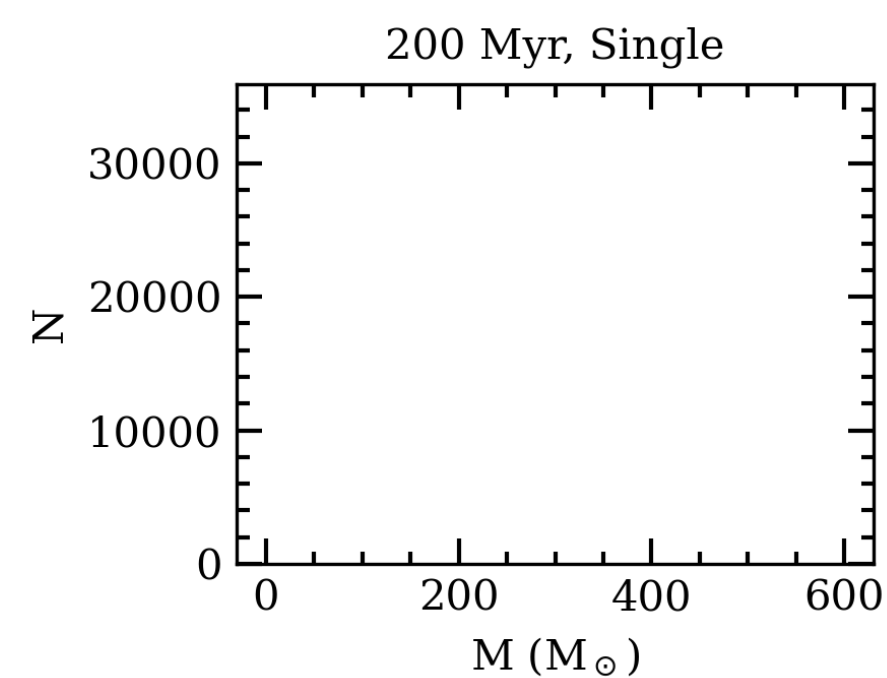
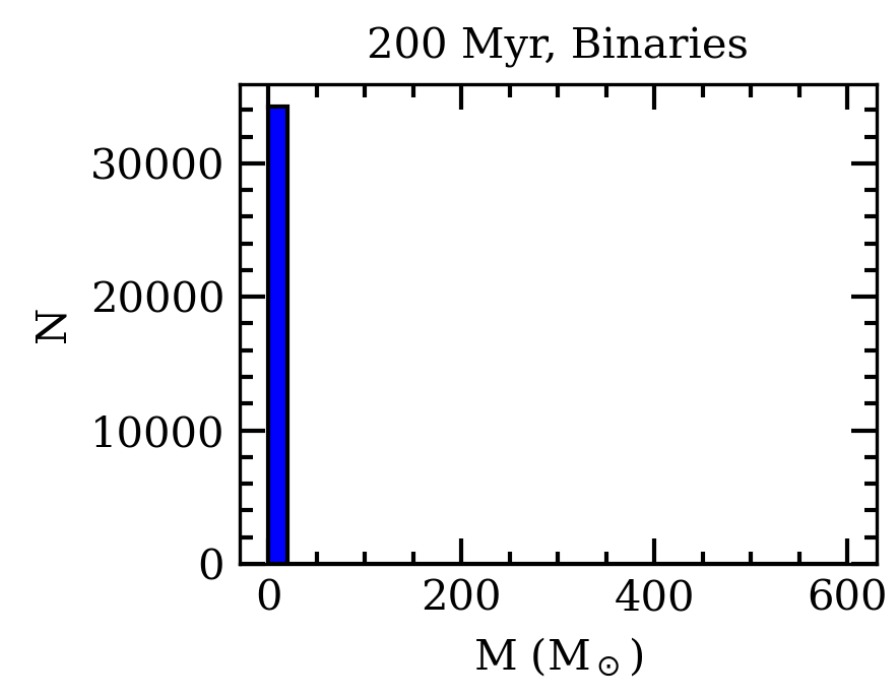
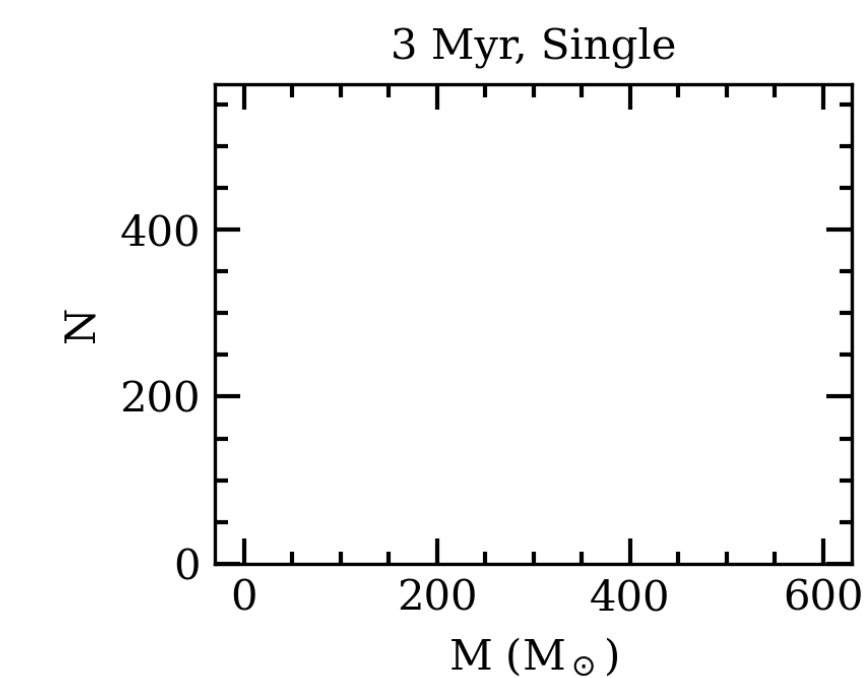
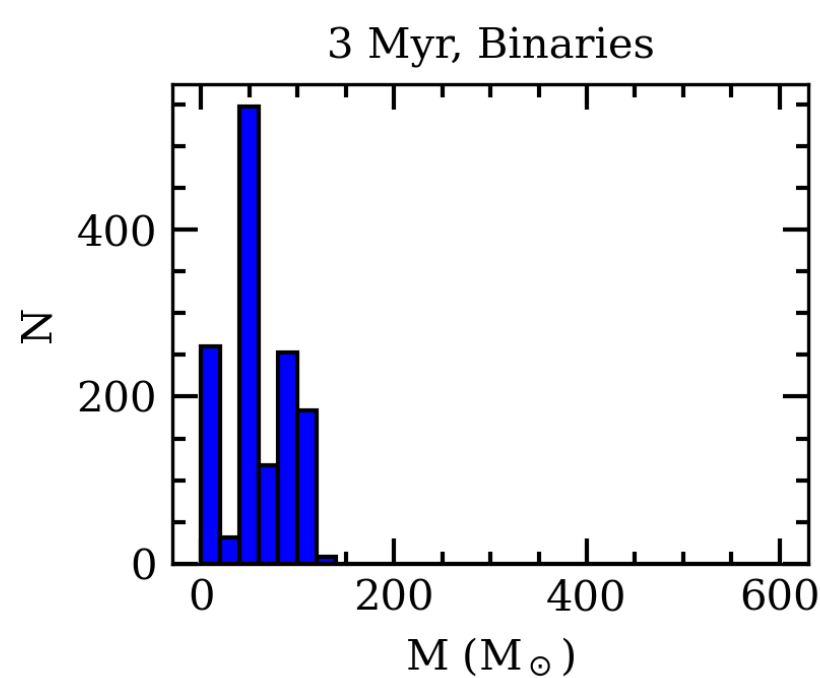
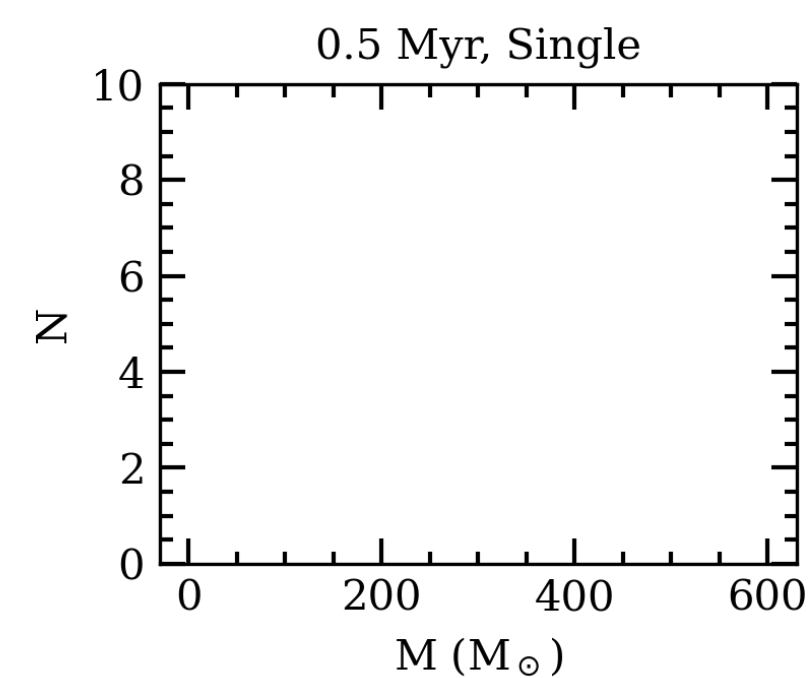
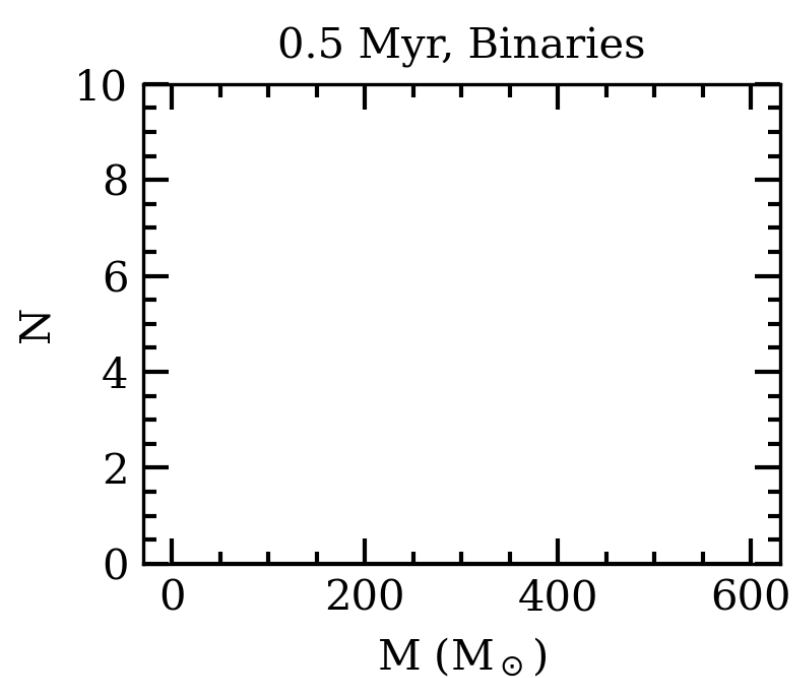
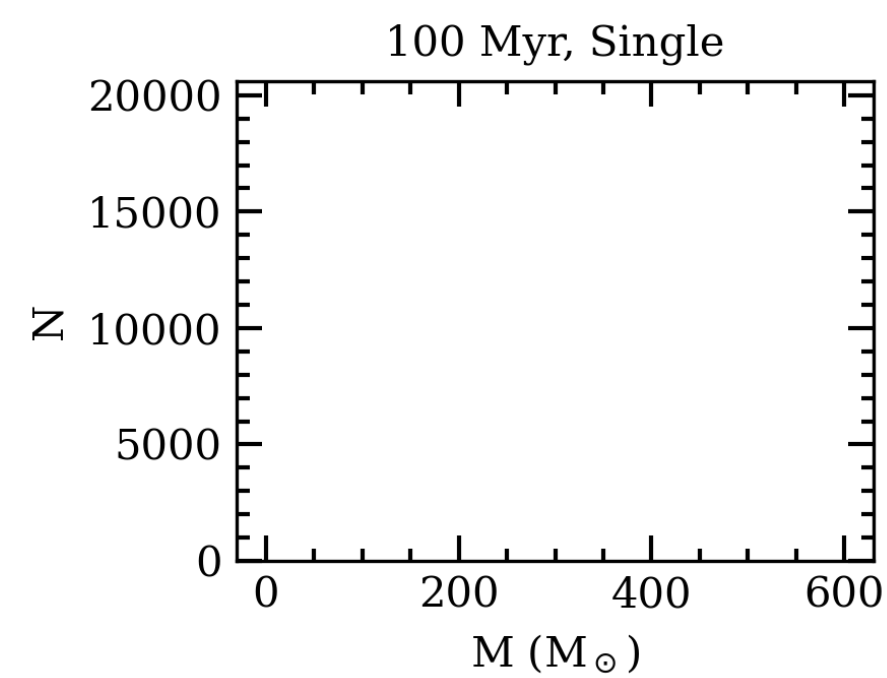
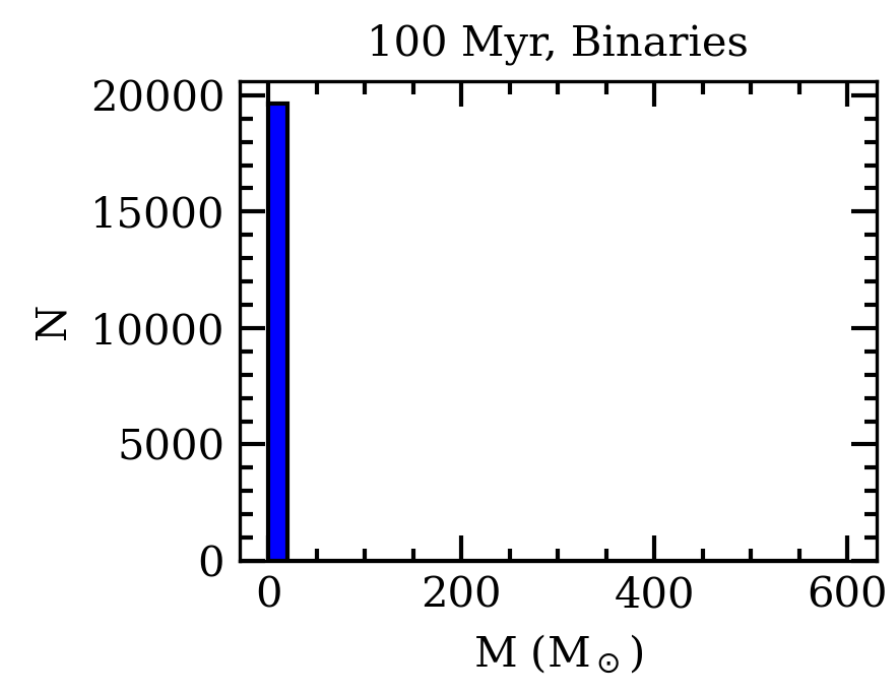
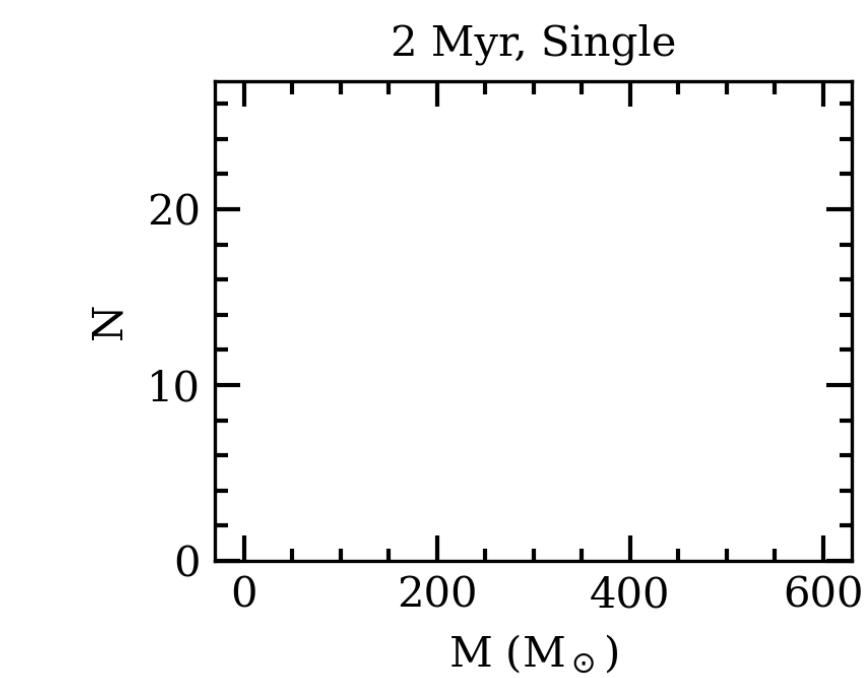
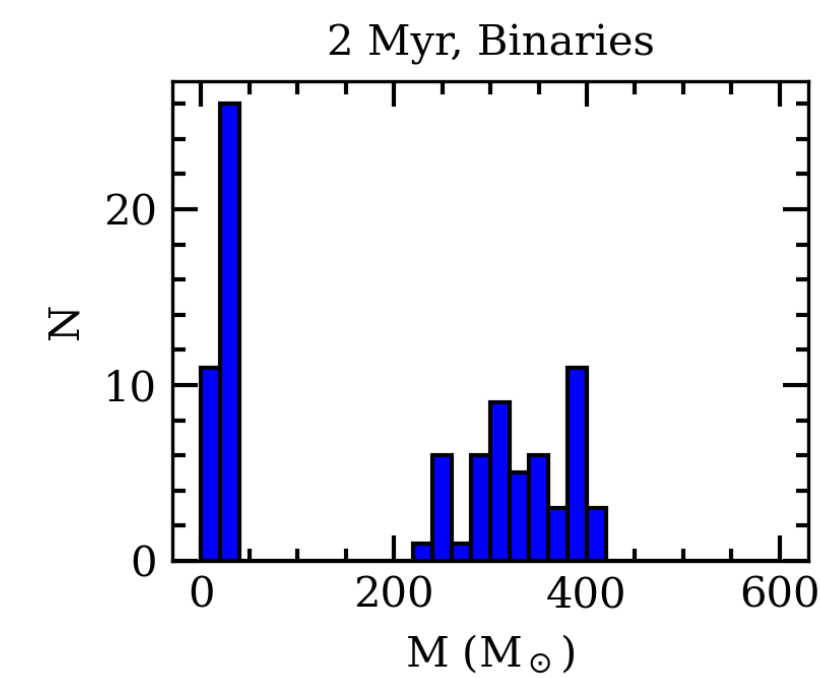
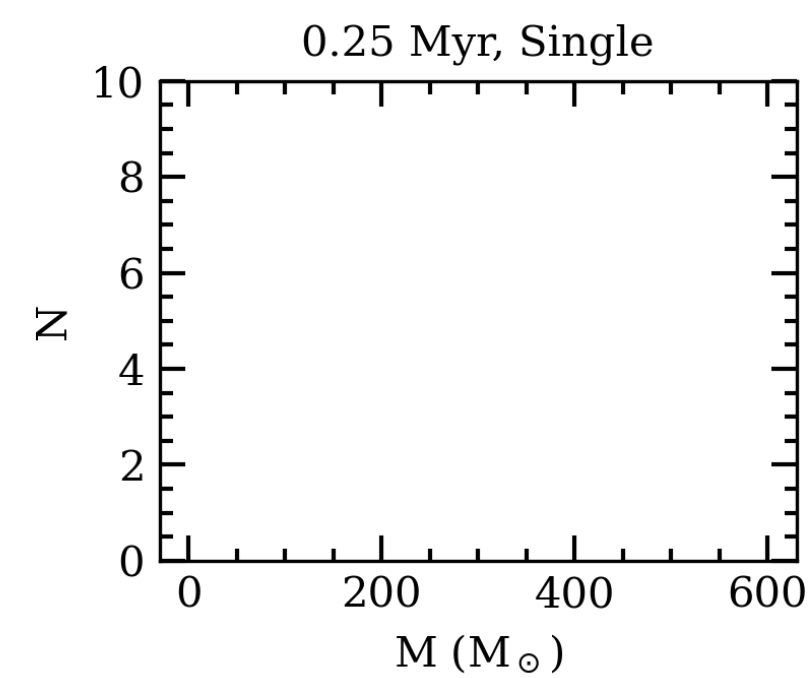
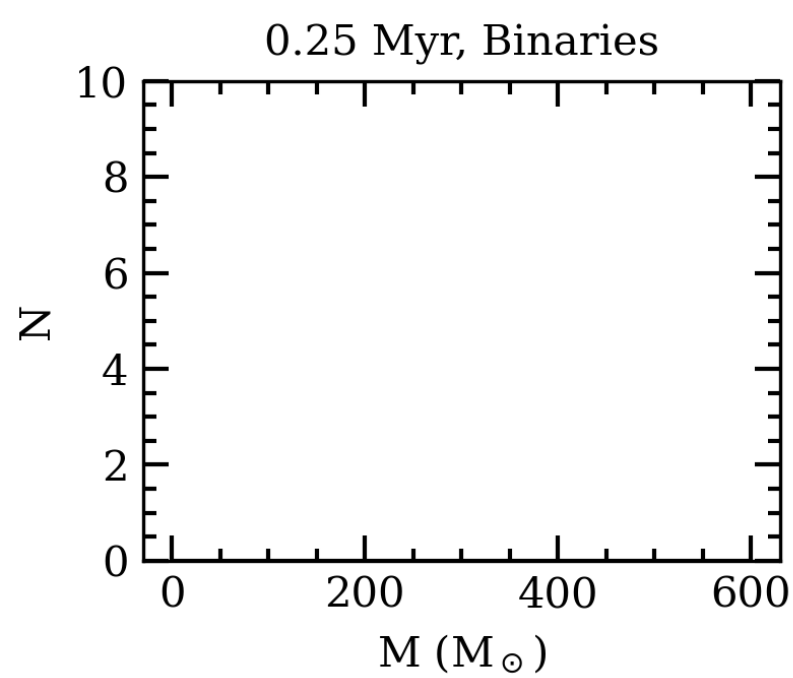
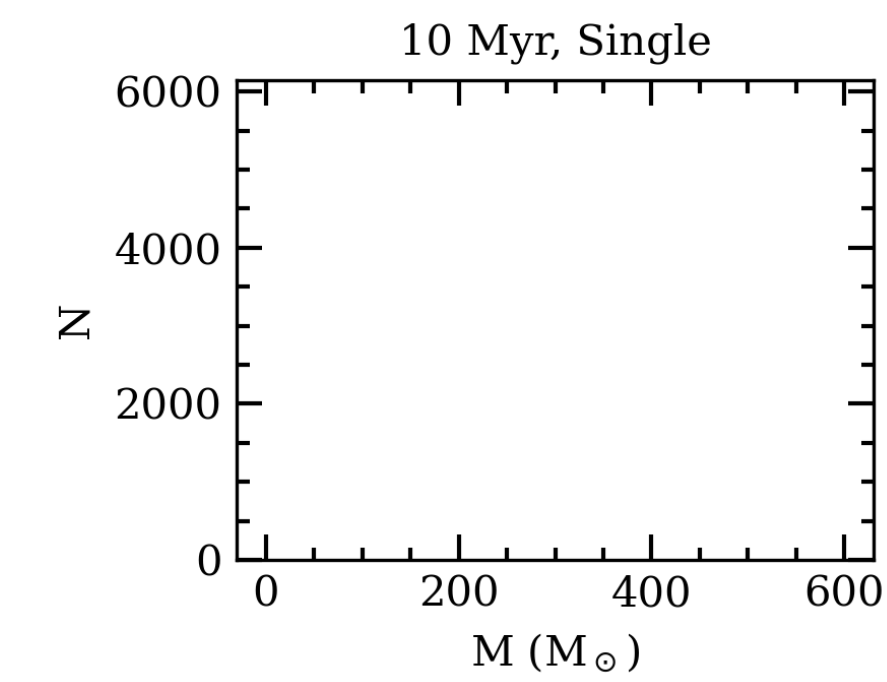
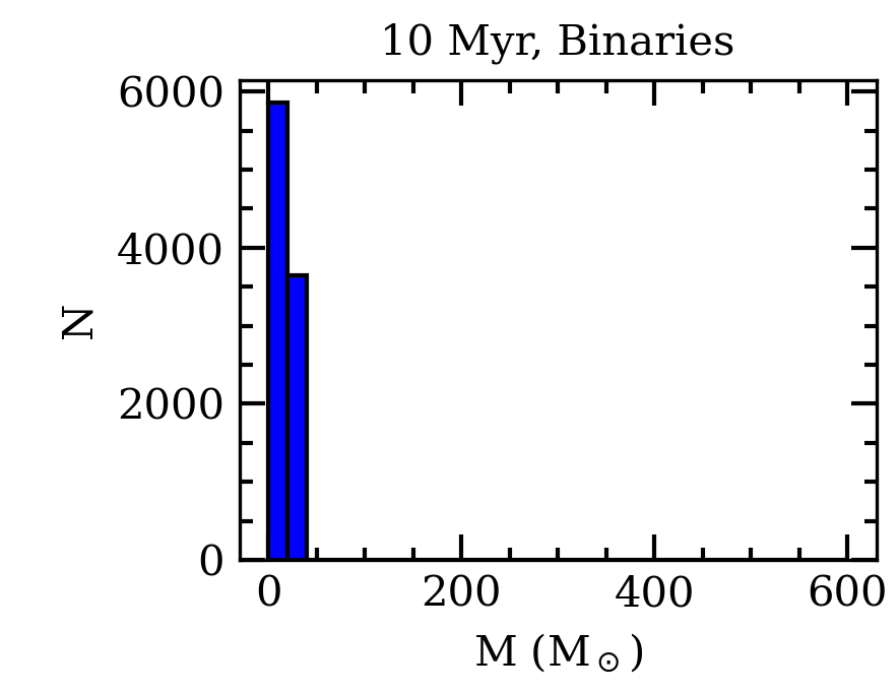
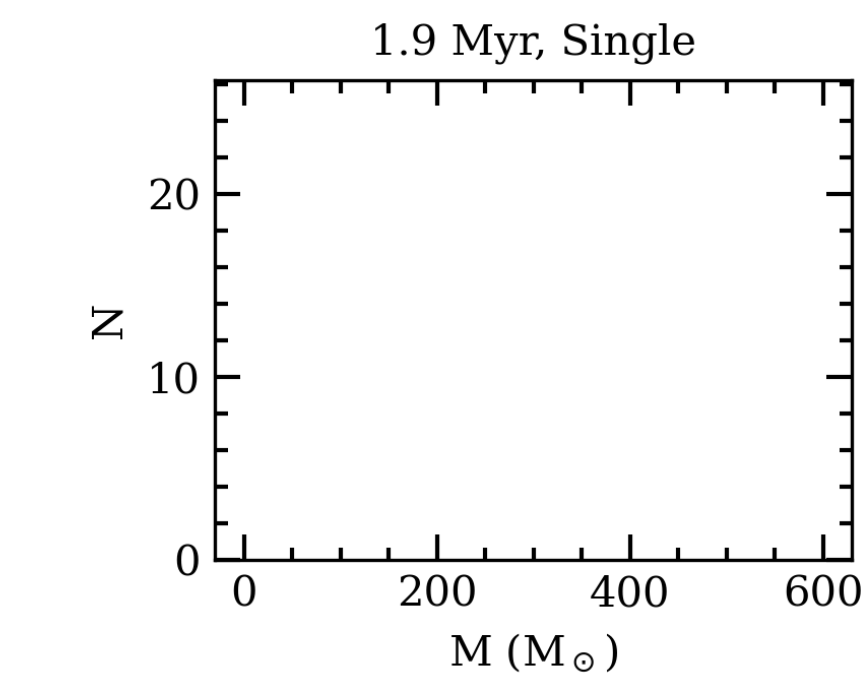
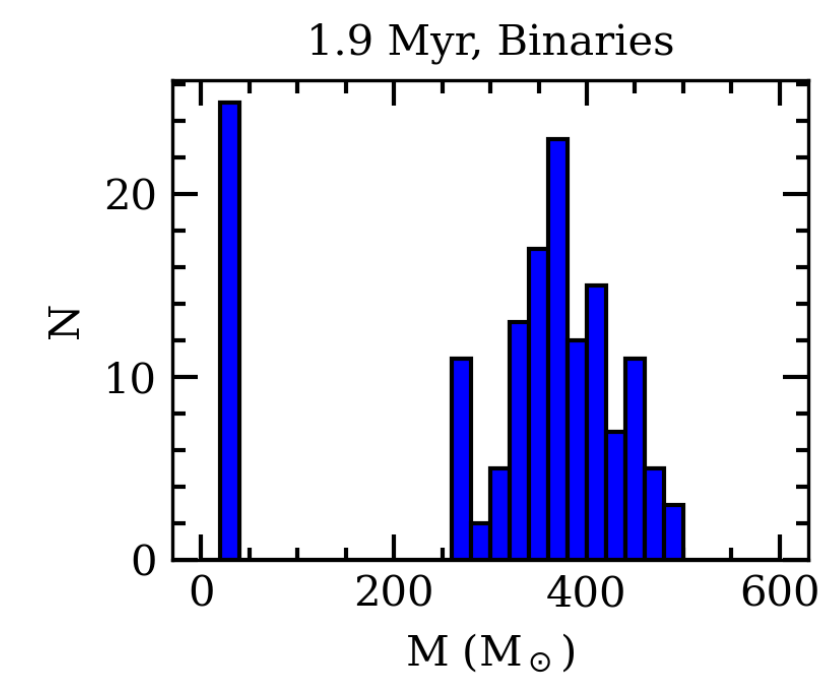
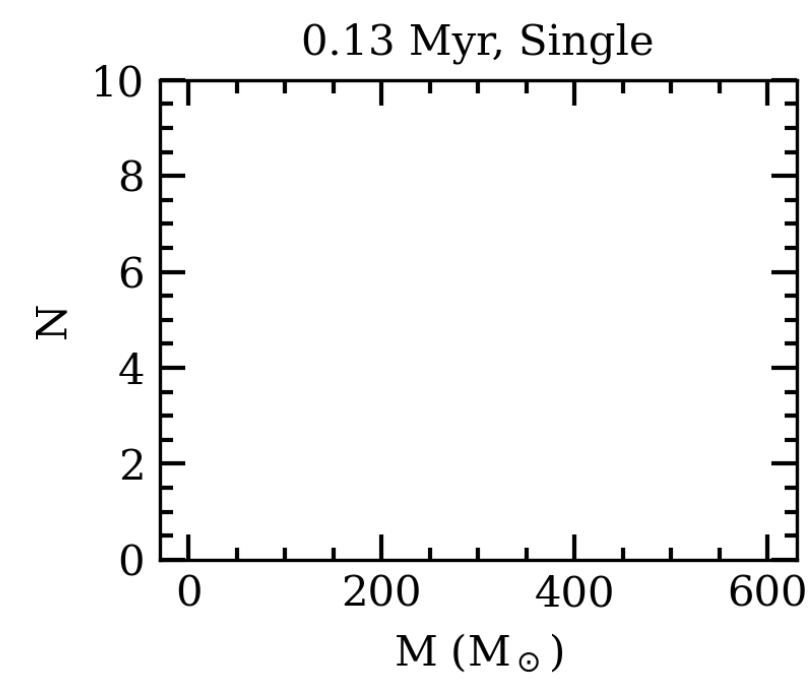
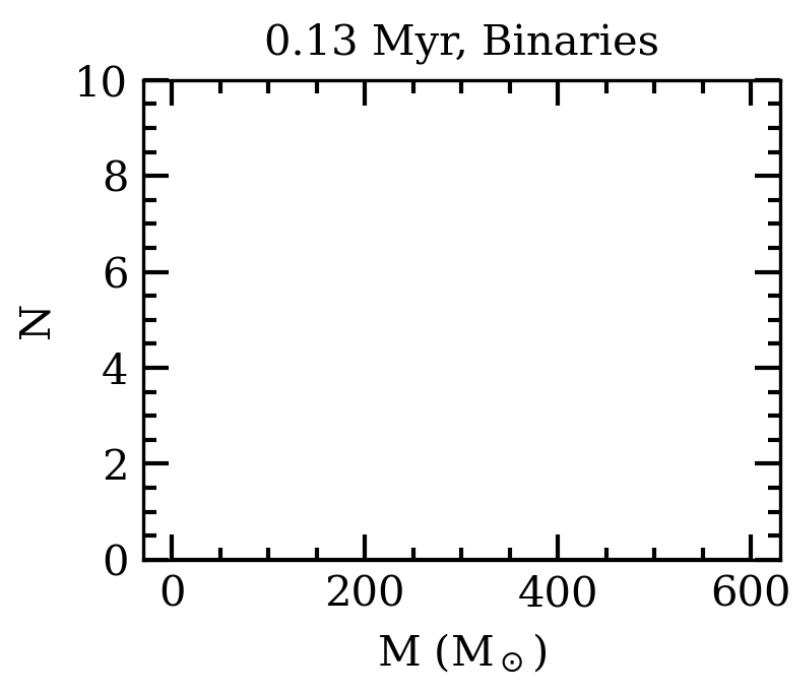


GALSEVN 2024 SSP models, various Binary Fractions,  $Z=0.001$ , Chabrier IMF,  $M_{UP}=300 M_{\odot}$





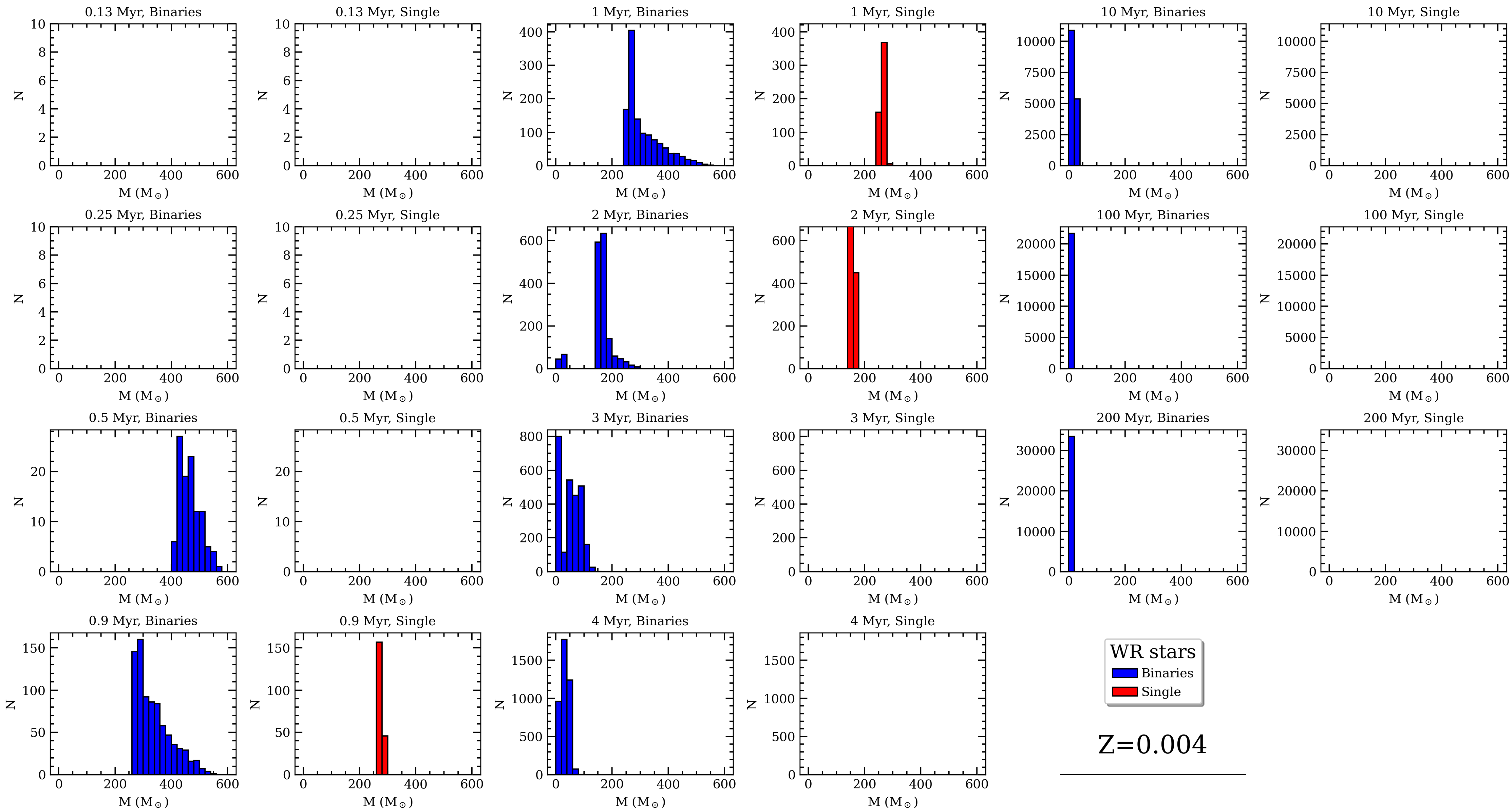
- WR star distribution

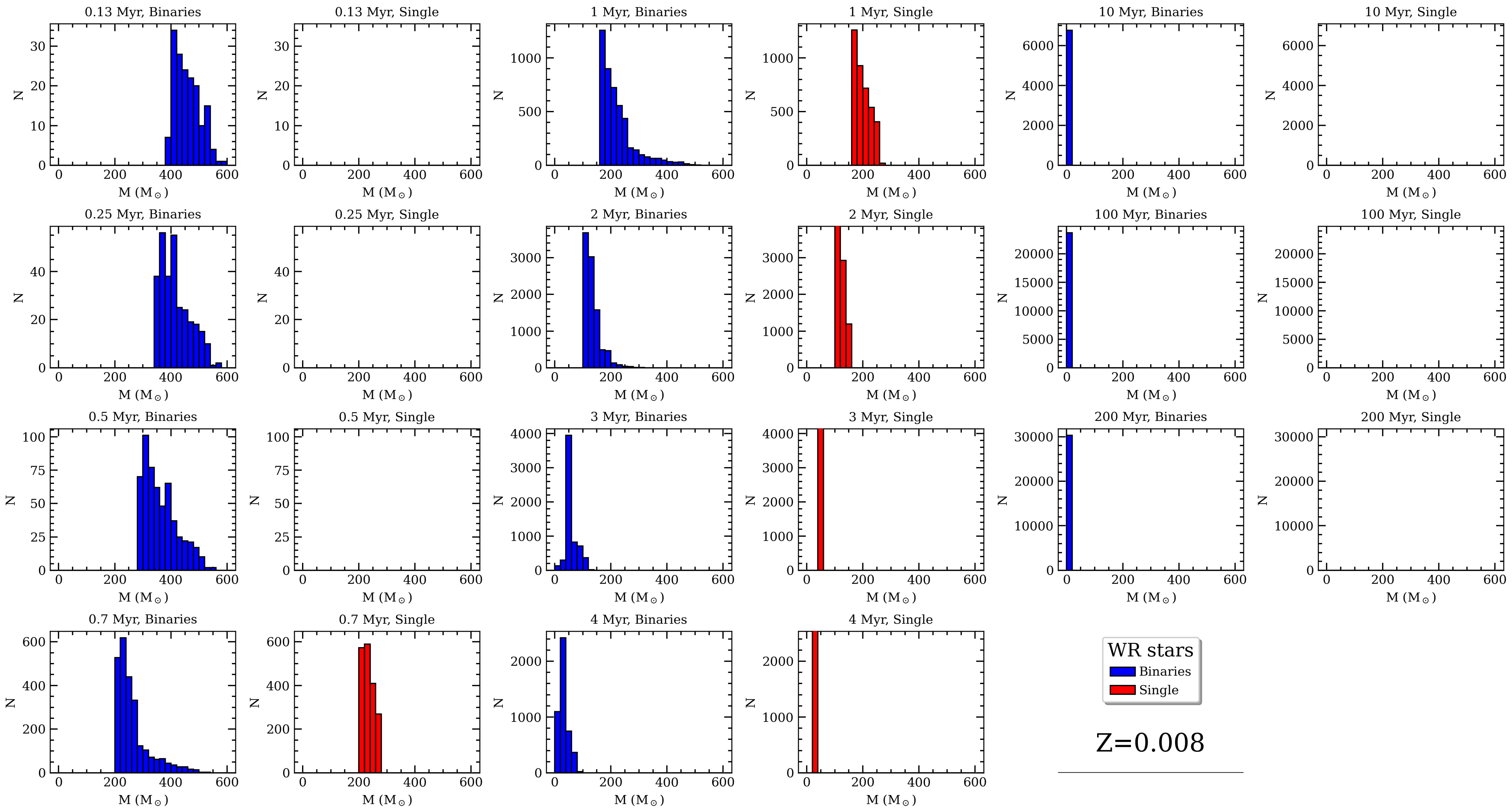


WR stars

- Binaries
- Single

Z=0.001





- VMS star distribution

